

**STUDIES IN CATALYSIS AND REACTION  
ENGINEERING OF MULTIPHASE  
HYDROGENATION REACTIONS**

**A THESIS  
SUBMITTED TO  
THE UNIVERSITY OF PUNE  
FOR THE DEGREE OF  
DOCTOR OF PHILOSOPHY**

**IN  
CHEMISTRY  
BY  
DEBDUT ROY**

**AT  
HOMOGENEOUS CATALYSIS DIVISION  
NATIONAL CHEMICAL LABORATORY  
PUNE-411 008  
INDIA**

**September 2006**



राष्ट्रीय रासायनिक प्रयोगशाला  
(वैज्ञानिक तथा औद्योगिक अनुसंधान परिषद)  
डॉ. होमी भाभा मार्ग पुणे - 411 008. भारत  
**NATIONAL CHEMICAL LABORATORY**  
(Council of Scientific & Industrial Research)  
Dr. Homi Bhabha Road, Pune - 411 008. India.



## CERTIFICATE

This is to certify that the work incorporated in the thesis, “**Studies in Catalysis and Reaction Engineering of Multiphase Hydrogenation Reactions**” submitted by **Mr. Debdut Roy**, for the Degree of **Doctor of Philosophy**, was carried out by the candidate under my supervision in the Homogeneous Catalysis Division, National Chemical Laboratory, Pune – 411 008, India. Such material as has been obtained from other sources has been duly acknowledged in the thesis.

**Dr. R. V. Chaudhari**  
(**Research Supervisor**)

## **DECLARATION**

I hereby declare that the thesis “**Studies in Catalysis and Reaction Engineering of Multiphase Hydrogenation Reactions**” submitted for the degree of Doctor of Philosophy to the University of Pune has not been submitted by me for a degree to any other University.

**Date:**

**Debdut Roy**

**Place:**

---

*Dedicated to*

*My Beloved Family*

*- Till Death Do Us Part*

---

## List of Contents

	<b>Description</b>	<b>Page No.</b>
	List of Figures	v
	List of Schemes	x
	List of Tables	xii
	Abstract of the Thesis	xiv
<b>Chapter 1</b>	<b>Introduction and Literature Survey</b>	
1.1.	General Introduction	2
1.2.	Multiphase Hydrogenation Reactions	6
1.2.1.	Catalysts for Hydrogenation Reactions	7
1.2.2.	Issues Heterogeneous Catalytic Hydrogenation Reactions	9
1.2.2.1.	Catalysis Issues	9
1.2.2.2	Reaction Engineering Aspects	10
1.2.3.	Reductive Alkylation of Amines	15
1.2.1.1	Reaction Pathway and Product Distribution:	15
1.2.3.2.	Substrates	17
1.2.3.3.	Catalysts	18
1.2.2.	Dearomatization Reaction	28
1.3.	Gas-Liquid-Liquid-Solid Four-Phase Systems	28
1.4.	Catalysis by Metal Nanoparticles	33
1.4.1.	Synthesis and Stabilization of Metal Nanoparticles	34
1.4.2.	Immobilization of Metal Nanoparticles	36
1.4.3.	Catalysis by Immobilized Heterogeneous Metal Nanoparticles	39
1.5.	Multiphase Reactors	45
1.5.1.	Slurry Reactors	46
1.5.1.1.	Agitated Slurry Reactors	46
1.5.1.2.	Bubble Column Reactors	48
1.5.1.3.	Fluidized-Bed Reactors	48

1.5.1.4.	Loop Recycle Reactors	50
1.5.2.	Fixed Bed Reactors	50
1.6.	Scope of the Present Work	51
	References	52
<b>Chapter 2</b>	<b>Reductive Alkylation of Aniline with Acetone Using Pd/Al<sub>2</sub>O<sub>3</sub> Catalyst: Kinetics and Modeling of Trickle Bed Reactor</b>	
2.1.	Introduction	62
2.2.	Experimental Section	64
2.2.1.	Chemicals	64
2.2.2.	Reactor Set-up	66
2.2.2.1.	Slurry Reactor	66
2.2.2.2.	Fixed Bed Reactor	67
2.2.3.	Analysis	69
2.3.	Results and Discussion	70
2.3.1	Preliminary Experiments	70
2.3.1.1.	Catalyst Selection	70
2.3.1.2.	Product Distribution	71
2.3.1.3.	Catalyst Stability and Recycle Studies	74
2.3.2.	Solubility Data	75
2.3.3.	Analysis of Initial Rate Data	76
2.3.4.	Analysis of Mass Transfer Effects	77
2.3.4 5.	Kinetic Modeling	81
2.3.6.	Trickle Bed Reactor Model	89
2.3.6.1.	Mathematical Model	90
2.3.6.2.	Comparison of Experimental Results with Model Predictions	97
2.4.	Conclusion	101
	Nomenclature	101
	References	104

<b>Chapter 3</b>	<b>Analysis of a Gas-Liquid-Liquid-Solid Catalytic Reaction: Kinetics and Modeling of a Semi Batch Slurry Reactor</b>	
3.1.	Introduction	107
3.2.	Experimental Section	108
3.2.1.	Materials	108
3.2.2.	Analysis	108
3.2.3.	Catalyst preparation and Characterization	108
3.2.4.	Reactor Set-up	111
3.3.	Results And Discussions	112
3.3.1.	Preliminary Experiments	112
3.3.1.1.	Reaction Mechanism and Product Distribution	113
3.3.2.	Solubility Data	116
3.3.2.1.	Solubility data for hydrogen in water	116
3.3.2.2.	Solubility data for hydrogen in cyclohexane	116
3.3.2.3.	Partition coefficient of hydrogen and aniline in cyclohexane – water binary system	117
3.3.3.	Analysis of Initial Rate Data	117
3.3.4.	Analysis of Mass Transfer Effects	121
3.3.5.	Intrinsic Kinetics	124
3.4.	Analysis Of A Gas-Liquid-Liquid-Solid System	132
3.4.1.	Mathematical Model	135
3.4.1.1.	Comparison of the model predictions with experimental results	143
3.5.	Conclusion	145
	Nomenclature	145
	Literature Cited	147

<b>Chapter 4</b>	<b>Pt and Pd Nanoparticles Immobilized on Amine-functionalized Zeolite: Catalytic Applications for Hydrogenation and Heck Reactions</b>	
4.1.	Introduction	150
4.2.	Experimental Section	152
4.2.1.	Chemicals	152
4.2.2.	Synthesis	152
4.2.3.	Instrumentation	154
4.3.	Results And Discussion	156
4.3.1.	Characterization	156
4.3.2.	Catalysis	164
4.3.2.1.	Trojan Horses or Truly Heterogeneous?	173
4.3.2.2.	Active Pd species for Heck Reaction	174
4.3.2.3.	Role of Surface Modification by APTS	176
4.4.	Conclusion	177
	Reference	179
	<b>Publications/Symposia</b>	182



## List of Figures

<b>Figure No.</b>	<b>Description</b>	<b>Page No.</b>
1.1.	Classification of catalytic hydrogenation reactions	7
1.2.	(A) Mean chemisorption enthalpies of hydrogen as a function of the transition metals in the periodic table, (B) ethylene hydrogenation rate as a function of metal-metal distance in (100) planes	9
1.3.	The flow regimes in a trickle bed reactor (G and L are superficial mass flow rates for gas and liquid respectively)	11
1.4.	Automotive converters: an application of metal nanoparticles	33
1.5.	(a) Electrostatic and (b) steric stabilization of metal nanoparticles	36
1.6.	Immobilization of metal nanoparticles through amide linkage	38
1.7.	Immobilization of metal nanoparticles on solid supports	39
1.8.	Agitated slurry reactors	47
1.9.	Schematics of different types of fixed bed reactors	50
2.1.	Schematic of a slurry reactor set-up	67
2.2.	Schematic of the fixed bed reactor	69
2.3.	Concentration-time profile for reductive alkylation of aniline with acetone	73
2.4.	Concentration-time profiles for homogeneous reaction between aniline and acetone: effect of hydrogen and Pd/Al <sub>2</sub> O <sub>3</sub> on the equilibrium	73
2.5.	Recycle experiments for reductive alkylation of aniline using 3% Pd/Al <sub>2</sub> O <sub>3</sub>	74
2.6.	(A) Effect of agitation speed and (B) Effect of aniline concentration on initial rate of hydrogenation for reductive alkylation of aniline and acetone using 3% Pd/Al <sub>2</sub> O <sub>3</sub>	77
2.7.	(A) Effect of partial pressure of hydrogen and (B) Effect of catalyst loading on initial rate of hydrogenation for reductive alkylation of aniline and acetone using 3% Pd/Al <sub>2</sub> O <sub>3</sub>	78

2.8.	Concentration-Time profile at 378 K	85
2.9.	Concentration-Time profile at 393 K	86
2.10.	Concentration-Time profile at 408 K	86
2.11.	H <sub>2</sub> consumption-Time profiles at different temperatures	87
2.12.	%RR values at different aniline concentrations	87
2.13.	%RR values at different partial pressures of hydrogen	88
2.14.	%RR values at different catalyst loadings	88
2.15.	Temperature dependence of rate constants	89
2.16.	Effect of liquid velocity on conversion of aniline in trickle bed reactor at different aniline inlet concentrations	99
2.17.	Effect of liquid velocity on selectivity to N-IPA in trickle bed reactor at different aniline inlet concentrations	99
2.18.	Effect of liquid velocity on selectivity to N-IPC in trickle bed reactor at different aniline inlet concentrations	100
2.19.	Effect of liquid velocity on selectivity to N-IPC in trickle bed reactor at different aniline inlet concentrations	100
3.1.	Set-up for Ru/Al <sub>2</sub> O <sub>3</sub> catalyst preparation	109
3.2.	XRD patterns of (A) $\gamma$ -alumina, and (B) 2% Ru/Al <sub>2</sub> O <sub>3</sub> recorded in the 2 $\theta$ range 10°-80°. The Bragg reflections for Ru/Al <sub>2</sub> O <sub>3</sub> sample are indexed.	110
3.3.	TEM image of 2%Ru/Al <sub>2</sub> O <sub>3</sub> Catalyst	110
3.4.	Recycle experiments for hydrogenation of aniline using 2% Ru/Al <sub>2</sub> O <sub>3</sub> catalyst: a comparison between four-phase and three-phase systems	115
3.5.	Effect of aqueous phase hold-up on initial rate of hydrogenation for hydrogenation of aniline in a four phase system using 2% Ru/Al <sub>2</sub> O <sub>3</sub>	118
3.6.	Effect of agitation speed on initial rate of hydrogenation for hydrogenation of aniline in a four phase system using 2% Ru/Al <sub>2</sub> O <sub>3</sub>	119

3.7.	Effect of catalyst loading on initial rate of hydrogenation for hydrogenation of aniline in a four phase system using 2% Ru/Al <sub>2</sub> O <sub>3</sub>	119
3.8.	Effect of aniline concentration on initial rate of hydrogenation for hydrogenation of aniline in a four phase system using 2% Ru/Al <sub>2</sub> O <sub>3</sub>	120
3.9.	Effect of hydrogen partial pressure on initial rate of hydrogenation for hydrogenation of aniline in a four phase system using 2% Ru/Al <sub>2</sub> O <sub>3</sub>	121
3.10.	Concentration-time profile at 378 K	129
3.11.	Concentration-time profile at 398 K	129
3.12.	Concentration-time profile at 418 K	130
3.13.	Temperature dependence of rate constants	130
3.14.	Temperature dependence of adsorption constants	131
3.15.	Photographs of the glass reactor containing aniline in cyclohexane (organic phase; top yellow layer), water (aqueous phase; colorless bottom layer) and catalyst (black colored) at different hold ups of aqueous and organic phases. The total volume of the liquid phase was kept constant. A glass jar was fitted physically below the reactor head, which was used for the slurry reactions. A hot plate was used to heat the contents of the glass jar and temperature was controlled by the thermocouple fitted to the reactor.	134
3.16.	Concentration profile of species A and B in a gas-liquid-liquid-solid catalytic system	137
3.17.	Concentration profile of species A and B in a gas-liquid-liquid-solid catalytic system	141
3.18.	Comparison of experimental and predicted results for initial rate of hydrogenation as a function of aqueous phase hold up at constant amount of aniline and catalyst	144
4.1.	(A) UV-vis spectra recorded for the samples <b>[Pt]-APTS-Y</b>	157

- (curve 1) and **[Pd]-APTS-Y** (curve 2) after dispersion in water; (B) FTIR spectra recorded from drop-coated films of amine-functionalized zeolite (curve 1) and platinum-nanoparticle-bound zeolite (sample **[Pt]-APTS-Y**) material (curve 2) on Si(111) substrates.
- 4.2. TGA data recorded from a carefully weighed quantity of the APTS functionalized Na-Y zeolite powder (curve 1), after immobilization of palladium and platinum nanoparticles on the amine-functionalized zeolite (curves 2 and 3 for **[Pd]-APTS-Y** and **[Pt]-APTS-Y** samples respectively). 158
- 4.3. (A) XRD patterns recorded from the samples of Na-Y zeolite (curve 1), amine-functionalized Na-Y zeolite (curve 2), **[Pt]-APTS-Y** (curve 3) and **[Pd]-APTS-Y** (curve 4) in the  $2\theta$  range  $5^\circ$ - $30^\circ$ ; (B) XRD patterns recorded from the samples **[Pd]-APTS-Y** (curve 1) and **[Pt]-APTS-Y** (curve 2) in the  $2\theta$  range  $35^\circ$ - $85^\circ$ . The Bragg reflections for both samples are indexed. 160
- 4.4. (A) - (C) Representative TEM images of amine-functionalized zeolite, **[Pt]-APTS-Y** before reaction and **[Pt]-APTS-Y** after reaction respectively on a carbon-coated TEM grid (see text for details). (D) Selected area electron diffraction (SAED) pattern recorded from the platinum nanoparticles shown in B. 162
- 4.5. (A) and (B) - Pt 4f and Pd 3d core level spectra recorded for **[Pt]-APTS-Y** and **[Pd]-APTS-Y** samples respectively. 164
- 4.6. (A) Recycle experiments for hydrogenation of styrene to ethylbenzene using **[Pt]-APTS-Y**; and (B) Pt 4f core level spectra from **[Pt]-APTS-Y** after 1<sup>st</sup> (curve 1) and 3<sup>rd</sup> recycle (curve 2) of the hydrogenation reaction. 168
- 4.7. (A) - (D) Representative TEM images of the samples of amine-functionalized zeolite, **[Pd]-APTS-Y** before reaction, 170

- [Pd]-APTS-Y** after hydrogenation reaction and after 2<sup>nd</sup> cycle of Heck reaction respectively on a carbon-coated TEM grid.
- 4.8. (A) Reaction scheme for Heck arylation of styrene: an application of **[Pd]-APTS-Y** catalyst; (B) A typical conversion-time profile (**1**: iodobenzene; **2**: *trans*-stilbene; **3**: *cis*-stilbene) 171
- 4.9 Hot filtration experiment to check the heterogeneity of **[Pd]-APTS-Y** catalyst for Heck arylation of styrene with iodobenzene. (A) **[Pd]-APTS-Y** catalyzed reaction; (B) reaction continued with liquid separated out from **[Pd]-APTS-Y** by filtration after ~50% conversion. Conditions are as given in Table 4.3. 174
- 4.10. Pd 3d core level spectra recorded from **[Pd]-APTS-Y** sample after keeping in hydrogen atmosphere (curve 1) and after 2<sup>nd</sup> recycle (curve 2) of the Heck reaction. The spectrum in curve 2 has been decomposed into two components by a nonlinear least-squares procedure and the spin-orbit components are shown. 176
- 4.11. Representative TEM images of Pd nanoparticles immobilized on the surface of Na-Y zeolite without APTS modification 177

## List of Schemes

Scheme No.	Description	Page No.
1.1.	Synthesis of Ibuprofen <sup>®</sup> by Boots route and Hoechst-Celanese process	3
1.2.	Mechanism of N-monoalkylation of aniline	15
1.3.	Reaction pathway of N-dialkylation of aniline	16
1.4.	Ring alkylation of aromatic amines by carbonyl compounds	16
1.5.	N-alkylation of sterically hindered amines with alcohols	19
1.6.	Reductive alkylation of nitro-compounds with aldehydes	23
1.7.	Reductive alkylation of amides	25
1.8.	Reductive alkylation reactions of chiral amines and $\alpha$ -ketoesters	26
1.9.	Synthesis of optically active amines by reductive alkylation reaction	26
1.10.	Synthesis of Metolachlor by reductive alkylation reaction	27
1.11.	Synthesis of <i>p</i> -amino phenol in a gas-liquid-liquid-solid system	30
1.12.	Selective hydrogenation of $\alpha,\beta$ -unsaturated aldehyde in a gas-liquid-liquid-solid system	30
1.13.	Hydrogenolysis of carbobenzoxy phenylalanine in a gas-liquid-liquid-solid system	31
2.1.	Reaction scheme for reductive alkylation of aniline with acetone	63
2.2.	Reaction scheme for reductive alkylation of aniline with acetone in presence of 3% Pd/Al <sub>2</sub> O <sub>3</sub> catalyst	72
3.1.	Stepwise hydrogenation of aniline to cyclohexylamine	113
3.2.	Mechanism of formation of dicyclohexylamine during hydrogenation of aniline	114
3.3.	Reaction scheme for hydrogenation of aniline in a gas-	114

	liquid-liquid-solid system using 2% Ru/Al <sub>2</sub> O <sub>3</sub> catalyst	
4.1.	Schematic representation of selective outer-cage synthesis of <b>[Pt]/[Pd]-APTS-Y</b> nanocomposites	163
4.2.	Schematic diagram of (A) HDA capped colloidal Pt nanoparticle and (B) <b>[Pt]-APTS-Y</b> nanocomposite catalysts. Active catalyst surface is more accessible with <b>[Pt]-APTS-Y</b> for the substrate molecules for catalytic hydrogenation reactions.	165

## List of Tables

<b>Table No.</b>	<b>Description</b>	<b>Page No.</b>
1.1.	Commercial applications of hydrogenation reactions using heterogeneous catalysts	5
1.2.	Catalytically active metals for hydrogenation reactions	8
1.3.	Gas-liquid-solid catalytic hydrogenation reactions: A Literature Review	12
1.4.	Comparison of transition metals for reductive alkylation of aniline and acetone	18
1.5.	Comparison of Pt and Pd metals for reductive alkylation of PAPD and MIBK	19
1.6.	Literature survey on reductive alkylation of aromatic amines and carbonyl compounds (and their precursors)	20
1.7.	Summary of catalytic hydrogenation of aromatic compounds	28
1.8.	Commonly used reducing agents in synthesis of colloidal metal nanoparticles	35
1.9.	Commonly used stabilizers in synthesis of colloidal metal nanoparticles	36
1.10.	Catalysis by immobilized metal nanoparticles	41
1.11.	Reactor modeling studies in semi batch slurry reactors	49
2.1.	Literature on reductive alkylation of aromatic amines	65
2.2.	Range of experimental conditions	67
2.3.	Catalyst screening for reductive alkylation of aniline and acetone	71
2.4.	Comparison of transition metals for reductive alkylation of aniline and acetone (Greenfield's report)	71
2.5.	Solubility data (Henry's constant) for H <sub>2</sub> -in aniline/acetone mixture at different temperatures and compositions	76
2.6.	Specifications of reactor parameters and $k_1a_b$ calculation	79
2.7.	Values of different parameters used in mass transfer analysis	80
2.8.	Comparison of various models for reductive alkylation of	84



	aniline with acetone using 3% Pd/Al <sub>2</sub> O <sub>3</sub>	
2.9.	Dimensionless parameters used in the model	93
2.10.	Correlations used for Trickle bed reactor modeling	97
3.1.	Comparison of catalytic performance for three-phase and four-phase catalytic systems for different aromatic functionalities	113
3.2.	Range of operating conditions for kinetic study	115
3.3.	Solubility data (Henry's constant) for H <sub>2</sub> in water at different temperatures	116
3.4.	Solubility data (Henry's constant) for H <sub>2</sub> in various compositions of aniline in cyclohexane at different temperatures	116
3.5.	Values of different parameters used in mass transfer analysis for hydrogen	123
3.6.	Rate equations and kinetic parameters	127
3.7.	Values of enthalpy and entropy of adsorption	132
4.1.	Hydrogenation reactions using immobilized Pt nanoparticles on APTS modified NaY zeolite	166
4.2.	Performance of <b>[Pd]-APTS-Y</b> catalyst for hydrogenation reactions	169
4.3.	Heck arylation of iodobenzene with styrene using <b>[Pd]-APTS-Y</b>	172

## Abstract of the Thesis

Catalysis has wide ranging applications in our day-to-day life due to its application in food, cloth, medicinal industries, waste water treatment, pollution control etc. While the petroleum refining industries developed due to catalysis, its application on pharmaceuticals, specialty chemicals expanded rapidly because catalysis showed promising advantages over the stoichiometric routes practiced by the industries previously to produce these high quality products. This leads to minimum waste generation and on the other hand improved product quality and cost effectiveness. Due to the increasing awareness of environmental issues and competitiveness of the global market, the industries look for alternative routes providing a more cleaner and atom efficient transformation of the starting materials to the desired product. In this context, heterogeneous catalysis played an important role and among the various types of reactions, catalytic hydrogenation of various organic functionalities is most commonly encountered in fine chemicals and pharmaceutical industries. Similarly, with the advancement in the catalysis research and related processes, development of multiphase catalytic reactors has become equally important.<sup>1</sup> Thus, we can realize the importance of integrated efforts of catalysis and reaction engineering in new generation processes, which will not only give better quality of life to us but will also be useful in achieving economical processes. Though extensive work on theoretical as well as experimental multiphase reactions is reported previously, in most of these single step reactions with isothermal conditions have been considered. Only in a few cases, experimental studies on multistep multiphase hydrogenation reactions have been addressed.<sup>2</sup> On the other hand, the reactions practiced in the industries are exothermic, multi-step and with complex reaction network. Therefore, there is a need of experimental studies on multistep, complex reactions. Similarly, in order to develop economically competitive processes, several new types of catalytic systems also have been found to be advantageous. For example, four-phase reactions in which catalytic hydrogenations are carried out in the presence of two immiscible liquid phases and a solid catalyst has not been well studied. Similarly, several reactions involving combinations of non-catalytic and catalytic reactions, complexities of equilibrium reactions, reactions with complex network where selective synthesis of an intermediate compound is important, or catalytic reactions

in non-ideal reaction media (such as CO<sub>2</sub>, H<sub>2</sub>O, ionic liquids) have not also been addressed with detailed experimental studies. In this thesis, few such cases of hydrogenation reactions are addressed, which demand attention from chemical engineering as well as catalysis point of view. The following catalytic systems were chosen for the present work:

1. Reductive alkylation reaction of aromatic amines
2. Hydrogenation reaction in gas-liquid-liquid-solid four phase catalytic system
3. Catalysis by immobilized metal nanoparticles

The thesis is presented in four chapters, a brief summary of which is outlined here.

Chapter 1 presents a general review on hydrogenation reaction with an emphasis on reductive alkylation, catalysis in gas-liquid-liquid-solid reactions and synthesis and applications of metal nanoparticles on hydrogenation reactions. A general discussion on catalysis and reaction engineering aspects of hydrogenation reactions is presented in this chapter. At the end of this chapter, a brief discussion on multiphase reactors used for hydrogenation reactions has been addressed.

N-alkyl aromatic amines are important products for the dyes, fuels and rubber industries and synthesized by the reductive alkylation of an aromatic amine and a carbonyl compound in the presence of a supported transition metal catalyst. The first step in the synthesis is a non-catalytic homogeneous reaction, followed by hydrogenation in the second step to the desired N-alkylated product. The literature reports reveal that the unique class of reaction, which is a combination of non-catalytic and catalytic reactions though has been practiced for decades in the industries and huge number of publications addressed the catalysts and substrates, there are only few reports<sup>3</sup> on the analysis of the reaction system from chemical engineering point of view. A detailed literature review on reductive alkylation reactions is presented as a part of this chapter.

It is well documented in the literature that in many occasions a gas-liquid-liquid-solid system is beneficial over the conventional gas-liquid-solid three phase catalytic systems for hydrogenation of organic compounds.<sup>4</sup> One can consider the revolutionary process of Asahi Chemicals for partial hydrogenation of benzene to cyclohexene in a four phase system. But the issues like phase behavior, mass transfer of the reactants and product

molecules, swelling and shrinking of a particular phase during the course of a reaction and its effect on overall reactor performance and phase behavior are not well studied. Therefore, the analysis of a gas-liquid-liquid-solid four phase system is very much important to understand these issues. In Chapter 1, the literature reports on gas-liquid-liquid-solid systems and unique features of the individual reaction systems are addressed.

Metal nanoparticles are of immense interest to the catalysis researchers for last two decades. But majority of the reports are with colloidal metal nanoparticles, which suffers from agglomeration during high temperature - high pressure reaction conditions. Immobilization of metal nanoparticles immersed as a new strategy to over come this problem. In this chapter a detailed review on synthesis and stabilization of colloidal metal nanoparticles, strategies of immobilization of metal nanoparticles has been presented. Applications of metal nanoparticles in catalysis have also been addressed with an emphasis on hydrogenation reactions.

Chapter 2 presents the experimental study on reductive alkylation of aniline and acetone using 3% Pd/Al<sub>2</sub>O<sub>3</sub> catalyst as a model system. The first step of this reaction is a non-catalytic equilibrium one, whereas hydrogenation over the metal surface takes place after that. The kinetic experiments of the reaction were carried out in a slurry reactor. Due to unique combination of non-catalytic and catalytic reactions, the conventional approach for analysis of initial rates is misleading for the present system. For example, the initial rate of hydrogenation was observed to be constant with increase in catalyst loading, which usually means that the reaction is in mass transfer controlled regime. Therefore, a detailed analysis of initial rate based on quantitative criteria is presented to ensure that the experiments were carried out under kinetically controlled conditions. Several theoretical models considering non-catalytic as well as catalytic reaction steps have been presented to develop semi-batch slurry reactor models and the strategy to chose the appropriate model has been discussed. It was observed that a rate model considering competitive adsorption of hydrogen (in dissociative manner) and other reactants on the metal surface as the rate-limiting step for the catalytic reactions was found to represent the experimental data at different reaction conditions satisfactorily.

Further, the kinetic model was used to develop a trickle bed reactor model using the well known approach reported by Rajashekharam et al.<sup>5</sup> Trickle bed experiments were

carried out for different inlet concentrations of aniline and different flow rates at 393K. The observed results were compared with the model predictions for conversion of aniline, selectivity to products and temperature rise as a function of liquid flow rate at different aniline inlet concentrations. It was observed that the experimental and predicted results were agreeing reasonably well.

Chapter 3 presents the analysis of a gas-liquid-liquid-solid system using hydrogenation of aniline using 2% Ru/Al<sub>2</sub>O<sub>3</sub> catalyst as a model reaction. Aniline in cyclohexane constituted the organic phase and water was used as the second immiscible liquid phases. The system showed an unusual property of the liquid-liquid-solid system when the aqueous phase hold up was increased keeping the total liquid volume constant. It was observed that at low liquid hold up ( $\epsilon_w < 0.4$ ), the catalyst was in the aqueous phase and went to the organic phase above that. This phase inversion of catalyst is not reported in the literature for gas-liquid-liquid-solid reactions. It was further observed that, the catalytic activity (initial rate of hydrogenation) of the system increased with aqueous phase hold up, passed through maxima and then decreased. To model this observed trend, as a first step, a detailed kinetic modeling of a semibatch slurry reactor for hydrogenation of aniline in the gas-liquid-liquid-solid four phase system and evaluation of kinetic parameters have been presented. Using the rate equations based on the availability of the catalyst in a particular phase (aqueous or organic), two different models were developed. The mass transfer of hydrogen and hydrodynamic factors were accounted in these models. The observed trend of initial rate of hydrogenation as a function of aqueous phase hold up was compared with the predicted results of the models and observed that the theoretical model predicted the trend properly.

Chapter 4 presents a strategy of synthesizing immobilized Pt and Pd metal nanoparticles on the surface of Na-Y zeolite. Na-Y zeolite was synthesized following the reported literature procedure<sup>6</sup> and was grafted by 3-aminopropyltrimethoxysilane (APTS). The amine functionality in the APTS molecule was used to stabilize Pt and Pd metal nanoparticles ([Pt]-APTS-Y and [Pd]-APTS-Y). The synthesized materials were characterized using several techniques and the results are summarized here: (A) UV-visible spectra confirm the formation of Pt and Pd metal nanoparticles; (B) FTIR spectra and TGA (Thermo gravimetric analysis) data confirm that the Pt and Pd nanoparticles are bound to

the zeolite surface through the amine functionality of APTS molecule; (C) TGA data also indicates that the [Pt]-APTS-Y and [Pd]-APTS-Y nanocomposites are stable till 145°C; (D) Powder XRD data indicates that the zeolite structure remains unchanged during the surface grafting by APTS molecules and metal immobilization. The formation of face centered cubic Pt and Pd nanoparticles on the outer surface of Na-Y zeolite is also interpreted by the XRD (X-ray diffraction) data. These observations are supported by TEM (Transmission electron microscopy) measurements; (E) Different oxidation states of Pt and Pd present in the [Pt]-APTS-Y and [Pd]-APTS-Y nanocomposites are confirmed by XPS (X-ray photoemission spectroscopy) studies.

The [Pt]-APTS-Y and [Pd]-APTS-Y were tested as a catalyst for hydrogenation of several organic compounds and compared with commercially available catalysts. It was observed that the synthesized materials showed better activity compared to the conventional heterogeneous catalysts. The [Pt]-APTS-Y catalyst was recycled three times successfully for styrene hydrogenation at 353K. [Pd]-APTS-Y nanocomposite was also showed very good activity (TOF: 1881 h<sup>-1</sup>) and recyclability for Heck coupling reaction between iodobenzene and styrene. Due to solid zeolite matrix, the nanoparticles were easily separable from the reaction mixture and hence it was very easy to reuse the catalyst. The TEM analysis showed that the catalysts didn't agglomerated even after the recycle studies. XPS studies showed that Pt(IV) and Pd(II) species were present in minor quantities along with the Pt(0) and Pd(0) species in [Pt]-APTS-Y and [Pd]-APTS-Y nanocomposites respectively. The active species responsible for hydrogenation (studied on [Pt]-APTS-Y, Pt(0)) and Heck reactions (studied on [Pd]-APTS-Y, Pd(0)) were confirmed by XPS studies. The role of APTS as a grafting agent was studied separately and observed that without APTS the metal loading decreased from 3.6% to 0.3% for Pd.

## Reference

- <sup>1</sup>. (a) Mills, P. L.; Ramachandran, P. A.; Chaudhari R. V. Multiphase reaction engineering for fine chemicals and pharmaceuticals. *Rev. Chem. Eng.*, **1992**, 8, 1. (b) Ramachandran P. A.; Chaudhari R. V. Three phase catalytic reactors, Gordon Breach Science Publishers, New York, 1983. (c) Carpenter K. J. Chemical reaction engineering aspects of fine chemicals manufacture, *Chem. Eng. Sc.*, **2001**, 56, 305.
- (a) Rajashekharan, M. V.; Nikalje, D. D.; Jaganathan, R.; Chaudhari, R. V. Hydrogenation of 2,4-dinitrotoluene using a Pd/Al<sub>2</sub>O<sub>3</sub> catalyst in a slurry reactor: a molecular level approach to kinetic modeling and nonisothermal effects. *Ind. Eng. Chem. Res.*, **1997**, 36(3), 592. (b) Benaissa, M.; Le Roux, G. C.; Joulia, X.; Chaudhari, R. V.; Delmas, H. Kinetic modeling of the hydrogenation of 1,5,9-

- 
- cyclododecatriene on Pd/Al<sub>2</sub>O<sub>3</sub> catalyst including isomerization. *Ind. Eng. Chem. Res.*, **1996**, 35(7), 2091.
- (c) Lylykangas, M. S.; Rautanen, P. A.; Krause, A. O. I. Hydrogenation and Deactivation Kinetics in the Liquid-Phase Hydrogenation of Isooctenes on Pt/Al<sub>2</sub>O<sub>3</sub>. *Ind. Eng. Chem. Res.*, **2004**, 43(7), 1641.
- (d) Chaudhari, R. V.; Jaganathan, R.; Kolhe, D. S.; Emig, G.; Hofmann, H. Kinetic modeling of a complex consecutive reaction in a slurry reactor: hydrogenation of phenyl acetylene. *Chem. Eng. Sci.*, **1986**, 41(12), 3073.
3. (a) Lehtonen, J. Salmi, T., Vuori, A., Tirronen, E. On the principles of modeling of homogeneous-heterogeneous reactions in the production of fine chemicals. A case study: Reductive alkylation of aromatic amines. *Org. Process Res. Dev.*, **1998**, 2(2), 78. (b) Salmi, T., Lehtonen, J., Kaplin, J., Vuori, A., Tirronen, E., Haario, H. A homogeneous-heterogeneously catalyzed reaction system in a loop reactor. *Catal. Today*, **1999**, 48(1-4), 139.
4. (a) Drinkard W. C. Selective hydrogenation of aromatic compounds to cycloolefinic compounds, *GB patent 1381048 A* to Dupont de Nemours, **1972**. (b) Yamada, H., Urano, H.; Goto, S. Selective hydrogenation of unsaturated aldehydes in gas-liquid-liquid-solid four phases. *Chem. Eng. Sci.*, **1999**, 54, 5231. (c) Rode, C. V.; Vaidya, M. J.; Jaganathan, R.; Chaudhari, R. V. Hydrogenation of nitrobenzene to *p*-aminophenol in a four-phase reactor: reaction kinetics and mass transfer effects. *Chem. Eng. Sci.*, **2001**, 56, 1299.
5. Rajashekharam, M. V.; Jaganathan, R.; Chaudhari, R. V. A trickle-bed reactor model for hydrogenation of 2,4-dinitrotoluene: Experimental verification. *Chem. Eng. Sci.*, **1998**, 53 (4), 787.
6. Mukhopadhyay, K.; Mandale A. B.; Chaudhari, R. V. Encapsulated HRh(CO)(PPh<sub>3</sub>)<sub>3</sub> in microporous and mesoporous supports: Novel heterogeneous catalysts for hydroformylation. *Chem. Mater.*, **2003**, 15(9), 1766.

# **Chapter 1**

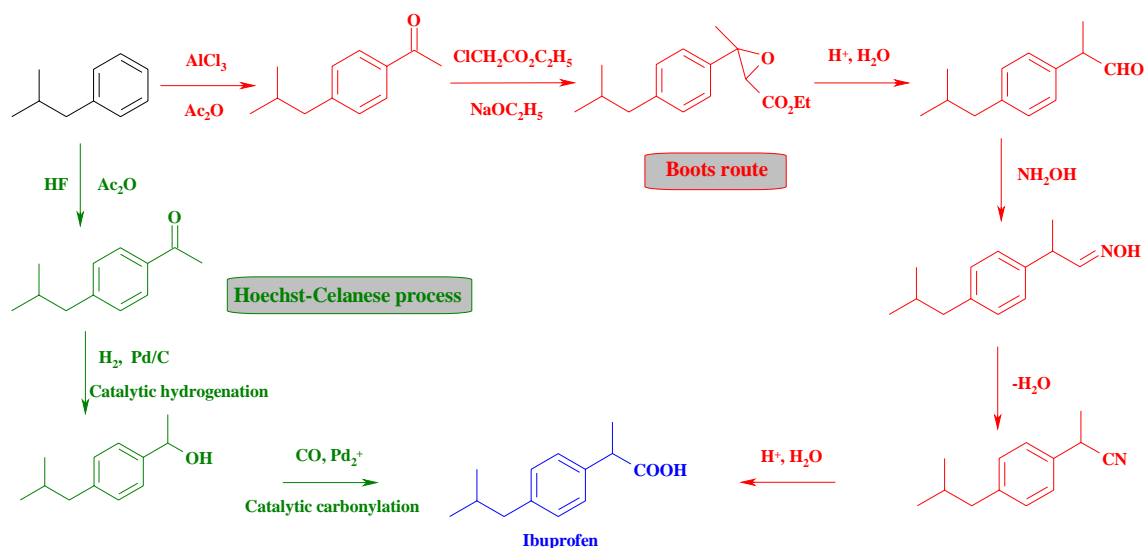
## **Introduction and Literature Survey**



## 1.1. GENERAL INTRODUCTION

Catalysis has played an important role in improving the quality of human life, though it is not obvious to the community. The applications of catalysis are wide ranging, some examples of which are the chemical or biochemical transformations ending up with products useful in petrochemicals, food, clothing, pollution control etc. While, the petrochemical and petroleum refining industries developed due to catalysis, a recent trend shows its expanding applications even in fine chemicals, pharmaceuticals and specialty products, which were commonly manufactured using stoichiometric organic synthesis. The stoichiometric synthetic routes often involve toxic and corrosive reagents, byproducts and waste products consisting of inorganic salts. Due to the high cost of the final products in these applications, these drawbacks and even lower yields were acceptable with a focus on product specifications and quality. However, with the increasing awareness of the environmental issues (pollution, difficulties in waste disposal and hazards) and competition in the global market, it is becoming imperative to look for alternative processes, which are clean, atom efficient and use hazardless and non-toxic raw materials. In this context, both homogeneous and heterogeneous catalysis has played a vital role. Similarly, with the advancement in the catalysis research and related processes, development of multiphase catalytic reactors has become equally important. Thus, we can realize the importance of integrated efforts of catalysis and reaction engineering in new generation processes, which will not only give better quality of life to us but will also be useful in achieving economical processes.

Several examples of catalytic applications in the fine chemicals and pharmaceutical processes are known. For example, the synthesis of ibuprofen by the conventional Boots route (by the name of the inventor of the drug) involves a six-step process wherein stoichiometric amounts of aluminium chloride, ethylchloroacetate etc. are used in different steps leading to formation of large amount of inorganic salts (13 kg/kg of product) as by products with only 50% overall yield of the desired product. In a subsequent development, a new Hoechst-Celanese process<sup>1</sup> involving only three catalytic steps (Scheme 1.1) has replaced the conventional route giving more than 95% regioselectivity to ibuprofen with no waste products. This catalytic process now meets 50% global requirement of this anti-inflammatory drug.



**Scheme 1.1.** Synthesis of Ibuprofen<sup>®</sup> by Boots route and Hoechst-Celanese process

Few other examples where catalysis replaced the conventional processes are: (a) auto-oxidation of *p*-di-isopropylbenzene to hydroquinone,<sup>2</sup> (b) hydroxylation of phenol to hydroquinone and catechol using zeolite based catalysts, (c) oxidative carbonylation of methanol to dimethyl carbonate,<sup>3</sup> (d) L-dopa synthesis by asymmetric hydrogenation,<sup>4</sup> (e) multistep synthesis of vanillin<sup>5</sup>. Depending upon the physical nature of the catalyst employed, these catalytic reactions can be categorized into two major classes, viz. homogeneous catalysis and heterogeneous catalysis. Homogeneous catalysis includes the class of reactions where soluble metal complexes are used. On the other hand, in heterogeneous catalysis, catalyst remains immiscible or as a separate phase to the reaction system. Though, homogeneous catalysis has unique advantages over the heterogeneous systems like high activity and selectivity even at milder reaction conditions, catalyst-product separation difficulties have limited their practical applications. Therefore, only 20% of the catalytic industrial processes use homogeneous catalysts, whereas the rest of the processes employ heterogeneous catalysts.

Among the various types of reactions, catalytic hydrogenation of various organic functionalities is most commonly encountered with wide ranging applications in fine chemicals and pharmaceuticals (Table 1.1). Depending on the nature of the reactants and products and their volatility, the reactions are either carried out in vapour phase or liquid phase mode. Due to the advantage of easy catalyst-product separation, heterogeneous

catalysts consisting of supported metal or composites of metal oxides are often used as catalyst precursors. Except the processes for low boiling commodity chemicals, most of the hydrogenation reactions are carried out in a liquid phase with either suspended solid catalysts or a fixed bed of catalyst. A detailed description of such multiphase reactions and their engineering analysis has been well developed as described in the well known textbooks and reviews.<sup>6</sup> Though extensive work on theoretical as well as experimental multiphase reactions is reported previously, in most of these single step reactions with isothermal conditions have been considered. Only in a few cases, experimental studies on multistep multiphase hydrogenation reactions have been addressed.<sup>7</sup> In order to develop economically competitive processes, several new types of catalytic systems have been found to be advantageous. For example, four-phase reactions in which catalytic hydrogenations are carried out in the presence of two immiscible liquid phases and a solid catalyst has not been well studied. Similarly, several reactions involving combinations of non-catalytic and catalytic reactions, complexities of equilibrium reactions, reactions with complex network where selective synthesis of an intermediate compound is important, or catalytic reactions in non-ideal reaction media (such as CO<sub>2</sub>, H<sub>2</sub>O, ionic liquids) have not also been addressed with detailed experimental studies. It is the objective of this thesis to understand in detail the catalysis and reaction engineering aspects of a few important hydrogenation reactions, which have some unique features. The following catalytic systems were chosen for the present work:

❖ **Reductive alkylation of amines:** N-alkyl anilines are important products for the dyes, fuels and rubber industries and synthesized by the reductive alkylation of an aromatic amine and a carbonyl compound in the presence of a supported transition metal catalyst. The first step in the synthesis is a non-catalytic homogeneous reaction, followed by hydrogenation in the second step to the desired N-alkylated product. But, after formation of N-alkyl aniline, hydrogenation of the aromatic ring can occur and the reaction ends with N-alkyl cyclohexylamine, which is of lesser importance than the former. Therefore, proper analysis of the reaction engineering issues like mass and heat transfer parameters coupled with reaction kinetics is required to understand and select suitable reaction conditions to obtain improved selectivity of the intermediate product, N-alkyl aniline. It is an example of a complex multistep catalytic reaction in the presence of non-catalytic equilibrium steps.

**Table 1.1.** Commercial applications of hydrogenation reactions using heterogeneous catalysts

No.	Process	Catalyst	Product	Application	Ref.
1	Selective hydrogenation of sorbic acid, hexyn-1-ol or hexadienols	Supported Pd colloids	Hexane-1-ols	Fruit, vegetable fragrances and flavors	8
2	Hydrogenation of methyl sorbate	Pd/C	Methyl-2-hexenoate	Flavors	9
3	Partial hydrogenation of cis-propenyl pyrethroids	Lindlar catalyst	Pyrethrins	Insecticides	10
4	Selective hydrogenation of dehydrolinalool	Pd-Bi catalyst	Citral, linalool	Perfumes and cosmetics	11
5	Production of 1,4-butanediol and THF	Fe promoted Raney-Ni, co-promoted with Cr, Mo, W, Co, Mn and Ti	1,4-butanediol and THF	Intermediate for polymers and solvent	12
6	Enantioselective carbonyl group hydrogenation of $\alpha$ -ketoester	Chinchona-modified Pt/Al <sub>2</sub> O <sub>3</sub>	Chiral $\alpha$ -hydroxyester	Intermediate for Benazepril <sup>®</sup> , a medicine for high blood pressure	13
7	Reductive amination of methanol	SiO <sub>2</sub> -Al <sub>2</sub> O <sub>3</sub> in the 1st step and mordenite in the 2 <sup>nd</sup> step	Dimethyl-amine	Intermediate for pharmaceuticals, herbicides, rocket fuels. Dehairing agent in leather processing.	14
8	Hydrogenation of aromatic nitro compounds	Vandium doped precious metal powder	Aromatic amines	Intermediates for agrochemicals, dyes and fluorescent whitening agent	15
9	Hydrogenation of halonitro aromatics	Ir-Fe/C	Halo amino aromatics	Cosmetics	16
10	Partial hydrogenation of benzene	Supported Ru catalyst	Cyclohexene	Intermediates for polyamides and lysines	17
11	Dearomatization of aniline	5% containing Deloxan <sup>®</sup> catalyst	Pd Cyclohexyl-amine	Intermediates for rubber, food and pharmaceuticals	18
12	N-debenzylation to form Nebivolol <sup>®</sup>	Pd/C	Nebivolol <sup>®</sup>	Anti-depression drug	19

❖ **Hydrogenation in four phase reaction system:** Four phase reactions (gas-liquid-liquid-solid) are advantageous in many cases compared to the corresponding three phase catalytic reactions. But the issues like phase behavior, mass transfer of the reactants and product molecules, swelling and shrinking of particular phase during the course of a reaction and its effect on overall reactor performance and phase behavior are not well studied. Therefore, the reaction kinetics and importance of mass transfer parameters for hydrogenation of aniline in a gas-liquid-liquid-solid four phase system was investigated.

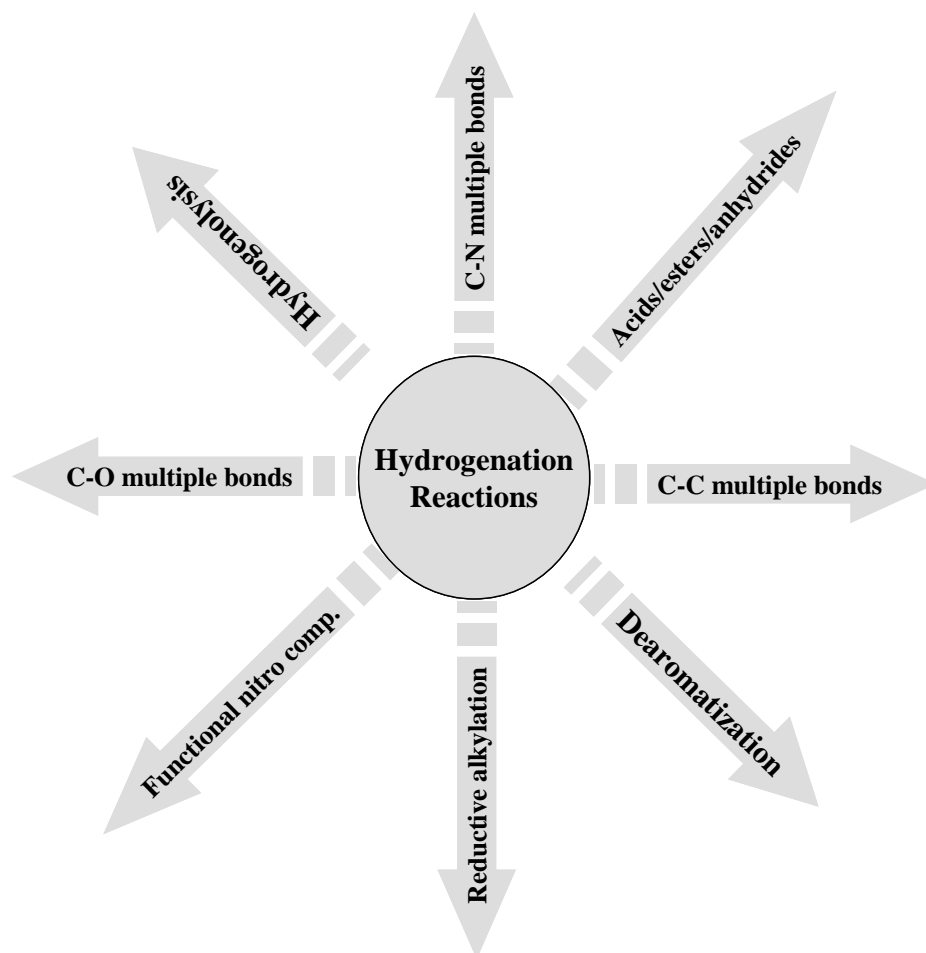
❖ **Catalysis by supported nano-materials:** Among the various new concepts, catalysis by metal nanoparticles received immense interest to the researchers because of their potential in achieving higher catalytic activity. At the same time, agglomeration at higher reaction temperatures, efficient separation and reuse of metal nanoparticles from the reaction systems are considered as the major challenges for their applications. A need for developing new synthetic approaches for supported nano-metals to overcome these drawbacks is most essential. It was also the aim of this work to synthesize supported nano Pd and Pt catalysts by anchoring to mesoporous supports like NaY. Further the catalytic activity and selectivity of these catalysts was also investigated. The objective was also to understand how significant is the influence of nanosize materials on the performance of catalysts.

In this chapter, a literature review on catalysis and reaction engineering aspects of hydrogenation reactions with a special emphasis on reductive alkylation of aromatic amines, dearomatization of aromatic compounds and applications of gas-liquid-liquid-solid four phase systems are presented. Application of nanomaterials as catalysts in multiphase reactions has also been reviewed. Finally, the multiphase catalytic reactors in hydrogenation reactions and the current trend in their analysis have also been reviewed.

## **1.2. MULTIPHASE HYDROGENATION REACTIONS**

One of the important classes of catalytic reactions, which made significant impact in replacing stoichiometric synthetic routes by catalytic one, is the hydrogenation of organic compounds with a variety of functional groups. Some important features of catalytic hydrogenation reactions in general and specific literature on reductive alkylation and dearomatization reactions have been presented in this part. Catalytic hydrogenation of

organic functional groups is one of the most common applications of heterogeneous catalysis in the synthesis of organic compounds. The usefulness of these reactions has been well covered by several books and reviews.<sup>20</sup> Liquid phase hydrogenation reactions using heterogeneous catalysts can be broadly classified into a few classes as shown in Figure 1.1. Among these, reductive alkylation and dearomatization reactions are discussed in detail and other classes of reactions are presented in Table 1.3.



**Figure 1.1.** Classification of catalytic hydrogenation reactions

### 1.2.1. Catalysts for hydrogenation reactions

The most frequently used heterogeneous catalysts and the typical crystal structures of the bulk metals used for hydrogenation reactions are shown in Table 1.2. The choice of

the metal depends on several factors but the most commonly used metals as catalysts are indicated with darker bands.

**Table 1.2.** Catalytically active metals for hydrogenation reactions

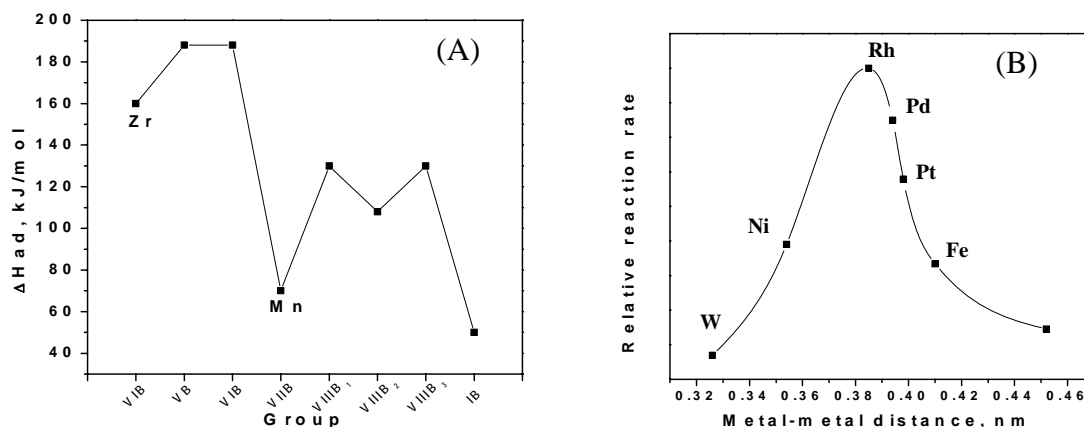
VIIA	VIII		IB
		Co <i>fcc</i>	Ni <i>fcc</i>
	Ru <i>hcp</i>	Rh <i>fcc</i>	Pd <i>fcc</i>
Re <i>hcp</i>	Os <i>hcp</i>	Ir <i>fcc</i>	Pt <i>fcc</i>
			Au <i>fcc</i>

*fcc*: face centered cubic, *hcp*: hexagonal close packed

■ > ■ > ■

For hydrogenation reactions, generally catalytic activity is considered to be a function of both *electronic factors* and *geometric factors* associated with the active sites.<sup>21</sup> The chemisorption of gases on a metallic surface requires vacancies within *d*-band capable of accepting electrons donated by the adsorbate. When the number of *d*-vacancies is large, for example Gr. III-A and VII-A metals, the substrate may be strongly adsorbed irreversibly. In such cases, catalytic activity is heavily suppressed. Similarly, for metals of Gr. I-B, with no such vacancies in *d*-band, substrates may adsorb weakly and, as catalytic reaction rates are directly related to the surface coverage, overall activity is also correspondingly decreased. Maximum activity is expected for those metals with the smallest number of *d*-vacancies and this corresponds to the metals of Gr. VIII. This is termed as ‘*electronic factor*’ in catalytic activity. This is clear from the chemisorption enthalpies of transition metals as shown in Figure 1.2(A).

The metal atoms of the surface exposed to the adsorbing medium should be spaced such that the transition state complex formed has the lowest possible potential energy. It follows, therefore, that reaction activation energies will be reduced and progress under considerable milder reaction conditions than required for the equivalent non-catalyzed process. This constitutes the ‘*geometric factor*’. For example, Figure 1.2(B) shows the rate of ethylene hydrogenation as a function of metal-metal distance. Therefore, both the factors happen to be optimum for the Gr. VIII metals. In the following sections we will see that most of the catalytic hydrogenation reactions are conducted using these metals only.



**Figure 1.2.** (A) Mean chemisorption enthalpies of hydrogen as a function of the transition metals in the periodic table, (B) ethylene hydrogenation rate as a function of metal-metal distance in (100) planes

## 1.2.2. Issues in Heterogeneous Catalytic Hydrogenation Reactions

In catalytic hydrogenation reactions on heterogeneous metal surfaces, the effectiveness of the system may be considered from two perspectives, viz. *catalysis* and *chemical reaction engineering*. Before going to the specific examples of hydrogenation reactions, these issues are highlighted briefly in this section.

### 1.2.2.1. Catalysis Issues:

*Support:* The catalytic activity of heterogeneous catalysts is due to the metal atoms present at the surface of the bulk metals. Therefore, to get a better activity or maximizing the active surface, dispersion of metal particles on a high surface area solid support such as alumina ( $\text{Al}_2\text{O}_3$ ), activated carbon, titania ( $\text{TiO}_2$ ), silica ( $\text{SiO}_2$ ), magnesia ( $\text{MgO}$ ) etc. are commonly practiced. These support materials also keep the individual small metal particles apart from each other and prevent agglomeration or sintering of metal particles to larger and less efficient entities. There are a number of physical characteristics of the support such as hardness, density, pore volume, pore size, pore distribution, particles size, particles shape etc. which have to be considered to achieve the required performance of a supported metal catalyst.<sup>22,23</sup>



*Metal-support interactions:* Sometimes the support materials influence the activity of metal catalysts by changing its electronic environment or geometry (number of active sites) of the catalyst particles. This is termed as metal-support interaction. Metal-support interaction indicates the strength of binding between the metal and the support particles and prevents sintering of metal particles. Among the commonly used supports, alumina, carbon or silica are known to exhibit weak metal-support interaction whereas titania showed a strong metal-support interaction with hydrogenation catalysts.<sup>24</sup>

*Hydrogen spillover:* In some supported metal catalysts, adsorbed hydrogen atoms migrate from the metal surface to the interstitial volume of the support material. This phenomenon is termed as *hydrogen spillover*. An interesting illustration on hydrogen spillover over macroscopic distances was demonstrated in isomerization of 1-butene.<sup>25</sup> When a noble metal (Pd on graphitic carbon) and bimetallic catalysts (base metal and a lanthanide metal on graphitic carbon) were used in a dual bed reactor, 2.7 times greater activity was observed compared to that of the noble metal alone. The activity increase was attributed to hydrogen spillover i.e., molecular hydrogen adsorbed and dissociated on the noble metal catalyst was transported via surface diffusion to the bimetallic catalyst surface and activated those sites for the reaction.

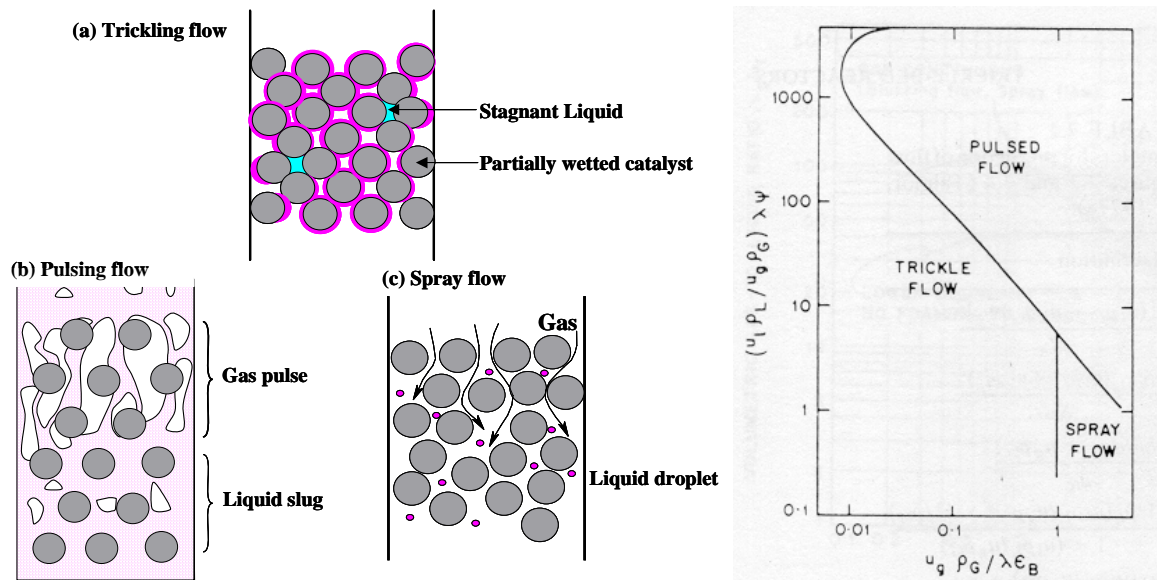
#### **1.2.2.2. Reaction Engineering Aspects:**

*Interphase Mass transfer:* For a gas-liquid-solid (three phase) catalytic hydrogenation reactions, a number of mass transfer steps have to occur before the gas phase (A) and liquid phase (B) reactants are converted to products. These steps are: (a) transport of A from bulk gas phase to gas-liquid interface, (b) transport of A from gas-liquid interphase to bulk liquid, (c) transport of A and B from bulk liquid to the catalyst surface, (d) intraparticle diffusion of A and B through the pores of catalyst, (e) adsorption of A and B on the active catalyst sites, (f) chemical reaction between A and B and (g) product desorption from the active catalyst sites. The approaches for analysis of mass transfer effects in gas-liquid-solid catalytic reactions are described in detail by Ramachandran and Chaudhari.<sup>6b</sup>

*Non-isothermal effect:* Many gas-liquid-solid catalyzed reactions are highly exothermic in nature and this influences several parameters like rate of reaction, vapour pressure, solubility, mass transfer coefficients, diffusivity etc. Therefore, one should

consider the non-isothermal effects on the overall rate of reaction and reactor performance for an exothermic reaction. Few important studies on this topic are, (a) hydrogenation of *m*-nitrochlorobenzene to *m*-chloroaniline using sulphided Pt/C catalyst,<sup>26</sup> (b) hydrogenation of 2,4-dinitrotoluene using Pd/Al<sub>2</sub>O<sub>3</sub>,<sup>27</sup> (c) hydrogenation of *p*-nitrocumene to *p*-cumidine over supported palladium catalyst<sup>28</sup> etc. In these reports a detailed analysis of a non-isothermal batch reactor has been discussed along with experimental verification of reactor models.

*Flow regimes in trickle bed reactor:* The flow pattern in a trickle bed reactor had been studied by several authors and reviewed by Gianetto et al.<sup>29</sup> The gas-liquid two phase concurrent down flow for nonfoaming system may be classified in four regimes: (i) trickling flow (at low gas and liquid velocity), (ii) pulsing flow (relatively higher gas and liquid velocities), (iii) spray flow (high gas velocities and low liquid velocities) and (iv) bubble flow (high liquid velocities and low gas velocities). The flow regimes are represented in Figure 1.3. Normal laboratory and commercial reactors are operated in trickle or pulse flow regime.



**Figure 1.3.** The flow regimes in a trickle bed reactor<sup>30</sup> (G and L are superficial mass flow rates for gas and liquid respectively)

**Table 1.3.** Gas-liquid-solid catalytic hydrogenation reactions: A Literature Review

Reaction class	Catalyst	Reactor	Remarks	Ref.
<b><i>Hydrogenation of C-C bonds</i></b>				
Alkene or alkyne to alkane	Rany-Ni; Ni on oxides; Pd/C		Operates at milder conditions (room temp and atmospheric pressure). Pd is mostly used among Gr.VIII metals for selective and non-selective alkene hydrogenation. Activated carbon or low-acid Al <sub>2</sub> O <sub>3</sub> is the most common support material. Acidic support may accelerate polymerization. Stirred reactors with efficient cooling are oftenly used for fine chemicals and specialties. Recirculated reactor with exterior cooling is useful. Trickle bed reactors are also used. Liquid flow removes oligomers from catalyst surface.	31
	Cinchona modified Pd; Pd/C	Slurry reactor Slurry reactor	Enantioselective alkene hydrogenation of $\alpha,\beta$ -unsaturated acids and ketones. Reactions performed in gas-liquid-liquid-solid system with alkali promoters.	32
Alkyne to alkene	Pd-Pb/CaCO <sub>3</sub>		>95% <i>cis</i> -olifins under mild conditions. Reaction stops after uptake of one mole of hydrogen	33
	Pd/CaCO <sub>3</sub> -NH <sub>3</sub> ; Pt/CaCO <sub>3</sub> -NH <sub>3</sub>	Slurry reactor Slurry reactor	Kinetic modeling for 2-butyne-1,4-diol to <i>cis</i> -2-butene-1,4-diol using Pd/CaCO <sub>3</sub> -NH <sub>3</sub> and Pt/CaCO <sub>3</sub> -NH <sub>3</sub> catalyst system was studied.	
<b><i>Hydrogenation of acids, esters and anhydrides</i></b>				
Acids, esters and anhydrides to alcohols	CuCrO doped with barium		Alcohol is the major product, but metal leaches out into the solution	34
	Rany-Cu doped with Fe or Mn		Environmentally benign alternative of Cu Chromite catalyst; operates at relatively milder conditions	
Anhydrides to alcohols	Re-Pd;	Fixed bed	Re insert between C- of carbonyl gr. and O- of anhydride ring to form	35
	Re-Rany-Ni;	Fixed bed	oxometallacycle, which acts as a promoter.	
	Ru-Re	Slurry reactor	Kinetic modeling in batch slurry reactor using bimetallic Ru-Re catalyst and bubble column slurry reactor modeling with a mixing cell model is reported.	
Acids, esters to aldehydes	ZrO <sub>2</sub> ; Cr <sub>2</sub> O <sub>3</sub>	Fixed bed Fixed bed	Carboxylic acids to aldehyde selectively. ZrO <sub>2</sub> showed better activity for aromatic acids while Cr <sub>2</sub> O <sub>3</sub> is good for aliphatic acids.	36

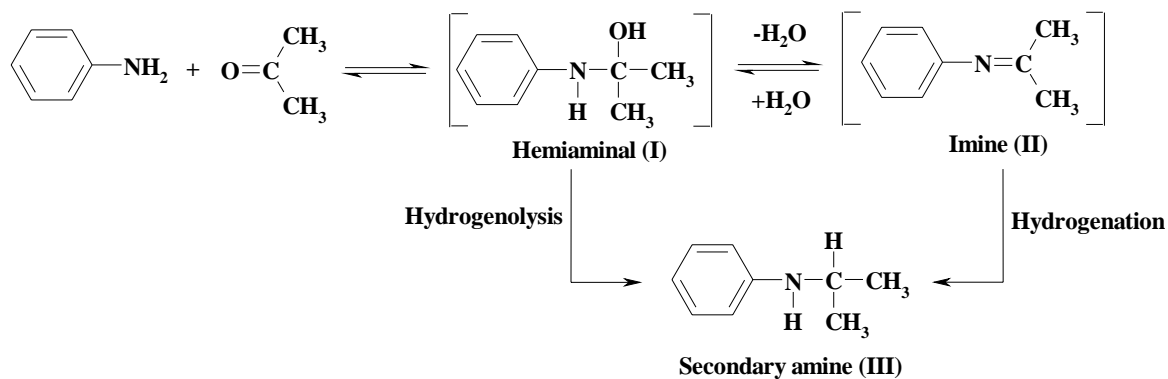
Reaction class	Catalyst	Reactor	Remarks	Ref.
<b>Hydrogenation of C-N bonds</b>				
Nitrile hydrogenation	Rany-Co; Rany-Ni	Slurry reactor	Rany-Co and Rany-Ni are considered as the best catalysts for Nitrile to 1° amine. Rany-Co or –Ni activity depends upon the type and amount of base additives. For butyronitrile hydrogenation, Ru/C, Rh/C and Pt/C produced 1°, 2° and 3° amines respectively.	37
	Ru, Rh, Pt on activated C			
Dinitriles (adiponitrile) hydrogenation	Rany-Co or –Ni with	Fixed bed	Raney catalyst used as tablets, extrudates and hollow spheres for adiponitrile to hexamethylene diamine. Hollow sphere catalyst showed the best activity due to high porosity.	38
	Rany-Ni	Bubble column	Langmuir-Hinshelwood model developed considering competitive adsorption between hydrogen and nitriles on the catalyst surface and reaction as the rate limiting step Based on hydrodynamic and intrinsic kinetics data, a bubble column slurry reactor model proposed	
<b>Hydrogenolysis</b>				
	Pd/C	Slurry reactor	Pd/C is the most common catalyst. Operates at ambient temperature and pressure conditions. Often with acids or bases as promoters	39
<b>Hydrogenation of C-O bonds</b>				
Aliphatic carbonyls	Pt;		Readily hydrogenated to alcohols under milder condition. Pt works in acidic media.	40
	Rh or Ru		Rh or Ru works in neutral or basic conditions.	
$\alpha,\beta$ -unsaturated carbonyls	Pt/C	Slurry reactor	Reactions performed in gas-liquid-liquid-solid system with alkali promoters.	41
	Pt or Ni with metal chlorides (eg. FeCl <sub>3</sub> , GeCl <sub>4</sub> )	Slurry reactor	Fe increases electron density on Pt leading to an electron deficient Fe species that coordinates to carbonyl gr. and the electron rich Pt species becomes less likely to accept $\pi$ -electron form C=C gr.	42
Aromatic carbonyls	Pd; Raney-Ni	Slurry reactor Slurry & fixed bed reactor	Aromatic moiety activates carbonyl gr., therefore, hydrogenation occurs at relatively milder conditions. Pd is the most preferred metal in neutral non-polar solvents. Slurry and TBR model developed for benzaldehyde to benzyl alcohol. For acetophenone to 1-phenylehanol, selectivity and dielectric constant of the solvent was correlated for Raney-Ni catalyst.	43

Reaction class	Catalyst	Reactor	Remarks	Ref.
Enantio-selective hydrogenation of $\alpha$ -ketoesters	Cinchona modified Pt	Slurry reactor	A Langmuir-Hinshelwood model developed. A modified active site is formed by adsorption of one cinchona molecule. A protonated adsorbed modifier interacts with the $\alpha$ -ketoester and forms a stabilized half hydrogenated intermediate. The rate-determining step for the preferred enantiomer is the addition of the second hydrogen. The rate acceleration and the enantio-discrimination are due to the preferential stabilization of one of the two-diastereomeric intermediates. Catalyst characterization, mass transfer calculations and kinetic experiments integrated to quantify the contribution of mass transfer parameters. It concluded that lower ee in few cases were due to liquid-solid mass transfer resistance.	44
<b>Hydrogenation of <math>-NO_2</math> group</b>				
Aliphatic and aromatic nitro compounds	Pt; Pd; Ni	Slurry reactor	Hydrogenation to amine follows the Haber's mechanism. Hydroxylamine intermediate may accumulate, which is toxic. Vanadium used as a promoter for faster reaction and purer amine compound. Vanadium works as a 'catalytic by-pass'.	45
Chemo-selective hydrogenation	Pt- $H_3PO_2$ -V;	Slurry reactor	Applied firstly for halonitrobenzene and then applied successfully for other functionalized nitro aromatics, even for selective hydrogenation of acetylnic nitroaromatics.	46
	Pt-Pb- $CaCO_3$ (Pt-Lindlar catalyst)	Slurry reactor	Pt-Pb is suitable except acetylnic nitroaromatics. Pt-Pb catalyst gives the best results in aprotic polar solvents with $FeCl_2$ and $Bu_4NCl$ . Pt- $H_3PO_2$ -V works best in toluene-water using $VO(acac)_2$ as a promoter. Fe or V promoters suppress accumulation of hydroxylamines.	
Di-nitrobenzene to nitro aniline	Pt; Rh; CuCrO		Pt or Rh is better catalyst than Pd.	47
	Raney-Cu		Selectivity increases with decreasing metal loading. Highest selectivity for 2-amino-6-nitrotoluene is achieved at 313K and 0.1% Pt/ $Al_2O_3$ . Regioselective hydrogenation of unsymmetrical alkyl dinitrobenzene (2,4-DNT) to alkyl amino nitrobenzene (2-nitro-4-amino toluene) is related to the steric factor of alkyl group (selectivity: 68% for unsubstituted; 70% for methyl; 93% for tert-butyl).	
	Pd/charcoal	Slurry reactor	2,4-DNT hydrogenation carried out in isopropanol-water mixture. <i>p</i> -amino isomer was predominant at mass transfer limited conditions.	

### 1.2.3. Reductive Alkylation of Amines

#### 1.2.3.1 Reaction Pathway and Product distribution:

Reductive alkylation is a class of reaction, which involves the condensation of an amine or ammonia and a carbonyl compound followed by reduction of the intermediate imine derivative to the desired amine. This reaction can also be termed as reductive amination when it is looked from the perspective of the carbonyl compound. Mechanism of this reaction is well documented in the textbooks though only limited information is available on catalytic reaction mechanism on a molecular scale. The reaction occurs in three steps as shown in Scheme 1.2 in which aniline and acetone are considered as the representative reaction of amine and carbonyl compound respectively. The condensation of amine and a carbonyl compound produces hemiaminal (I, also called carbinolamine), which may undergo dehydration reaction to form the imine intermediate (II, commonly termed as Schiff's base) or may undergo hydrogenolysis to produce the secondary amine (III). The imine compound may hydrogenate catalytically to III.

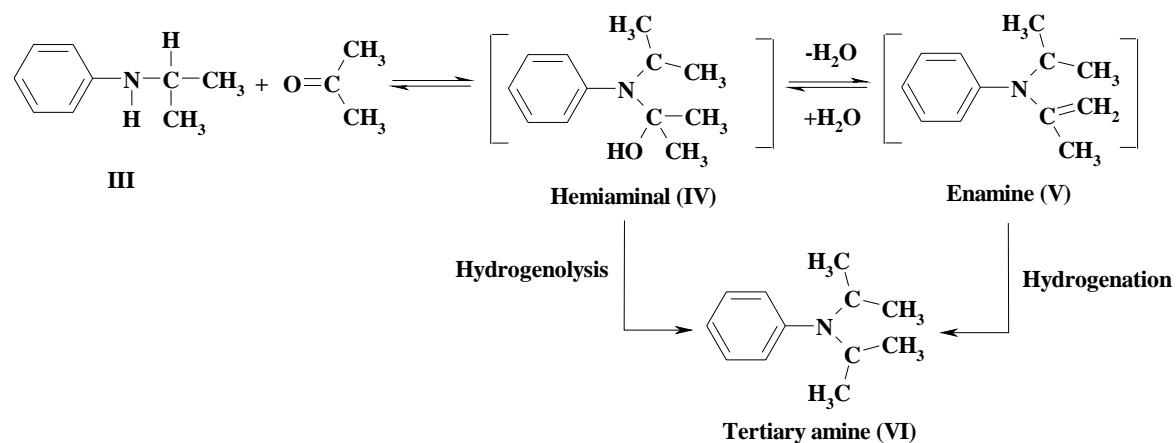


**Scheme 1.2.** Mechanism of N-monoalkylation of aniline

The equilibrium-controlled formation of the Schiff's base [SB] is believed to be the slowest step in the consecutive reaction sequence. Acids and bases are reported to promote the formation of Schiff's base (II).<sup>48</sup> Continuous removal of water from the reaction mixture by azeotropic distillation<sup>49</sup> or using molecular sieves<sup>50</sup> can shift the equilibrium towards the right side and enhance the overall rate of reductive alkylation.

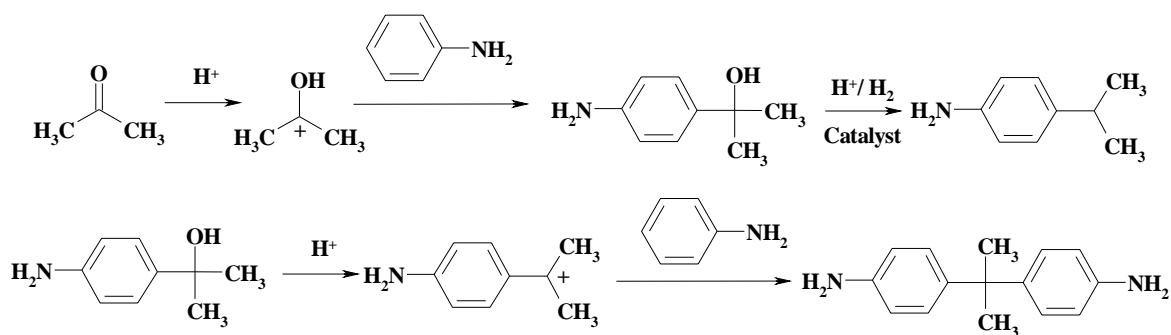
The secondary amine (III) may further condense with another molecule of a carbonyl compound to form hemiaminal (IV) that cannot dehydrate to an imine but Enamine (V) (Scheme 1.3). Hydrogenolysis of IV or hydrogenation of V gives N-

dialkylamine (VI). In reality, due to the lower reactivity and bulkier size of ketones, the reaction stops at monoalkylamine.<sup>51</sup> N-dialkylation requires severe conditions and very selective catalysts.<sup>52</sup> On the other hand, alkylation continues for the aldehyde substrates to the N-dialkylated products. Due to the stepwise reaction mechanism, monoalkylated product can be formed with aldehyde by optimizing the reaction conditions.<sup>53</sup>



**Scheme 1.3.** Reaction pathway of N-dialkylation of aniline

Alkylation of aromatic moiety is one more possibility in this reaction. This may be a probable side product in reductive N-alkylation reaction when acids are used as promoters for formation of II and V, because C-alkylation is reported to be catalyzed by acids and accelerated by *o*-, *p*- directing groups like  $-\text{NH}_2$  or  $-\text{OH}$  in the aromatic moiety.<sup>54</sup> The reaction is a typical aromatic electrophilic substitution by the carbonium ion as shown in Scheme 1.4.



**Scheme 1.4.** Ring alkylation of aromatic amines by carbonyl compounds

Hydrogenation of the carbonyl functionality to the corresponding alcohol and aromatic ring hydrogenation are also important side products in this class of reaction. Alcohol formation may be a crucial problem in a commercial process, because it utilizes the carbonyl compound and hydrogen, and leads to a separation problem. Archar et al.<sup>55</sup> allowed the carbonyl compound to stand together overnight with the amine compound before hydrogenation in presence of Adams platinum oxide, so that the imines could be available on the catalyst surface on an appreciable concentration to hydrogenate and that could suppress the carbonyl hydrogenation. Emerson<sup>56</sup> isolated the imine from the reaction mixture before hydrogenation reaction to eliminate the formation of alcohol. The complex product distributions in reductive alkylation due to ring hydrogenation of aniline analogues have been reviewed by Stieber et al. and Greenfield.<sup>57</sup> Stieber et al. suggested the use of highly pure starting materials and selective catalysts under controlled reaction conditions to reduce the impurities in the reaction mixture. According to Greenfield, reactions at lower temperature, high pressure and high catalyst loading can be a solution for minimizing side products.

Aromatic N-alkylated products have wide variety of applications in dyestuff industries as intermediates, in petroleum and rubber industries as anti-oxidant and anti-ozonant, in agrochemical industries as intermediates.

#### ***1.2.3.2. Substrates:***

Reductive alkylation has been investigated previously using a wide range of alkylating agents and catalysts. Any type of amine precursors like nitro, nitroso or nitrile compounds, are suitable for this reaction, which hydrogenate in-situ to generate the amine.<sup>58</sup> Secondary amines like amides are also reported for reductive alkylation with aldehydes and ketones in good yield (>80%) without any O- or C- alkylated products.<sup>59</sup> Due to the lower cost and less toxicity compared to amines, nitro compounds are often used as the starting compounds in industrial processes.

Alcohols were used in some cases as the alkylating agents,<sup>60</sup> which first dehydrogenated to the corresponding carbonyl compounds and then initiated the condensation reaction with the amine functionality.<sup>61</sup> Due to the severe conditions required for *in-situ* generation of the carbonyl compounds, the reactions are conducted in a gas phase and selectivity to unsymmetric amines may decrease. A review on aniline alkylation



with alcohols in the vapor phase over solid acid catalysts such as oxides, clays and zeolites is made by Narayanan and Deshpande<sup>62</sup> and the mechanism of this reaction on different solid surfaces at different conditions are proposed.

### 1.2.3.3. Catalysts:

The choice of a catalyst and reaction conditions are two strong factors in the performance of reductive alkylation reactions. In the early literature, Raney-Ni was reported as the preferred catalyst at elevated temperature and pressure, and seems to be a good choice for synthesis of primary amines. Supported Ni, Cu, Co, copper chromite (2CuO.Cr<sub>2</sub>O<sub>3</sub>) was also suggested. Among the transition metals, palladium is the most preferred catalyst because,

- ❖ Pd is the most active metal for the saturation of double bonds in conjugation with aromatic ring,
- ❖ Pd is least active metal for hydrogenation of aromatic ring at lower temperatures (<423K)
- ❖ Pd has lower activity for hydrogenation of aliphatic aldehydes and ketones.

As an example, the performances of different transition metal catalysts for reductive alkylation of aniline with acetone at identical conditions are presented in Table 1.4.<sup>57b</sup>

**Table 1.4.** Comparison of transition metals for reductive alkylation of aniline and acetone

Catalyst	Temp. (K)	Time (h)	Conv. (%) Aniline	Sel. (%) N-IPA	Sel. (%) N-IPC	Low boiling amines	IPA <sup>a</sup> (%)
5% Pd/C	378	1	100	67	14	6	0
5% Pt/C	378	1	60	47	<2	>1	33
5% Rh/C	378	10	100	0	81	21	>90
5% Ru/C	378	1.8	100	0	74	23	100
5% Pd/C	378	4.7	>99	50	20	13	0
5% Pd/C	418	1	>98	40	39	18	0

Reaction conditions: aniline, 1 mol; acetone, 15 mole; catalyst, 6 g (all are procured from Engelhard Industries); P<sub>H<sub>2</sub></sub>, 400-600 psig; reaction taken in 1 gallon stirred autoclave.

a: IPA formed w.r.t. excess acetone used.

N-IPA: N-isopropylaniline; N-IPC: N-isopropylcyclohexylamine; IPA: isopropylalcohol.

It is clear from Table 1.4 that Pd is far superior to the other catalysts for reductive alkylation of aniline and acetone. Pt showed less tendency for ring hydrogenation, but it suffers from lower conversion, which may be due to severe catalyst poisoning by amines. But, interestingly, the activity and selectivity of Pt catalyst was reported to increase over Pd

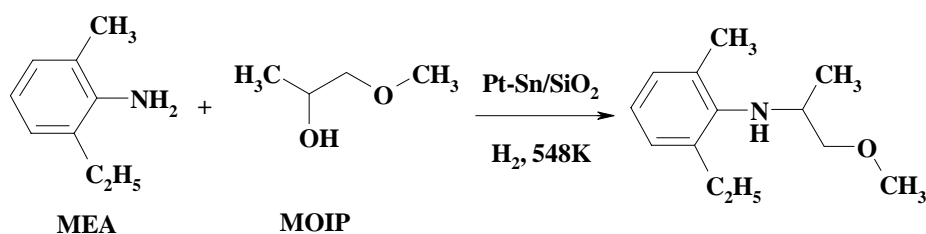
for higher molecular weight of ketones and amines as substrates as shown in Table 1.5. Therefore, the nature of amine and ketone are also important in selecting a suitable catalyst for this class of reaction. A detailed literature report on reductive alkylation with specific examples of amines (or precursors), carbonyls (or alkylating agents), catalysts and reactors are reported in Table 1.6.

**Table 1.5.** Comparison of Pt and Pd metals for reductive alkylation of PAPD and MIBK

Catalyst	Temp (K)	Time (h)	Conversion (%)	Yield (%) based on conv.
5% Pd/C	393	12.5	76	78
5% Pt/C	373	10	92	93

Reaction conditions: PAPD, 0.40 mole; MIBK, 1.6 mol; catalyst, 3 g (procured from Engelhard Industries);  $P_{H_2}$ , 150-300 psig; reaction done in 600 ml Magne Drive autoclave.  
 PAPD: *p*-amino diphenylamine; MIBK: methyl isobutyl ketone.

Rusek reported the N-monoalkylation of sterically hindered amines with secondary alcohols with Pt/SiO<sub>2</sub> catalyst in presence of metallic promoters like Sn, Ge, Re etc. and found that Pt-Sn/SiO<sub>2</sub> pretreated with Ca<sup>2+</sup> gave the best result (Scheme 1.5 and Table 1.6). The author proposed that the alcohol dehydrogenates to the corresponding ketone, which reacts with the amine to form imine intermediate. In contrast to copper chromite catalyst, which is the active catalyst for primary alcohols only, this Pt based catalyst was active for secondary alcohols too.



**Scheme 1.5.** N-alkylation of sterically hindered amines with alcohols

The influence of acidity or basicity of faujasites and effect of temperature are discussed for gas phase alkylation of aniline with methanol. As proposed by Su et al.,<sup>64</sup> the reaction starts with the formation of methyl carbocation (CH<sub>3</sub><sup>+</sup>).

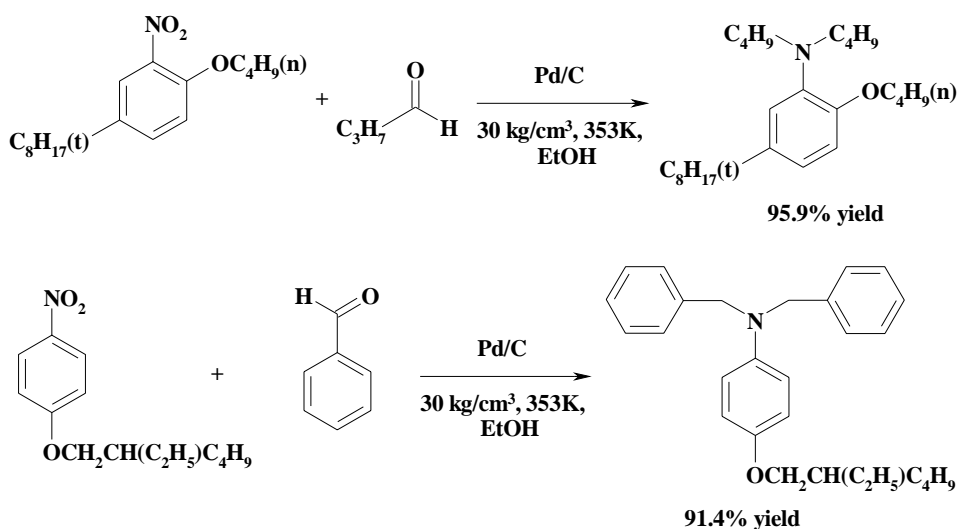
**Table 1.6.** Literature survey on reductive alkylation of aromatic amines and carbonyl compounds (and their precursors)

No.	Substrates	Catalyst	Reaction conditions	Reactor	Conversion, Selectivity (%)	Ref.
1	2-Methyl-6-ethylaniline (MEA) and methoxy-2-propanol (MOIP)	Pt-Sn/SiO <sub>2</sub> pretreated with Ca <sup>2+</sup>	Feed: MEA: MIOP=0.5 (3ml/h); P <sub>H2</sub> : 1 atm; H <sub>2</sub> : 4.7 ml/min.; 548K	Microreactor quartz tube	Conversion (MEA): 36.4; selectivity (N-alkylated product): 76.2.	Rusek, M. <sup>63</sup>
2	Aniline and methanol	LiY and NaY non-protic and non-basic zeolites	Aniline: MeOH, 3:1; 623-723K	Fixed bed	Conv. (aniline): 100; Sel. (N-methyl aniline, N, N-dimethyl aniline and toluidine): 60, 6 and 34 respectively.	Su et al. <sup>64</sup>
3	2-Butoxy-5-tert-octylnitrobenzene and butanal p-alkoxy nitrobenzene and benzaldehyde	Pd/C Pd/C	353K; P <sub>H2</sub> : 30kg/cm <sup>2</sup> ; solvent: EtOH; time: 5h	Stirred autoclave	N, N-dibutyl-2-butoxy-5-tert-octylaniline is the major product (yield 98.1%). N,N-dibenzyl compound (yield 91.4).	Kaneko et al. <sup>65</sup>
4	3-Aminobenzoic acid and aqueous HCHO	Pd/C	323K; P <sub>H2</sub> : 5kg/cm <sup>2</sup> ; solvent: MeOH; time: 1 h		3-dimethylamino benzoic acid is the major product (95.5%)	Nishimura et al. <sup>66</sup>
5	Aromatic amines and aldehydes	3-5% Pt/C	303-348K; P <sub>H2</sub> : 15 bar; solvent: MeOH	Slurry reactor (2 lit)	Conv (aniline): 100%, sel. (N-mono and di alkylated pdt.): 47 and 18% at 3.5 h at 314K. Conv (aniline): 100%, sel. (N-mono and di alkylated pdt.): 10 and 47% at 10 h at 314K.	Lehtonen et al. <sup>67</sup>

No.	Substrates	Catalyst	Reaction conditions	Reactor	Conversion, Selectivity (%)	Ref.
6	Aromatic amines and aldehydes	3-5% Pt/C	303-348K; P <sub>H2</sub> : 15 bar; solvent: MeOH	Loop slurry reactor		Salmi et al. <sup>68</sup>
7	<i>p</i> -Phynelenediamine and isobutyl ketone	63% Ni on kieselguhr; organic/inorganic acid; organic sulfur containing compound	438K; P <sub>H2</sub> : 750-1000 ponds; 4h	Slurry reactor (1 lit)		Wilson <sup>69</sup>
8	3,4-Me <sub>2</sub> C <sub>6</sub> H <sub>3</sub> NH <sub>2</sub> (3,4-xylidine) and 2-heptanone	5% Pt/C; 2-napthalene sulfonic acid	P <sub>H2</sub> : 47 psi; 343K; 0.75 h	Slurry reactor	Conv. 100; yield and purity (N-2-heptyl-3,4-xylidine) 99 and 100.	Ross et al. <sup>70</sup>
9	NH(C <sub>6</sub> H <sub>4</sub> NO <sub>2</sub> ) <sub>2</sub> and methyl isobutylketone	Pt/C	353-383K; P <sub>H2</sub> : 100 kg/cm <sup>2</sup>	Slurry reactor	Sel. NH(C <sub>6</sub> H <sub>4</sub> NHCH MeCH <sub>2</sub> CHMe <sub>2</sub> ): 100.	Watanabe <sup>71</sup>
10	Aniline and acetophenone	3% PtS <sub>x</sub> /C (sulfided catalyst)	398K; 500-800 psig; 3.5h; solvent: aniline	Slurry reactor (1 lit)	Yield of N-phenyl- $\alpha$ -methylbenzylamine: 94%.	Malz et al. <sup>72</sup>
11	Amides and carbonyls	10% Pd/C; sodium sulfate	373K; 40 bar; solvent: ethyl acetate	Slurry reactor	Isolated yield: 81-98	Fache et al. <sup>59a</sup>
12	Nitro aromatics and $\alpha$ -ketoester	10% Pd/C; sodium sulfate	293K; 50 bar; solvent: cyclohexane	Slurry reactor	Isolated yield: $\geq$ 60	Fache et al. <sup>59b</sup>
13	L- $\alpha$ -Methyl benzylamine and $\alpha$ -ketobutanoicacid	10% Pd/C	303K; 50 psi; solvent: EtOH; 10h		L-2-aminobutanoic acid (after debenzoylation): yield 84.9, enantioselective excess: 81.4%.	Hiskey et al. <sup>73</sup>

No.	Substrates	Catalyst	Reaction conditions	Reactor	Conversion, Selectivity (%)	Ref.
14	4-nitrodiphenylamine, methyl isoamyl ketone (MIAK); methyl isobutyl ketone (MIBK) (after the rx <sup>n</sup> with MIAK)	1% Pd/C (63% water) and acidic carbon co-catalyst	393K; ~3 Mpa; 113 min. 423K; ~3 Mpa; 95 min	Slurry reactor	N-(1,4-dimethylamyl)-N'phenyl- <i>p</i> -phynelene diamine (50.8); N-(1,3-dimethylbutyl)-N'-phenyl- <i>p</i> -phynelene diamine (48.7)	Merten et al. <sup>74</sup>
15	2-methyl-5-ethyl-aniline (MEA) and methoxy acetone (MOA)	5%Pt/C, H <sub>2</sub> SO <sub>4</sub>	323K, 5 bar	Batch reactor	N-methoxy propyl-2-methyl-5-ethyl-aniline (intermediate for metolachlor)	Vogel et al. <sup>75</sup>

Use of nitro compounds as precursors for amine compounds in the reductive alkylation reactions are reported by Kaneko et al. Aromatic nitro compounds containing alkyl, alkoxy, carboxylic, ester functionalities in *o*-, *m*-, *p*- positions are reductively alkylated with a wide range of aliphatic and aromatic aldehydes in presence of Pd or Pt catalysts. It was observed that lower homologues of aliphatic aldehydes (e.g., butyraldehyde or iso- butyraldehyde) give N, N-dialkylated products in good yields (>85%) even if there is an *o*- substitution in the nitro compound. Benzaldehyde was reported to produce N,N-dialkylated product with the nitro compound having no *o*-substituents (Scheme 1.6).



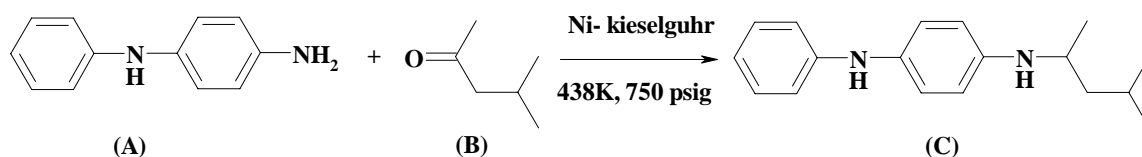
**Scheme 1.6.** Reductive alkylation of nitro-compounds with aldehydes

Watanabe reported reductive alkylation of di-nitro compounds with aliphatic ketones in presence of Pt/C or copper-chromium bimetallic catalysts.

Malz et al. reported the N-alkylation of aniline using acetophenone as a carbonyl compound. The product, N-phenyl- $\alpha$ -methylbenzylamine is useful as an antioxidant in petroleum and synthetic industries. As reported by Rylander,<sup>76</sup> the main issue in using acetophenone is its hydrogenolysis to ethyl benzene in the presence of normal transition metal catalysts and hydrogen. Sulfur poisoned catalysts solved this problem and Pt was reported as the best catalyst (yield: 94%). 5% RuS<sub>x</sub>/C and RhS<sub>x</sub>/C gave N-phenyl- $\alpha$ -methylbenzylamine in 80% and 72% yields respectively.

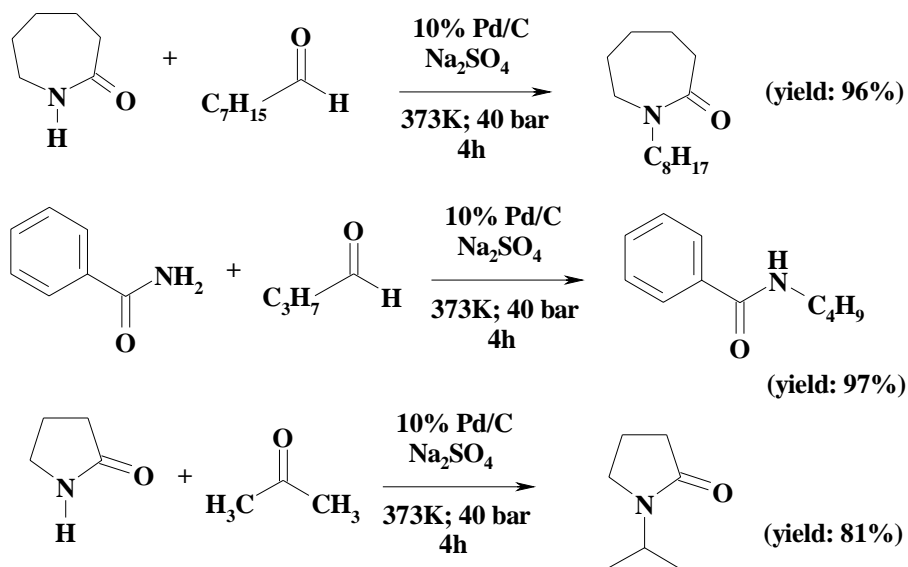
Lehtonen et al. have proposed a kinetic model for reductive alkylation of aromatic amine with alkyl substituents in the ring and a short chain aldehyde (having less than three carbon atoms), applicable for laboratory as well as industrial scale semibatch slurry reactor considering the mass transfer at the gas-liquid interface. Imine formation by homogeneous reaction was found to be non-catalytic. The imine reacts with hydrogen on the active Pt metal surface to produce the N-alkylated amine. Further, the catalytic three-phase reaction including homogeneous liquid-phase steps were simulated in a loop reactor by Salmi et al. The loop reactor was modeled using tanks-in series or alternatively, axial dispersion models. Kinetics of the reductive alkylation of aromatic amines, which was determined from the experiments in a laboratory autoclave, was used for verifying the reactor model and for concentration profile simulations in the loop reactor.

There are few reports on the use of mineral or organic acids in reductive alkylation reactions. Wilson reported that use of acids with or without sulfur containing modifiers improves the productivity of this reaction for all types of amine precursors and carbonyls. The yield of the reaction (C) at the identical conditions without any promoter was 75.5 %, whereas in the presence of *p*-toluene sulphonic acid or sulfuric acid, the yield increased to >90%. Again, the promoter reduces the hydrogenation of the ketone from 10% to < 5%. It was further observed that, addition of sulfur containing modifier (e.g., xylene monosulfide or thiodipropionic acid) increased the yield of C to 100%.



Ross et al. also described the use of acid promoters of pKa value in the range of 0.3-1.5 for reductive alkylation of amines (or their oxidized precursors) with ketones. A large number of acids like  $\beta$ -naphthalene sulphonic acid (pKa: 0.57), *p*-toluene sulfonic acid (pKa: 0.9), trifluoro acetic acid (pKa: 0.3) and benzene sulfonic acid (pKa: 0.7) were used to produce the N-alkylated products with high yields and purity (>90%). The authors have demonstrated that the acids of pKa value above or below this range gave poor yields. For example, with H<sub>2</sub>SO<sub>4</sub> and HCl (pKa: 0) as promoters, the yields were 65.7 and 70.5% respectively and 72.2% with acetic acid (pKa: 4.75) under identical reaction conditions.

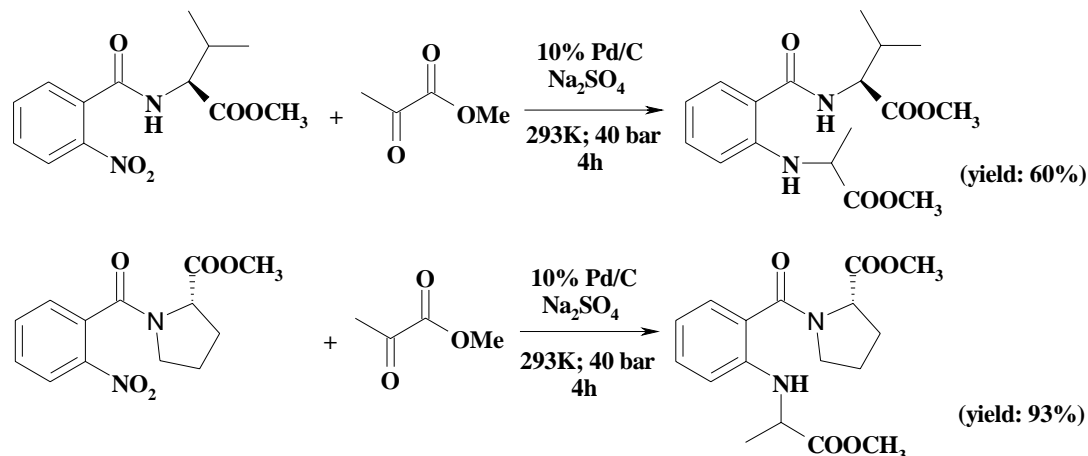
Fache et al.<sup>59a</sup> addressed the synthesis of N-alkylated amides from a series of amides and carbonyl compounds. It was observed that aromatic, cyclic or acyclic amides were giving the products in high yields (80-98%) with aliphatic as well as aromatic aldehydes and ketones (Scheme 1.7). Only formaldehyde was reported not to give the desired alkylated product with amides.



**Scheme 1.7.** Reductive alkylation of amides

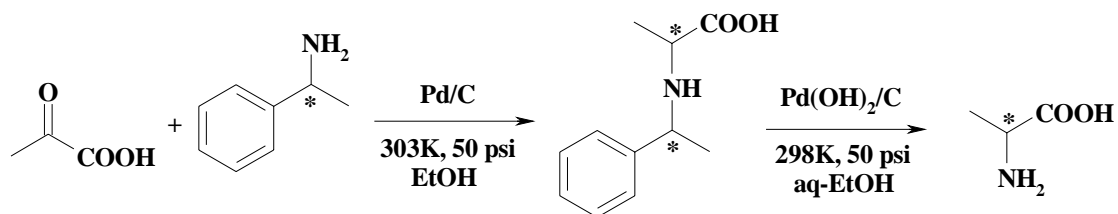
This catalyst system was equally active for amine compounds and various carbonyls.<sup>59b</sup> For substituted anilines and carbonyls, the isolated yields were in the range of 85-95% except octanaldehyde (0%). The catalyst gave good selectivity to the N-alkylated product too when  $\alpha$ -ketoesters were used (60-83%) (Scheme 1.8). Interestingly, the reactions were carried out at room temperature and chirality of the starting compound was retained after reaction. Therefore, the catalyst has an application in a large variety of substrates to produce the desired N-alkylated products.





**Scheme 1.8.** Reductive alkylation reactions of chiral amines and  $\alpha$ -ketoesters

Synthesis of optically active amines or amino acids is also possible by reductive alkylation (Scheme 1.9). Hiskey et al. synthesized a large number of amino acids, which is believed to occur in two steps: (i) reductive alkylation of the  $\alpha$ -ketoacid and benzylketone over Pd/C catalyst; (ii) hydrogenolysis (debenzylation) of the product to the amino acid over palladium hydroxide. L- $\alpha$ -amino acid was formed when reductive alkylation started with a L-amine. The optical purity varied in a broad range (12-81%) depending upon the chain length of the alkyl group in the  $\alpha$ -ketoacids.



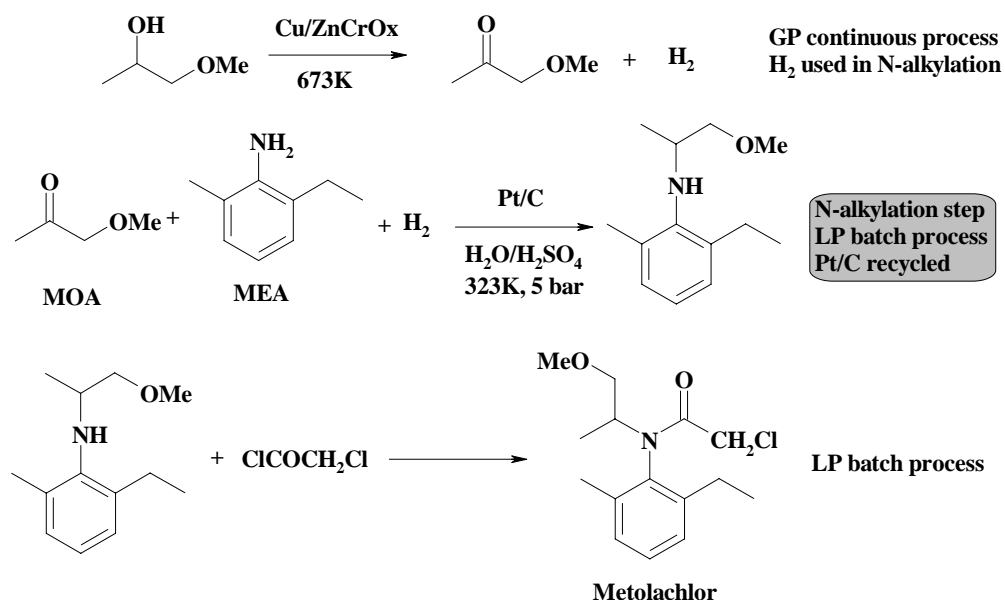
**Scheme 1.9.** Synthesis of optically active amines by reductive alkylation reaction

Reductive alkylated derivatives of *p*-phenylene diamines, N, N'-disubstituted *p*-phenylene diamines (NNPPDA) are used as antidegradants of rubber, in particular effective in protecting vulcanized rubber from ozone attack. Blends of two or more NNPPDA are more useful in rubber industries and sold commercially after mixing them. This needs separate mixing and storage equipment. Merten et al. reported the synthesis of two NNPPDAs by sequential reaction of 4-nitrodiphenylamine (or its reduced forms) with two

ketones. 4-nitrodiphenylamine, methyl isoamyl ketone (MIAK) was treated in a stirred reactor in the presence of Pt/C and acidic carbon co-catalysts to produce NNPPDA1 [N-(1,4-dimethylamyl)-N'-phenyl-*p*-phenylene diamine]. After cooling the reaction mixture, methyl isobutyl ketone (MIBK) was added into the reaction mixture and conducted the reaction at similar conditions to react remaining unconverted 4-nitrodiphenylamine to form NNPPDA2 [N-(1,3-dimethylbutyl)-N'-phenyl-*p*-phenylene diamine]. The final product constituted 50.8 and 48.7% of NNPPDA1 and NNPPDA2 respectively.

Malone and Merten<sup>77</sup> compared the reactor performance of laboratory scale (1 lit) stirred tank, Buss-Loop (50 lit) and industrial plant for reductive alkylation 4-nitrodiphenylamine with ketone at similar conditions used by Merten et al. (with single ketone in contrary to the ref. 76). The authors concluded that Buss-Loop reactor improved the rate by about 100%. The efficient mixing and better heat exchange ability of the Buss-Loop reactor was responsible for higher reaction rate and controlling the product selectivity.

Metolachlore is the active ingredient of Dual<sup>®</sup>, one of the most important grass herbicides for use in maize and a number of other crops. It is synthesized by the following transformations (Scheme 1.10):



**Scheme 1.10.** Synthesis of Metolachlor by reductive alkylation reaction

Ciba-Giegy Corporation introduced the product to the market in 1976 as a mixture of four stereoisomers. Later in 1982, it was found that only two isomers were active as herbicides. It was found that enantioselective hydrogenation of the imine (Schiff's Base) compound formed in the reductive alkylation gives the desired active metolachlors. In 1997, [Ir(cod)Cl]<sub>2</sub> with xylyphos ligand was reported as the catalyst for the imine hydrogenation at 80 bar and 323K.

#### 1.2.4. Dearomatization Reaction

There are several monographs and papers available for dearomatization of carbo- or heterocyclic compounds.<sup>78</sup> The summary of literature reports on hydrogenation of aromatic ring compounds is given in Table 1.7. In general, aromatic rings are very stable and need severe conditions to hydrogenate. Therefore, the other functionalities attached to the aromatic ring hydrogenate under the conditions used for ring hydrogenation.

**Table 1.7.** Summary of catalytic hydrogenation of aromatic compounds

Sr. No.	Reaction	Catalyst	Conditions	Conv./Sel. (%)	Ref.
1	Benzene to cyclohexane	Ru/ macro porous support	353K, 20 bar	Conv.: 100 Sel: 99.99	79
2	Benzene to cyclohexene	Ru/La <sub>2</sub> O <sub>3</sub> , ZnO, NaOH	423K, 50 bar, (g-l-l-s system)	Conv.: 52.3; Sel.: 70.4	80
3	Aniline to cyclohexylamine	Ru/Al <sub>2</sub> O <sub>3</sub>	433K, 230 bar	Conv.: 99.9; Sel.: 99.3	81
4	Aniline to dicyclohexylamine	Pd/Nb <sub>2</sub> O <sub>5</sub>	413K, 270 bar	Conv.: 100 Sel.: 92	82
5	<i>o-t</i> -butyl phenol to <i>o-t</i> -butyl cyclohexanol	Raney Ni-Fe	373K, 20 bar	Yield: 99; Sel: 95:5 ( <i>cis:trans</i> )	83
6	Phenol to cyclohexanone	Pd/C	333-423K, 1-20 bar	Conv.: 80; Sel.: 79	84
7	Pyridines to piperidines	Pd/C	353K, 10-50 bar	Conv.: 100 Sel: >90	85
8	Furan to tetrahydrofuran	Rh/Re/C	433K, 100 bar	Conv.: 100 Sel: 75	86

### 1.3. GAS-LIQUID-LIQUID-SOLID FOUR-PHASE SYSTEMS

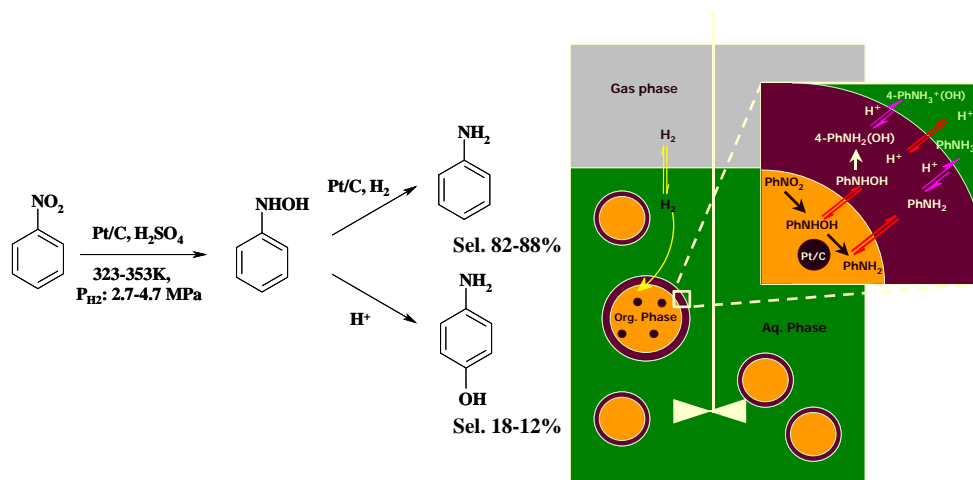
We have discussed at the beginning that though the introduction of a liquid phase brings considerable engineering complexities in gas-liquid-solid (three phase) catalytic systems, the liquid phase provides a better heat removal efficiency and good control over

the selectivity to the desired product. There are only a few reports in the literature, where the addition of an immiscible liquid phase (to form a gas-liquid-liquid-solid (four phase) system) gives a better process performance. We can consider the revolutionary process for benzene to cyclohexene developed by Asahi Chemicals, Japan that produces 60,000 TPA of cyclohexene since 1990.<sup>80a</sup> Hydrogenation of benzene in a three-phase system using lower alcohols as solvents was reported to produce cyclohexane along with trace amount of cyclohexene (2 mol % of benzene).<sup>87</sup> In 1972, Drinkard from DuPont Company patented the selective synthesis of cyclohexene from benzene (highest conv. 54%; sel.: 39%) for the first time in a gas-liquid-liquid-solid system with water and benzene as the two immiscible liquid phases and Ru as the catalyst.<sup>88</sup> The catalytic system required large quantity of alkali and additives like carbonyl compounds of chromium or other metals, which reduced the conversion of benzene and caused severe corrosion problem. The system was further developed by supporting Ru on rare earth oxides and oxides of Zn or Al as a catalyst and performing the reaction in a four phase system (conversion. 48.5%; sel.: 74.5%).<sup>80a</sup>

Benzene to cyclohexene is the most studied reaction system in gas-liquid-liquid-solid system.<sup>89</sup> Ru catalyst (on suitable support) dispersed in aqueous phase was used in all the cases strategically. Ru is known as a good catalyst for hydrogenation of aromatic unsaturated double bonds but not so effective for olefinic double bonds. Therefore, benzene loses its aromaticity in presence of Ru but the reaction slows down for hydrogenation of cyclohexene to cyclohexane. The supports and additives in these reactions are also very important to control the selectivity. Again, the low solubility of hydrogen in water reduces the rate of surface reaction. Hence, concentration of cyclohexene becomes high in aqueous phase and due to its low solubility in water, is transported rapidly to the organic (benzene) phase.

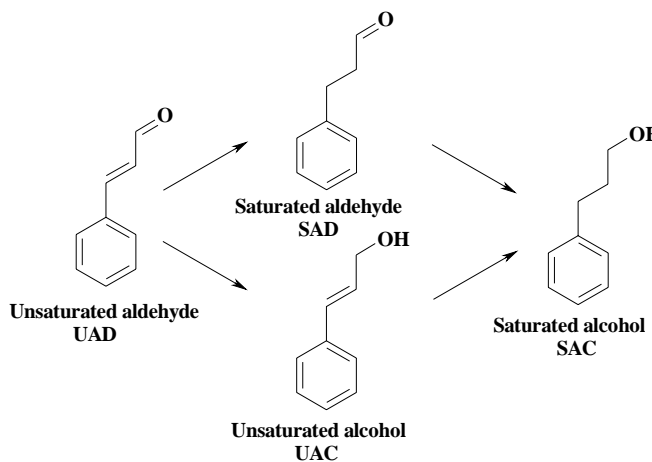
Synthesis of *p*-amino phenol, an intermediate for paracetamol (an analgesic drug), from nitrobenzene in a gas-liquid-liquid-solid system is another important example where two immiscible liquid phases are used.<sup>90</sup> For this reaction, Pt/C is most commonly used catalyst in the presence of a mineral acid (H<sub>2</sub>SO<sub>4</sub>) in a four-phase system. Due to the adhesion property of Pt/C, the catalyst remains in organic phase and initiates hydrogenation of nitrobenzene to the intermediate phenylhydroxylamine, which rearranges to *p*-aminophenol in the presence of acid by Bamberger rearrangement. The rearrangement

reaction is proposed to take place at the water-organic interface as shown in Scheme 1.11. The products *p*-aminophenol and aniline remain in the aqueous phase and easily separated from the catalyst.



**Scheme 1.11.** Synthesis of *p*-aminophenol in a gas-liquid-liquid-solid system

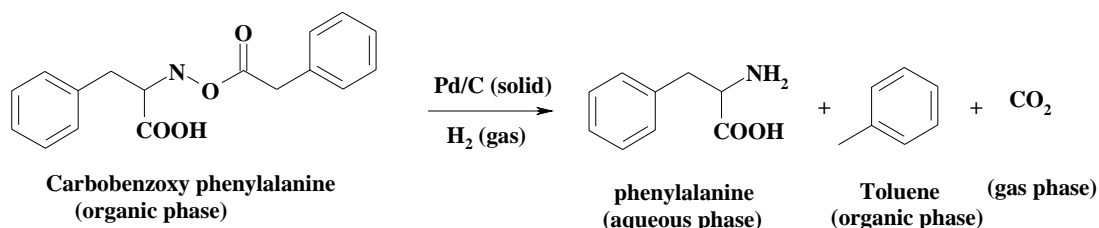
Satagopan and Chandalia<sup>91</sup> reported the selective hydrogenation of  $\alpha,\beta$ -unsaturated aldehydes (UAD, e.g. cinnamaldehyde) in a g-l-l-s system. The reaction scheme is shown in Scheme 1.12. Toluene containing UAD was the organic phase and alkaline (KOH or NaOH) aqueous solution was used as second immiscible liquid phase. The authors showed that Pd/C catalyst selectively hydrogenated the C=C bond to produce hydrocinnamaldehyde (conv. 100%, sel. to SAD: ~95% and SAC: ~5%). On the other hand, Pt/C catalyst gave high selectivity to UAC (cinnamyl alcohol, ~90%).



**Scheme 1.12.** Selective hydrogenation of  $\alpha,\beta$ -unsaturated aldehyde in a gas-liquid-liquid-solid system

Yamada et al.<sup>32b</sup> further studied the effects of base and water for this reaction using both Pd and Pt on carbon catalysts. The selectivity of SAD decreased to 20% (SAC: 80%) when the reaction was carried out in a four-phase system without a base for Pd/C catalyst. On the other hand, in the absence of an aqueous phase, the selectivity to SAD (~92%) was not affected for the three phase system (KOH impregnated Pd/C used as a catalyst), but the reaction rate decreased to 0.23 times with respect to the four phase one. The selectivity profile for Pt catalyzed reaction is highly influenced by the aqueous phase. The three phase reaction (KOH impregnated Pt/C used as catalyst) showed zero selectivity to UAC where as the four-phase reaction gave 90% selectivity. Thus, the control over reaction rate and selectivity for hydrogenation of  $\alpha,\beta$ -unsaturated aldehydes is possible by performing the reaction in a gas-liquid-liquid-solid system.

Protecting groups are used to mask special functional groups in organic compounds to avoid undesired reactions and removed later to obtain the final product. For example, phenylalanine is frequently protected to carbobenzoxy phenylalanine and the protecting group was removed by hydrogenolysis in a gas-liquid-liquid-solid system over Pd/C catalyst as shown below (Scheme 1.13).<sup>92</sup>



**Scheme 1.13.** Hydrogenolysis of carbobenzoxy phenylalanine in a gas-liquid-liquid-solid system

Hydrogenolysis of carbobenzoxy phenylalanine dissolved in 1,2-dichloroethane over Pd/C catalyst took place in the organic phase and the product transferred to the aqueous phase due to its dominant hydrophilic nature. It was observed that the reaction did not proceed without the aqueous phase. This reflects that the reaction is highly influenced by product inhibition. Water reduced the product concentration drastically in the reacting (organic) phase and hence higher reaction rate was obtained.

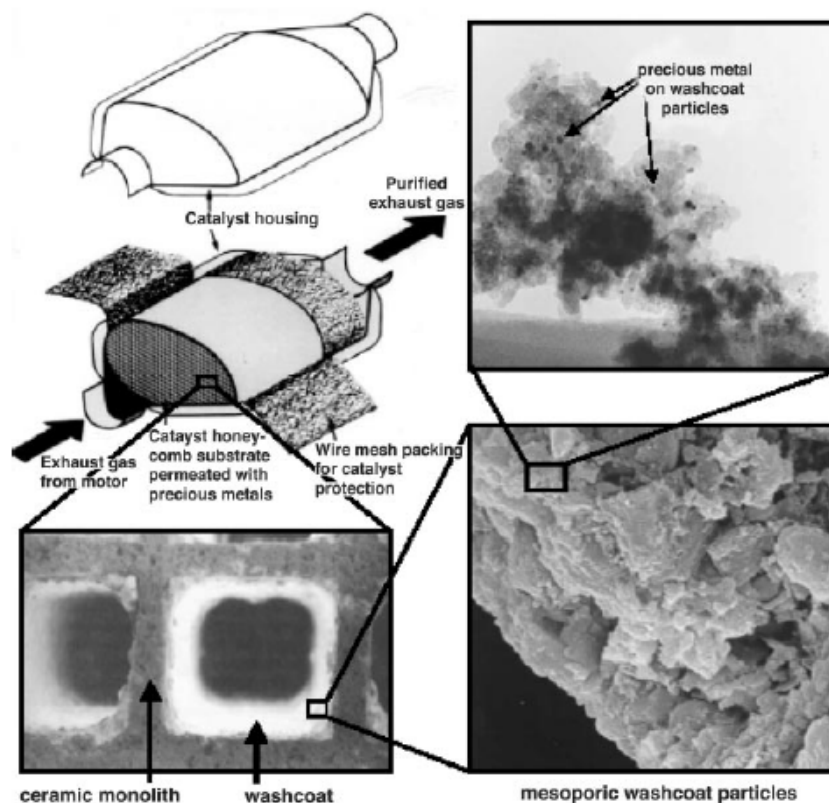
Carbonylation of allyl chloride is an important example of a four-phase catalytic reaction wherein the reaction occurred on the catalyst surface at the liquid-liquid

interface.<sup>93</sup> In this reaction, CO was the gas phase, allyl chloride and phosphine dissolved in toluene constituted the organic phase and aqueous NaOH was the second immiscible liquid phase. Metallic Pd catalyst was present as the solid phase. It was observed that, the reaction had almost negligible activity if it was carried out as a three-phase system. On the contrary, the activity was ~100 times higher in a wide range of four-phase conditions with organic to aqueous phase holdup in a range of 0.1-0.6. The catalyst present at the interface accessed the organic phase reactants and promoters present in both the phases. The organic acid produced by the reaction formed salts with the base and transferred to the aqueous phase. Therefore, volume of aqueous phase increased during the course of a reaction and hence affected the interfacial area. This effect could be pronounced when the reaction took place at very low or high organic phase holdups.

It is clear from the above examples that each one of these have different characteristics though they are conducted in a gas-liquid-liquid-solid (four-phase) system. For example, in selective hydrogenation of benzene to cyclohexene, cyclohexene formed in the aqueous phase, came back to the organic phase. But, in a few cases the product did not reside in the same phase where the reactant was present (e.g., hydrogenolysis example), which caused the swelling of the other phase. As a result, hold up and interfacial area varied with conversion level. Secondly, it is very important to ensure the phase in which reaction occurs because the solubility of the reactants, products and promoters would not be the same in all the phases. For example, in selective synthesis of cyclohexene, the catalyst remained in the aqueous phase and high selectivity is achievable due to poor solubility of cyclohexene in the aqueous medium. If the catalyst is present in the organic phase, high selectivity to cyclohexene might be difficult to achieve due to longer residence time on the catalyst surface. In summery, the overall rate, selectivity and reactor performance for a gas-liquid-liquid-solid system requires consideration of the reaction engineering issues like: (i) dispersion of catalyst and promoters, (ii) dispersion characteristics of two immiscible liquid phases, (iii) identification of reactions occurring in each phase, interfacial reactions and kinetics and (iv) gas-liquid, liquid-liquid and liquid-solid mass transfer.

## 1.4. CATALYSIS BY METAL NANOPARTICLES

An industrial process always looks for catalysts with high activity and selectivity. The former can be achieved by using high surface area solids in which an active catalyst is dispersed in the form of very small particles. These highly dispersed particles having dimensions of 1 to 20 nm are commonly termed as ‘nanoparticles’. The impact of nanomaterials in catalysis is evidenced by large number of publications on this subject<sup>94</sup> and can be illustrated by the example of a catalyst for automotive exhaust used in cars. The catalytic converter has a honeycomb structure, the walls of which are coated with porous alumina as shown in Figure 1.4.<sup>95</sup>



**Figure 1.4.** Automotive converters: an application of metal nanoparticles

Metal nanoparticles like Pt, Rh and metal oxides like ceria ( $\text{CeO}_2$ ), zirconia ( $\text{ZrO}_2$ ), lanthana ( $\text{La}_2\text{O}_3$ ) and baria ( $\text{BaO}$ ) are impregnated on alumina supports to prepare the catalysts for automotive exhaust applications. Pt catalyses oxidation of hydrocarbons and CO, Rh reduces  $\text{NO}_x$ , ceria in combination with zirconia acts as an oxygen storage



component and lanthana stabilizes the alumina against loss of surface area. Baria is used occasionally to trap SO<sub>3</sub>, which is known to deactivate the catalyst. Therefore, it is evident that the finely dispersed metal and metal oxides are highly active as catalysts at their nano-size range.

The reasons why nanosize materials show high catalytic activity, can be explained as follows:<sup>96</sup>

- High surface-to-volume ratio compared to bulk materials. A nanoparticle of 10 nm diameter has ~10% atoms on the surface, while a 1 nm particle has ~100%.
- Different shapes and fraction of atoms located on corners or edges enhance catalytic activity. Metal atoms at the edges and corners have a smaller coordination number than those on the planar faces. These low-coordination sites are higher in energy and hence show high activity. The activity of low-coordination defect sites can be so large that in spite of their very low concentrations, their presence determines the catalytic activity of a material to a very large extent.<sup>97</sup>

#### **1.4.1. Synthesis and Stabilization of Metal Nanoparticles**

Synthesis of metal nanoparticles can be done by (i) physical and (ii) chemical methods. In the physical method, metallic aggregates are subdivided mechanically to produce nanoparticles. But this method produces relatively larger particles (>10 nm) with very broad particle size distribution. This method has a drawback of reproducibility in synthesis, which leads to inconsistent catalytic activity.<sup>98</sup>

Chemical methods like reduction of metal salts are used most commonly due to its simplicity, reproducibility and control over narrow particle size distribution. A number of reducing agents like alcohols, hydrogen or hydrides are reported in the literature and the details are reviewed by Roucoux et al.<sup>99</sup> and Burda et al.<sup>100</sup> A summary of commonly used reduction methods are shown in Table 1.8.

Unfortunately, the bare metallic nanoparticles are unstable and agglomerate to form larger particles and eventually bulk materials due to its thermodynamic stability. Then it loses its characteristics like high surface-to-volume ratio and the unique chemical and physical properties associated with it. Therefore, stabilizers are used to restrict the close

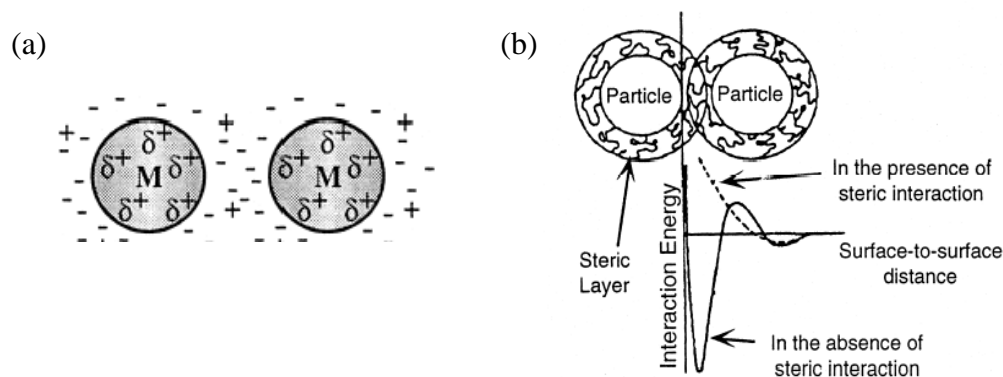
proximity of metal nanoparticles and aggregation. Two methods of stabilizations as reported by Aiken and Finke are described below.<sup>101</sup>

*Electrostatic stabilization:* Adsorption of ionic compounds (in aqueous phase) such as halides, carboxylates or polyoxoanions on electrophilic metal surface generates an electrical double layer around the metal surface. Therefore, a Coulombic electrostatic repulsion is generated between the metal particles, which prevents aggregation (Figure 1.5a).

**Table 1.8.** Commonly used reducing agents in synthesis of colloidal metal nanoparticles

Sr. No.	Reducing agent	Remarks	Ref.
1	Alcohols	Alcohols having $\alpha$ -hydrogen (eg. MeOH, EtOH), acts as reducing agent in reflux conditions. Alcohol oxidizes to corresponding carbonyl compound.	102
2	Hydrogen	Aqueous solutions of chloride salts are used oftenly.	103
3	Hydrides	Borohydrides (e.g., NaBH <sub>4</sub> or KBH <sub>4</sub> ) are used to produce metal nanoparticles in aqueous phase.	104
4	Hydrazine	Hydrazine can be used in all its forms like hydrochlorides or sulfates.	105
5	4-Hexadecyl aniline	Used for synthesis of hydrophobic metal nanoparticles from water-soluble metal precursors. 4-Hexadecyl aniline acts as a phase transfer agent, reducing agent as well as stabilizing agent.	106
6	Sodium citrate	Act as a reducing agent as well as ionic stabilizer. Forms intermediate acetone dicarboxylic acid, which causes ill-defined colloids.	107
7	Photo chemical reduction	Reduction by radiolytically produced reducing agents or degradation of organometallic complex by radiolysis	108
8	Sonochemical reduction	Occurs in three steps: (i) generation of H <sup>•</sup> and OH <sup>•</sup> into cavitation bubble; (ii) reduction of metal precursor at the bubble-solution interface and (iii) growth of colloids.	109
9	Electrochemical reduction	Anode acts as the metal source, oxidized in presence of quaternary ammonium salt (which act as electrolyte as well as stabilizing agent) and the ions reduced at the cathode to produce metal nanoparticles.	110

*Steric stabilization:* Stabilization of metal nanoparticles can also be achieved by using macromolecules such as polymers or surfactants. The macromolecule forms a steric layer, which prevents aggregation as shown in Figure 1.5b.



**Figure 1.5.** (a) Electrostatic and (b) steric stabilization of metal nanoparticles

Other than these two types of stabilizations, combination of electronic as well as steric stabilization by polyoxoanions ( $P_2W_{15}Nb_3O_{62}^{9-}$ ) and tetrabutyl ammonium halides ( $Bu_4N^+$ ),<sup>111</sup> stabilization by ligands (amines, thiols etc) are also reported in the literature. Solvent molecules are reported in a few cases to act as the stabilizer of metal nanoparticles,<sup>112,113</sup> but are not well accepted. It is believed that halide anions from the precursors remain on the metal surface to give electronic stabilization in those cases.<sup>113</sup> A brief summary of stabilizing agents is shown in Table 1.9.

**Table 1.9.** Commonly used stabilizers in synthesis of colloidal metal nanoparticles

Sr. No.	Stabilizer	Remarks	Ref.
1	Surfactants	The first nanoscale metals stabilized by surfactants were reported in 1976 by Lisichkin et al. and 1979 by Kiwi and Grätzel.	113
2	Dendrimers	Dendrimers are fairly uniform in composition and structure, and yield well-defined nanoparticles. Nanoparticles are confined by steric effect; therefore metal surface is mostly unpassivated and available. The dendrimer branches can be used as selective gates to control access of small molecules (substrates) to the encapsulated (catalytic) nanoparticles.	114
3	Polymers		115
4	Amines	Sometimes amines act a phase transfer agent, reducing agent as well as capping agent.	116
5	Thiols	Dispersible in organic as well as inorganic solvents. Bisthiolate ligands are useful to link individual clusters.	117

### 1.4.2. Immobilization of Metal Nanoparticles

From the discussion above, it is evident that the area of synthesis, stabilization and characterization of colloidal metal nanoparticles are well developed. These suspended

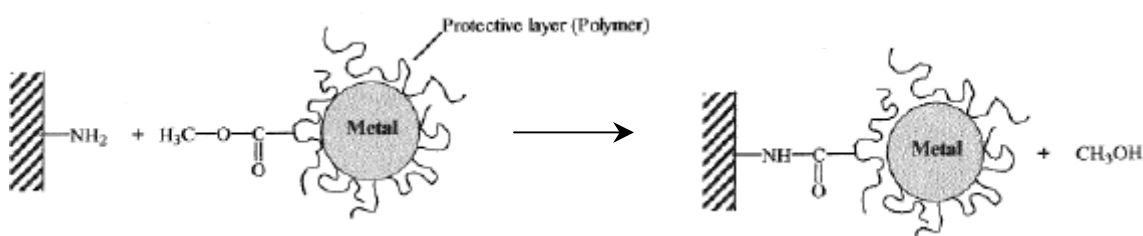
nanoparticles showed very good activity as catalysts,<sup>100,101</sup> but separation of these materials from the reaction mixture is difficult. Therefore, syntheses of catalytically active, reproducible and isolable metal nanocomposites are important to researchers in this domain. Finke et al.<sup>118</sup> reported the '*bottolable*', solid Ir and Rh nanoparticles, which can be dispersed in various organic solvents to use as a catalyst and termed them as '*soluble heterogeneous catalysts*'. Reek and co-authors<sup>119</sup> showed the use of membrane reactors for recovery of transition metal nanocomposites supported on dendrimers. But these are not satisfactory options for separable catalysis because of their limitation on applicability. Immobilization of transition metal nanoparticles on some solid supports such as inorganic oxides, zeolites or polymeric materials can be an interesting alternative, because the catalyst can be filtered from the reaction mixture and recycled easily.

There are two major chemical ways for the preparation of supported metal nanocomposites: (i) adsorption of nanoparticles on support, (ii) grafting of nanoparticles on support. Fabrication of nanostructures on support by electron beam lithography technique is also an important area explored by the solid-state researchers.<sup>120</sup> In this section chemical synthesis of supported nanocomposites will be discussed with a few highlights to show the spectrum of supports used for immobilization of nanomaterials.

(i) *Adsorption of nanoparticles on support:* Usually metal nanoparticles are synthesized first in the liquid phase and then impregnated on the solid supports. Bönemann and co-workers<sup>121</sup> reported wide range of metal nanoparticles chemically synthesized (hydrotriorganoborates as the reducing agent) and stabilized by tert-ammonium halides in tetrahydrofuran and supported on charcoal. Electrochemically synthesized nanoparticles are also supported on charcoal and alumina (cortex catalyst) by Reetz and co-workers<sup>122</sup> in the same way. Lang et al.<sup>123</sup> immobilized dendrimer stabilized Pt nanoparticles on silica support and thermally removed the support to achieve Pt/SiO<sub>2</sub> catalyst. There are also many reports where metal precursor is adsorbed first on the solid support and then reduced to nanosize particles.<sup>124</sup> For example, Joo et al. and Lu et al.<sup>125</sup> obtained highly dispersed Pt and magnetically separable Pd nanoparticles on ordered nanoporous carbon, synthesized using SBA-15 (Si/Al=20) as a template, by simple incipient wetness followed by reduction using hydrogen. Kralik and co-authors<sup>126</sup> reviewed

the polymers and resins as useful supports for synthesis of supported transition metal nanoparticles.

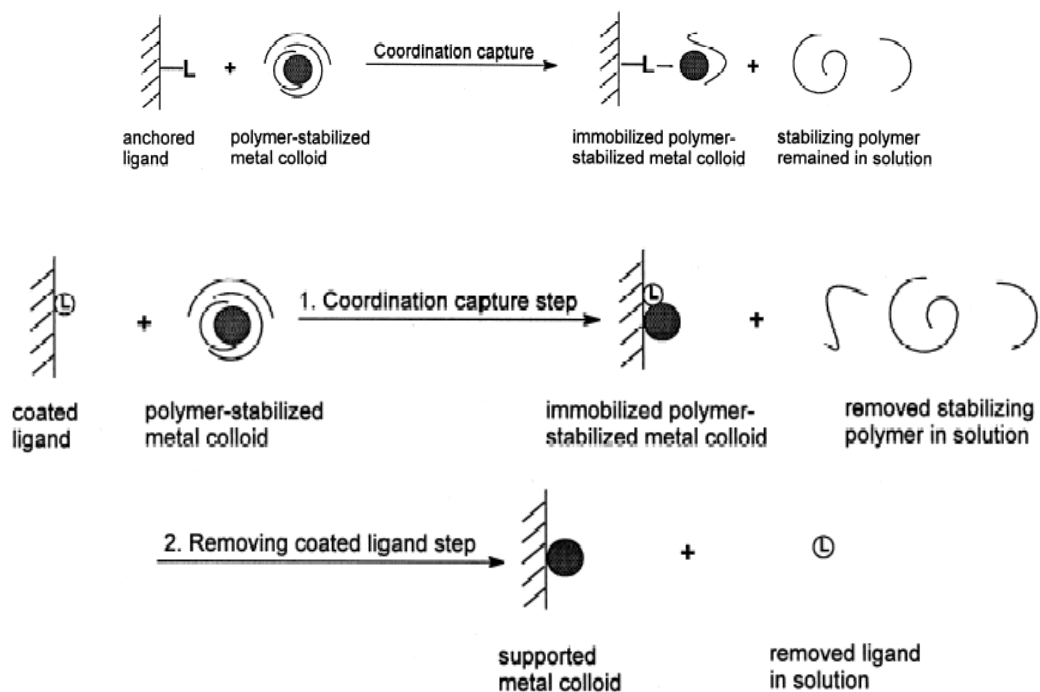
(ii) *Grafting of nanoparticles on support:* Ohtaki et al.<sup>127</sup> reported ultra fine Rh and Pt particles prepared by alcohol reduction in the presence of a protective polymer and were immobilized covalently onto a cross-linked polymer support. Methylacrylate residue in the protective polymer formed an amide bond with the primary amino group in the support as shown in Figure 1.6. Grafted nanoparticles remain unchanged after immobilization and no leaching was observed under hydrogenation reaction conditions.



**Figure 1.6.** Immobilization of metal nanoparticles through amide linkage

Chen et al.<sup>128</sup> synthesized well-dispersed Pt, Ag colloids on polystyrene nanospheres with surface-grafted poly-N-(isopropylacrylamide) by reduction of PtCl<sub>6</sub><sup>2-</sup> or AgNO<sub>3</sub> using ethanol. The approach was also applied successfully for Pt nanoparticles using silica as a solid matrix.<sup>129</sup>

Liu and co-workers<sup>130</sup> have reported a synthetic route for immobilization of Pt, Pd, Rh and Ir on solid supports like polymers, alumina or magnesia. As an illustration, triphenyl-phosphine (TPP) supported on polystyrene (PS) and poly *N*-vinyl-2-pyrrolidone (PVP) stabilized Pt nanoparticles were dispersed in ethanol to get the PS supported Pt nanoparticles. The stepwise mechanism is shown below (Figure 1.7):



**Figure 1.7.** Immobilization of metal nanoparticles on solid supports

### 1.4.3. Catalysis by Immobilized Heterogeneous Metal Nanoparticles

Heterogeneous metal nanoparticles have been reported for a wide variety of reactions such as in fuel cells, hydrogenation, oxidations and coupling reactions. Among them fuel cells have the major industrial application of heterogeneous metal nanoparticles and this topic is reviewed in several publications.<sup>131</sup> Applications of immobilized metal nanoparticles in other reactions are summarized in Table 1.10 and discussed for hydrogenation reactions in this section.

Schmid et al. reported Pd on TiO<sub>2</sub> and Al<sub>2</sub>O<sub>3</sub> as powerful catalysts in various olefin hydrogenation reactions. Diolefins like 1,3-cyclooctadiene or dicyclo-pentadiene could be semi hydrogenated selectively. 1-Hexyne was transformed to 1-hexene with 98% yield. All hydrogenation processes were heterogeneously catalyzed, as no case had been observed where the filtered products showed catalytic activities. The activities of repeatedly used catalyst samples were constant.

Lu et al.<sup>125b</sup> used Pd nanoparticles supported on Co-ordered mesoporous carbon (Co-OMC) for hydrogenation reactions. The Co-OMC made the catalyst magnetically

separable from the reaction mixture after completion of 1-octene hydrogenation. The catalyst was stable enough and reported to be recycled efficiently two times.

Bönnemann et al. synthesized Pt, Pd and Rh nanoparticles on charcoal and studied their catalytic activity for C=C hydrogenation reactions. The activity was compared with commercial Degussa catalysts which was made by simple precipitation method and showed that the ligand stabilized synthesis of metal nanoparticles produced better catalysts from activity and stability perspective. Activity of the conventionally precipitated catalyst (Pd/C) expires completely after the performance of  $38 \times 10^3$  catalytic cycles per palladium atom, whereas the colloidal Pd/C catalyst still showed a residual activity even after  $96 \times 10^3$  catalytic turnovers.

Karlik and co workers have reviewed the polymers and resins as the potential supports for immobilization of metal nanoparticles and highlighted their applications in catalysis. Chen et al<sup>133</sup> grafted the polystyrene surface with poly-(N-isopropyl acryl amide) (PNIPAAm) and immobilized Pt nanoparticles. This catalyst showed 5 times higher catalytic activity for allyl alcohol hydrogenation in comparison to Pt/C catalyst prepared by precipitation technique. Furthermore, the catalyst showed constant activities till seven recycles whereas Pt/C catalyst became inactive after one reaction. The authors proved that the bulky PNIPAAm stabilizers prevent agglomeration and hence showed constant activity. If Pt is supported on polystyrene beads, the activity reduced to 50% on its 5<sup>th</sup> recycle.

**Table 1.10.** Catalysis by immobilized metal nanoparticles

Sr. No.	Catalyst	Substrate (conv. %)	Product (sel. %)	Reaction conditions	Remarks	Ref.
<i>Hydrogenation Reactions</i>						
1	Pd on TiO <sub>2</sub> or Al <sub>2</sub> O <sub>3</sub>	1-Hexyne	1-hexene (98% yield)	--	Di-olefins could be semi hydrogenated selectively. Pd leaching was not observed. The activities of repeatedly used catalyst samples were constant.	132
2	1% Pd- 9% Co-ordered mesoporous carbon	1-Octene	n-Octane	Hydrogen bubbled	Co on ordered mesoporous carbon (Co-OMC) made the catalyst magnetically separable. Recycled efficiently two times.	125b
3	5% Pd/C  5% Pt/C	Cyclohexene Cinnamic acid  Crotonic acid	Cyclohexane Phenylpropionic acid Butanoic acid	--	Activity: 566 (N ml/g min) Activity: 826 (N ml/g min) Degussa E10R (Pd/C): 356 (Nml/g min) Activity: 415 (N ml/g min) Degussa E10R (Pt/C): 254 (Nml/g min)	121a
4	Pd-cortex catalyst (5% Pd/Al <sub>2</sub> O <sub>3</sub> )	Cyclooctene	Cyclooctane	--	Three times more active compared to 5% Pd/Al <sub>2</sub> O <sub>3</sub> Aldrich catalyst.	122
5	Pt-(N-isopropyl acrylamide)-polystyrene	Allyl alcohol	Propanol	1 bar, 298K, water	Activity (TOF, mol <sub>H2</sub> /mol <sub>Pt</sub> min) is 5 times higher than Pt/C catalyst. Recycled six times without loss of activity.	133
6	Pd on heterocyclic polyamide resin	2-methyl-1,3-pentadiene (35) Phenylacetylene (100) 2-Hexyne (70)	2-methyl-2-pentene (88) Styrene (100) Cis-2-hexene (87)	1 bar, 298K, methanol	Comparison with Pd/C catalyst: Conv.: 100, Sel.: 0. Conv.: 100, Sel.: 0. Conv.: 100, Sel.: 0.	134



Sr. No.	Catalyst	Substrate (conv. %)	Product (sel. %)	Reaction conditions	Remarks	Ref.
7	Pt on polystyrene (Pt-PS)	Cinnamaldehyde (79.7)	Cinnamyl alcohol (94.7); hydrocinnamaldehyde (5.3)	4 Mpa, 333K, EtOH:H <sub>2</sub> O=5:1, NaOH	PVP used to stabilize Pt nanoparticles and removed after immobilization. TOF: 233.3 mol <sub>H<sub>2</sub></sub> /(mol <sub>Pt</sub> h) Stable and reusable	135
8	5% Rh (colloid) on charcoal 5% Rh (cluster) on charcoal 5% Rh on charcoal (commercial)	Butyronitrile	n-Pentyl amine	1 bar, 313K, 2000 rpm, EtOH	Very small parts of all catalysts were oxygenated to stabilize. Activity after 5 min of reaction (Nml/gm.min) for with & without TiO <sub>2</sub> : 262 & 203  230 & 167  124 & 83	136
9	Pt-PS Pt-Al <sub>2</sub> O <sub>3</sub>	<i>o</i> -Chloro nitrobenzene (100)	<i>o</i> -Chloro aniline (81.9) (79.9)	303K, 0.1 MPa	TPP used as ligand to capture Pt-PVP and removed after formation of supported catalyst. With Pt-PVP sel.: 60.2 for <i>o</i> -chloronitrobenzene at 100% conv.	130
	Pt-PS Pt-Al <sub>2</sub> O <sub>3</sub>	Citronellal (100) (95.5)	Citronellol (81.2) (92.8)	333K, 6 MPa, EtOH : H <sub>2</sub> O = 5:1, 2h	With Pt-PVP conv.: 70.6, sel.: 44.5 for citronellal after 2 h.	
<b>Coupling Reactions (Heck and Suzuki Coupling)</b>						
1	Pd-SiO <sub>2</sub> Me	Iodobenzene (58) and styrene	Stilbene (86)	NaOAc or Et <sub>3</sub> N, 423K,	Silica surface modified with various chlorohydrosilanes (eg., methyl, phenyl).	137
	Pd-SiO <sub>2</sub> Ph	Iodobenzene (80) and styrene	Stilbene (83)	N-methyl phormamide, 5h	Applied for various haloarenes and vinylic compounds. Leaching observed.	

Sr. No.	Catalyst	Substrate (conv. %)	Product (sel. %)	Reaction conditions	Remarks	Ref.
2	[Pd(0)]-NaY	4-bromofluorobenzene (100) and styrene	cis- and trans-p-fluorobenzyl-2-benzyl ethene	NaOAc, DMAc, 373-413K, 20h	Yield: 90.3 and 86.1% at 373 and 413 K. TOF: 20 and 16 h <sup>-1</sup> at 373 and 413 K. Truly heterogeneous and recycled efficiently.	138
3	LDH-Pd	<i>p</i> -chloroanisole and styrene	<i>p</i> -methoxystilbene (yield: 76%)	Bu <sub>3</sub> N, [NBu <sub>4</sub> ]Br  Thermal heating, 403K 40h.	Layered double hydroxide supported Pd (LDH-Pd) had superior activity over Pd/C, Pd/SiO <sub>2</sub> , Pd/Al <sub>2</sub> O <sub>3</sub> (yield: 76, 28, 15, 22% respectively). Microwave irradiated reaction is the highest reported TOF for Heck reaction till date for activated and deactivated chloroarenes.	139
		<i>p</i> -chloroanisole and styrene	<i>p</i> -methoxystilbene (yield: 80)	Microwave irradiation, 1h	Truly heterogeneous catalyst. Recycled 5 times with almost constant activity.	
4	LDH-Pd	<i>p</i> -Chloroanisole and phenylboronic acid	<i>p</i> -Methoxy biphenyl (yield: 90%)	KF in 1,4-dioxane/H <sub>2</sub> O (5:1), 373K, 8h	Recycled 5 times without loss in activity.	139
		Chlorobenzene and phenylboronic acid	Biphenyl (yield: 93%)		LDH-Pd is active for Sonogashira and Still coupling reactions also without deactivation in prolong use.	
5	4.2% Pd-PVP on C	Phenyl benzoic acid and iodobenzene	Biphenyl	Phenylboronic acid, NaOAc, acetonitrile: H <sub>2</sub> O=3:1, 373 K, 12 h	Activity reduced to 69% in 2 <sup>nd</sup> recycle and retained constant till 5 <sup>th</sup> run. Colloidal Pd-PVP showed better activity (~2 times) in fresh run, but reduced to 37% in 2 <sup>nd</sup> recycle and further slowly reduced to 16% in 5 <sup>th</sup> recycle	140

Sr. No.	Catalyst	Substrate (conv. %)	Product (sel. %)	Reaction conditions	Remarks	Ref.
<b>Oxidation Reactions:</b>						
1	5% Pt/C 5% Pt/graphite 5% Pd/C 5% Pd/graphite 1% Au/activated C 1% au/graphite	Glycerol 63.1 58.6 57.2 53 56 91	Glyceric acid 73.7 65.7 67 50 100 92	3 bar, 333K, H <sub>2</sub> O, NaOH	At 1 bar, Pt and Pd catalysts were less selective to glyceric acid and Au was totally inactive. Proposed that NaOH aids the initial dehydrogenation via H-abstraction of one of the primary OH groups of glycerol and, in this way, the rate-limiting step in the oxidation process was overcame.	141
2	Au/C (X40S, high surface area C) Au/C (XC72R, high surface area C)  Au/C (X40S) Au/C (XC72R)	Glucose 100 (2h) 100 (1.5 h)  Ethylene glycol 52 22	$\delta$ -glucono-lactone   Glycolic acid 94 94	O <sub>2</sub> bubbled, pH: 9.5 (NaOH), 323K  NaOH, 303 kPa, 343K, 30 min	Particle size seems to be a major factor to influence the reactivity of the catalysts. The trends in activity are not explained.	142
3	1% Au/C  1% Au/C 1% Au/Al <sub>2</sub> O <sub>3</sub>	Ethylene glycol  2-amino-propanol 65 100	Glycolate (98)  2-amino-propanoate	Aq. Medium, alkali, 3 atm., 343 K  Aq. Medium, alkali, 3 atm., 343 K, 2h	Au/C is compared with 5% Pd/C and Pt/C (Sel. and TOF, h <sup>-1</sup> : 98, 77, 71 and 1000, 500, 475 respectively).  5% Pd/C and Pt/C are inactive at these conditions. Au on C, Al <sub>2</sub> O <sub>3</sub> and SiO <sub>2</sub> synthesized and applied for selective oxidation of various diols, aminoalcohols and oxidation of aldehydes and glucose.	143

Michalska et al. reported synthesis of Pd nanoparticles on heterocyclic (pyridine) polyamide resins by ligand exchange method using  $\text{PdCl}_2(\text{PhCN})_2$ . The resin functional groups (i.e. N- and O-) acted as coordination sites for the palladium and mixed valence state species are formed, giving a selective palladium catalyst. The catalyst showed high selectivity towards partial hydrogenation of alkenes and alkynes. Evaluation of the stability of the supported palladium catalyst was tested in eleven successive runs involving 4300 catalytic cycles and neither loss of activity nor selectivity was reported.

Yu et al. synthesized Pt nanoparticles on polystyrene beads (PS) with or without stabilizers (PVP) and showed that Pt-PS catalyst was relatively more active and selective in gas-liquid-liquid-solid four-phase hydrogenation of cinnamaldehyde (CAL) to cinnamylalcohol (COL) than Pt-PS-PVP (TOF: 233.3 & 204.3  $\text{h}^{-1}$ ; conv: 79.7 & 69.9%; sel (COL): 94.7 & 92.1% respectively). PVP blocked the active Pt surfaces through which the carbonyl moiety coordinated to the metal surface, resulting in lower activity and selectivity. This was further evident when Pt-PS was compared with Pt-PVP (colloidal homogeneous suspension) catalyst (TOF: 84.2  $\text{h}^{-1}$ ; conv: 37.5%; sel (COL): 12%).

Bonnemann et al. reported the immobilization of Rh metal nanoparticles on charcoal in the form of clusters as well as colloids for hydrogenation of butyronitrile. Strong metal-support interaction and hence better activity was observed when the support surface was modified with  $\text{TiO}_2$ . The catalyst was compared with commercial Rh on charcoal catalysts and the nanoparticles showed better catalytic activity.

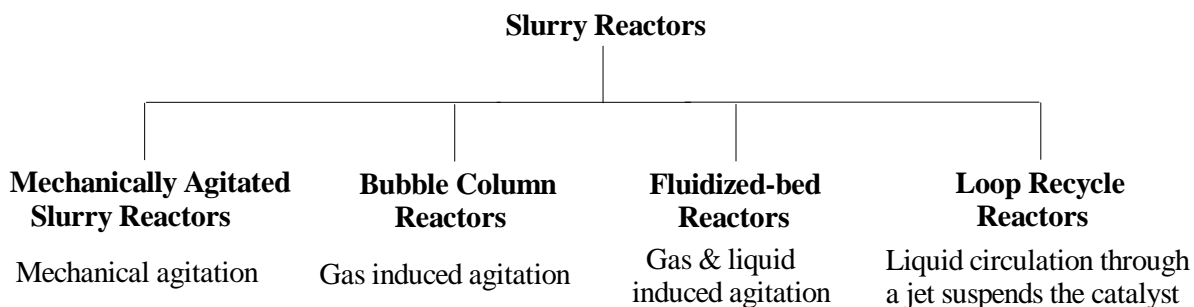
## 1.5. MULTIPHASE REACTORS

In most of the chemical process manufacturing operations, the reactor represents the heart of the plant.<sup>144</sup> The reactor type used for multiphase reactions generally depends on reaction class and type of phases involved. Due to the presence of gas-liquid-solid (and one more liquid phase occasionally) phases, the analysis and design of these reactors is important to achieve effective mixing of fluid phases, heat and mass transfer to get the desired performance of the process. These reactors are mainly classified into two classes: (i) slurry reactors and (ii) fixed bed reactors. Ramachandran and Chaudhari, Satterfield, Shah, Chaudhari and Ramachandran, Doraiswamy and Sharma, reviewed the design and

analysis of the different types of slurry and fixed bed reactors.<sup>145</sup> In this section, a brief review of these two types of reactors is presented.

### 1.5.1. Slurry Reactors

In these reactors, catalysts are suspended in the form of fine particles. Depending on the mode by which the catalysts are suspended, these reactors are classified into four major classes as shown below:



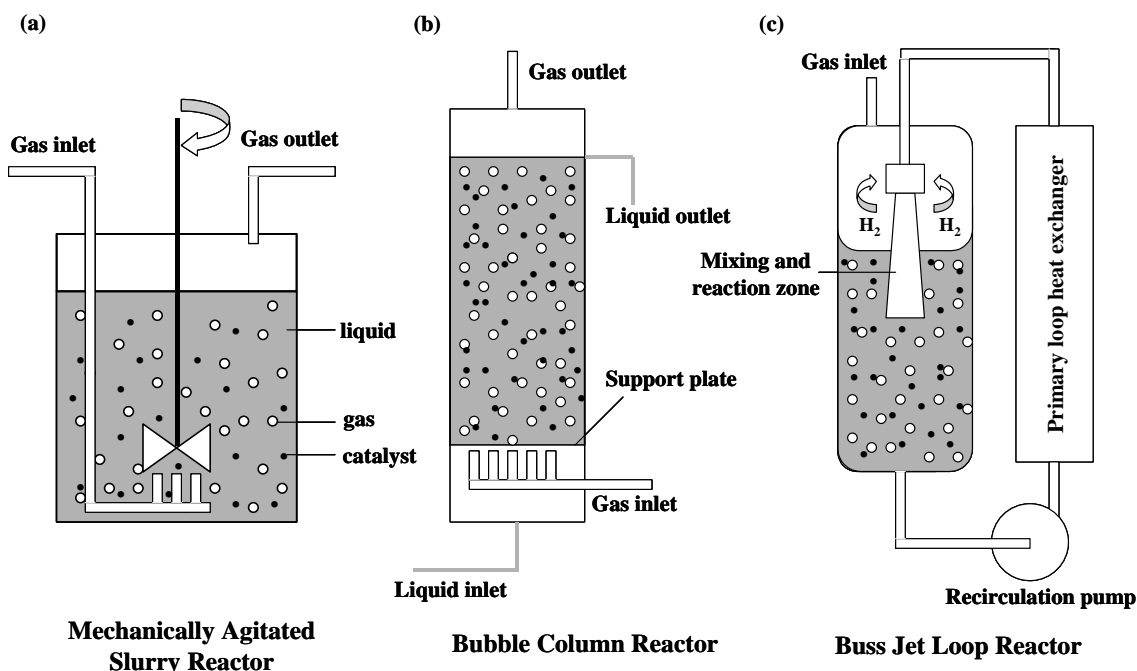
#### 1.5.1.1. Agitated Slurry Reactors

The agitated slurry reactors are most commonly used in industrial scale liquid phase hydrogenation, alkylation, oxidation reactions. The catalyst particles, which are commonly used in the powder form, are suspended by means of mechanical agitation. Due to the smaller particle size, intraparticle diffusion effects are negligible in these reactors. These reactors are preferred for mass transfer limited and highly exothermic reactions.

A mechanically agitated reactor is shown in Figure 1.8 (a). Small volume specialty chemicals are often synthesized in batch slurry reactors. A dead-end operation without discharging hydrogen is very common due to its safe operation. Agitated slurry reactors can also be operated in a semi batch mode where, the gas phase flows continuously through the system without any inflow or out flow of liquid phase. Semibatch slurry reactors are commonly used to evaluate catalyst performance and to determine the reaction kinetics of a particular reaction. A few studies on semibatch slurry reactor modeling of hydrogenation reactions are summarized in Table 1.11 and some examples are discussed here.

Jaganathan et al. reported the intrinsic kinetics of hydrogenation of *p*-nitrocumene to *p*-cumidine over supported Pd catalysts in a mechanically agitated slurry reactor. Intraparticle diffusion effects were studied using pelleted catalysts and equations for overall effectiveness factor were derived for Langmuir-Hinshelwood type kinetics. To verify the

applicability of the kinetic model experimentally, a semibatch slurry reactor model was developed for both isothermal and non-isothermal conditions.



**Figure 1.8.** Agitated slurry reactors

Rajashekharam et al. studied the kinetics of hydrogenation of 2,4-dinitrotoluene (2,4-DNT) in a semibatch slurry reactor using a 5% Pd/Al<sub>2</sub>O<sub>3</sub> catalyst at 323-363 K. A fundamental approach based on a molecular level description of the catalytic cycle was used to derive the rate models. It was found that the intraparticle diffusional effects were important for particle sizes ( $d_p$ )  $> 3 \times 10^{-4}$  m, but the external mass-transfer (g-l and l-s) effects were unimportant. For the complex rate equation observed, an approximate expression for the overall effectiveness factor was derived and the experimental data for different particle sizes were found to agree with the predictions of the model incorporating intraparticle diffusion effects. A mathematical model to predict the temperature and concentration profiles in a semibatch reactor under non-isothermal conditions had also been proposed.

Topinen et al. reported the kinetics and semibatch slurry reactor modeling for hydrogenation of benzene and three mono-substituted alkyl benzenes in a three-phase system. The analysis of the experimental data with a reaction-diffusion model revealed that the kinetics was influenced by pore diffusion. Rate equations based on a sequential

addition mechanism of adsorbed hydrogen to the aromatic nucleus was derived, and the kinetic parameters were estimated from the reaction-diffusion model with nonlinear regression analysis.

Rode et al had investigated the kinetics of catalytic hydrogenation of nitrobenzene to p-aminophenol in acidic medium in a batch slurry reactor at 323-353 K using a Pt/C catalyst. Based on the initial rate data in the kinetic regime and considering that the reaction was taking place in both organic as well as aqueous phases, a Langmuir-Hinshelwood type of rate equation was proposed. Since this was a four-phase system, the rate equation was suitably modified to include gas-liquid and liquid-liquid mass transfer steps.

#### **1.5.1.2. Bubble Column Reactors**

In this type of a reactor, gas passes through the liquid pool containing the fine catalyst particles and suspends it by the gas-induced agitation (Figure 1.8b). As very small catalyst particles are used, intraparticle diffusion limitations are negligible and maximum catalyst utilization is possible. Due to the high liquid hold-up, bubble column reactors are very much efficient in heat transfer also. Power requirement for operation is the lowest among the slurry reactors. Considerable back mixing and hence poor reactor performance are the major disadvantage of this reactor.

#### **1.5.1.3. Fluidized-bed Reactors**

In this reactor, gas bubble and liquid phase moves upward and induces catalyst suspension. Relatively larger catalyst particles are used in this reactor and the liquid flow is mainly responsible for the suspension. As there are no moving parts, similar to bubble column reactors, these reactors are also easy to design mechanically. Non-uniform catalyst distribution and hence poor reactor performance is a major disadvantage of fluidized-bed reactors.

**Table 1.11.** Reactor modeling studies in semi batch slurry reactors

Sr. No.	Reaction system	Catalyst	Conditions	Remarks	Ref.
1	p-nitrocumene to p-cumidine	1% Pd/Al <sub>2</sub> O <sub>3</sub>	0.5-2.2 MPa, 313-353 K	Methodology for development of slurry reactor model to predict isothermal and non-isothermal performances Kinetic model combined with mass transfer resistances	146
2	2,4-dinitrotoluene to 2,4-toluene-diamine	5% Pd/ Al <sub>2</sub> O <sub>3</sub>	0.34-2.75MPa, 323-363 K	Molecular level approach to kinetic modeling and non-isothermal effects	147
3	1,5,9-cyclododecatriene to cyclododecene	Pd/ Al <sub>2</sub> O <sub>3</sub>	0.3-1.2 MPa	Kinetic model was developed considering all the parallel isomerization and consecutive reactions	148
4	Phenylacetylene to ethyl benzene	0.1% Pd/C	2-7.5 MPa, 288-318K	L-H model developed under strong substrate inhibition conditions	149
5	Isooctenes to isooctane	0.3% Pt/Al <sub>2</sub> O <sub>3</sub>	10-40 bar, 353-413 K	Hydrogenation kinetics was combined with catalyst deactivation kinetics	150
6	Cinnamaldehyde	1-4% Ru/ Al <sub>2</sub> O <sub>3</sub>	283-333 K	A L-H rate equation considering two-site model was used to describe the kinetic experiments. Effect of Sn promoter on kinetic parameters were evaluated	151
7	Benzene to cyclohexane	16.6% Ni/Al <sub>2</sub> O <sub>3</sub>	20-40 bar, 368-398 K	Kinetics and reactor modeling in presence of significant pore diffusion was proposed.	152
8	Lactic acid to propylene glycol	5 % Ru/C	6.8-13.6 MPa, 403-423 K, Aqueous phase	Through mass transfer analysis showed that there was no transport limitations in the operating conditions.	153
9	Nitrobenzene to p-aminophenol	3% Pt/C	0.5-7 MPa, 323-353 K, g-l-l-s system	Langmuir-Hinshelwood type model was proposed considering the reaction took place in both organic as well as aqueous phase.	90b

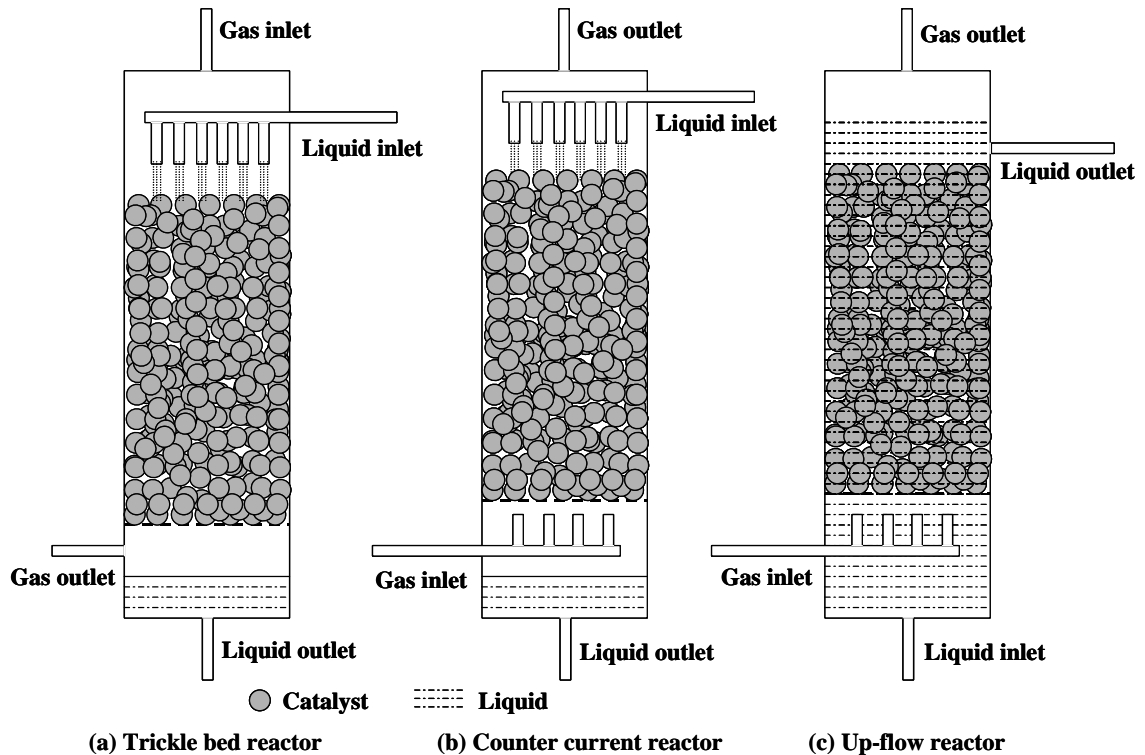


#### 1.5.1.4. Loop Recycle Reactors

In this reactor, the catalyst particles are suspended by means of liquid circulation through a jet using circulation pump or gas lift device (Figure 1.8c). Simple design, high heat and mass transfer efficiency are the advantages of this reactor. Unlike the other slurry reactors, loop recycle reactors are operated only in a batch mode.

#### 1.5.2. Fixed Bed Reactors

In a fixed bed reactor, the catalyst particles (average diameter range from 1/32 to 1/8 inches) are in a stationary phase and the gas-liquid mixture flows over the catalyst bed. Depending upon the mode of operation, these reactors can be classified into two classes, viz., (a) Trickle bed reactor which uses either co-current down flow or countercurrent flow of gas and liquid and (b) Packed bubble column reactor where cocurrent up flow of gas and liquid phases is used as shown in Figure 1.9.



**Figure 1.9.** Schematics of Different types of Fixed Bed Reactors

## 1.6. SCOPE OF THE PRESENT WORK

It is evident from the literature review presented here that even though extensive work on theoretical development of reaction rate/reactor performance models has been carried out, the experimental validation of models were limited. Particularly, the focus to analyze multistep, complex multiphase reactions has been inadequate. Considering the increasing importance of catalysis in complex catalytic reactions for fine chemicals, pharmaceuticals and specialty products, there is a need to investigate case studies on catalysis and reaction engineering aspects. At the same time, it is also important to explore new types of catalysts and catalytic systems, which can provide better activity, selectivity to the desired products. Considering the importance of catalysis and reaction engineering studies in hydrogenation reactions with complex reaction pathways, the following specific problems were chosen for the present work:

- ❖ Kinetics and modelling of a semi-batch slurry reactor under isothermal conditions and experimental and theoretical investigations on performance of a trickle bed reactor under non-isothermal conditions for reductive alkylation of aniline with acetone using Pd/Al<sub>2</sub>O<sub>3</sub> catalyst
- ❖ Analysis of a gas-liquid-liquid-solid catalytic system considering hydrogenation of aniline using Ru/Al<sub>2</sub>O<sub>3</sub> catalyst as a model reaction
- ❖ Synthesis of immobilized Pt and Pd metal nanoparticles and its catalytic applications for hydrogenation and Heck coupling reactions

## REFERENCES

1. Elango, V.; Davenport, K. G. Method for producing ibuprofen. EP 400892, 1990.
2. Sheldon, R.A. Fine chemicals by catalytic oxidation. *CHEMTECH*, **1991**, 566.
3. (a) Romano, U.; Rivetti, F.; Nicola, D. M. Process for producing dimethylcarbonate. US 4318862, 1981. (b) Romano, U.; Tesei, R.; Mauri, M. M.; Rebora, P. Synthesis of dimethyl carbonate from methanol, carbon monoxide, and oxygen catalyzed by copper compounds. *Ind. Eng. Chem. Proc. Res. Dev.* **1980**, *19*(3), 396.
4. Knowles, W. S.; Sabacky, M. J.; Vineyard, B. D. L-Dopa process and intermediates. US 4005127, 1977.
5. Ratton, S. Heterogeneous catalysis in the fine chemicals industry. From dream to reality. *Chem. Today*, **1998**, *16*(3/4), 33.
6. (a) Mills, P. L.; Ramachandran, P. A.; Chaudhari R. V. Multiphase reaction engineering for fine chemicals and pharmaceuticals. *Rev. Chem. Eng.*, **1992**, *8*, 1. (b) Ramachandran P. A.; Chaudhari R. V. Three phase catalytic reactors, Gordon Breach Science Publishers, New York, 1983. (c) Carpenter K. J. Chemical reaction engineering aspects of fine chemicals manufacture, *Chem. Eng. Sc.*, **2001**, *56*, 305.
7. (a) Rajashekharan, M. V.; Nikalje, D. D.; Jaganathan, R.; Chaudhari, R. V. Hydrogenation of 2,4-dinitrotoluene using a Pd/Al<sub>2</sub>O<sub>3</sub> catalyst in a slurry reactor: a molecular level approach to kinetic modeling and nonisothermal effects. *Ind. Eng. Chem. Res.*, **1997**, *36*(3), 592. (b) Benaissa, M.; Le Roux, G. C.; Joulia, X.; Chaudhari, R. V.; Delmas, H. Kinetic modeling of the hydrogenation of 1,5,9-cyclododecatriene on Pd/Al<sub>2</sub>O<sub>3</sub> catalyst including isomerization. *Ind. Eng. Chem. Res.*, **1996**, *35*(7), 2091. (c) Lylykangas, M. S.; Rautanen, P. A.; Krause, A. O. I. Hydrogenation and Deactivation Kinetics in the Liquid-Phase Hydrogenation of Isooctenes on Pt/Al<sub>2</sub>O<sub>3</sub>. *Ind. Eng. Chem. Res.*, **2004**, *43*(7), 1641. (d) Chaudhari, R. V.; Jaganathan, R.; Kolhe, D. S.; Emig, G.; Hofmann, H. Kinetic modeling of a complex consecutive reaction in a slurry reactor: hydrogenation of phenyl acetylene. *Chem. Eng. Sci.*, **1986**, *41*(12), 3073.
8. Bonnemann, H.; Brijoux, W.; Tilling, A. S.; Siepen, K. Application of heterogeneous colloid catalysts for the preparation of fine chemicals. *Top. Catal.*, **1998**, *4*(3,4), 217.
9. Kukula, P.; Cerveny, L. The kinetics of methyl sorbate hydrogenation. *Appl. Catal., A*, **1999**, *177*(1), 79.
10. Mori, T.; Matsuo, N. Preparation of trans-3-(1-propynyl)-2,2-dimethylcyclopropanecarboxylate compounds. EP 955287, 1999.
11. Broecker, F.-J.; Arnold, L.; Grafen, P. Palladium catalysts, their preparation, and their use as hydrogenation catalysts. EP 412415, 1991 by BASF.
12. (a) Zajacek, J. G.; Shum, W. P. Hydroformylation process and rhodium-dimethyl(alkyl)phosphine catalysts for the manufacture of 1,4-butanediol from allyl alcohol and synthesis gas. WO 00/63143, 2000 by Arco Chemical Technology. (b) Chen, S. C.; Chu, C. C.; Lin, F. S.; Chou, J. Y.; Huang, C. C. Modified Raney nickel catalyst and a process for preparing diols by using the same. US 5888923, 1999 by Dairen Chemical Corporation, Taiwan.
13. (a) Blaser, H.-U.; Studer, M. Critical issues for using enantioselective catalysis for fine chemicals production. *Chirality*, **1999**, *11*(5/6), 459. (b) Chen, B.; Dingerdissen, U.; Krauter, J. G. E.; Lansink Rotgerink, H. G. J.; Moebus, K.; Ostgard, D. J.; Panster, P.; Riermeier, T. H.; Seebald, S.; Tacke, T.; Trauthwein, H. New developments in hydrogenation catalysis particularly in synthesis of fine and intermediate chemicals. *Applied Catalysis A: General*, **2005**, *280*(1), 17.
14. Ashina, Y.; Fujita, T.; Fukatsu, M.; Yagi, J. Dimethylamine. EP 130407 A1, 1985 by Nitto Chemical Industry Co., Ltd., Japan.
15. Studer, M.; Baumeister, P. Process for the catalytic hydrogenation of aromatic nitro compounds. WO 9636597, 1996 by Ciba Geigy AG.
16. Auer, E.; Freund, A.; Gross, M.; Hartung, R. Multimetallic catalyst and method for production of substituted aromatic amines. US 6316381, 1998 by Degussa AG.
17. Mitsui, O.; Fukuoka, Y. Process for producing cycloolefins. US 4678861, 1987 by Asahi Chemical Industry Co., Ltd., Japan
18. Ross, S. K.; Meehan, N. J.; Poliakoff, M.; Daniel N. Supercritical hydrogenation of substrates. WO 2002081414, 2002 by Thomas Swan & Co. Ltd., UK.
19. Chen, B.; Dingerdissen, U.; Krauter, J. G. E.; Lansink Rotgerink, H. G. J.; Moebus, K.; Ostgard, D. J.; Panster, P.; Riermeier, T. H.; Seebald, S.; Tacke, T.; Trauthwein, H. New developments in hydrogenation catalysis particularly in synthesis of fine and intermediate chemicals. *App. Cat. A: Gen.*, **2005**, *280*(1), 17.

- 
20. (a) Ertl, G.; Knoezinger, H.; Ed. Handbook of Heterogeneous Catalysis, 5 Volume Set. (Wiley-VCH: Weinheim, Germany), 2800, 1997. (b) Augustine, R. L. Heterogeneous catalysis for synthetic chemist. Marcel Dekker, New York, 1996.
21. Baily, S.; King, F. catalytic hydrogenation and dehydrogenation. Fine chemicals through heterogeneous catalysis. Sheldon, R. A.; van Bekkum, H. (Ed.), Wiley-VCH, 351, 2001.
22. Stiles, A. B. Catalyst support and supported catalysts. Ed. Stiles, A. B., Butterworths, Boston, 1987, 87
23. Augustine, R. L. Heterogeneous catalysis for the synthetic chemist, Marcel Dekker, New York, 153, 1996.
24. Bond, G. C.; Burch, R. Strong metal-support interactions. *Catalysis*, **1983**, 6, 27,.
25. Weigle J. C.; Phillips J. Novel Dual-Bed Reactors: Utilization of Hydrogen Spillover in Reactor Design. *Langmuir*, **2004**, 20(4), 1189.
26. Rode C. V.; Chaudhari R. V. Hydrogenation of m-nitrochlorobenzene to m-chloroaniline: reaction kinetics and modeling of a non-isothermal slurry reactor. *Ind. Eng. Chem. Res.*, **1994**, 33, 1645.
27. Rajashekharam M. V.; Nikhalje D. D.; Jaganathan R.; Chaudhari R. V. Hydrogenation of 2,4-Dinitrotoluene using a Pd/Al<sub>2</sub>O<sub>3</sub> catalyst in a slurry reactor: A molecular level approach to kinetic modeling and nonisothermal effects. *Ind. Eng. Chem. Res.*, **1996**, 35, 1824.
28. Jaganathan R.; Ghugikar V. G.; Gholap R. V.; Chaudhari R. V.; Mills P. L. Catalytic hydrogenation of p-nitrocumene in a slurry reactor, *Ind. Eng. Chem. Res.*, **1999**, 38, 4634.
29. Gianetto, A.; Baldi, G.; Specchia, V.; Sicardi, S. Hydrodynamics and solid-liquid contacting effectiveness in trickle-bed reactors. *AIChE J.*, **1978**, 24(6), 1087 and the references thereof.
30. Ng K. M.; Chu C. F. Trickle-bed reactors. *Chem. Eng. Prog.*, Nov. **1987**, 55.
31. Augustine, R. L. Selective heterogeneously catalyzed hydrogenations. *Catal. Today*, **1997**, 37, 419. (b) Rase, H. F. handbook of commercial catalysts. CRC publication, Florida. 131, 2000.
32. Blaser, H.-U.; Indolese, A.; Schnyder, A.; Steiner, H.; Studer, M. Supported palladium catalysts for fine chemicals synthesis. *J. Mol. Catal. A: Chemical*, **2001**, 173(1-2), 3. (b) Yamada, H.; Urano, H.; Goto, S. Selective hydrogenation of unsaturated aldehyde in gas-liquid-liquid-solid four phases. *Chem. Eng. Sci.*, **1999**, 54(21), 5231.
33. (a) Rylander, P. N. Hydrogenation methods. Bench top edition, Academic Press, New York, 29, 1990. (b) Telkar, M. M.; Rode, C. V.; Rane, V. H.; Jaganathan, R.; Chaudhari, R. V. Selective hydrogenation of 2-butyne-1,4-diol to 2-butene-1,4-diol: roles of ammonia, catalyst pretreatment and kinetic studies. *App. Cat., A: Gen.*, **2001**, 216(1-2), 13. (c) Telkar, M. M.; Rode, C. V.; Jaganathan, R.; Rane, V. H.; Chaudhari, R. V. Platinum catalyzed hydrogenation of 2-butyne-1,4-diol. *J. Mol. Catal. A: Chemical*, **2002**, 187(1), 81.
34. (a) Liang, S.; Fischer, R. H.; Pinkos, R.; Stein, F.; Breitscheidel, B. Hydrogenation process and catalysts for the manufacture of 1,6-hexanediol from adipic acid diesters and/or 6-hydroxyhexanoic acid esters. DE 19757554, 1999 by BASF, Germany. (b) Hirayama, H. Preparation of alcohols from catalytic hydrogenation of carbonyl compounds. JP 07206737, 1995 by Showa Denko Kk, Japan.
35. (a) Ostgard, D.; Bender, B.; Berweiler, M.; Moebus, K.; Stein, G. Fixed bed catalysts. US 6284703, 2002 by Degussa AG. (b) Chaudhari, R. V.; Rode, C. V.; Deshpande, R. M.; Jaganathan, R.; Leib, T. M.; Mills, P. L. Kinetics of hydrogenation of maleic acid in a batch slurry reactor using a bimetallic Ru-Re/C catalyst. *Chem. Eng. Sci.*, **2003**, 58(3-6), 627. (c) Thakar, N. N.; Jaganathan, R.; Chaudhari, R. V.; Mills, P. L. Modeling of hydrogenation of maleic acid in a bubble-column slurry reactor. *AIChE Journal*, **2003**, 49(12), 3199.
36. (a) Yokoyama, T.; Yamagata, N. Hydrogenation of carboxylic acids to the corresponding aldehydes. *App. Cat., A: Gen.*, **2001**, 221(1-2), 227. (b) Yokoyama, T.; Setoyama, T. Carboxylic acids and derivatives. Fine chemicals through heterogeneous catalysis, 370, ed: Sheldon R. A.; van Bekkum, H. Wiley-VCH Verlag GmbH: Weinheim, Germany, 2001.
37. (a) De Bellefon, C.; Fouilloux, P. Homogeneous and heterogeneous hydrogenation of nitriles in a liquid phase: chemical, mechanistic, and catalytic aspects. *Catal. Rev. - Sci. Eng.*, **1994**, 36(3), 459. (d) Augustine, R. L. hydrogenation VI: nitrogen containing functional groups. (Heterogeneous catalysis for the synthetic chemist, Marcel Dekker, New York.) 473, 1996. (e) Rase, H. F. handbook of commercial catalysts. CRC publication, Florida. 138, 2000.
38. (a) Ostgard, D.; Berweiler, M.; Roeder, S. Production of primary and secondary amines by hydrogenation of nitriles and imines using Raney-type catalysts in the form of hollow bodies. WO 2002051791, 2002 by Degussa A.-G., Germany. (b) Gavroy, D.; Joly-Vuillemin, C.; Cordier, G.; Fouilloux, P.; Delmas, H.

- Continuous hydrogenation of adiponitrile on Raney nickel in a slurry bubble column. *Catal. Today*, **1995**, 24(1-2), 103.
39. (a) Notheisz, F.; Bartok, M. Hydrogenolysis of C-O, C-N and C-X bonds. Fine chemicals through heterogeneous catalysis. Wiley-VCH, Sheldon, R. A.; van Bekkum, H. (Ed.), 415, 2000. (b) Greene, T. W.; Wuts, P. G. M. protective groups in organic synthesis. Wiley-VCH, Newyork, 1991.
40. Augustine, R. L. Heterogeneous catalysis for the synthetic chemist. Dekker, New York, 1996.
41. (a) Gallezot, P.; Richard, D. Selective hydrogenation of  $\alpha,\beta$ -unsaturated aldehydes. *Catal. Rev. - Sci. Eng.*, **1998**, 40(1-2), 81. (b) Ref. 28(b)
42. (a) Galvagno, S.; Donato, A.; Nerl, G.; Pietropaolo, T. Hydrogenation of cinnamaldehyde over platinum catalysts: influence of addition of metal chlorides. *J. Mol. Catal.* **1989**, 49, 223. (b) Gallezot, P.; Cerino, P. J.; Blanc, B.; Fleche, G.; Fuertes, P. J. Glucose hydrogenation on promoted Raney-nickel catalysts. *J. Catal.*, **1994**, 146(1), 93.
43. (a) Saeki, K.; Shima, K. Preparation of aromatic carbinols from aromatic ketones. JP 02062837, 1990 by Daicel Chemical Industries, Ltd., Japan. (b) De Thomas, W. R.; Hort, E. V. Catalyst comprising Raney nickel with adsorbed molybdenum compound. US 4153578, 1979 by GAF Corp (c) Herskowitz, M. hydrogenation of benzaldehyde to benzyl alcohol in a slurry and fixed bed reactor. *Stud. Surf. Sci. Catal.*, **1991**, 59, Ed. Guisnet, M. et al. Elsevier Science Publishers B. V., Amsterdam.
44. (a) Blaser, H. U.; Jalett, H. P.; Muller, M.; Studer, M. Enantioselective hydrogenation of  $\alpha$ -ketoesters using cinchona modified platinum catalysts and related systems: a review. *Catal. Today*, **1997**, 37(4), 441. (b) Garland, M.; Jalett, H. P.; Blaser, H. U. Mass transfer considerations for the enantioselective hydrogenation of  $\alpha$ -keto esters catalyzed by cinchona modified platinum/alumina. *Stud. Surf. Sci. Catal.*, **1991**, 59 (Heterog. Catal. Fine Chem. 2), 177.
45. Augustine, R. L. hydrogenation VI: nitrogen containing functional groups. (Heterogeneous catalysis for the synthetic chemist, Marcel Dekker, New York,) 473, 1996.
46. (a) Siegrist, U.; Baumeister, P.; Blaser, H.-U.; Studer, M. The selective hydrogenation of functionalized nitroarenes: new catalytic systems. *Chem. Ind. (Dekker)*, 75(Catalysis of Organic Reactions), 207, 1998. (b) Chen, B.; Dingerdissen, U.; Krauter, J. G. E.; Lansink Rotgerink, H. G. J.; Moebus, K.; Ostgard, D. J.; Panster, P.; Riermeier, T. H.; Seebald, S.; Tacke, T.; Trauthwein, H. New developments in hydrogenation catalysis particularly in synthesis of fine and intermediate chemicals. *Applied Catalysis A: General*, **2005**, 280(1), 17.
47. (a) Ref. 40c (b) Geus, J. W. energetics of hydrogen adsorption on porous and supported metals. (Hydrogenation effects in catalysis) Ed. Pall, Z.; Menon, P. G. Marcel Dekker Inc., New York, 85, 1988.
48. (a) Texier-Boullet, F. A simple, convenient and mild synthesis of imines on an alumina surface without solvent. *Synthesis*, **1985**, 6-7, 679. (b) Ross, L. J.; Levy, S. D. Reductive alkylation of substituted anilines. US 4261926, 1981 by American Cyanamid Co., USA.
49. Gilbert, S.; Brizzolara, A.; Landesman, H.; Szmuszkovicz, J.; Terrell, R. The enamine alkylation and acylation of carbonyl compounds. *J. Amer. Chem. Soc.*, **1965**, 85, 207.
50. Taguchi, K.; Westheimer, F. H. Catalysis by molecular sieves in the preparation of ketimines and enamines. *J. Org. Chem.*, **1971**, 36(11), 1570.
51. (a) Kaneko, M., Tanaka, S. Method of manufacturing alkylaniline compounds. European Patent 760360, 1997 by Konica Corporation, Japan (b) Nishimura, T., Takeda, F., Wada, M., kanemura, Y. Preparation of N-alkyl-Substituted aromatic amines. JP 2000095739, 2000 by Mitsui Chemicals Inc., Japan.
52. Greenfield, H.; Malz, R. E. Jr. *Catalysis of organic reactions*, Ed. Kosak, J. R. Marcel Dekker, New York. 1984, 309.
53. Bonds, A. P.; Greenfield, H. The reductive alkylation of aromatic amines with formaldehyde. *Catalysis of organic reactions*, Ed. Pascoe, W. E. Marcel Dekker, New York. **1991**, 47, 65.
54. de Angelis, A.; Ingallina, P.; Perego, C. Solid acid catalysts for industrial condensations of ketones and aldehydes with aromatics. *Ind. & Eng. Chem. Res.*, **2004**, 43(5), 1169.
55. Archer, S.; Lewis, T. R.; Unser, M. J.; Hoppe, J. O.; Lape, H. 1 -Ethyl-4-(3-tropanyl) -tetrahydro-1 H-1,4-benzodiazepine. *J. Amr. Chem. Soc.*, **1957**, 79, 5783.
56. Emerson, W. S. *Organic reactions*, **1948**, 4, 174.
57. (a) Stieber, J.; Reynolds, M. Impurity formation during the reductive alkylation of aniline with methyl isoamyl ketone. *Catalysis of organic reactions*, Ed. Pascoe, W. E. Marcel Dekker, New York. **1991**, 47, 87.

- (b) Greenfield, H. Side reactions in reductive alkylation of aromatic amines with aldehydes and with ketones. *Catalysis of organic reactions*, **1995**, 53, 265.
58. (a) Klyuev M. V.; Bulatov A. V.; Kushch L. A.; Khidekel M. L. Method of preparing n-alkylaromatic amines. SU Patent 802264, 1981, By Institute of chemical physics, USSR. (b) Harada T.; Arita H. Preparation of N-alkylaminodiarylamine. JP 55139343, 1980 by Mitsui Petrochemical Ind. (c) Yoshigaki S.; Ando S.; Otsuki T.; Kawasaki T. Production Of N-Alkyl-N'-Phenyl-P-Phenylenediamines as stabilizers for rubbers. JP 63051362, 1988 by Ouchi Shinko Chemical Industrial Co. Ltd., Japan.
59. (a) Fache, F.; Jacquot, L.; Lemaire, M. Extension of the Eschweiler-Clarke procedure to the N-alkylation of amides. *Tetrahedron Lett.*, **1994**, 35(20), 3313. (b) Fache, F.; Bethmont, V.; Jacquot, L.; Valot, F.; Milenkovic, A.; Lemaire, M. Reductive O- and N-alkylations. Alternative catalytic methods to nucleophilic substitution. *Stud. Surf. Sci. Catal.*, **1997**, 108(Heterogeneous Catalysis and Fine Chemicals IV), 115.
60. (a) Zhou, X., Wu, Zuwang, Lin, L., Wang, G., Li, J. Synthesis of N-ethyl-m-toluidine from m-nitrotoluene by reductive alkylation. *Dyes Pigm.*, **1998**, 36 (4), 365. (b) Zhou, X., Wu, Zuwang, Lin, L., Wang, G. Studies on the selective synthesis of N-monoalkyl aromatic amines. *Dyes Pigm.*, **1999**, 40(2-3), 205. (c) Simon, J., Becker, R., Lebjucher, R., Neuhauser, H. Catalytic N-alkylation of amines with alcohols. EP 863140, **1998** by BASF-AG, Germany. (d) Su, B., Barthomeuf, D. Effect of reaction temperature on the alkylation of aniline by methanol over almost neutral zeolites LiY and NaY. *Stud. Sur. Sc. Catal.* (Catalysis by microporous materials): Elsevier Science. **1995**, 94, 598.
61. Rusek M. Effect of promoters on Pt/SiO<sub>2</sub> catalysts for the N-alkylation of sterically hindered anilines in the vapor phase. *Het. Cat. and fine chem. II*, Elsevier Science Publishers B. V., Amsterdam. **1991**, 359.
62. Narayanan, S.; deshpande, K. aniline alkylation over solid acid catalysts. *App. Catal. A: General*, **2000**, 199, 1.
63. Rusek M. Effect of promoters on Pt/SiO<sub>2</sub> catalysts for the N-alkylation of sterically hindered anilines in the vapor phase. *Het. Cat. and fine chem. II*, Elsevier Science Publishers B. V., Amsterdam. **1991**, 359.
64. Su, B., Barthomeuf, D. Effect of reaction temperature on the alkylation of aniline by methanol over almost neutral zeolites LiY and NaY. *Studies in surface science and catalysis* (Catalysis by microporous materials): Elsevier Science. **1995**, 94, 598.
65. Kaneko, M., Tanaka, S. Method of manufacturing alkylaniline compounds. EP 760360, 1997 by Konica Corporation, Tokyo, Japan.
66. Nishimura, T., Takeda, F., Wada, M., kanemura, Y. Preparation of N-alkyl-Substituted aromatic amines. JP 2000095739, 2000 by Mitsui Chemicals Inc.
67. Lehtonen, J. Salmi, T., Vuori, A., Tirronen, E. On the principles of modeling of homogeneous-heterogeneous reactions in the production of fine chemicals. A case study: Reductive alkylation of aromatic amines. *Org. Process Res. Dev.*, **1998**, 2(2), 78.
68. Salmi, T., Lehtonen, J., Kaplin, J., Vuori, A., Tirronen, E., Haario, H. A homogeneous-heterogeneously catalyzed reaction system in a loop reactor. *Catal. Today*, **1999**, 48(1-4), 139.
69. Wilson, Jr. Modified nickel catalyst systems and their use in reductive alkylation reactions. US 4043942, 1977 by Goodyear Tire and Rubber Co., Ohio.
70. Ross, L. J.; Levy, S. D. Reductive alkylation of substituted anilines. US 4261926, 1981 by American Cyanamid Company, Stanford.
71. Watanabe, T. Preparation of di-(substituted amino) diphenylamines as antioxidants and antiozonants for polymers. JP 10168038, 1998 by Yanai Kagaku Kogyo K. K., Japan.
72. Malz, R. E. Jr.; Jancis, E. H.; Reynolds, M. P.; O'Leary, S. T. Reductive alkylation of acetophenone with aniline. *Chem. Ind. (Dekker)*, **1995**, 62 (Catalysis of organic reactions), 263.
73. Hiskey R. G.; Northrop R. C. Azomethine chemistry. I. Formation of optically active  $\alpha$ -amino acids by asymmetric induction. *J. Amr. Chem. Soc.*, **1961**, 83, 4798.
74. Merten, H. L.; Baclawski, L. M. Process for producing N, N'-disubstituted paraphenylene diamine mixtures by sequential reductive alkylation. US 4900868, 1990 by Monsanto Company.
75. Vogel, C.; Aebi, R. Herbicidal and plant growth inhibiting agent. US 4324580, 1982 by Ciba-Geigy Corporation, Newyork.
76. Rylander, P. N. Catalytic hydrogenation over platinum metals. Academic Press, New York. 277, 1967.
77. Malone, R. J.; Merten, H. L. A comparative mass transfer study in the reductive N-alkylation of aromatic nitro compounds. *Catalysis of organic reactions*, Ed. Pascoe, W. E. Marcel Dekker, New York. **1991**, 47, 79.

- 
78. (a) Augustine, R. L. Hydrogenation IV: Aromatic compounds. (Heterogeneous catalysis for the synthetic chemist) Marcel Dekker, New York, 1996, 403. (b) Rase, H. F. handbook of commercial catalysts. CRC publication, Florida. 2000, 120. (c) Sheldon, R. A.; van Bekkum, H. Fine chemicals through heterogeneous catalysis. Wiley-VCH, Sheldon, R. A.; van Bekkum, H. (Ed.), 2000, 407. (d) Sanati, M.; Harrysson, B.; Faghihi, M.; Gevert, B.; Jaras, S. Catalytic hydrodearomatization. *Catalysis*, **2002**, *16*, 1.
79. Boettcher, A.; Henkelmann, J.; Funke, F. Hydrogenation of aromatics using catalyst with macroporous support. WO 00/63142, 2000 by BASF A.-G., Germany.
80. (a) Mitsui, O.; Fukuoka, Y. Process for producing a cycloolefin. US 4678861 by Asahi Chemical Ind., 1987. (b) Nagahara, H.; Konishi, M. Process for producing cycloolefins. US 4734536 by Asahi Chemical Ind., 1988.
81. Rutter, H.; Ruhl, T.; Breitscheidel, B.; Henkelmann, J.; Henne, A.; Wettling, T. Hydrogenation of aromatic compounds in which at least one amino group is bonded to an aromatic nucleus using ruthenium catalysts. US 5773657, 1998 by BASF A.-G., Germany.
82. Immel, O.; Darsow, G.; Waldmann, H.; Petruck, G. M. Supported noble metal catalysts and their preparation and use in manufacture of mixture of mono- and dicyclohexylamines. EP 501265, 1992 by Bayer A.-G., Germany.
83. Kuhn, W. Method for producing cis-2-tert-butylcyclohexanol by the stereoselective catalytic hydrogenation 2-tert-butylphenol in the presence of 2-tert-butylcyclohexyl acetates. WO 2002048079 A2, 2002 by Haarmann & Reimer, Germany).
84. Joris, G. G.; Vitrone Jr., J. Hydrogenation of phenol. US 2829166, 1958 by Allied chemical and Dye Corporation, New York.
85. (a) Giffels, G.; Diehl, H.; Martin, Georg; Frohn, L.; Hammerschmidt, Erich Process for the preparation of piperidines from activated pyridines using chemoselective palladium hydrogenation catalysts. EP1153918, 2001 by Bayer A.-G., Germany.
86. Pinkos, R.; Fischer, R. Process for preparation of 1,4-butanediol and tetrahydrofuran from furan. WO 9629322, 1996 by BASF A.-G., Germany.
87. (a) Hartog, F. Preparation of cyclic alkenes. US 3391206, 1968 by Stamicarbon, Netherlands. (b) Odenbrand, C. U. I.; Lundin, S. T. Hydrogenation of benzene to cyclohexene on an unsupported ruthenium catalyst: effect of poisons. *J. Chem. Technol. Biotechnol.*, **1981**, *31*, 660.
88. Drinkard W. C. Selective hydrogenation of aromatic compounds to cycloolefinic compounds. GB 1381048, 1972 by Dupont de Nemours, USA.
89. (a) Struijk, J.; Moene, R.; Van der Kamp, T.; Scholten, J. J. F. Partial liquid-phase hydrogenation of benzene to cyclohexene over ruthenium catalysts in the presence of an aqueous salt solution. II. Influence of various salts on the performance of the catalyst. *Appl. Catal. A: General*, **1992**, *89*(1), 77. (b) Ronchin, L.; Toniolo, L. Selective hydrogenation of benzene to cyclohexene using a suspended Ru catalyst in a mechanically agitated tetraphase reactor. *Catal. Today*, **1999**, *48*(1-4), 255. (d) Augustine, R. L. (Heterogeneous catalysis for the synthetic chemist) Marcel Dekker, New York, 1996, 403.
90. (a) Rode, C. V.; Vaidya, M. J.; Jaganathan, R.; Chaudhari, R. V. Hydrogenation of nitrobenzene to p-aminophenol in a four-phase reactor: Reaction kinetics and mass transfer effects. *Chem. Eng. Sc.*, **2001**, *56*(4), 1299. (b) Rode, C. V.; Vaidya, M. J.; Chaudhari, R. V. Synthesis of p-Aminophenol by Catalytic Hydrogenation of Nitrobenzene. *Org. Process Res. Dev.*, **1999**, *3*(6), 465. (c) Caskey, D. C.; Chapman, D. W. p-Aminophenol and alkyl-substituted p-aminophenol. US 4571437, 1986 by Mallinckrodt, Inc., USA.
91. (a) Satagopan, V.; Chandalia, Sampatraj B. Selectivity aspects in the multi-phase hydrogenation of  $\alpha,\beta$ -unsaturated aldehydes over supported noble metal catalysts: part I. *J. Chem. Technol. Biotechnol.*, **1994**, *59*(3), 257. (b) Satagopan, V.; Chandalia, Sampatraj B. Selectivity aspects in the multiphase hydrogenation of  $\alpha,\beta$ -unsaturated aldehydes over supported noble metal catalysts: Part III. *J. Chem. Technol. Biotechnol.*, **1994**, *60*(1), 17.
92. (a) Yamada, H.; Tagawa, T.; Goto, S. Hydrogenolysis for deprotection of amino acid in a stirred tank reactor containing gas-liquid-liquid-solid four phases. *J. Chem. Eng. Jpn.*, **1996**, *29*(2), 373. (b) Yamada, H.; Goto, S. Periodic operation of trickle bed reactor for hydrogenolysis in gas-liquid-liquid-solid four phases. *J. Chem. Eng. Jpn.*, **1997**, *30*(3), 478. (c) Yamada, H.; Goto, S. Continuous operation of upflow reactors for hydrogenolysis in gas-liquid-liquid-solid four phases. *J. Chem. Eng. Jpn.*, **1997**, *30*(4), 769. (d) Yamada, H.; Goto, S. Gas and liquid holdups in multi-stage bubble columns for gas-liquid-liquid-solid four-phase system. *J. Chem. Eng. Jpn.*, **1998**, *31*(5), 813.

93. Gupte, S. P.; Krishnamurthy, V. P.; Chaudhari, R. V. Kinetics and mechanism of carbonylation of allyl chloride using a Pd catalyst: a case of gas-liquid-liquid-solid catalytic reaction. *Chem. Eng. Sci.*, **1996**, *51*(10), 2069.
94. (a) Thomas, J. M.; Johnson, B. F. G.; Raja, R.; Sankar, G.; Midgley, P. A.; High-Performance Nanocatalysts for Single-Step Hydrogenations. *Acc. Chem. Res.*, **2003**, *36*(1), 20. (b) Raimondi, F.; Scherer, G. G.; Koetz, R.; Wokaun, A. Nanoparticles in energy technology: Examples from electrochemistry and catalysis. *Angew. Chem., Int. Ed.*, **2005**, *44*(15), 2190. (c) Moreno-Manas, M.; Pleixats, R. Formation of Carbon-Carbon Bonds under Catalysis by Transition-Metal Nanoparticles. *Acc. Chem. Res.*, **2003**, *36*(8), 638. (d) Raja, R.; Thomas, J. M. Shape-selective regiospecific and bifunctional nanoporous catalysts for single step solvent free processes. *Nanotechnology in Catalysis*, **2004**, *1*, 249. Ed: Zhou, B; Hermans, S; Somorjai, G A. Kluwer Academic/Plenum Publishers: New York. (e) Lewis, L. N. Chemical catalysis by colloids and clusters. *Chem. Rev.*, **1993**, *93*, 2693. (f) Haruta, M. When gold is not noble: Catalysis by nanoparticles. *Chemical Record*, **2003**, *3*(2), 75.
95. Bell, A. T. The Impact of Nanoscience on Heterogeneous Catalysis. *Science*, **2003**, *299*(5613), 1688.
96. (a) Raimondi, F.; Scherer, G. G.; Koetz, R.; Wokaun, A. Nanoparticles in energy technology: Examples from electrochemistry and catalysis. *Angewandte Chemie, International Edition*, **2005**, *44*(15), 2190. (b) Link, S.; El-Sayed, M. A. Optical properties and ultrafast dynamics of metallic nanocrystals. *Ann. Rev. Phys. Chem.*, **2003**, *54*, 331.
97. Dahl, S.; Logadottir, A.; Egeberg, R. C.; Larsen, J. H.; Chorkendorff, I.; Tornqvist, E.; Norskov, J. K. Role of Steps in N<sub>2</sub> Activation on Ru(0001). *Phys. Rev. Lett.*, **1999**, *83*(9), 1814.
98. Willner, I.; Mandler, D. Characterization of palladium- $\beta$ -cyclodextrin colloids as catalysts in the photosensitized reduction of bicarbonate to formate. *J. Am. Chem. Soc.*, **1989**, *111*(4), 1330.
99. Roucoux, A.; Schulz, J.; Patin, H. Reduced transition metal colloids: A novel family of reusable catalysts? *Chem. Rev.*, **2002**, *102*(10), 3757.
100. Burda, C.; Chen, X.; Narayanan, R.; El-Sayed, M. A. Chemistry and properties of nanocrystals of different shapes. *Chem. Rev.*, **2005**, *105*(4), 1025.
101. Aiken, J. D., III.; Finke, R. G. A review of modern transition-metal nanoclusters: their synthesis, characterization, and applications in catalysis. *J. Mol. Catal. A: Chem.*, **1999**, *145*(1-2), 1.
102. (a) Teranishi, T.; Miyake, M. Size control of palladium nanoparticles and their crystal structures. *Chem. Mater.*, **1998**, *10*(2), 594. (b) Bonet, F.; Delmas, V.; Grugeon, S.; Urbina, R. Herrera; Silvert, P-Y.; Tekaiia-Elhsissen, K. Synthesis of monodisperse Au, Pt, Pd, Ru and Ir nanoparticles in ethylene glycol. *Nanostruct. Mater.*, **2000**, *11*(8), 1277.
103. (a) Boutonnet, M.; Kizling, J.; Stenius, P.; Maire, G. The preparation of monodisperse colloidal metal particles from microemulsions. *Colloids Surf.*, **1982**, *5*(3), 209. (b) Ahmadi, T. S.; Wang, Z. L.; Green, T. C.; Henglein, A.; El-Sayed, M. A. Shape-controlled synthesis of colloidal platinum nanoparticles. *Science*, **1996**, *272*(5270), 1924.
104. (a) Zhao, M.; Crooks, R. M. Homogeneous hydrogenation catalysis with monodisperse, dendrimer-encapsulated Pd and Pt nanoparticles. *Angew. Chem., Int. Ed.*, **1999**, *38*(3), 364. (b) Masaru T.; Hisashi F. Chiral Bisphosphine BINAP-Stabilized Gold and Palladium Nanoparticles with Small Size and Their Palladium Nanoparticle-Catalyzed Asymmetric Reaction. *J. Am. Chem. Soc.*, **2003**, *125*, 15742.
105. Boudjahem, A. G.; Monteverdi, S.; Mercy, M.; Bettahar, M. M. Study of nickel catalysts supported on silica of low surface area and prepared by reduction of nickel acetate in aqueous hydrazine. *J. Catal.*, **2004**, *221*(2), 325.
106. Mandal, Saikat; Selvakannan, P. R.; Roy, Debdut; Chaudhari, Raghunath V.; Sastry, Murali A new method for the synthesis of hydrophobized, catalytically active Pt nanoparticles. *Chem. Comm.*, **2002**, (24), 3002.
107. (a) Harriman, A.; Thomas, J. M.; Millward, G. R. Catalytic and structural properties of iridium-iridium dioxide colloids. *New J. Chem.*, **1987**, *11*(11-12), 757. (b) Furlong, D. Neil; Launikonis, Anton; Sasse, Wolfgang H. F.; Sanders, John V. Colloidal platinum sols. Preparation, characterization, and stability towards salt. *J. Chem. Soc., Faraday Trans. 1*, **1984**, *80*(3), 571.
108. (a) Aiken, J. D., III.; Finke, R. G. Polyoxoanion- and tetrabutylammonium-stabilized Rh(0)<sub>n</sub> nanoclusters: unprecedented nanocluster catalytic lifetime in solution. *J. Am. Chem. Soc.*, **1999**, *121*(38), 8803. (b) Aiken, J. D., III.; Finke, R. G. A review of modern transition-metal nanoclusters: their synthesis, characterization, and applications in catalysis. *J. Mol. Catal. A: Chem.*, **1999**, *145*(1-2), 1.



109. (a) Dhas, N. Arul; Gedanken, A. Sonochemical preparation and properties of nanostructured palladium metallic clusters. *J. Mater. Chem.*, **1998**, 8(2), 445. (b) Fujimoto, T.; Terauchi, S.; Umehara, H.; Kojima, I.; Henderson, W. Sonochemical Preparation of Single-Dispersion Metal Nanoparticles from Metal Salts. *Chem. Mater.*, **2001**, 13(3), 1057.
110. (a) Reetz, M. T.; Helbig, W.; Quaiser, S. A. *Active Metals: Preparation, Characterization, Applications*; Ed. Furstner, A., VCH: New York, 1996.
111. Aiken J. D. III; Lin, Y.; Finke, R. G. A perspective on nanocluster catalysis: polyoxoanion and (n-C<sub>4</sub>H<sub>9</sub>)<sub>4</sub>N<sup>+</sup> stabilized Ir(0)<sub>~300</sub> nanocluster 'soluble heterogeneous catalysts'. *J. Mol. Catal. A: Chem.*, **1996**, 114(1-3), 29. (b) Aiken, J. D., III; Finke, R. G. Polyoxoanion- and tetrabutylammonium-stabilized, near-monodisperse, 40 ± 6 Å Rh(0)~1500 to Rh(0)~3700 nanoclusters: synthesis, characterization, and hydrogenation catalysis. *Chem. Mater.*, **1999**, 11(4), 1035.
112. Vidoni, O.; Philippot, K.; Amiens, C.; Chaudret, B.; Balmes, O.; Malm, J.-O.; Bovin, J.-O.; Senoq, F.; Casanove, M.-J. Novel, spongelike ruthenium particles of controllable size stabilized only by organic solvents. *Angew. Chem., Int. Ed.*, **1999**, 38(24), 3736.
113. (a) Bonnemann, H.; Braun, G.; Brijoux, W.; Brinkmann, R.; Schulze A.; Seevogel, T. K.; Siepen, K. Nanoscale colloidal metals and alloys stabilized by solvents and surfactants preparation and use as catalyst precursors. *J. Organomet. Chem.*, **1996**, 520, 143. (b) Mevellec, V.; Mattioda, C.; Schulz, J.; Rolland, J.-P.; Roucoux, A. Enantioselective hydrogenation of ethyl pyruvate in biphasic liquid-liquid media by reusable surfactant-stabilized aqueous suspensions of platinum nanoparticles. *J. Catal.*, **2004**, 225(1), 1.
114. (a) Crooks, R. M.; Zhao, M.; Sun, L.; Chechik, V.; Yeung, L. K. Dendrimer-encapsulated metal nanoparticles: synthesis, characterization, and applications to catalysis. *Acc. Chem. Res.*, **2001**, 34(3), 181. (b) Narayanan, R.; El-Sayed, M. A. Effect of Colloidal Catalysis on the Nanoparticle Size Distribution: Dendrimer-Pd vs PVP-Pd Nanoparticles Catalyzing the Suzuki Coupling Reaction. *J. Phy. Chem. B*, **2004**, 108(25), 8572.
115. (a) Kralik, M.; Biffis, A. Catalysis by metal nanoparticles supported on functional organic polymers. *J. Mol. Catal. A: Chem.*, **2001**, 177(1), 113. (b) Narayanan, R.; El-Sayed, M. A. Effect of catalytic activity on the metallic nanoparticle size distribution: electron-transfer reaction between Fe(CN)<sub>6</sub> and thiosulfate ions catalyzed by PVP-Platinum nanoparticles., **2003**, 107(45), 12416.
116. (a) Schmid, G.; Emde, S.; Maihack, V.; Meyer-Zaika, W.; Peschel, St. Synthesis and catalytic properties of large ligand stabilized palladium clusters. *J. Mol. Catal. A: Chem.*, **1996**, 107(1-3), 95. (b) Ref. 105.
117. (a) Chen, S.; Kimura, K. Synthesis of thiolate-stabilized platinum nanoparticles in protolytic solvents as isolable colloids. *J. Phys. Chem. B*, **2001**, 105, 5397. (b) Schmid, G.; Beyer, N. A new approach to well-ordered quantum dots. *Eur. J. Inorg. Chem.*, **2000**, (5), 835.
118. (a) Lint, Y.; Finke, R. G. Novel polyoxoanion- and Bu<sub>4</sub>N<sup>+</sup>-stabilized, isolable, and redissolvable, 20-30-Å Ir<sub>~300-900</sub> nanoclusters: the kinetically controlled synthesis, characterization, and mechanism of formation of organic solvent-soluble, reproducible size, and reproducible catalytic activity metal nanoclusters. *J. Am. Chem. Soc.*, **1994**, 116, 8335. (b) Ref 113b.
119. van Heerbeek, R.; Kamer, P. C. J.; van Leeuwen, P. W. N. M.; Reek, J. N. H. Dendrimers as support for recoverable catalysts and reagents. *Chem. Rev.* **2002**, 102, 3717.
120. (a) Eppler, A.; Rupprechter, G.; Guzzi, L.; Somorjai, G. A. Model Catalysts Fabricated Using Electron Beam Lithography and Pulsed Laser Deposition. *J. Phys. Chem. B*, **1997**, 101(48), 9973. (b) Zhu, J.; Somorjai, G. A. Formation of Platinum Silicide on a Platinum Nanoparticle Array Model Catalyst Deposited on Silica during Chemical Reaction. *Nano Letters*, **2001**, 1(1), 8.
121. (a) Boennemann, H.; Brijoux, W.; Brinkmann, R.; Fretzen, R.; Jousen, T.; Koepler, R.; Korall, B.; Neiteler, P.; Richter, J. Preparation, characterization, and application of fine metal particles and metal colloids using hydrotriorganoborates. *J. Mol. Catal.*, **1994**, 86(1-3), 129. (b) Boennemann, H.; Brinkmann, R.; Neiteler, P. Preparation and catalytic properties of NR<sub>4</sub><sup>+</sup>-stabilized palladium colloids. *Appl. Organomet. Chem.*, **1994**, 8(4), 361.
122. (a) Ref. 112b. (b) Reetz, M. T.; Quaiser, S. A.; Breinbauer, R.; Tesche, B. A new strategy in heterogeneous catalysis: the design of cortex catalysts. *Angew. Chem., Int. Ed.* **1996**, 34(23/24), 2728.
123. Lang, H.; May, R. A.; Iversen, B. L.; Chandler, B. D. Dendrimer Encapsulated Nanoparticle Precursors to Supported Platinum Catalysts. *J. Am. Chem. Soc.*, **2003**, 125, 14832.
124. (a) Yang, C.; Kalwei, M.; Schüth, F.; Chao K. Gold nanoparticles in SBA-15 showing catalytic activity in CO oxidation. *App. Catal. A*, **2003**, 254, 289. (b) Ref. 107b.

125. (a) Joo, S. H.; Choi, S. J.; Oh, I.; Kwak, J.; Liu, Z.; Terasaki, O.; Ryoo, R. Ordered nanoporous arrays of carbon supporting high dispersions of platinum nanoparticles. *Nature*, **2001**, 412(6843), 169. (b) Lu, A.-H.; Schmidt, W.; Matoussevitch, N.; Bonnemann, H.; Spliethoff, B.; Tesche, B.; Bill, E.; Kiefer, W.; Schuth, F. Nanoengineering of a Magnetically Separable Hydrogenation Catalyst. *Angew. Chem. Int. Ed.*, **2004**, 43, 4303.
126. (a) Kralik, M.; Biffis, A. Catalysis by metal nanoparticles supported on functional organic polymers. *J. Mol. Catal. A: Chem.*, **2001**, 177(1), 113. (b) Corain, B.; Centomo, P.; Lora, S.; Kralik, M. Functional resins as innovative supports for catalytically active metal nanoclusters. *J. Mol. Catal. A: Chem.*, **2003**, 204-205, 755.
127. (a) Ohtaki, M.; Komiyama, M.; Hirai, H.; Toshima, N. Effects of polymer support on the substrate selectivity of covalently immobilized ultrafine rhodium particles as a catalyst for olefin hydrogenation. *Macromolecules*, **1991**, 24(20), 5567. (b) Ohtaki, M.; Toshima, N.; Komiyama, M.; Hirai, H. Covalent immobilization of ultrafine platinum particles onto crosslinked polymer support and their application to catalysis. *Bull. Chem. Soc. Jpn.*, **1990**, 63(5), 1433.
128. (a) Chen, C.-W.; Chen, M.-Q.; Serizawa, T.; Akashi, M. In situ synthesis and the catalytic properties of platinum colloids on polystyrene microspheres with surface-grafted poly(N-isopropylacrylamide). *Chem. Commun.*, **1998**, 831. (c) Chen, C.-W.; Serizawa, T.; Akashi, M. Synthesis and characterization of poly(N-isopropylacrylamide)-coated polystyrene microspheres with silver nanoparticles on their surfaces. *Langmuir*, **1999**, 15(23), 7998.
129. Suzuki, K.; Yumura, T.; Mizuguchi, M.; Tanaka, Y.; Chen, C.-W.; Akashi, M. Poly(N-isopropylacrylamide)-grafted silica as a support of platinum colloids: preparation method, characterization, and catalytic properties in hydrogenation. *J. Appl. Polym. Sci.*, **2000**, 77(12), 2678.
130. Yu, W.; Liu, M.; Liu, H.; An, X.; Liu, Z.; Ma, X. Immobilization of polymer-stabilized metal colloids by a modified coordination capture: preparation of supported metal colloids with singular catalytic properties. *J. Mol. Catal. A: Chem.*, **1999**, 142(2), 201. See the ref. therein.
131. (a) Watanabe, M. Design of electrocatalysts for fuel cells. 2003, 827. *Catalysis and Electrocatalysis at Nanoparticle Surfaces*, Ed: Wieckowski, A.; Savinova, E. R.; Vayenas, C. G. Marcel Dekker, New York. (b) Wieckowski, A. Nanostructures in electrochemical surface science and heterogeneous electrocatalysis. *Electrochemistry*, **2003**, 71(3), 206.
132. Schmid, G.; Harms, M.; Malm, J. O.; Bovin, J. O.; Van Ruitenbeck, J.; Zandbergen, H. W.; Fu, W. T. Ligand-stabilized giant palladium clusters: promising candidates in heterogeneous catalysis. *J. Am. Chem. Soc.*, **1993**, 115(5), 2046.
133. Chen, C.-W.; Chen, M.-Q.; Serizawa, T.; Akashi, M. *In situ* synthesis and the catalytic properties of platinum colloids on polystyrene microspheres with surface-grafted poly-(N isopropylacrylamide) *Chem. Commun.*, **1998**, 831.
134. Michalska, Z. M.; Ostaszewski, B.; Zientarska, J.; Sobczak, J. W. Catalytic hydrogenation of alkadienes and alkynes by palladium catalysts supported on heterocyclic polyamides. *J. Mol. Catal. A: Chem.*, **1998**, 129(2-3), 207.
135. Yu, W.; Liu, H.; An, X. Novel catalytic properties of supported metal nanoclusters. *J. Mol. Catal. A: Chem.*, **1998**, 129(1), L9.
136. Boennemann, H.; Brijoux, W.; Brinkmann, R.; Dinjus, E.; Fretzen, R.; Jousen, T.; Korall, B. Highly dispersed metal clusters and colloids for the preparation of active liquid-phase hydrogenation catalysts. *J. Mol. Catal.*, **1992**, 74(1-3), 323.
137. (a) Molnar, A.; Papp, A.; Miklos, K.; Forgo, P. Organically modified Pd-silica catalysts in Heck coupling. *Chem. Commun.*, **2003**, 2626. (b) Papp, A.; Miklos, K.; Forgo, P.; Molnar, A. Heck coupling by Pd deposited onto organic-inorganic hybrid supports. *J. Mol. Catal. A: Chem.*, **2005**, 229, 107.
138. Djakovitch, L.; Koehler, K. Heck Reaction Catalyzed by Pd-Modified Zeolites. *J. Am. Chem. Soc.*, **2001**, 123(25), 5990.
139. Choudary, B. M.; Madhi, S.; Chowdari, N. S.; Kantam, M. L.; Sreedhar, B. Layered double hydroxide supported nanopalladium catalyst for Heck-, Suzuki-, Sonogashira-, and Stille-type coupling reactions of chloroarenes. *J. Am. Chem. Soc.*, **2002**, 124(47), 14127.
140. Narayanan, R.; El-Sayed, M. A. Carbon-supported palladium nanoparticles as potential recyclable catalysts for the Suzuki coupling. *J. Catal.*, **2005**, 234, 384.
141. Carretin, S.; McMorn, P.; Johnston, P.; Griffin, K.; Kiely, C. J.; Hutchings, G. Oxidation of glycerol using supported Pt, Pd and Au catalysts. *J. Phy. Chem. Chem. Phy.*, **2003**, 5(6), 1329.

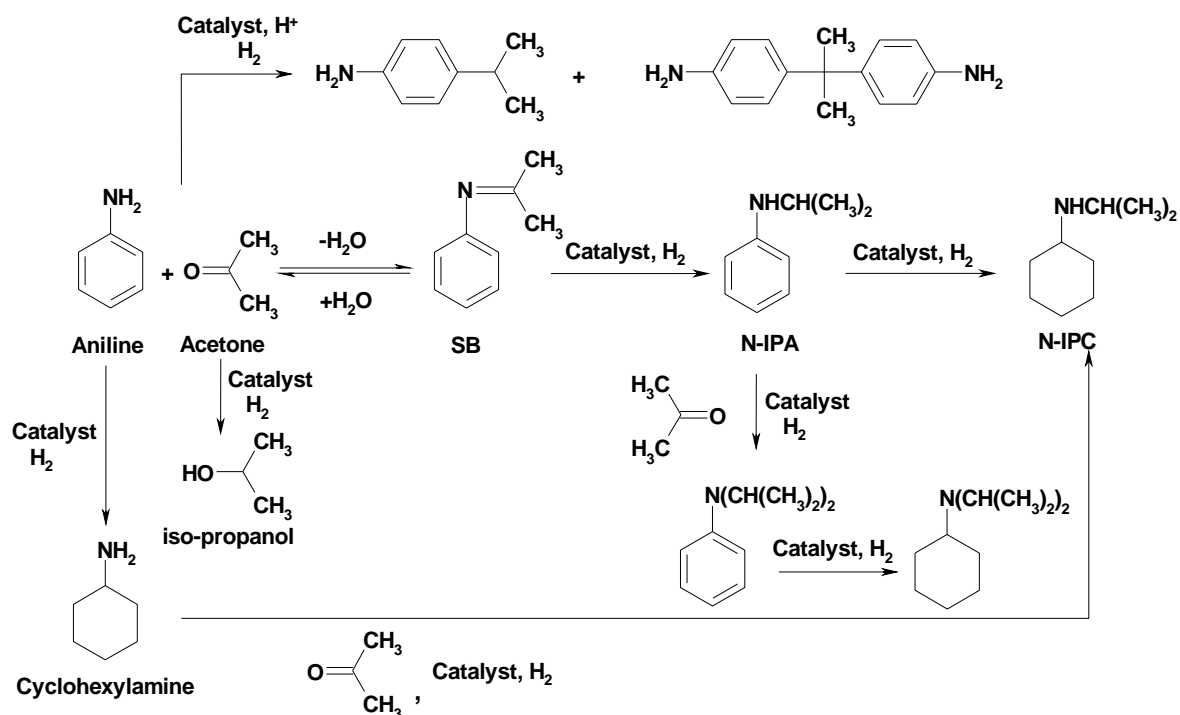
- 
142. Comotti, M.; Pina, C. D.; Matarrese, R.; Rossi, M.; Siani A. Oxidation of alcohols and sugars using Au/C catalysts Part 2. Sugars. *App. Cat. A: Gen.*, **2005**, *291*, 204.
143. Biella, S.; Castiglioni, G. L.; Fumagalli, C.; Prati, L.; Rossi, M. Application of gold catalysts to selective liquid phase oxidation. *Catal. Today*, **2002**, *72*(1-2), 43.
144. Cusack R. W. A fresh look at reaction engineering. *Chemical Engineering*, **1999**, *106*(11), 134.
145. (a) Ref 10b. (b) Satterfield, C. N. Trickle bed reactors. *AIChE J.*, **1975**, *21*, 209. (c) Shah Y. T. Gas-Liquid-Solid reactor design, McGraw-Hill, New York, 1979. (d) Ref. 10d. (e) Doraiswamy L. K.; Sharma M. M., Heterogeneous reactions, vol.2, Wiley, New York, 1984.
146. Jaganathan, R.; Ghugikar, V. G.; Gholap, R. V.; Chaudhari, R. V.; Mills, P. L. Catalytic hydrogenation of *p*-nitrocumene in a slurry reactor. *Ind. Eng. Chem. Res.*, **1999**, *38*(12), 4634.
147. Rajashekharam, M. V.; Nikalje, D. D.; Jaganathan, R.; Chaudhari, R. V. Hydrogenation of 2,4-dinitrotoluene using a Pd/Al<sub>2</sub>O<sub>3</sub> catalyst in a slurry reactor: a molecular level approach to kinetic modeling and nonisothermal effects. *Ind. Eng. Chem. Res.*, **1997**, *36*(3), 592.
148. Benaissa, M.; Le Roux, G. C.; Joulia, X.; Chaudhari, R. V.; Delmas, H. Kinetic modeling of the hydrogenation of 1,5,9-cyclododecatriene on Pd/Al<sub>2</sub>O<sub>3</sub> catalyst including isomerization. *Ind. Eng. Chem. Res.*, **1996**, *35*(7), 2091.
149. Chaudhari, R. V.; Jaganathan, R.; Kolhe, D. S.; Emig, G.; Hofmann, H. Kinetic modeling of a complex consecutive reaction in a slurry reactor: hydrogenation of phenyl acetylene. *Chem. Eng. Sci.*, **1986**, *41*(12), 3073.
150. Lylykangas, M. S.; Rautanen, P. A.; Krause, A. O. I. Hydrogenation and Deactivation Kinetics in the Liquid-Phase Hydrogenation of Isooctenes on Pt/Al<sub>2</sub>O<sub>3</sub>. *Ind. Eng. Chem. Res.*, **2004**, *43*(7), 1641.
151. Neri, G.; Bonaccorsi, L.; Mercadante, L.; Galvagno, S. Kinetic analysis of cinnamaldehyde hydrogenation over alumina-supported ruthenium catalysts. *Ind. Eng. Chem. Res.*, **1997**, *36*(9), 3554.
152. Toppinen, S.; Rantakylae, T.-K.; Salmi, T.; Aittamaa, J. Kinetics of the liquid-phase hydrogenation of benzene and some monosubstituted alkylbenzenes over a nickel catalyst. *Ind. Eng. Chem. Res.*, **1996**, *35*(6), 1824.
153. Zhang, Z.; Jackson, J. E.; Miller, D. J. Kinetics of aqueous-phase hydrogenation of lactic acid to propylene glycol. *Ind. Eng. Chem. Res.*, **2002**, *41*(4), 691.

## **Chapter 2**

### **Reductive Alkylation of Aniline with Acetone Using Pd/Al<sub>2</sub>O<sub>3</sub> Catalyst: Kinetics and Modeling of Trickle Bed Reactor**

## 2.1. INTRODUCTION

Synthesis of secondary or tertiary amine compounds by reductive alkylation of aromatic amines is an important class of reaction, as the products are used in dyestuff industries as intermediates<sup>1</sup>, in rubber and petroleum industries as antioxidants<sup>2</sup>, as intermediates in agrochemicals etc. It is a unique example of a tandem one-pot synthesis with a reversible condensation reaction in liquid phase followed by catalytic hydrogenation using solid catalysts. Because of the homogeneous-heterogeneous combination, this is an important class of reaction from academic point of view also. The reaction starts through a condensation reaction between an amine compound or its precursor and a carbonyl compound or alcohol to form an imine compound (Shiff's base)<sup>3</sup>, which is hydrogenated in the presence of a metallic catalyst to N-alkylated products.<sup>4</sup> Depending upon the substrates, reaction conditions and the solid catalyst and promoter used, various other products also may form. For example, in reductive alkylation of aniline and acetone, hydrogenation of acetone to iso-propanol may be important when Pt, Rh or Ru catalysts are used, but it is negligible for a Pd catalyzed reaction. On the other hand, C-alkylation may occur when acids are used as promoters.<sup>5</sup> The possible product distribution for reductive alkylation of aniline and acetone is presented in Scheme 2.1. The equilibrium-controlled formation of the Shiff's base [SB] is believed to be the slowest step in the consecutive reaction sequence. Hence, continuous removal of water from the reaction mixture by azeotropic distillation or using molecular sieves can shift the equilibrium and enhance the overall rate of reductive alkylation. Hydrogenation of [SB] also shifts the equilibrium reaction towards the right hand side. Organic or inorganic acids and bases are also reported to accelerate the formation of [SB]<sup>6</sup> and hence the reductive alkylation products.



**Scheme 2.1.** Reaction scheme for reductive alkylation of aniline with acetone

Reductive alkylation of nitro or amine compounds has been investigated previously using a wide range of alkylating agents and catalysts. Alcohols<sup>7</sup> were used in some cases as the alkylating agents, which first dehydrogenated to the corresponding carbonyl compound and initiated the condensation reaction with the amine functionality<sup>8</sup>. Among the carbonyl compounds, aldehydes and ketones differ from each other from the activity and product distribution point of view. For Aldehydes, N, N-dialkylated products are reported in most of the cases.<sup>9</sup> Lehtonen et al.<sup>10</sup> discussed the probable product distribution for reductive alkylation with carbonyl compounds and developed a semi batch slurry reactor model for aniline and short chain aldehydes in presence of Pt/C catalyst. The system was also modeled considering mass transfer limitations at the gas-liquid interface. Salmi et al.<sup>11</sup> used this kinetic data for verification of the performance of a loop reactor.

In contrary to aldehydes, with ketones as the alkylating agents, N-mono alkylated compounds were the major products<sup>2, 12</sup> due to the relatively higher molecular size and less reactivity of the ketones. Greenfield<sup>13</sup> studied reductive alkylation of aromatic amines with aldehydes and ketones using different transition metals as catalysts for the selectivity

improvement of N-alkylated products and reported that palladium was a better catalyst than platinum, rhodium or ruthenium at lower temperatures. Ring hydrogenation and hydrogenation of the carbonyl compounds to corresponding alcohols were relatively higher for these three metal catalysts. But selective synthesis of the N-alkylated products was the major focus in the above reports. A summary of previous work on this subject is presented in Table 2.1. While, numerous reports on catalyst performance evaluation have appeared in the previous literature, no attempts have been made to study the kinetics of reductive alkylation of amines using ketones as alkylation agents for any of the catalysts.

In this chapter, a study of intrinsic kinetics of reductive alkylation of aniline with acetone using 3% Pd/Al<sub>2</sub>O<sub>3</sub> as a catalyst in a batch slurry reactor is reported. The overall reaction involves a combination of a non-catalytic reaction followed by two catalytic hydrogenation steps, where the selectivity of the intermediate N-IPA (N-isopropylaniline) is an important issue. The effect of aniline concentration, partial pressure of hydrogen and catalyst concentration on the concentration-time profiles were studied. Rate equations have been proposed for the non-catalytic as well as catalytic reaction steps using a model discrimination approach and the rate parameters were estimated.

## **2.2. EXPERIMENTAL SECTION**

### **2.2.1. Chemicals**

Aniline and acetone were procured from E-Merck, India and used without any further treatment. A 3% Pd/Al<sub>2</sub>O<sub>3</sub> catalyst was purchased from M/s Aldrich Chemicals, USA. The catalyst was spherical with average diameter of  $3 \times 10^{-3}$  m. For kinetic studies in a batch slurry reactor, the catalyst was crushed and sieved to obtain very fine powder. The specifications of the powdered catalyst were as follows: palladium content: 3% (w/w); support: Al<sub>2</sub>O<sub>3</sub>; particle size:  $1 \times 10^{-5}$  m; particle density:  $2 \times 10^3$  kg/m<sup>3</sup>; surface area:  $1.75 \times 10^5$  m<sup>2</sup>/kg.

**Table 2.1.** Literature on reductive alkylation of aromatic amines

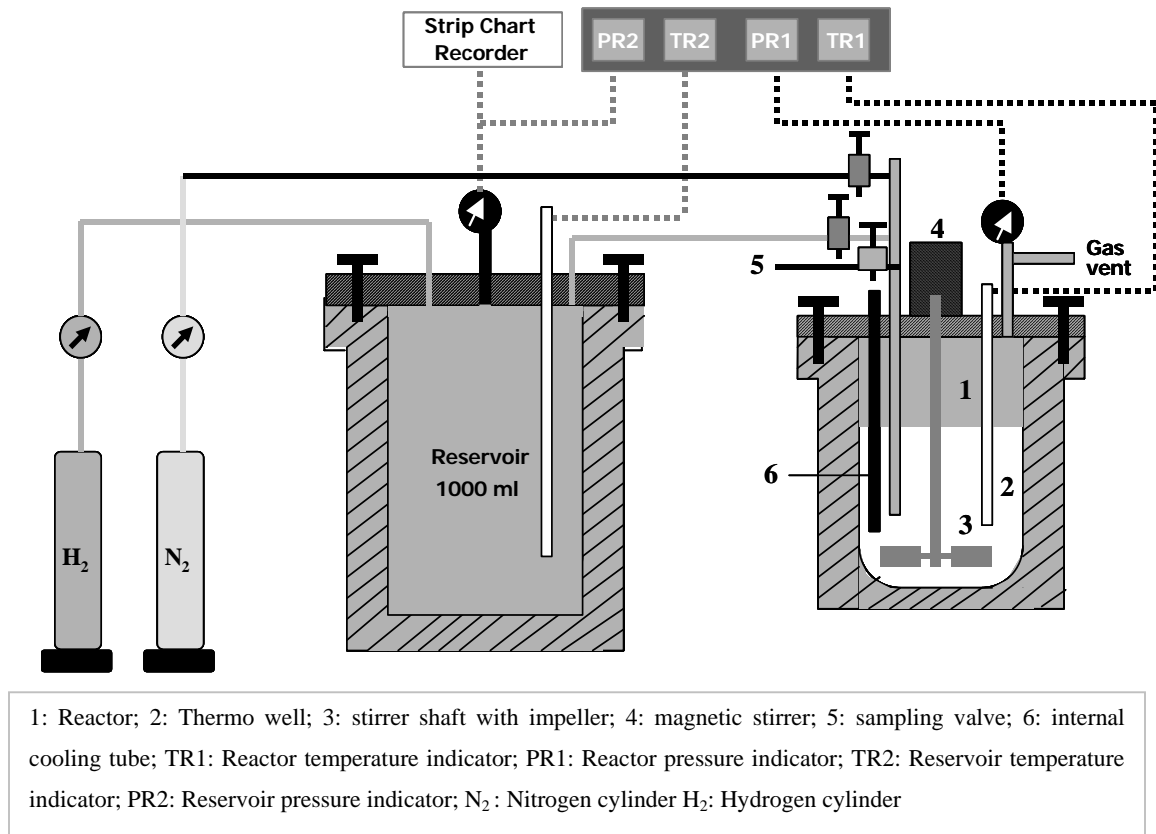
Substrates	Catalyst	Reaction conditions	Remarks	Ref.
Aniline and methanol	LiY and NaY non-protic and non-basic zeolites	623-723K	Selectivity to N-alkylated product increases with temperature while C-alkylation selectivity decreases	7d
2-Methyl-6-ethylaniline (MEA) and methoxy-2-propanol (MOIP)	Pt-Sn/SiO <sub>2</sub> catalyst pretreated with Ca <sup>2+</sup>	Feed: MEA: MOIP=0.5 (3ml/h); P <sub>H2</sub> : 1 atm; H <sub>2</sub> : 4.7 ml/min.; 448K; micro reactor	Conversion (MEA): 36.4; selectivity (N-alkylated product): 76.2.	8
2-Butoxy-5-tert-octyl-nitrobenzene and butanal	Pd/C	353K; P <sub>H2</sub> : 30kg/cm <sup>2</sup> ; solvent: EtOH; 5h	N,N-dibutyl-2-butoxy-5-tert-octylaniline is the major product (98.1%)	9a
3-Aminobenzoic acid and aqueous HCHO	Pd/C	323K; P <sub>H2</sub> : 5kg/cm <sup>2</sup> ; solvent: MeOH; 1h	3-dimethylamino benzoic acid is the major product (95.5%)	9b
Aromatic amines and aldehydes	3-5% Pt/C	303-348K; P <sub>H2</sub> : 15 bar; solvent: MeOH	A three-phase semibatch reactor model proposed and kinetic parameters evaluated.	10
Aromatic amines and aldehydes	3-5% Pt/C	303-348K; P <sub>H2</sub> : 15 bar; solvent: MeOH	A loop slurry reactor model proposed.	11
4-H <sub>2</sub> NC <sub>6</sub> H <sub>4</sub> NHPh and Me <sub>2</sub> CHCH <sub>2</sub> COMe	63% Ni on kieselguhr; organic/inorganic acid; organic S-containing compound	438K; P <sub>H2</sub> : 750-1000 ponds; 4h	Yield of N-alkylated products increased by addition of small amount of an organic/inorganic acid and an organic S-containing compound	6c
3,4-Me <sub>2</sub> C <sub>6</sub> H <sub>3</sub> NH <sub>2</sub> and Et <sub>2</sub> CO	5% Pt/C; 2-naphthalene sulfonic acid	P <sub>H2</sub> : 47 psi; 333-338K; 0.75 h	Yield of 3,4-Me <sub>2</sub> C <sub>6</sub> H <sub>3</sub> NHCH <sub>2</sub> Et <sub>2</sub> increased using acid promoters.	6a
NH(C <sub>6</sub> H <sub>4</sub> NO <sub>2</sub> ) <sub>2</sub> and methyl isobutylketone	Pt/C	353-383K; P <sub>H2</sub> : 100 kg/cm <sup>2</sup>	NH(C <sub>6</sub> H <sub>4</sub> NHR) <sub>2</sub> is the only product formed (R = CHMeCH <sub>2</sub> CHMe <sub>2</sub> ).	2
Aniline and acetophenone	3% PtS <sub>x</sub> /C (sulfided catalyst)	398K; 500-800 psig; 3.5h; solvent: aniline	Yield of N-phenyl- $\alpha$ -methylbenzylamine: 94%. Role of sulfide poisoning on side reactions, solvent and temperature effect were studied.	12c
Aniline and acetone	Pt, Pd, Rh, Ru (metal loading:5; support: Carbon for all cases)	400-600 psig, temp.: 378-413K; stirred autoclave (1-gal. capacity)	With Pd catalyst, conv. (aniline): 100%; yield (N-IPA): 67%; yield (N-IPC): 14%. With Pt, Rh, Ru ring hydrogenation and acetone hydrogenation significant	13



## 2.2.2. Reactor Set-up

### 2.2.2.1. Slurry Reactor

All the reductive alkylation batch reactions were carried out in a  $3 \times 10^{-4} \text{ m}^3$  capacity high pressure stirred autoclave supplied by Parr Instrument Company, Moline, USA. The autoclave was equipped with a heating arrangement, overhead stirrer, thermo well, internal cooling loop, pressure gauge as well as transducer, gas inlet, gas outlet, sampling valve and a rupture disc. There was a separate controller for agitation speed and temperature. Water circulation through the internal cooling loop equipped with automatic cut-off arrangement controlled the temperature inside the reactor with an accuracy of  $\pm 1^\circ \text{ C}$ . A schematic of the slurry reactor set-up is shown in Figure 2.1. In a typical experiment, required amount of aniline dissolved in acetone was charged into the reactor. Total volume of the liquid phase was always kept to  $1 \times 10^{-4} \text{ m}^3$ . A required amount of powered 3% Pd/Al<sub>2</sub>O<sub>3</sub> catalyst was charged into the reactor bomb carefully and the vessel was closed. The reactor was purged 2-3 times with nitrogen and twice with hydrogen at room temperature. The reactor bomb was heated to the desired temperature and after attaining the desired temperature; hydrogen gas was introduced through the gas inlet valve to the desired pressure. Liquid sample was collected as the initial sample and reaction started by putting the agitation to a set value. A constant pressure regulator maintained the pressure inside the reactor and the consumption of H<sub>2</sub> due to reaction was monitored from the pressure drop in the reservoir. Samples were withdrawn at regular intervals and analyzed by gas chromatography. In each experiment, concentration –time as well as H<sub>2</sub> consumption-time data were recorded. The reaction was stopped after a certain time and the reactor contents cooled to room temperature. The range of operating conditions studied in this work is given in Table 2.2.



**Figure 2.1.** Schematic of a slurry reactor set-up

**Table 2.2.** Range of experimental conditions

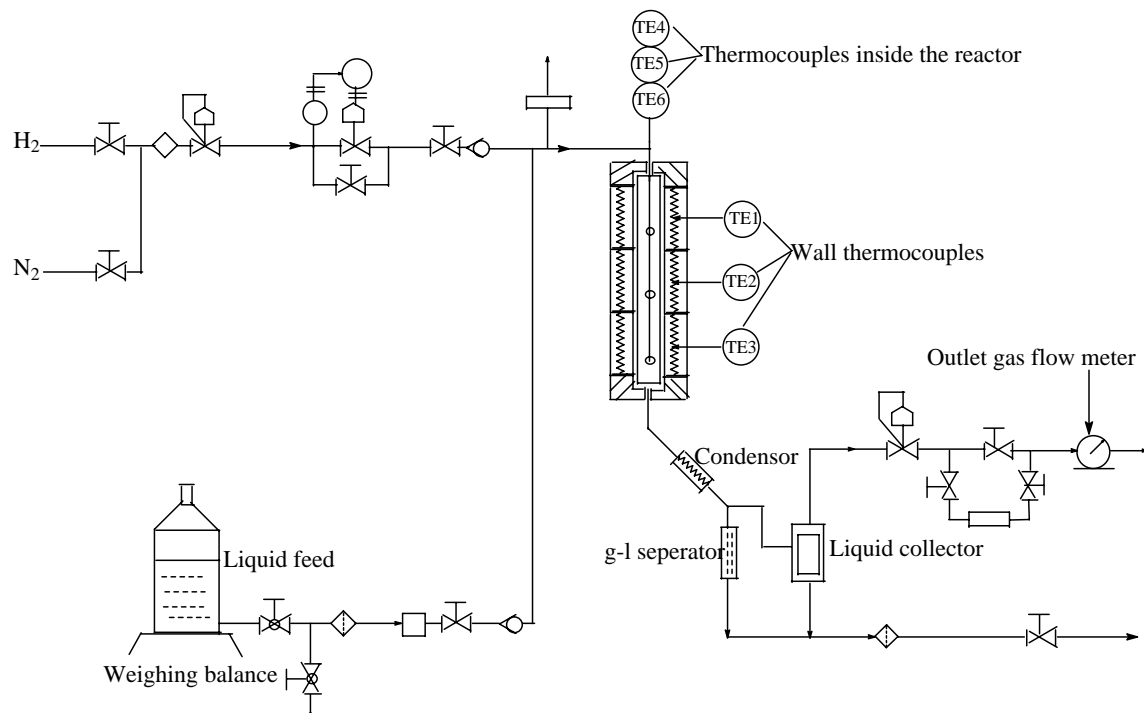
Catalyst loading	2-8 kg/m <sup>3</sup>
Aniline concentration	0.5-2.0 kmol/m <sup>3</sup>
Hydrogen partial pressure	1.4-8.3, MPa
Agitation speed	11.6-18.3 Hz
Temperature	378-408 K
Volume of liquid	1×10 <sup>-4</sup> m <sup>3</sup>
Reaction time	3 h

### 2.2.2.2. Fixed Bed Reactor

The experiments in continuous mode were carried out in a trickle bed reactor procured from M/s. "Vinci Technologies", France. The schematic of the reactor set-up is shown in Figure 2.2. The reactor consists of a stainless steel tube of 0.53 m length and 1.9

$\times 10^{-2}$  m inner diameter. The reactor was also provided with three thermocouples [Chromel-Alumel, type K] to measure temperatures at three different points viz. along the length of the reactor. A thermo well made of stainless steel of outer diameter  $0.8 \times 10^{-2}$ , m placed axially along the reactor length had the thermocouples in it. An electronically controlled furnace split into three separate sections heated the reactor and the corresponding wall temperatures could also be noted from the electronic display along with that of the reactor bed temperature. The temperature of each of these furnaces could be controlled independently. The gas flow rate was adjusted by mass flow controller of range 0-60 Nl/h and could be read from the electronic display. The reactor pressure was adjusted with the manual pressure controller and the pressure was indicated by the pressure gauge fitted at the reactor inlet. For quick pressurization of the unit, the mass flow controller can be bypassed by a manual valve. A storage tank with the liquid feed was kept on a weighing balance with an accuracy of 0.5gm and from the weight drop observed from the weighing balance the exact flow rate of liquid feed was calculated. The pump had a maximum capacity of  $2.5 \times 10^{-3}$  m<sup>3</sup>/hr. The outlet of the reactor was equipped with a condenser and a high-pressure gas-liquid separator, and a liquid level indicator. The gas outlet line was equipped with a backpressure controller, which maintained a constant pressure in the unit by continuous pressure release. A wet gas flow meter measured the total gas outflow. The liquid product from the gas liquid separator could be drained by means of a 'block and bleed valve'. In each experiment, required amount of catalyst was charged in the reactor and the sections above and below the catalyst bed were packed with inert packing (carborundum). The lines of the reactor are flushed with the feed solution before the start of any experiment. In the beginning, the reactor was flushed with nitrogen well and the wall temperatures of the different zones were set to the desired limit. The liquid flow was started after adjusting the required flow rate. Once the temperature of the wall was attained and the temperature inside the reactor was stable, the reactor was pressurized after setting the gas flow rate. Liquid samples were withdrawn from the exit at regular intervals of time and were analysed by Gas Chromatography. The temperatures inside the reactor were monitored at three positions inside the reactor. The catalyst was filled in such a way that the first thermocouple was at the inlet of the catalyst bed, second one at the middle of the catalyst bed and the third thermocouple at the exit of the catalyst bed. Following this

procedure, experiments were carried out at different inlet conditions and steady state performance of the reactor observed by analysis of reactants and products in the exit streams.



**Figure 2.2.** Schematic of the fixed bed reactor

### 2.2.3. Analysis

The liquid samples were analyzed by gas chromatography (GC) technique (HP 6890 instrument) using a HP-5 capillary column (5% phenyl methyl siloxane as the stationary phase, 30 m × 320 μm × 0.25 μm). The conditions of GC analysis were: injector temperature: 523K; column temperature: 313 K for 3 min - @ 20 K min<sup>-1</sup> up to 453 K - hold 3 min - @ 10 K min<sup>-1</sup> up to 513 K - hold 2 min; FID temperature: 523K. Helium and air were used as the carrier gas and makeup gas respectively. A few samples were characterized using GC-MS (Shimadzu QP 2000A) for identification of products.

The metal content in the catalysts was determined using a Perkin Elmer Plasma 1000 ICP-OES spectrometer. Surface area of the powered catalyst was measured using a CHEMBET-3000, Quantachrome instrument at 30% nitrogen.

## 2.3. RESULTS AND DISCUSSION

### 2.3.1 Preliminary Experiments

#### 2.3.1.1. Catalyst Selection

To select a suitable catalyst for selective synthesis of N-isopropyl aniline (N-IPA) by reductive alkylation of aniline and acetone, we screened Pd, Pt, Ru and Rh catalysts supported on alumina. The catalyst screening results were compared in terms of conversion, selectivity and turnover frequency (TOF) and the results are shown in Table 2.3. The terms conversion, selectivity and TOF were defined as follows:

$$\text{Conversion (\%)} = \frac{\text{Amount of aniline consumed (kmol)}}{\text{Total amount of aniline initially taken (kmol)}} \times 100 \quad (2.1)$$

$$\text{Selectivity (\%)} = \frac{\text{Amount of the particular product formed (kmol)}}{\text{Total amount of aniline converted (kmol)}} \times 100 \quad (2.2)$$

$$\text{TOF (h}^{-1}\text{)} = \frac{\text{Amount of N-IPA formed (kmol)}}{[\text{Amount of metal in the catalyst (kmol)}] \times [\text{reaction time (h)}]} \quad (2.3)$$

The TOF is defined in terms of N-IPA because the primary aim of this catalyst screening study was to find out a suitable catalyst for selective synthesis of N-IPA. From Table 2.3, it is envisaged that under identical conditions Pd and Pt gave the highest selectivity to N-IPA. With Ru/Al<sub>2</sub>O<sub>3</sub> and Rh/Al<sub>2</sub>O<sub>3</sub>, N-isopropyl cyclohexylamine (N-IPC) and hydrogenation of acetone to iso-propanol (IPA) were the major products. On the other hand, though the conversion of aniline and selectivity to N-IPA were good with Pt/Al<sub>2</sub>O<sub>3</sub> catalyst, hydrogenation of acetone to iso-propanol (IPA) was significant. A comparison of catalysts for reductive alkylation of aniline and acetone based on literature report is presented in Table 2.4. As the reactor size, metal content, support and reaction temperature are not same for the data presented in Table 2.3 and 2.4, the catalyst performance data might be different but it is very much clear that the trends were quite similar. Therefore, Pd/Al<sub>2</sub>O<sub>3</sub> was chosen as the suitable catalyst for selective synthesis of N-IPA.

Few experiments were also carried out using 1, 3 and 5% (w/w) Pd/Al<sub>2</sub>O<sub>3</sub> catalysts. The investigations revealed that the reaction rate was very slow with 1% Pd/Al<sub>2</sub>O<sub>3</sub>, while it

was very fast for 5% Pd/Al<sub>2</sub>O<sub>3</sub> catalyst. Hence, a 3% Pd/Al<sub>2</sub>O<sub>3</sub> catalyst was used for further study.

**Table 2.3.** Catalyst screening for reductive alkylation of aniline and acetone

Catalyst	Temp. (K)	Time (h)	Conv., % Aniline	Selectivity, %		
				N-IPA	N-IPC	IPA <sup>#</sup>
3% Pd/Al <sub>2</sub> O <sub>3</sub>	398	3	95	86	14	0
3% Pt/Al <sub>2</sub> O <sub>3</sub>	398	3	98	89	10	26
3% Ru/Al <sub>2</sub> O <sub>3</sub>	398	3	72	41	51	48
3% Rh/Al <sub>2</sub> O <sub>3</sub>	398	3	66	49	42	56

Reaction conditions: aniline: 1.0 kmol/m<sup>3</sup>, catalyst: 4 kg/m<sup>3</sup>; P<sub>H2</sub>: 4 MPa; Agitation: 16.66 Hz; reaction volume: 1×10<sup>-4</sup> m<sup>3</sup>; acetone is the solvent and one of the reactants  
IPA<sup>#</sup>: *iso*-propanol, formed with respect to excess acetone used

**Table 2.4.** Comparison of transition metals for reductive alkylation of aniline and acetone (Greenfield's report)

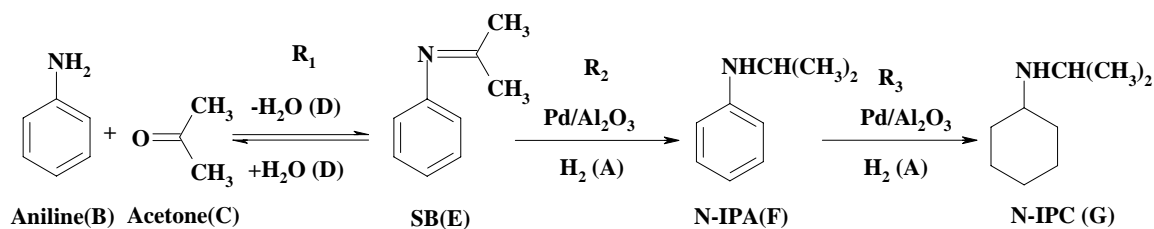
Catalyst	Temp. (K)	Time (h)	Conv., % Aniline	Selectivity, %		
				N-IPA	N-IPC	IPA <sup>#</sup>
5% Pd/C	378	1	100	67	14	0
5% Pt/C	378	1	60	47	<2	33
5% Rh/C	378	10	100	0	81	>90
5% Ru/C	378	1.8	100	0	74	100
5% Pd/C	378	4.7	>99	50	20	0

Reaction conditions: aniline, 1 mol; acetone, 15 mole; catalyst, 6 g; P<sub>H2</sub>, 400-600 psig; reaction taken in 1 gallon stirred autoclave.  
IPA<sup>#</sup>: *iso*-propanol, formed with respect to excess acetone used

### 2.3.1.2. Product Distribution

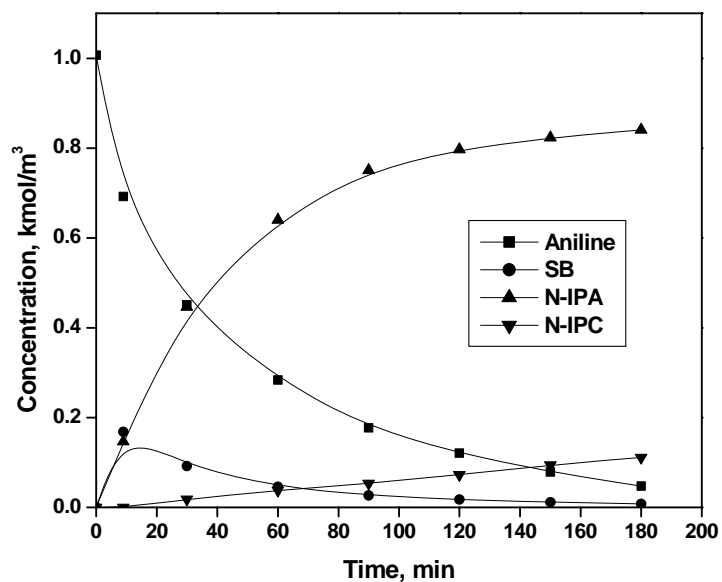
In order to investigate the intrinsic kinetics of reductive alkylation of aniline with acetone using Pd/Al<sub>2</sub>O<sub>3</sub> catalyst, a few initial experiments were carried out to identify the key products formed during the reaction and material balance in the overall reaction. For all the reactions, acetone was used as one of the reactant in excess that also served the role of a

solvent. A typical concentration-time profile observed is shown in Figure 2.3, which indicates that Schiff's base [SB], N-isopropyl aniline (N-IPA) and N-isopropyl cyclohexyl amine (N-IPC) were the major products. The ring-hydrogenated product N-IPC was not observed at the initial period of reaction (e.g. first 15 min of the concentration-time profile shown in Figure 2.3), which indicates that aromatic ring hydrogenation starts only after N-IPA formed. Therefore, the possibility of parallel hydrogenation of aniline to cyclohexylamine followed by reductive alkylation was discarded. The formation of dimerization products of the aromatic amine compound and hydrogenation of acetone to iso-propanol were observed to be negligible (<0.5%) for all the cases. In all the reactions, the material balance of aniline and hydrogen consumed agreed with the products formed to the extent of >95 % and hence the modified reaction scheme considered for reductive alkylation of aniline with acetone using Pd/Al<sub>2</sub>O<sub>3</sub> catalyst is shown in Scheme 2.2.

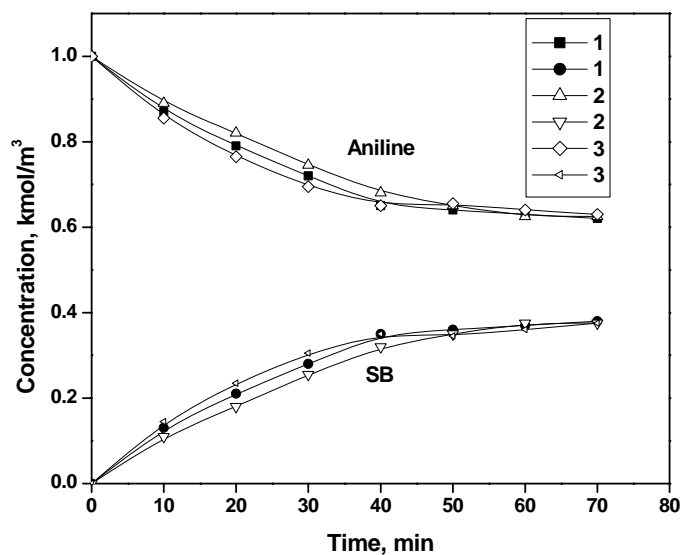


**Scheme 2.2.** Reaction scheme for reductive alkylation of aniline with acetone in presence of 3% Pd/Al<sub>2</sub>O<sub>3</sub> catalyst

To check the possibilities of homogeneous non-catalytic reactions, a few reactions were carried out without the catalyst and hydrogen. It was observed that Schiff's base was the only product formed and maintained an equilibrium state after a certain reaction time (Figure 2.4). The effects of hydrogen and catalyst on the equilibrium reaction were also studied separately and it was observed that the equilibrium was not disturbed due to the presence of these two components (Figure 2.4).



**Figure 2.3.** Concentration-time profile for reductive alkylation of aniline with acetone  
 Reaction conditions: aniline: 1.0 kmol/m<sup>3</sup>, catalyst (3% Pd/Al<sub>2</sub>O<sub>3</sub>): 4 kg/m<sup>3</sup>; P<sub>H<sub>2</sub></sub>: 4 MPa; temp.: 393K;  
 Agitation: 16.66 Hz; reaction volume: 1×10<sup>-4</sup> m<sup>3</sup>; acetone is the solvent and one of the reactants; reaction  
 time: 3h

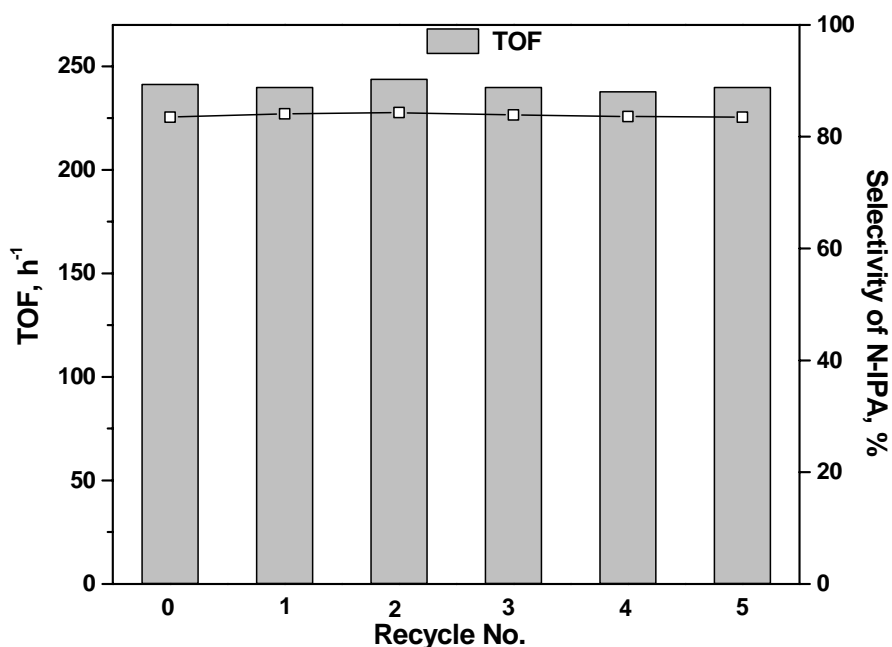


**Figure 2.4.** Concentration-time profiles for homogeneous reaction between aniline and acetone: effect of hydrogen and Pd/Al<sub>2</sub>O<sub>3</sub> on the equilibrium  
 (1,1): without hydrogen or catalyst; (2,2): with hydrogen but no catalyst; (3,3): with catalyst but no hydrogen.  
 Reaction conditions: aniline: 1.0 kmol/m<sup>3</sup>; temp.: 393K; Agitation: 16.66 Hz; reaction volume: 1×10<sup>-4</sup> m<sup>3</sup>;  
 acetone is the solvent and reactant; reaction time: 1.2 h



### 2.3.1.3. Catalyst Stability and Recycle Studies

It is important to ensure the consistent activity of the Pd/Al<sub>2</sub>O<sub>3</sub> catalyst through out a reaction. Otherwise, if the catalyst deactivates during a reaction, reactor performance will be a function of catalyst deactivation rate and may give falsified kinetic parameters. Therefore, activity of the catalyst was checked for consecutive batch reactions with the same catalyst reused (recycle of catalyst). The results are shown in Figure 2.5, which indicate that the intrinsic activity of the catalyst was constant during the batch experiments even after 5 recycles. The initial rates of hydrogenation for each recycle reactions were also calculated and it was observed that those values are identical. ICP-OES analysis of the catalyst and the liquid samples collected after reactions showed no leaching of Pd metal during the reductive alkylation reaction.



**Figure 2.5.** Recycle experiments for reductive alkylation of aniline using 3% Pd/Al<sub>2</sub>O<sub>3</sub>

Reaction conditions: aniline: 1.0 kmol/m<sup>3</sup>, catalyst (3% Pd/Al<sub>2</sub>O<sub>3</sub>): 4 kg/m<sup>3</sup>; P<sub>H<sub>2</sub></sub>: 4 MPa; temp.: 393K; Agitation: 16.66 Hz; reaction volume: 1×10<sup>-4</sup> m<sup>3</sup>; acetone is the solvent and one of the reactants; reaction time: 3 h

### 2.3.2. Solubility Data

For the quantitative analysis of mass transfer effects and interpretation of kinetic data for reductive alkylation of aniline and acetone, the concentrations of hydrogen (solubility) in various compositions of aniline in acetone at different temperatures are essential. The solubility of hydrogen in different aniline and acetone mixtures were determined experimentally using the procedure reported in the literature.<sup>14</sup>

In a typical experiment, for the measurement of hydrogen solubility, a known volume ( $1 \times 10^{-4} \text{ m}^3$ ) of aniline in acetone solution (with a known concentration of aniline) was charged into the reactor and the reactor closed properly. The reactor was flushed thrice with nitrogen to replace air inside the reactor and then flushed twice with hydrogen. The contents were heated to a desired temperature under slow stirring and the reactor pressurized up to a desired pressure when the temperature was attained. Then liquid was stirred at 16.6 Hz for 10-15 min to equilibrate with the gas phase. The pressure drop in the autoclave was recorded when the pressure drop ceased, which indicated the saturation of the liquid phase with hydrogen at that temperature, composition and pressure. The concentration of hydrogen into the liquid phase was calculated assuming the ideal behavior of the gas phase.

The saturation solubility of hydrogen ( $A^*$ ,  $\text{kmol/m}^3$ ) at a particular temperature and composition was correlated with partial pressure of hydrogen ( $P_{H_2}$ , atm.) by Henry's Law as given below:

$$A^* = H_e P_{H_2} \quad (2.4)$$

where,  $H_e$  is the Henry's constant,  $\text{kmol/m}^3/\text{atm}$ . The partial pressure of hydrogen was calculated by subtracting the vapor pressure of solvent (acetone) at the experimental temperature from the total pressure digitally displayed in the automatic controller. The partial pressure of acetone ( $P_v$ , mmHg) at different temperatures were calculated using the correlation as given below:

$$\log(P_v) = (-0.2185 A/T) + B \quad (2.5)$$

where, A and B are constants and  $T$  is temperature (K) inside the reactor. The values of A and B are 7641.5 and 7.904024 respectively for acetone.<sup>15</sup>

The values of Henry's constant at different temperatures and compositions of aniline in acetone are given in Table 2.5.

**Table 2.5.** Solubility data (Henry's constant) for H<sub>2</sub>-in aniline/acetone mixture at different temperatures and compositions

Temperature, K	He × 10 <sup>3</sup> , kmol/m <sup>3</sup> /atm.		
	5% aniline in acetone	10% aniline in acetone	20% aniline in acetone
378	4.66	4.56	4.21
393	5.93	5.79	5.42
408	7.34	7.28	7.01

### 2.3.3. Analysis of Initial Rate Data

The initial rates of hydrogenation reactions were calculated from the H<sub>2</sub> consumption-time profiles observed in a semi batch slurry reactor for a wide range of conditions (Table 2.2). The H<sub>2</sub> consumption-time data were fitted by a second order polynomial of the form

$$Y = a + bt + ct^2 \quad (2.6)$$

where,  $Y$  is the hydrogen consumed in kmol/m<sup>3</sup>;  $t$  is reaction time in seconds;  $a$ ,  $b$  and  $c$  are constants. The rate of reaction at any time  $t$  can be calculated as

$$R_A = \frac{dY}{dt} = b + 2ct \quad (2.7)$$

where,  $R_A$  is the overall rate of hydrogenation reaction, kmol/m<sup>3</sup>/sec. When time  $t$  approaches to zero, Equation 2.7 can be written as

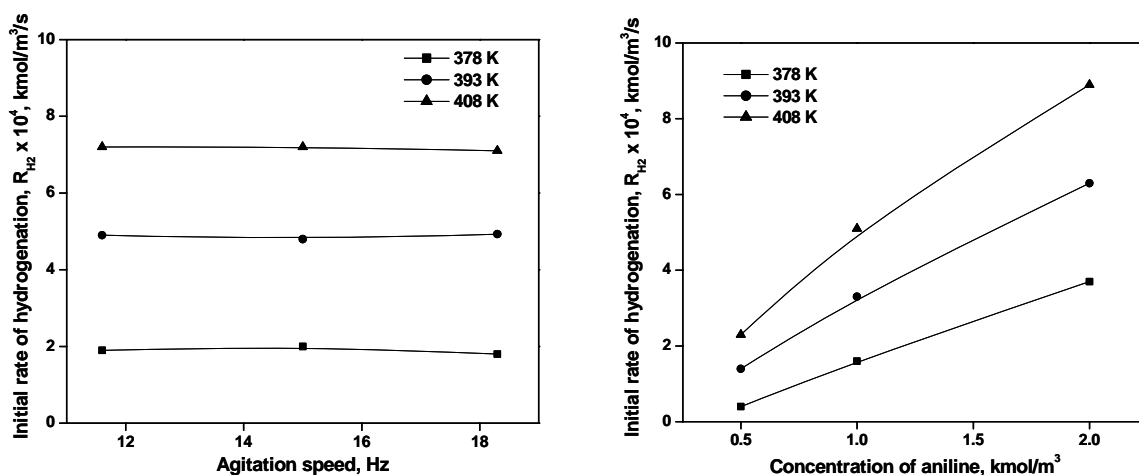
$$(R_A)_{t \rightarrow 0} = R_{H_2} = b \quad (2.8)$$

where,  $R_{H_2}$  is the initial rate of hydrogenation reaction, kmol/m<sup>3</sup>/sec.

The effects of agitation speed and aniline concentration on the initial rate of hydrogenation are shown in Figures 2.6. When the agitation speed was varied from 11.6 to

18.3 Hz (Figure 2.6 A), the rate of reaction was found to be unaffected indicating the absence of gas-liquid and liquid-solid mass transfer resistances.

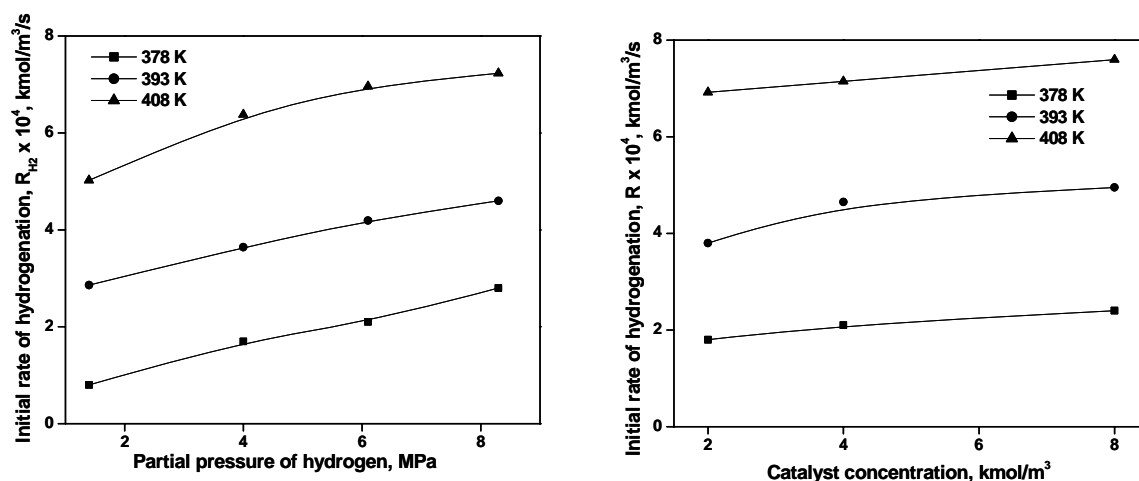
The initial rate of hydrogenation was found to increase linearly with aniline concentration (Figure 2.6 B).



**Figure 2.6.** (A) Effect of agitation speed and (B) Effect of aniline concentration on initial rate of hydrogenation for reductive alkylation of aniline and acetone using 3% Pd/Al<sub>2</sub>O<sub>3</sub>.

Reaction conditions: catalyst (3% Pd/Al<sub>2</sub>O<sub>3</sub>): 4 kg/m<sup>3</sup>; P<sub>H<sub>2</sub></sub>: 4 MPa; temp.: 393K; reaction volume: 1×10<sup>-4</sup> m<sup>3</sup>; acetone is the solvent and one of the reactants. For (A) aniline: 1.0 kmol/m<sup>3</sup>; for (B) agitation: 16.66 Hz

Partial pressure of hydrogen and catalyst loading showed a very negligible effect on initial rate of hydrogenation (Figures 2.7 A and B respectively). Here, it is important to note (see Scheme 2.2) that the hydrogenation step involves a reaction between imine intermediate (SB) and hydrogen on catalyst surface. The formation of SB is controlled by an equilibrium reaction step which is non-catalytic and hence changes in parameters which affect the hydrogenation reaction rate will show mild effects if the equilibrium reaction is rate limiting. The initial rate data indicate that the equilibrium reaction step to form the Schiff's Base [SB] is the rate-limiting step in the overall sequence of reactions.



**Figure 2.7.** (A) Effect of partial pressure of hydrogen and (B) Effect of catalyst loading on initial rate of hydrogenation for reductive alkylation of aniline and acetone using 3% Pd/Al<sub>2</sub>O<sub>3</sub>

Reaction conditions: aniline: 1.0 kmol/m<sup>3</sup>, temp.: 393K; Agitation: 16.66 Hz; reaction volume: 1 × 10<sup>-4</sup> m<sup>3</sup>; acetone is the solvent and one of the reactants. For (A) catalyst (3% Pd/Al<sub>2</sub>O<sub>3</sub>): 4 kg/m<sup>3</sup>; for (B) P<sub>H<sub>2</sub></sub>: 4 MPa

### 2.3.4. Analysis of Mass Transfer Effects

For the purpose of kinetic study, it is important to ensure that the rate data obtained are under kinetic controlled regime. Therefore, initial rate data were used to analyze the significance of various mass transfer resistances at the range of experimental conditions using the criteria discussed by Ramachandran and Chaudhari.<sup>16</sup>

1. Gas-liquid mass transfer resistance can be negligible if,

$$\alpha_1 = \frac{R_{H_2}}{k_l a_b A^*} < 0.1 \quad (2.9)$$

where  $k_l a_b$  is the gas-liquid mass transfer coefficient.

2. Liquid-solid mass transfer resistance can be negligible if,

$$\alpha_2 = \frac{R_{H_2}}{k_s a_p A^*} < 0.1 \quad (2.10)$$

where  $k_s a_p$  is the liquid-solid mass transfer coefficient.

3. Pore diffusion resistance can be considered as negligible if,

$$\phi_{\text{exp}} = \frac{d_p}{6} \left[ \frac{(m+1) \rho_p R_{H_2}}{2 D_e w A^*} \right]^{1/2} < 0.2 \quad (2.11)$$

where,  $D_e$  is the effective diffusivity.

To check if any one type of mass transfer is significant, a knowledge of the gas-liquid mass transfer coefficient,  $k_l a_b$ , the liquid-solid mass transfer coefficient,  $k_s a_p$ , effective diffusivity,  $D_e$ , overall rate of hydrogenation,  $R_A$  and the specific data for the catalyst used such as particle diameter,  $d_p$ , particle density,  $\rho_p$  are required.  $k_l a_b$  was calculated according to the correlation written below:<sup>17</sup>

$$k_l a_b = 1.48 \times 10^{-3} \times (N)^{2.18} \times \left( \frac{V_g}{V_l} \right)^{1.88} \times \left( \frac{d_i}{d_t} \right)^{2.16} \times \left( \frac{h_1}{h_2} \right)^{1.16} \quad (2.12)$$

The specification for slurry reactor used in this kinetic study and typical value of  $k_l a_b$  is presented in Table 2.6.

**Table 2.6.** Specifications of reactor parameters and  $k_l a_b$  calculation

$N$	Agitation speed, 16.7 Hz	$d_t$	Tank diameter, 0.064 m
$V_g$	Volume of gas in the reactor, $2.2 \times 10^{-4} \text{ m}^3$	$h_1$	Height of impeller from the bottom, 0.1 m
$V_l$	Volume of liquid in the reactor, $1 \times 10^{-4} \text{ m}^3$	$h_2$	Height of the liquid, 0.31 m
$d_i$	Impeller diameter, 0.04 m	$k_l a_b = 0.31 \text{ s}^{-1}$	

$k_s$  was calculated by the correlation proposed by Sano *et al.*<sup>18</sup>

$$\frac{k_s d_p}{D_M F_c} = 2 + 0.4 \left[ \frac{e (d_p)^4 \rho_l^3}{\mu_l^3} \right]^{0.25} \left[ \frac{\mu_l}{\rho_l D_M} \right]^{0.333} \quad (2.13)$$

where,  $e$ , the energy supplied to the liquid was calculated according to Calderbank,<sup>19</sup> and  $F_c$ , is the shape factor, was assumed to be unity for spherical particles.

$$e = \frac{N_p N^3 d_i^5 \Psi}{\rho_l V_l} \quad (2.14)$$

where  $N_p$  is the power number assumed to be 6.3 for flat blade turbine and  $\psi$ , the correction factor for gas bubbles was obtained from the correlation:

$$\Psi = 1 - 1.26 \left[ \frac{Q_g}{Nd_l^3} \right] \text{ when } \left[ \frac{Q_g}{ND_l^3} \right] < 3.5 \times 10^{-2} \quad (2.15)$$

$$\Psi = 0.62 - 1.85 \left[ \frac{Q_g}{Nd_l^3} \right] \text{ when } \left[ \frac{Qg}{Nd_l^3} \right] > 3.5 \times 10^{-2} \quad (2.16)$$

where,  $Q_g = R_{\max} \times V_l \times V_M$

Molecular diffusivity,  $D_M$  was calculated from the correlation proposed by Wilke and Chang<sup>20</sup>

$$D_M = \frac{7.4 \times 10^{-8} T (\chi M_w)^{1/2}}{\mu_l \nu_M^{0.6}} \quad (2.17)$$

where,  $\chi$ ,  $M_w$ ,  $\mu_l$  and  $\nu_m$  are the association factor of the solvent, molecular weight of solvent, viscosity of the liquid and molar volume of hydrogen respectively.

External surface area of the catalyst per unit volume,  $a_p$  was calculated from the following correlation:

$$a_p = \frac{6w}{\rho_p d_p} \quad (2.18)$$

where,  $\rho_p$  and  $d_p$  are the particle density and particle diameter respectively.

To calculate  $\phi_{exp}$ , effective diffusivity,  $D_e$  was calculated from the following correlation:

$$D_e = D_M \frac{\varepsilon}{\tau} \quad (2.19)$$

where,  $\varepsilon$  and  $\tau$  are the porosity and tortuosity of the catalyst, which are considered to be 0.5 and 3 respectively.

The values of different parameters required to calculate  $\alpha_1$ ,  $\alpha_2$  and  $\phi_{exp}$  are given in Table 2.7.

**Table 2.7.** Values of different parameters used in mass transfer analysis

Temperature, K	$k_l a_b, s^{-1}$	$k_s \times 10^3,$ m/s	$a_p, m^{-1}$	$D_M \times 10^8,$ m <sup>2</sup> /s	$D_e \times 10^8,$ m <sup>2</sup> /s
378	0.31	5.82	798	2.72	0.453
393	0.31	6.42	798	3.01	0.501
408	0.31	7.65	798	3.58	0.597

The saturation solubility of hydrogen,  $A^*$  at a particular temperature, composition and partial pressure of hydrogen was calculated from the data given in Table 2.5. Initial rate of hydrogenation,  $R_{H_2}$  for a reaction was obtained from the procedure described in Section 2.3.3. The highest calculated values of parameters  $\alpha_1$ ,  $\alpha_2$  and  $\phi_{\text{exp}}$  were 0.010, 0.0005 and 0.015 respectively indicating absence of mass transfer limitations.

Therefore, it is evident that the initial rate data will not be useful in determining the intrinsic kinetics for such a complex homogeneous-heterogeneous reaction system under consideration and integral concentration-time data should be considered in interpretation of the intrinsic kinetics.

### 2.3.4 5. Kinetic Modeling

For the purpose of kinetic modeling, the reaction scheme shown in Scheme 2.2 was considered in which the rate of non-catalytic equilibrium reaction involving condensation of aniline and acetone was assumed as follows:

$$R_1 = k_{1C} C_B C_C - k_2 C_E C_D \quad (2.20)$$

where,  $R_1$  is the net rate of reaction of aniline (Scheme 2.2),  $C_B$ ,  $C_E$ ,  $C_C$  and  $C_D$  are the concentrations of aniline, Schiff's base, acetone and water respectively. As we are using acetone in excess, and the concentration of water at any time can be expressed as  $(C_0 - C_1)$ , the Equation 2.20 becomes:

$$R_1 = k_1 C_B - k_2 C_E (C_0 - C_B) \quad (2.21)$$

where,  $k_1 = (k_{1C} C_C)$  and  $C_0$  is the initial concentration of aniline.

To represent the intrinsic kinetics of catalytic hydrogenation steps, several forms of rate equations were considered. Several authors have reported the activation of hydrogen in presence of palladium metal<sup>21</sup> in which the hydrogen may be present as an  $\alpha$ -hydride ( $\text{Pd}(\text{H})_2$ ) or a  $\beta$ -hydride ( $\text{Pd}(\text{H})$ ) species and that metal surface influences the reaction rate dramatically.<sup>22</sup> Molecular level description for activation of Schiff's base and aromatic ring in the presence of palladium metal surface are not well documented in the literature. Therefore, rate equations based on Langmuir-Hinshelwood (L-H) models were proposed based on the possible interactions of  $\text{H}_2$  and liquid phase components on Pd metal surface. The dual site mechanism was not considered since there was no substrate-inhibited kinetics



(characteristic of dual site model) observed with respect to either the amine or hydrogen. Several basic assumptions were made to develop the rate equations: (i) the rate of surface reaction is rate limiting for the hydrogenation steps (ii) adsorption and desorption rates are much higher than the rate of surface reaction (iii) adsorption of aniline and acetone on the catalyst surface is negligible (iv) N-IPC desorbed very fast from the catalyst surface to keep the catalyst surface free for reaction. The following models were considered:

**Model 1.** Reaction of adsorbed  $\alpha$ -hydride ( $\text{Pd}(\text{H})_2$ ) species with the liquid phase components as rate limiting steps for hydrogenation reactions.

**Model 2.** Reaction of adsorbed  $\alpha$ -hydride ( $\text{Pd}(\text{H})_2$ ) species with adsorbed liquid phase components as rate limiting steps ( a case of competitive adsorption).

**Model 3.** Reaction of  $\beta$ -hydride ( $\text{Pd}(\text{H})$ ) species with the liquid phase components as rate limiting steps.

**Model 4.** Competitive adsorption and reaction of  $\beta$ -hydride ( $\text{Pd}(\text{H})$ ) species and other reactants on the metal surface as rate limiting steps.

The rate equations derived for these models are presented in Table 2.8. It is important to mention here that the equilibrium reaction is the slowest step of the overall reaction sequence. Different rate limiting steps assumed in models 1-4 are only for the hydrogenation reactions.

In order to check the applicability of the rate models derived under isothermal and integral conditions, a semi batch reactor model was developed. Material balance of the liquid phase components based on Model 4 are given bellow as an example:

$$\frac{dC_B}{dt} = -R_1 = -(k_1 C_B - k_2 C_E (C_o - C_B)) \quad (2.22)$$

$$\frac{dC_E}{dt} = R_1 - R_2 = k_1 C_B - k_2 C_E (C_o - C_B) - \frac{k_3 w C_E (A^*)^{1/2}}{\left(1 + K_H (A^*)^{1/2} + \sum_{i=2,3} K_i C_i\right)^2} \quad (2.23)$$

$$\frac{dC_F}{dt} = R_2 - R_3 = \frac{w (A^*)^{1/2} (k_3 C_E - k_4 C_F)}{\left(1 + K_H (A^*)^{1/2} + \sum_{i=2,3} K_i C_i\right)^2} \quad (2.24)$$

$$\frac{dC_G}{dt} = R_3 = \frac{k_4 w C_F (A^*)^{1/2}}{\left(1 + K_H (A^*)^{1/2} + \sum_{i=2,3} K_i C_i\right)^2} \quad (2.25)$$

with the initial conditions:

$$\text{at } t = 0, C_B = C_0, C_E = C_F = C_G = 0 \quad (2.26)$$

where  $C_B$ ,  $C_E$ ,  $C_F$  and  $C_G$  are the concentrations of aniline, SB, N-IPA and N-IPC respectively (see Scheme 2.2) in  $\text{kmol/m}^3$ ,  $k_1$  to  $k_4$  are the rate constants of corresponding reaction steps shown in Scheme 2.2 and  $K_H$ ,  $K_E$  and  $K_F$  are the adsorption constants for hydrogen, [SB] (E) and N-IPA (F) respectively.

Total rate of hydrogenation can be represented as:

$$R_A = R_2 + 3R_3 \quad (2.27)$$

In order to select a rate equation, a non-linear least square regression analysis was used for each rate equation to get the best fit values of the parameters. An optimization program based on Marquardt's algorithm combined with Runge-Kutta method was used. The optimization method involved an objective function, the value of which was minimized during the optimization,

$$\phi_{\min} = \sum_{i=1}^4 \sum_{i=1}^n (Y_{i_{\text{exp}}} - Y_{i_{\text{mod}}}) \quad (2.28)$$

where,  $Y_{i_{\text{exp}}}$  and  $Y_{i_{\text{mod}}}$  represent experimental and predicted concentrations of  $i$ -th species and  $n$  represents the number of samples. The mean average of relative residuals (% RR) was also calculated based on the following expression:

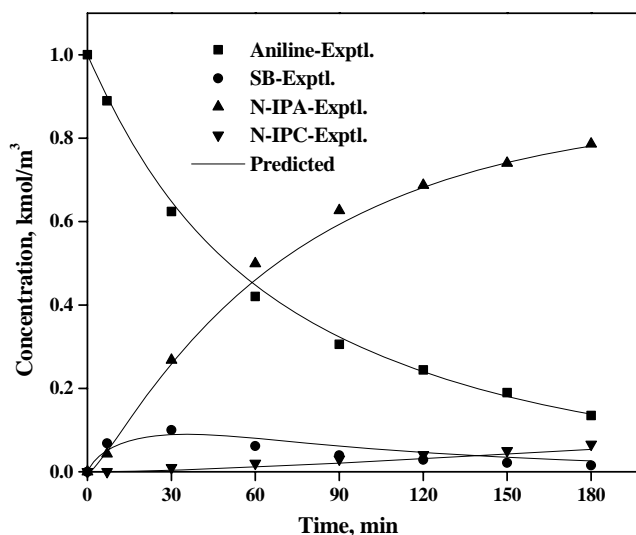
$$\% RR = \sum_{i=1}^4 \sum_{i=1}^n \frac{(Y_{i_{\text{exp}}} - Y_{i_{\text{mod}}})}{Y_{i_{\text{exp}}}} \times 100 \quad (2.29)$$

**Table 2.8.** Comparison of various models for reductive alkylation of aniline with acetone using 3% Pd/Al<sub>2</sub>O<sub>3</sub>

Model No.	Model	Temp., K	$k_1 \times 10^4$	$k_2 \times 10^4$	$k_3$	$k_4 \times 10^3$	$K_H$	$K_2$	$K_3$	% RR	$\phi_{min}$
1	$R_1 = k_1 C_B - k_2 C_E (C_0 - C_B)$	378	2.325	-2.77	0.1073	0.911	34.6	230.35	86.01	± 12	$7.2 \times 10^{-3}$
	$R_i = \frac{k_i w C_i A^*}{(1 + K_H A^* + \sum_{i=2,3} K_i C_i)}$	393	4.212	6.951	0.1912	2.428	86.805	377.23	161.2	± 16	$4.3 \times 10^{-4}$
		408	4.564	3.207	0.4084	-4.26	194.5	863.61	-116.7	± 16	$3.9 \times 10^{-4}$
2	$R_1 = k_1 C_B - k_2 C_E (C_0 - C_B)$	378	2.36	3.904	0.9847	7.706	53.749	66.17	17.256	± 19	$5.7 \times 10^{-3}$
	$R_i = \frac{k_i w C_i A^*}{(1 + K_H A^* + \sum_{i=2,3} K_i C_i)^2}$	393	4.37	8.745	2.494	31.73	89.42	71.029	23.989	± 16	$3.8 \times 10^{-3}$
		408	8.23	43.44	6.3707	78.14	116.24	119.74	25.395	± 18	$4.3 \times 10^{-2}$
3	$R_1 = k_1 C_B - k_2 C_E (C_0 - C_B)$	378	2.535	6.301	$5.703 \times 10^{-2}$	0.51	34.08	217.44	108.09	± 13	$4.7 \times 10^{-4}$
	$R_i = \frac{k_i w C_i (A^*)^{1/2}}{(1 + K_H (A^*)^{1/2} + \sum_{i=2,3} K_i C_i)}$	393	4.355	8.276	$7.508 \times 10^{-2}$	1.097	50.93	234.63	126.52	± 15	$4.1 \times 10^{-4}$
		408	4.899	8.572	$13.10 \times 10^{-2}$	1.306	56.79	588.61	51.04	± 16	$5.1 \times 10^{-4}$
4	$R_1 = k_1 C_B - k_2 C_E (C_0 - C_B)$	378	2.308	2.728	0.4593	4.892	45.58	44.96	26.87	± 6	$1.1 \times 10^{-6}$
	$R_i = \frac{k_i w C_i (A^*)^{1/2}}{(1 + K_H (A^*)^{1/2} + \sum_{i=2,3} K_i C_i)^2}$	393	4.047	5.342	0.5827	7.414	34.75	73.5	15.57	± 3	$4.5 \times 10^{-6}$
		408	5.354	14.99	0.9402	8.993	26.3	97.12	9.88	± 4	$7.6 \times 10^{-6}$

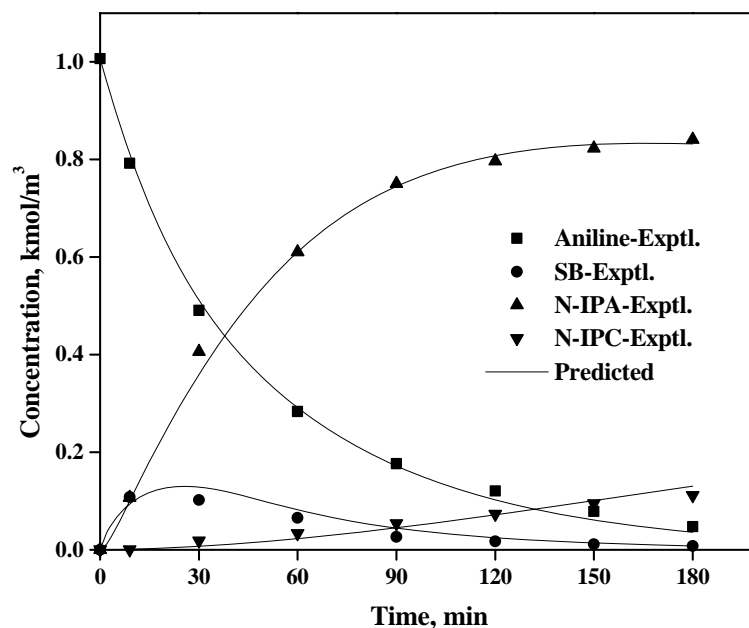
The rate models were discriminated based on  $\phi_{\min}$  and % RR values for each model. In addition, to thermodynamic criteria proposed by Vannice et al.<sup>23</sup> and Boudart<sup>24</sup> were also considered for model discrimination. These criteria are (i) rate constants and adsorption constants should be positive ( $k > 0$ ,  $K > 0$ ) and (ii) activation energy should be positive ( $Ea > 0$ ). The values of  $\phi_{\min}$  and %RR along with the optimized rate and adsorption parameters are presented in Table 2.8.

Based on above criteria, model 1 can be rejected, as some of the rate parameters predicted are negative. Among the remaining models, model-4 has the lowest  $\phi_{\min}$  and %RR. Hence, this model was selected as the best model. The experimental and predicted concentration-time profiles and hydrogen consumption-time data are shown in Figures 2.8-2.11. The relative residuals (%RR) as a function of operating parameters such as aniline concentration, partial pressure of hydrogen catalyst concentration and temperature are also shown in Figures 2.12-2.14, which showed that the scatter RR values are close to  $\pm 10$  for all temperatures without any particular trend. This indicates the stability of the model. The insets of Figures 2.12-2.14 showed the RR values based on Model 2 and 3. The results indicate that the semibatch reactor model developed in Equations 2.22-2.27 predicted the concentration-time as well as hydrogen consumption-time profiles reasonably well.



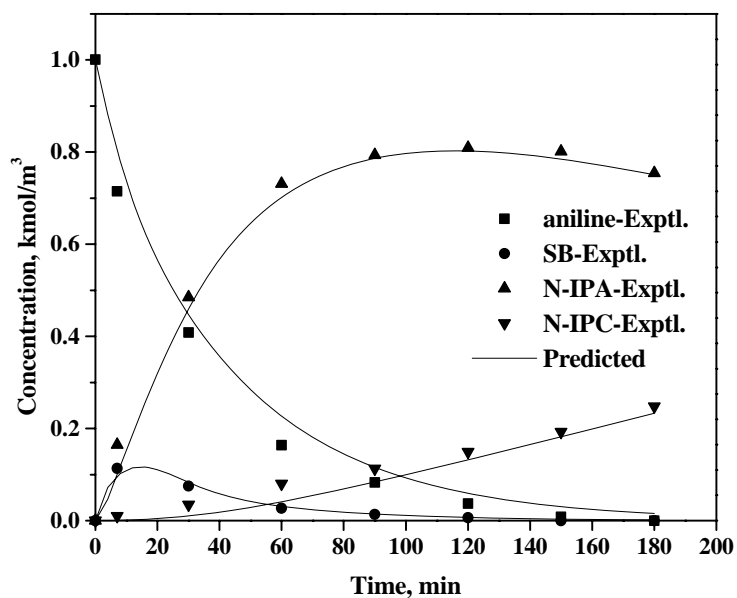
**Figure 2.8.** Concentration-Time profile at 378 K

Reaction conditions: aniline: 1.0 kmol/m<sup>3</sup>, catalyst loading: 4 kg/m<sup>3</sup>; P<sub>H<sub>2</sub></sub>: 4 MPa; Agitation: 16.66 Hz; reaction volume: 1×10<sup>-4</sup> m<sup>3</sup>; acetone is the solvent and one of the reactants; reaction time: 3h



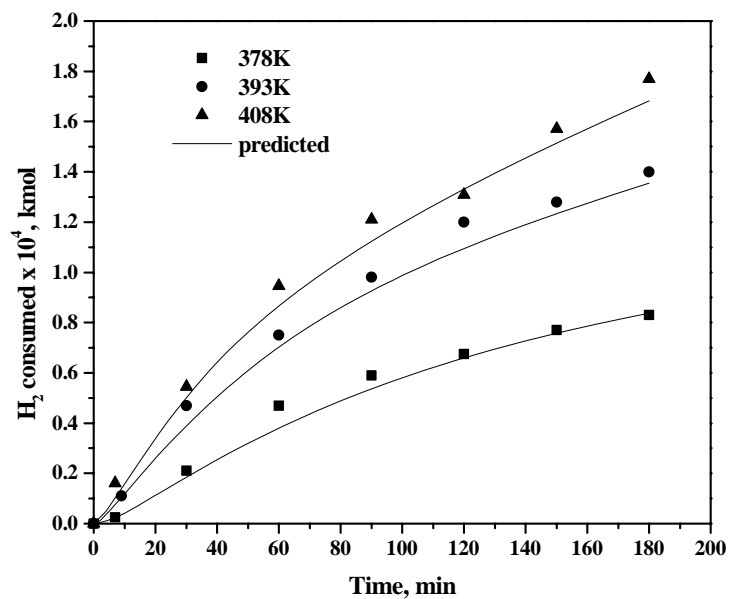
**Figure 2.9.** Concentration-Time profile at 393 K

Reaction conditions: aniline:  $1.0 \text{ kmol/m}^3$ , catalyst loading:  $4 \text{ kg/m}^3$ ;  $P_{\text{H}_2}$ : 4 MPa; Agitation: 16.66 Hz; reaction volume:  $1 \times 10^{-4} \text{ m}^3$ ; acetone is the solvent and one of the reactants; reaction time: 3h.

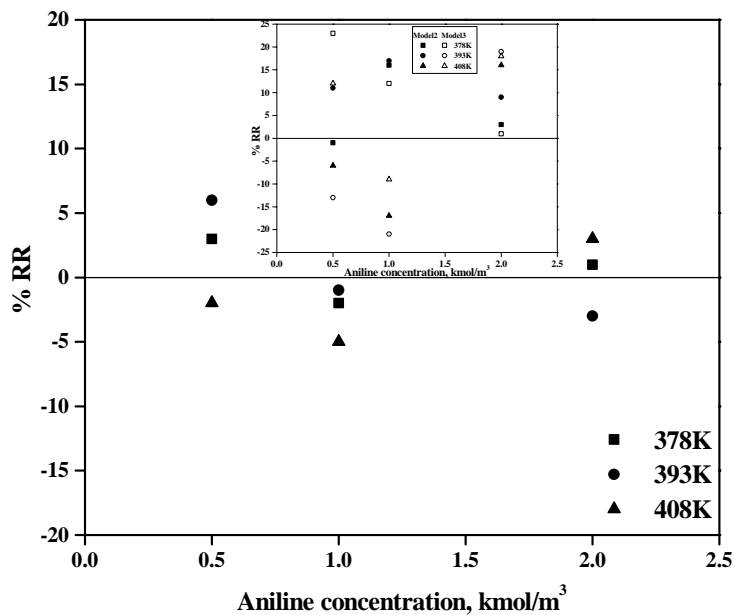


**Figure 2.10.** Concentration-Time profile at 408 K

Reaction conditions: aniline:  $1.0 \text{ kmol/m}^3$ , catalyst loading:  $4 \text{ kg/m}^3$ ;  $P_{\text{H}_2}$ : 4 MPa; Agitation: 16.66 Hz; reaction volume:  $1 \times 10^{-4} \text{ m}^3$ ; acetone is the solvent and one of the reactants; reaction time: 3h



**Figure 2.11.** H<sub>2</sub> consumption-Time profiles at different temperatures  
 Reaction conditions: aniline: 1.0 kmol/m<sup>3</sup>, catalyst loading: 4 kg/m<sup>3</sup>, P<sub>H<sub>2</sub></sub>: 4 MPa; Agitation: 16.66 Hz; reaction volume: 1×10<sup>-4</sup> m<sup>3</sup>; acetone is the solvent and one of the reactants; reaction time: 3h



**Figure 2.12.** %RR values at different aniline concentrations

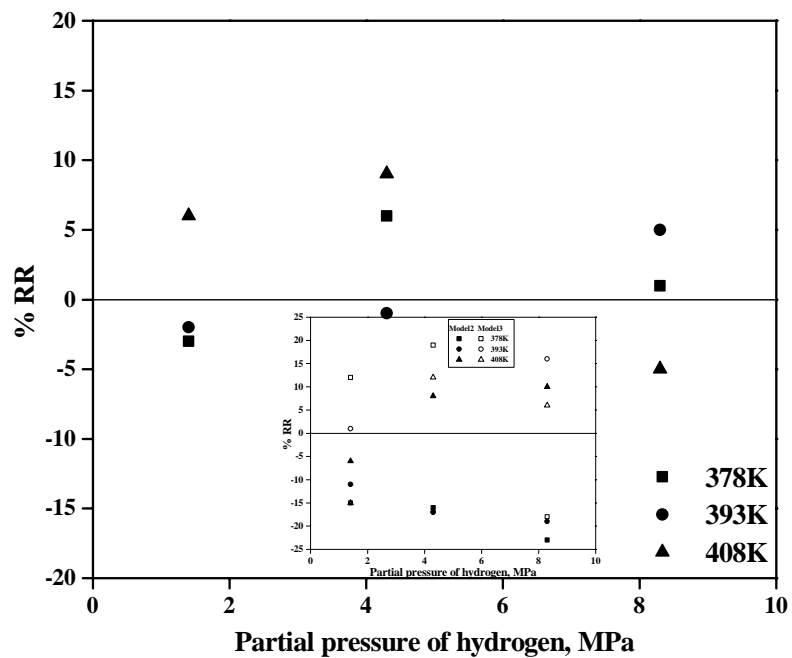


Figure 2.13. %RR values at different partial pressures of hydrogen

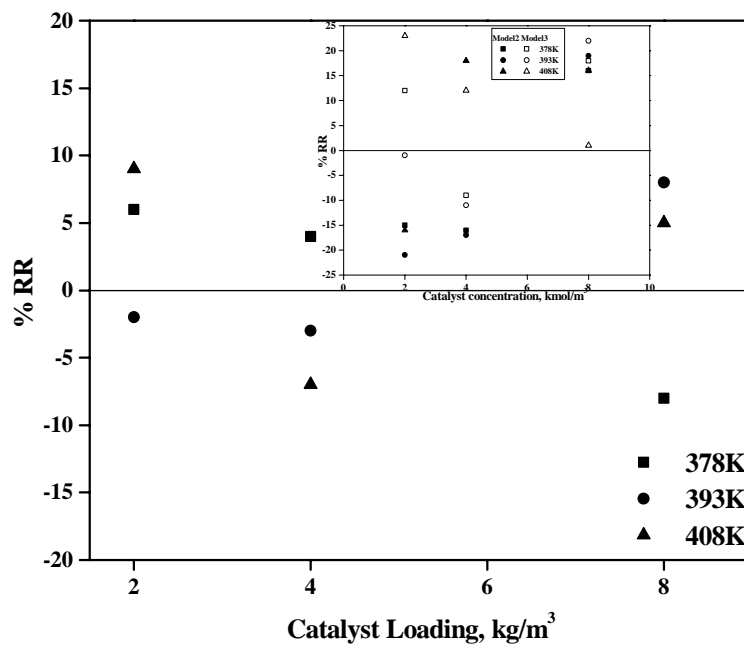


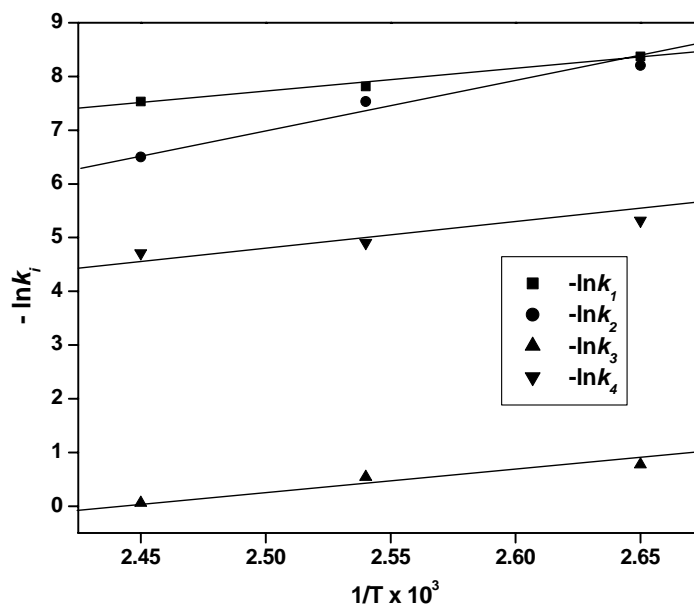
Figure 2.14. %RR values at different catalyst loadings

The temperature dependence of rate constants is shown in Figure 2.15 from which the activation energies of the individual reactions were calculated as 36.16, 72.59, 30.47 and 26.13 kJ/mol for steps R<sub>1</sub> to R<sub>3</sub> respectively.

The enthalpy of adsorption was calculated from the following equations:

$$K_i = K_{i0} \exp\left(-\frac{\Delta H_i}{RT}\right) \quad (2.30)$$

The calculated enthalpy of adsorption values ( $-\Delta H$ ) for  $K_H$ ,  $K_E$  and  $K_F$  are 23.85, -33.01 and 42.79 kJ/mol respectively. The negative value of enthalpy of adsorption for  $K_2$  indicates a possibility of endothermic chemisorption. Such observation, though uncommon, has also been previously reported by Broderick and Gates<sup>25</sup> and Chaudhari et al.<sup>26</sup> for hydrogenation reactions.



**Figure 2.15.** Temperature dependence of rate constants

### 2.3.6. Trickle Bed Reactor Model

In this section, a theoretical trickle bed reactor model has been developed considering reductive alkylation of aniline and acetone using 3% Pd/Al<sub>2</sub>O<sub>3</sub> catalyst and the model predictions results have been compared with experimental results.



### 2.3.6.1. Mathematical Model

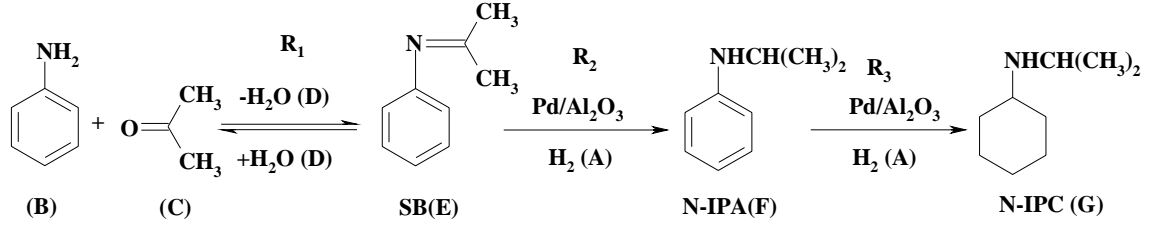
The present model was developed following the approach proposed earlier by Rajashekharam et al.<sup>27</sup> The features of the model are: The spherical catalyst particle was assumed to be divided into three zones which represented (i) a dry zone, (ii) a wetted zone covered by the flowing dynamic liquid and (iii) a wetted zone covered by the stagnant liquid. It was assumed that (a) gas and liquid phases are in plug flow; (b) liquid-phase reactant is non-volatile and is in excess compared to the gaseous reactant concentration in the liquid phase; (c) the gas-liquid, liquid-solid and intraparticle mass transfer resistances for H<sub>2</sub> are considered, whereas the liquid-solid and intraparticle mass transfer resistances for the liquid phase components are assumed to be negligible; (d) the interphase and intraparticle heat transfer resistances are negligible but bed to wall heat transfer has been considered to incorporate the non-isothermal effects; (e) the overall catalytic effectiveness factor can be expressed as a sum of the weighted average of the effectiveness factors in the dynamic liquid covered, stagnant liquid covered and gas covered zones, respectively, i.e.,

$$\eta_c = f_d \eta_{c_d} + f_s \eta_{c_s} + (1 - f_d - f_s) \eta_{c_g} \quad (2.31)$$

where,  $\eta_c$  is the overall catalytic effectiveness factor under conditions of partial wetting and stagnant liquid pockets and  $f_d$  and  $f_s$  are the fractions of catalyst particle covered by the dynamic and stagnant liquid zones.  $\eta_c$  is the catalyst effectiveness factor with  $\eta_{c_d}$ ,  $\eta_{c_s}$  and  $\eta_{c_g}$  representing the corresponding values for the dynamic, stagnant and dry zones, respectively. The overall catalytic effectiveness factor can be written as:

$$\eta_c = \frac{1}{\phi} \left( \coth 3\phi - \frac{1}{3\phi} \right) \quad (2.32)$$

The stepwise reactions of aniline and acetone in presence of a 3% Pd/Al<sub>2</sub>O<sub>3</sub> catalyst and hydrogen is shown below:



As already mentioned in Section 2.3.4.5, the following types of rate equations are suitable to represent the above homogeneous (non-catalytic) and heterogeneous (catalytic) reaction steps respectively:

$$R_1 = k_1 C_B - k_2 C_E (C_0 - C_B) \quad (2.33)$$

$$R_i = \frac{k_i w C_i (A^*)^{1/2}}{(1 + K_H (C_A^*)^{1/2} + \sum_{i=2,3} K_i C_i)^2} \quad (2.34)$$

where,  $C_i$  represents the concentration of  $i^{\text{th}}$  component,  $k_i$  is the rate constants of the respective steps and  $K_i$  is the adsorption constants of the  $i^{\text{th}}$  component.  $R_i$  represents the rate of reaction of the respective steps as presented in the above reaction scheme.

The catalytic effectiveness factor given in Equation 2.32 can be calculated following the well-known approaches by Ramachandran et al and Bischoff,<sup>16,28</sup> where the Thiele modulus,  $\Phi$  is defined as:

$$\phi = \frac{R}{3} \rho_p \Omega_A (A_s) \left[ \int_0^{A_s} 2D_e \rho_p \Omega_A (A) dA \right]^{-1/2} \quad (2.35)$$

For the kinetics given above, the Thiele modulus can be written as:

$$\phi = k''' \left\{ \frac{2k'}{K_A^3} \left[ (k'' + K_A \sqrt{A_s}) - 2k'' \ln(k'' + K_A \sqrt{A_s}) + 2k'' \ln k'' - \frac{(k'')^2}{(k'' + K_A \sqrt{A_s})} \right] \right\}^{-0.5} \quad (2.36)$$

or in terms of dimensionless concentrations

$$\phi = \phi_0 \left[ (k'' + k_a \sqrt{a_s}) - 2k'' \ln(k'' + k_a \sqrt{a_s}) + 2k'' \ln(k'') - \frac{(k'')^2}{(k'' + k_a \sqrt{a_s})} \right]^{-0.5} \quad (2.37)$$

with

$$\phi_0 = k''' \left[ \frac{K_A^3}{2k'} \right]^{0.5} \quad (2.38)$$

where,

$$k' = 2D_e \rho_p (e_l + 3k_{43} f_l) \quad (2.39)$$

$$k'' = 1 + k_e e_l + k_f f_l \quad (2.40)$$

$$\text{and } k''' = \frac{R}{3} \left[ \frac{\rho_p k_3 B_{li} \sqrt{A^*} (e_l + 3k_{43} f_l) \sqrt{a_s}}{(k'' + k_a \sqrt{a_s})^2} \right] \quad (2.41)$$

The dimensionless parameters used in expressing  $\phi$  are listed in Table 2.9.

The mass balance of hydrogen in dynamic liquid phase can be written as:

$$-u_l \frac{dA_{ld}}{dx} + k_L a_B (A^* - A_{ld}) = K_{ex} \varepsilon_{ls} (A_{ld} - A_{ls}) + f_d k_{sd} a_p (A_{ld} - A_{sd}) \quad (2.42)$$

At steady state conditions, the sum of the convection term and the gas-liquid mass transfer term are in equilibrium with the liquid-solid mass transfer term in the dynamic zone and the volumetric mass exchanged between the dynamic and stagnant zones. In a previous study by Hochmann et al,<sup>29</sup> it was shown that the exchange rates between the dynamic and stagnant zones could be explained by a volumetric mass exchange coefficient,  $K_{ex}$ , and with the help of a cross-flow model. Thus, in the dynamic zone, we also have:

$$f_d k_{sd} a_p (A_{ld} - A_{sd}) = \frac{f_d \eta_c \rho_p (1 - \varepsilon_B) (k_3 E_l + k_4 F_l) \sqrt{A_{sd}}}{(1 + K_A \sqrt{A_{sd}} + K_E E_l + K_F F_l)^2} \quad (2.43)$$

In the stagnant zone, we have

$$K_{ex} \varepsilon_{ls} (A_{ld} - A_{ls}) = f_s k_{ss} a_p (A_{ls} - A_{ss}) = \frac{f_s \eta_c \rho_p (1 - \varepsilon_B) (k_3 E_l + k_4 F_l) \sqrt{A_{ss}}}{(1 + K_A \sqrt{A_{ss}} + K_E E_l + K_F F_l)^2} \quad (2.44)$$

**Table 2.9.** Dimensionless parameters used in the model

Mass transfer parameters	
Gas-liquid mass transfer	$\alpha_{gl} = k_L a_B. L / u_l$
Liquid-solid mass transfer (dynamic zone)	$\alpha_{lsd} = k_s a_p. L/u_l$
Liquid-solid mass transfer (stagnant zone)	$\alpha_{ss} = k_{ss}. a_p. L/u_l$
Liquid-solid mass transfer (dry zone)	$\alpha_{gs} = k_{gs} a_p L/u_l$
Reaction rate and equilibrium constants	$k_a = K_A. \sqrt{A^*}; k_e = K_E. B_{li}; k_f = K_F. B_{li};$ $k_{43} = k_4/k_3$ $\alpha_{R1} = L.k_1/u_l; \alpha_{R2} = L.k_2.B_{li}/u_l$ $\alpha_{R3A} = L.w.k_3. \sqrt{B_{li}}/u_l; \alpha_{R3E} = L.w.k_3. \sqrt{A^*}/u_l$ $\alpha_{R4} = L.w.k_4. \sqrt{A^*}/u_l$
Heat transfer parameters	
	$\beta_1 = \frac{(-\Delta H_1)B_{li}}{T_o \rho_l C_{pl} \left[ 1 + \frac{u_g \rho_g C_{pg}}{u_l \rho_l C_{pl}} \right]}$ $\beta_2 = \frac{(-\Delta H_2)B_{li}}{T_o \rho_l C_{pl} \left[ 1 + \frac{u_g \rho_g C_{pg}}{u_l \rho_l C_{pl}} \right]}$ $\beta_3 = \frac{4U_w L}{u_l \rho_l C_{pl} d_T \left[ 1 + \frac{u_g \rho_g C_{pg}}{u_l \rho_l C_{pl}} \right]}$
	( $\Delta H_1$ and $\Delta H_2$ are the total heat of reaction for the non-catalytic and catalytic steps respectively)

The liquid entering to the stagnant zone from the dynamic zone, characterized by the volumetric mass exchange coefficient,  $K_{ex}$ , containing the dissolved gaseous species A, at steady state is in equilibrium with liquid-solid mass transfer term in the stagnant zone and the reaction in the catalyst particles in the stagnant zones (including pore diffusion effects).

The mass balance for species A in the dry zone can be written as:

$$(1-f_d-f_s)k_{g_s}a_p(A^*-A_{s_g})=\frac{(1-f_d-f_s)\eta_c\rho_p(1-\varepsilon_B)(k_3E_l+k_4F_l)\sqrt{A_{s_g}}}{(1+K_A\sqrt{A_{s_d}}+K_EE_l+K_FF_l)^2} \quad (2.45)$$

Equations 2.42-2.45 can be simplified and expressed in terms of dimensionless parameters. The unknown surface concentrations can be suitably expressed in terms of known parameters. The final mass balance equations for species A (hydrogen) in dimensionless form for the wetted and dry zone can be written as:

$$-\frac{da_{ld}}{dz}+\alpha_{gl}(1-a_{ld})=f_s\alpha_{s_s}(a_{ls}-a_{ss})+\alpha_{ls_d}(a_{ld}-a_{sd}) \quad (2.46)$$

$$f_d\alpha_{ls_d}(a_{ld}-a_{sd})=\frac{f_d\eta_c\alpha_{R3A}(e_l+k_{43}f_l)\sqrt{a_{sd}}}{(1+k_a\sqrt{a_{sd}}+k_e e_l+k_f f_l)^2} \quad (2.47)$$

$$\frac{L}{u_l}K_{ex}\varepsilon_{ls}(a_{ld}-a_{ls})=f_s\alpha_{s_s}(a_{ls}-a_{ss})=\frac{f_s\eta_c\alpha_{R3A}(e_l+k_{43}f_l)\sqrt{a_{ss}}}{(1+k_a\sqrt{a_{ss}}+k_e e_l+k_f f_l)^2} \quad (2.48)$$

$$(1-f_d-f_s)\alpha_{g_s}(1-a_{sg})=\frac{(1-f_d-f_s)\eta_c\alpha_{R3A}(e_l+k_{43}f_l)\sqrt{a_{sg}}}{(1+k_a\sqrt{a_{sg}}+k_e e_l+k_f f_l)^2} \quad (2.49)$$

Also, the mass balance of the homogeneous non-catalytic equilibrium reaction involving condensation of aniline and acetone can be written as:

$$-\frac{db_{ld}}{dx}=\alpha_{R1}b_l-\alpha_{R2}e_l(1-b_l) \quad (2.50)$$

Similarly, the mass balance equations of liquid phase components for the catalytic hydrogenation steps in dimensionless form can be written as:

$$\frac{de_{ld}}{dx}=\alpha_{R1}b_l-\alpha_{R2}e_l(1-b_l)-\eta_c\alpha_{R3E}e_l\chi \quad (2.51)$$

$$\frac{df_{ld}}{dx}=\left[\frac{f_s\eta_c\alpha_{R3E}}{3}\right](3e_l-k_{43}f_l)\chi \quad (2.52)$$

$$\frac{dg_{ld}}{dz} = \frac{f_s \eta_c \alpha_{R4} f_l \chi}{3} \quad (2.53)$$

with

$$\chi = \left\{ \begin{aligned} & \frac{f_d \sqrt{a_{sd}}}{\left(1 + k_a \sqrt{a_{sd}} + k_e e_l + k_f f_l\right)^2} + \frac{f_s \sqrt{a_{ss}}}{\left(1 + k_a \sqrt{a_{ss}} + k_e e_l + k_f f_l\right)^2} \\ & + \frac{(1 - f_d - f_s) \sqrt{a_{sg}}}{\left(1 + k_a \sqrt{a_{sg}} + k_e e_l + k_f f_l\right)^2} \end{aligned} \right\} \quad (2.54)$$

The dimensionless parameters used in these equations are defined in Table 2.9.

Lastly, in deriving a non-isothermal trickle bed reactor model, the dependencies of various parameters like reaction rate constants, equilibrium constants, effective diffusivity and saturation solubility on temperature are accounted for. The change in rate and equilibrium constants with respect to temperature can be represented as:

$$k_i(T) = k_i(T_o) \exp \left[ \frac{E_i}{RT_o} \left( 1 - \frac{1}{\theta} \right) \right] \quad (2.55)$$

$$K_i(T) = K_i(T_o) \exp \left[ \frac{-\Delta H_i}{RT_o} \left( 1 - \frac{1}{\theta} \right) \right] \quad (2.56)$$

where  $\theta = T / T_o$ . The variation of effective diffusivity with respect to temperature can be expressed as

$$D_e(T) = D_e(T_o) \exp \left[ \frac{E_D}{RT_o} \left( 1 - \frac{1}{\theta} \right) \right] \quad (2.57)$$

where,

$$D_e(T_o) = D_m \frac{\varepsilon}{\tau} \quad (2.58)$$

Here,  $D_m$  is the molecular diffusivity and is evaluated from the correlation of Wilke and Chang,  $\varepsilon$  and  $\tau$  represents the porosity and the tortuosity factors considered as 0.5 and 3. The dependence of saturation solubility on temperature is given as:

$$(A^*)_T = [P - (P_v)_T][(H_e)_T] \quad (2.59)$$

where,  $P_v$  is the change in vapor pressure of the solvent due to temperature rise, given as:

$$\log(P_v) = (-0.2185 \times 7641.5/T) + 7.90424 \quad (2.60)$$

and Henry's constant as a function of temperature can be written as:

$$(H_e)_T = -1.9 \times 10^{-3} + 1.82 \times 10^{-5} T - 1.89 \times 10^{-5} Y \quad (2.61)$$

The above equations [Equations 2.59-2.61] are applicable when acetone is used as a solvent. Owing to the exothermicity of the reaction, an increase in the bed temperature is expected and as a consequence might lead to enhance rates. The heat generated within the reactor is mainly carried away by the flowing liquid and also due to transfer of heat from the catalyst particle to the reactor wall which is characterized by the bed to wall heat transfer coefficient,  $U_w$ . Under such conditions, where the interphase and intraparticle heat transfer resistances are assumed to be negligible, the heat balance of the reactor can be written as:

$$(u_l \rho_l C_{p_l} + u_g \rho_g C_{p_g}) \frac{dT}{dx} = \left\{ \begin{array}{l} (-\Delta H_1)[k_1 B_l - k_2 E_l (B_{l_i} - B_l)] \\ + (-\Delta H_2) \left[ \frac{\eta_c \rho_p (1 - \varepsilon_B)(k_3 E_l - 3k_4 F_l) \sqrt{A_s}}{(1 + K_A \sqrt{A_s} + K_E E_l + K_F F_l)^2} \right] \\ - \frac{4U_w (T_b - T_w)}{d_T} \end{array} \right\} \quad (2.62)$$

The above equation in dimensionless form can be written as:

$$\frac{d\theta}{dz} = \beta_1 [\alpha_{R_1} b_l - \alpha_{R_2} e_l (1 - b_l)] + \beta_2 \eta_c \alpha_{R_{3A}} (e_l + 3k_{43} f_l) \chi - \beta_3 (\theta_b - \theta_w) \quad (2.63)$$

Equation 2.63 can be used to predict the maximum temperature rise along the length of the reactor. The various dimensionless parameters used in the above model are given in Table 2.9.

### 2.3.6.2. Comparison of Experimental results with Model Predictions

The model equations developed in the previous section (Equations 2.46, 2.50-2.53 combined with 2.63) allow prediction of experimental results for a given set of inlet conditions in a trickle bed reactor, for which, knowledge of kinetics, mass and heat transfer parameters and hydrodynamic parameters is essential. The intrinsic kinetic parameters used are given in Table 2.8. For other parameters, correlations from literature were used and are summarized in Table 2.10.

**Table 2.10.** Correlations used for Trickle bed reactor modeling

Parameter	Correlation	Reference
Gas-liquid mass transfer coefficient	$\frac{K_L a_B d_p}{D(1 - \varepsilon_L / \varepsilon_B)} = 2 \left( \frac{S_p}{d_p^2} \right)^{0.2} \text{Re}_L^{0.73} \text{Re}_G^{0.2} \left( \frac{\mu_L}{\rho_L D} \right)^{0.5} \left( \frac{d_p}{d_r} \right)^{0.2}$	30
Liquid-Solid mass transfer coefficient	$\frac{K_s d_p a_w}{D a_p} = 0.815 \text{Re}_L^{0.822} \left( \frac{\mu_L}{\rho_L D} \right)^{0.333}$	31
Total liquid holdup	$\log(1 - \varepsilon_l) = - \frac{1.22 \text{We}_L^{0.15}}{\text{Re}_L^{0.20} X_G^{0.15}}$	32
Bed to wall heat transfer coefficient	$\frac{U_w d_p}{\lambda_L} = 0.057 \left( \frac{\text{Re}_L}{\varepsilon_L} \right)^{0.09} \text{Pr}_L^{1/3}$	33
Pressure drop	$\frac{\Delta P}{Z} = \frac{2 \rho_g U_g^2}{d_K \left( X_G (\text{Re}_L \text{We}_L)^{\frac{1}{4}} \right)^{\frac{3}{2}}} \left[ 31.3 + \frac{17.3}{\sqrt{X_G (\text{Re}_L \text{We}_L)^{\frac{1}{4}}}} \right]$	32
Wetting efficiency	$f_w = 1.104 \text{Re}_L^{1/3} \left[ \frac{1 + [(\Delta P / Z) / \rho_L g]}{Ga_L} \right]^{1/9}$	34

Equations 2.32 and 2.47-2.49 were solved using IMSL (*International Mathematical and Statistical Libraries*) to evaluate  $\eta_c$ ,  $a_{s_d}$ ,  $a_{s_g}$  and  $a_{s_s}$ . These values were then used to solve Equations 2.46, 2.50-2.53 combined with 2.63 using a fourth order Runge-Kutta method with the following initial conditions:

$$\text{at } z = 0, a_1 = b_1 = 1; e_1 = f_1 = g_1 = 0; \theta = 1 \quad (2.64)$$



This model allows the prediction of the concentration of reactants/ products and the temperature profile along the length of the reactor. Thus, at any given length of the reactor the (fractional) conversion of Aniline ( $X_B$ ) is calculated as

$$X_B = 1 - b_l \quad (2.65)$$

The overall rate of hydrogenation is calculated as

$$R_A = \frac{u_l}{L} [f_l + 3g_l] \quad (2.66)$$

Here,  $u_l$  is the liquid velocity in m/s,  $L$  is the length of the catalyst bed in m,  $f_l$  and  $g_l$  are the concentrations of N-IPA and N-IPC respectively in kmol/m<sup>3</sup>. The selectivity to SB, N-IPA and N-I-IPC is evaluated using the following relationships:

$$S_{SB} = \frac{e_l}{1 - b_l} \times 100 \quad (2.67)$$

$$S_{NIPA} = \frac{f_l}{1 - b_l} \times 100 \quad (2.68)$$

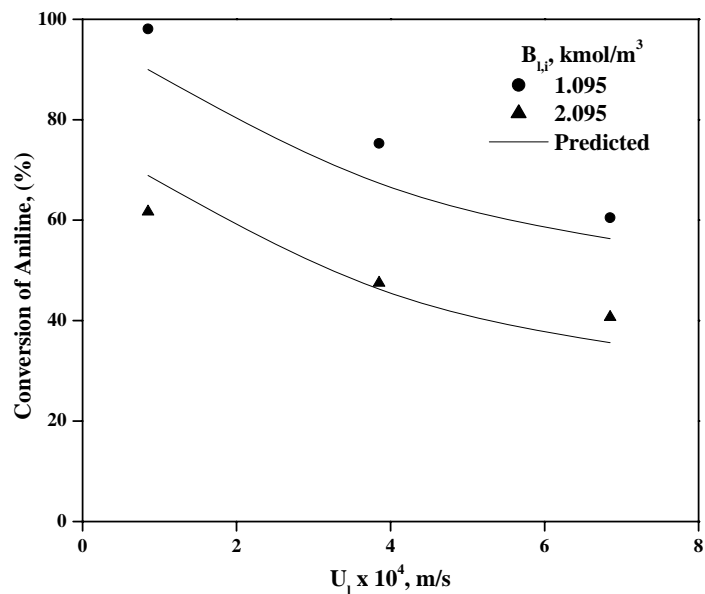
$$S_{NIPC} = \frac{g_l}{1 - b_l} \times 100 \quad (2.69)$$

and the maximum temperature rise is calculated as:

$$\Delta T_{\max} = T - T_o \quad (2.70)$$

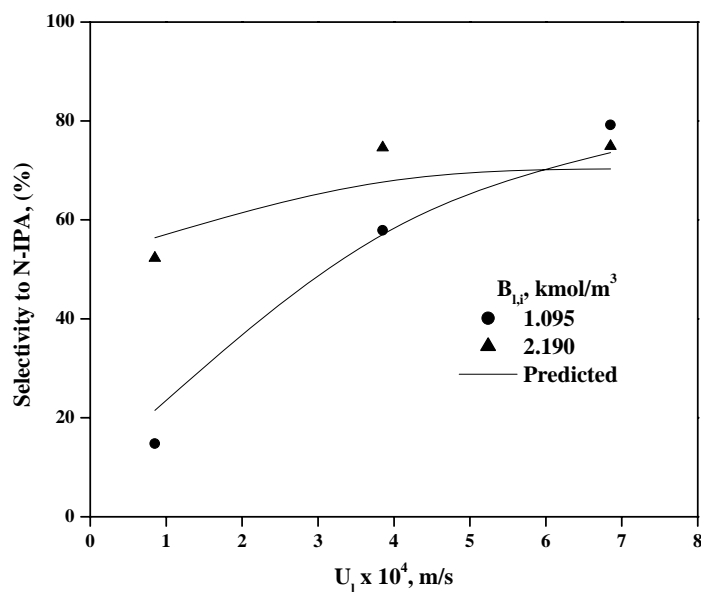
where,  $T$  represents the temperature calculated from Equation 2.63 and  $T_o$  represents the initial temperature. When calculations are performed for  $z = 1$ , we get the above quantities for the entire reactor.

Using the experimental procedure described in Section 2.2.2.2, trickle bed experiments were carried out for different inlet concentrations of aniline and different flow rates at 393K. The liquid samples coming out of the reactor were analyzed from which conversion and selectivity were calculated. The temperature at the exit of the reactor was also measured in all the experiments. The experimental and predicted results are compared in Figure 2.16-2.19, which indicates that the proposed model predicted the experimental trend reasonably well.



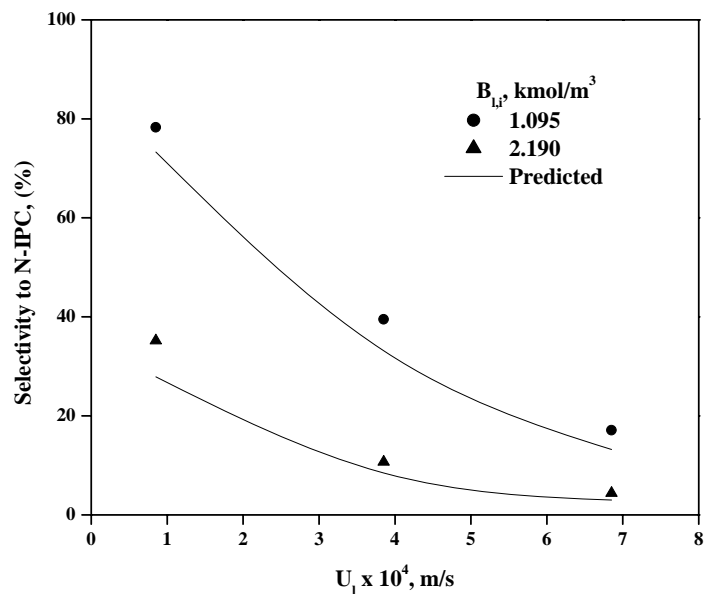
**Figure 2.16.** Effect of liquid velocity on conversion of aniline in trickle bed reactor at different aniline inlet concentrations

Reaction conditions:  $P_{H_2}$ : 4 MPa;  $U_g$ :  $2.14 \times 10^{-3} \text{ m/s}$ ; temperature: 393K



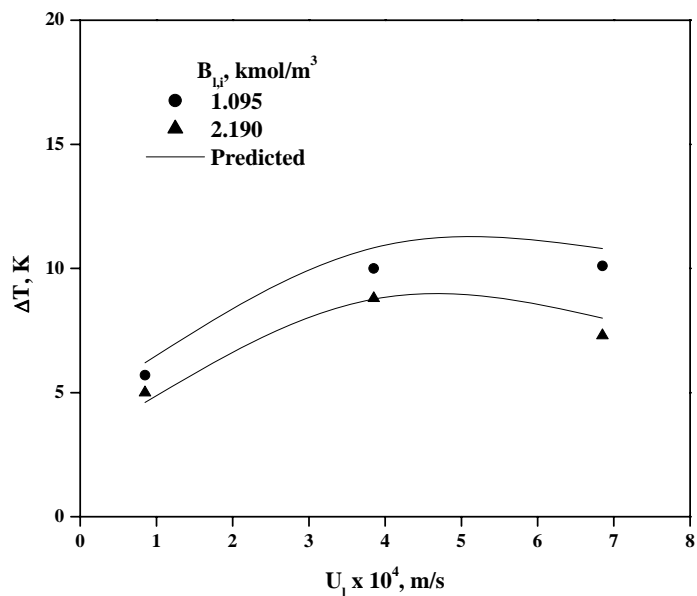
**Figure 2.17.** Effect of liquid velocity on selectivity to N-IPA in trickle bed reactor at different aniline inlet concentrations

Reaction conditions:  $P_{H_2}$ : 4 MPa;  $U_g$ :  $2.14 \times 10^{-3} \text{ m/s}$ ; temperature: 393K



**Figure 2.18.** Effect of liquid velocity on selectivity to N-IPC in trickle bed reactor at different aniline inlet concentrations

Reaction conditions:  $P_{H_2}$ : 4 MPa;  $U_g$ :  $2.14 \times 10^{-3}$  m/s; temperature: 393K



**Figure 2.19.** Effect of liquid velocity on selectivity to N-IPC in trickle bed reactor at different aniline inlet concentrations

Reaction conditions:  $P_{H_2}$ : 4 MPa;  $U_g$ :  $2.14 \times 10^{-3}$  m/s; temperature: 393K

The predicted results represent the experimental trends properly with an error limit of  $\pm 20$ . In our opinion this much error is acceptable because of the combination of experimental errors and the accuracy of the correlations used from the literature.

## 2.4. CONCLUSION

Kinetic modeling of reductive alkylation of aniline with acetone using 3% Pd/Al<sub>2</sub>O<sub>3</sub> catalyst has been studied in a slurry reactor in a temperature range of 378-408 K. Formation of the imine compound (Shiff's base) from aniline and acetone in the homogeneous, non-catalytic equilibrium reaction is the slowest step in the reaction sequence. Rate equations have been proposed for both the homogeneous and heterogeneous (catalytic) reactions and intrinsic kinetic parameters estimated based on the experimental concentration-time data. A rate model considering competitive adsorption of hydrogen (in dissociative manner) and other reactants on the metal surface as the rate limiting step for the catalytic reactions was found to represent the experimental data satisfactorily. Based on this kinetics, a non-isothermal trickle bed reactor model was developed for the same and compared with experimental results. The predicted and experimental results agreed reasonably well.

### Nomenclature

$A^*$  = saturation solubility of hydrogen in the liquid phase, kmol/m<sup>3</sup>  
 $a_B$  = gas-liquid interfacial area per unit volume of the liquid m<sup>2</sup>/m<sup>3</sup>  
 $A_l$  = concentration of hydrogen in the liquid phase, kmol/m<sup>3</sup>  
 $a_{li}$  = dimensionless concentration of hydrogen in liquid phase,  $(A_l/A^*)$   
 $a_p$  = external surface area of the catalyst per unit volume, m<sup>2</sup>/m<sup>3</sup>  
 $A_s$  = concentration of hydrogen at the catalyst surface, kmol/m<sup>3</sup>  
 $A_s$  = concentration of hydrogen at the catalyst surface, kmol/m<sup>3</sup>  
 $a_s$  = dimensionless concentration of hydrogen at the catalyst surface,  $(A_s/A^*)$   
 $a_t$  = packing external surface area of the per unit volume of reactor [ =  $S_{ex} (1 - \epsilon_B) / V_B$  ]  
 $a_w$  = catalyst area wetted, m<sup>-1</sup>  
 $A_s$  = concentration of hydrogen at the catalyst surface, kmol/m<sup>3</sup>  
 $B_{li}$  = Initial concentration of aniline in liquid phase, kmol/m<sup>3</sup>  
 $B_l$  = concentration of aniline in liquid phase, kmol/m<sup>3</sup>  
 $C_0$  = initial concentration of aniline, kmol/m<sup>3</sup>  
 $C_i$  = concentration of species  $i$ , kmol/m<sup>3</sup>

$C_{pg}$  = heat capacity of gas, kJ/kg/K  
 $C_{pl}$  = heat capacity of liquid, kJ/kg/K  
 $C_{ps}$  = heat capacity of solid catalyst, kJ/kg/K  
 $d_p$  = particle diameter, m  
 $De$  = effective diffusivity,  $m^2 / s$   
 $D_m$  = molecular diffusivity,  $m^2 / s$   
 $d_T$  = reactor diameter, m  
 $E_i$  = activation energy of  $i$ -th species, kJ/mol  
 $E_1$  = concentration of Schiff base in liquid phase,  $kmol/m^3$   
 $e_1$  = dimensionless concentration of Schiff base in liquid phase ( $E_1 / B_{li}$ )  
 $f_1$  = dimensionless concentration of N-IPA in liquid phase, ( $F_1 / B_{li}$ )  
 $F_1$  = concentration of N-IPA in liquid phase,  $kmol/m^3$   
 $f_d$  = fraction of the catalyst wetted by the dynamic liquid  
 $f_s$  = fraction of the catalyst wetted by the stagnant liquid  
 $f_w$  = total wetted fraction  
 $g_1$  = dimensionless concentration of N-IPC in liquid phase, ( $G_1 / B_{li}$ )  
 $G_1$  = concentration of N-IPC in liquid phase,  $kmol/m^3$   
 $\Delta H$  = enthalpy of adsorption, kJ/mol  
 $H_e$  = Henry's law constant,  $atm/kmol.m^3$   
 $k_1$  = rate constant for the forward equilibrium reaction,  $s^{-1}$   
 $k_2$  = rate constant for the backward equilibrium reaction,  $(kmol/m^3)^{-1/2} s^{-1}$   
 $k_3-k_4$  = rate constants for the hydrogenation steps,  $(kg/m^3)(kmol/m^3)^{-1/2} s^{-1}$   
 $k_{43}$  = dimensionless rate constant ( $k_4/k_3$ )  
 $k_a$  = dimensionless equilibrium constant for hydrogen,  $(kmol/m^3)^{-1/2}$   
 $K_H$  = adsorption equilibrium constant for hydrogen,  $(kmol/m^3)^{-1/2}$   
 $K_2-K_3$  = adsorption equilibrium constants for N-IPA and N-IPC respectively,  $(kmol/m^3)^{-1}$   
 $k_e-k_f$  = dimensionless equilibrium constants for N-IPA and N-IPC  
 respectively, ( $k_e = K_E.B_{li}$ ,  $k_f = K_F.B_{li}$ ),  $(kmol/m^3)^{-1}$   
 $K_{ex}$  = exchange coefficient between dynamic and stagnant liquid,  $s^{-1}$   
 $k_{ga}$  = gas-liquid mass-transfer coefficient,  $s^{-1}$   
 $k_{sa}$  = liquid-solid mass transfer coefficient,  $s^{-1}$   
 $L$  = reactor length, m  
 $L_m$  = superficial liquid mass velocity,  $kg / m^2 / s$   
 $N$  = speed of agitation, Hz  
 $Pr$  = Prandtl number for liquid phase ( $= C_{pl} \mu_l / \lambda_{eff}$ )  
 $Q_B$  = stoichiometric ratio [ $= (B_{li} / A^*)^{0.5}$ ]  
 $R_1-R_3$  = individual rates of reaction for the four steps,  $(kmol/m^3) s^{-1}$   
 $R_A$  = overall rate of hydrogenation,  $(kmol/m^3) s^{-1}$   
 $R_{H2}$  = initial rate of hydrogenation,  $(kmol/m^3) s^{-1}$   
 $R$  = radius of the pellet, m  
 $Re_l$  = Reynolds number for liquid phase  
 $R_g$  = universal gas constant,  $m^3.atm/kmol.K$   
 $S_{ex}$  = external surface area of the catalyst pellet,  $m^2$   
 $T_o$  = initial temperature, K  
 $T_b$  = bulk temperature, K  
 $T_w$  = wall temperature, K  
 $u_l$  = superficial velocity of the liquid, m/s  
 $u_g$  = superficial velocity of the gas, m/s  
 $U_w$  = bed-to-wall heat transfer coefficient,  $kJ/m^2/K/s$   
 $V_L$  = liquid volume,  $m^3$   
 $V_R$  = volume of the reactor,  $m^3$

$w$  = catalyst weight, kg/m<sup>3</sup>  
 $W_{el}$  = weber number for liquid ( =  $Lm^2 / \sigma_l \rho_l a_l$ )  
 $x$  = axial distance in the reactor, m  
 $z$  = reactor length, dimensionless, ( =  $x / L$ )

## Greek letters

$\alpha_1$  = parameter defined by Eq. 2.9  
 $\alpha_2$  = parameter defined by Eq. 2.10  
 $\alpha_{gl}$  = dimensionless gas-liquid mass transfer coefficient  
 $\alpha_{ls}$  = dimensionless liquid-solid mass transfer coefficient  
 $\alpha_{R3A}, \alpha_{R3E}$  = dimensionless reaction rate constant defined in table 3.  
 $\alpha_{R1}, \alpha_{R2}$  = dimensionless reaction rate constant defined in table 3.  
 $\beta_1, \beta_2, \beta_3,$  = dimensionless parameters defined in table 4  
 $\delta_l'$  = pressure drop per unit bed height with only liquid flowing, N / m<sup>2</sup>  
 $\delta_g'$  = pressure drop per unit bed height with only gas flowing, N / m<sup>2</sup>  
 $\Delta H_1$  = heat of reaction for equilibrium reaction step, kJ/kmol  
 $\Delta H_2$  = heat of reaction for heterogeneous reaction steps, kJ/kmol  
 $\varepsilon$  = porosity of the catalyst  
 $\varepsilon_b$  = bed voidage  
 $\varepsilon_l, \varepsilon_d, \varepsilon_s$  = liquid hold up, total dynamic and stagnant  
 $\eta_c$  = overall catalytic effectiveness factor  
 $\eta_{cd}, \eta_{cs}, \eta_{cg}$  = catalytic effectiveness factor in dynamic, stagnant and dry zones  
 $\theta$  = dimensionless temperature, (T / T<sub>o</sub>)  
 $\theta_b$  = dimensionless bed temperature, (T<sub>b</sub> / T<sub>o</sub>)  
 $\theta_w$  = dimensionless wall temperature, (T<sub>w</sub> / T<sub>o</sub>)  
 $\mu_l$  = viscosity of the liquid, kg / m / s  
 $\rho_g$  = density of the gas, kg/m<sup>3</sup>  
 $\sigma_l$  = surface tension, N / m  
 $\tau$  = tortuosity factor  
 $\phi$  = thiele parameter  
 $\phi_{exp}$  = parameter defined by Eq. 2A-6  
 $\phi_{min}$  = parameter defined by Eq. 2.7  
 $\mu_l$  = viscosity of the liquid, P  
 $\rho_l$  = density of liquid, kg/m<sup>3</sup>  
 $\varepsilon$  = porosity of the catalyst particle  
 $\tau$  = tortuosity  
 $\rho_p$  = particle density, kg/m<sup>3</sup>

## REFERENCES:

1. Mylorie, V. L. Reductive alkylation process to prepare tertiary aminoaryl cyan dye-transfer intermediates. *US 5861535*, **1999**.
2. Watanabe, T. Preparation of di-(substituted amino) diphenylamines as antioxidants and antiozonants for polymers. *JP 10168038*, **1998**.
3. Ege, S. *Organic Chemistry, Structure and Reactivity*, 3rd ed., D. C. Heath and Comp., Lexington, 1994, 535.
4. Fox, M. A.; Whitesell, J. K. *Organic Chemistry*, Jones and Bartlett Publishers, Boston, 1994, 72.
5. de Angelis, A.; Ingallina, P.; Perego, C. Solid acid catalysts for industrial condensations of ketones and aldehydes with aromatics. *Ind. & Eng. Chem. Res.*, **2004**, *43*(5), 1169.
6. (a) Ross, L. J.; Levy, S. D. Reductive alkylation of substituted anilines. *US 4261926*, **1981**. (b) Bader, R.; Flatt, P.; Radimerski, P. Process for the preparation of 2-alkyl-6-methyl-N-(1'-methoxy-2'-propyl)aniline and their chloracetanilides. *EP 605363*, **1995**. (c) Wilson, Jr. Modified nickel catalyst systems and their use in reductive alkylation reactions. *US 4043942*, **1977**. (d) Kirby, A. F., Willingboro, N. J. Reductive alkylation process for production of N-alkylated amines. *US 3522309*, **1970**.
7. (a) Zhou, X., Wu, Zuwang, Lin, L., Wang, G., Li, J. Synthesis of N-ethyl-m-toluidine from m-nitrotoluene by reductive alkylation. *Dyes Pigm.*, **1998**, *36* (4), 365. (b) Zhou, X., Wu, Zuwang, Lin, L., Wang, G. Studies on the selective synthesis of N-monoalkyl aromatic amines. *Dyes Pigm.*, **1999**, *40*(2-3), 205. (c) Simon, J., Becker, R., Lebjucher, R., Neuhauser, H. Catalytic N-alkylation of amines with alcohols. *EP 863140*, **1998**. (d) Su, B., Barthomeuf, D. Effect of reaction temperature on the alkylation of aniline by methanol over almost neutral zeolites LiY and NaY. *Studies in surface science and catalysis* (Catalysis by microporous materials): Elsevier Science. **1995**, *94*, 598.
8. Rusek M. Effect of promoters on Pt/SiO<sub>2</sub> catalysts for the N-alkylation of sterically hindered anilines in the vapor phase. *Heterogeneous catalysis and fine chemicals II*, Elsevier science publishers B. V., Amsterdam. **1991**, 359.
9. (a) Kaneko, M., Tanaka, S. Method of manufacturing alkyylaniline compounds. *EP 760360*, **1997**. (b) Nishimura, T., Takeda, F., Wada, M., Kanemura, Y. Preparation of N-alkyl-Substituted aromatic amines. *JP 2000095739*, **2000**.
10. Lehtonen, J. Salmi, T., Vuori, A., Tirronen, E. On the principles of modeling of homogeneous-heterogeneous reactions in the production of fine chemicals. A case study: Reductive alkylation of aromatic amines. *Org. Process Res. Dev.*, **1998**, *2*(2), 78.
11. Salmi, T., Lehtonen, J., Kaplin, J., Vuori, A., Tirronen, E., Haario, H. A homogeneous-heterogeneously catalyzed reaction system in a loop reactor. *Catal. Today*, **1999**, *48*(1-4), 139.
12. (a) Malz, R. E. Jr., Greenfield, H. Tertiary amine preparation by reductive alkylation of aliphatic secondary amines with ketones. *Heterogeneous catalysis and fine chemicals II*, Elsevier Science Publishers B. V., Amsterdam, **1991**, 351. (b) Mylroie, V. L., Valente, L., Fiorella, L., Osypian, M. A. Reductive alkylation optimized by techniques of experimental design. *Chem. Ind. (Dekker)*, **1996**, *68* (Catalysis of organic reactions), 301. (c) Malz, R. E. Jr., Jancis, E. H., Reynolds, M. P., O'Leary, S. T. Reductive alkylation of acetophenone with aniline. *Chem. Ind. (Dekker)*, **1995**, *62* (Catalysis of organic reactions), 263.
13. Greenfield, H. Side reactions in reductive alkylation of aromatic amines with aldehydes and with ketones. *Chem. Ind. (Dekker)*, **1994**, *53* (Catalysis of organic reactions), 265.
14. Purwanto, P.; Deshpande, R. M.; Chaudhari, R. V.; Delmas, H. Solubility of Hydrogen, Carbon Monoxide, and 1-Octene in Various Solvents and Solvent Mixtures. *J. Chem. Eng. Data*, **1996**, *41*(6), 1414.
15. Schlessinger, G. G. Vapour pressure of organic compounds, *Handbook of chemistry and physics*, Chemical Rubber Co. (CRC), **1970**, D153.
16. Ramachandran, P. A. and Chaudhari, R. V. *Three Phase Catalytic Reactors*. Gordon and Breach, New York, USA, **1983**.
17. Chaudhari, R. V.; Gholap, R. V.; Emig, G.; Hofmann, H. Gas-liquid mass transfer in dead end reactors. *Can. J. Chem. Eng.*, **1987**, *65*, 744.

- 
18. Sano, Y., Yamaguchi, N., Adachi, T. Mass transfer coefficients for suspended particles in agitated vessels and bubble columns. *J. Chem. Eng. Jpn.*, **1974**, *1*, 255.
  19. Calderbank, P. H. Physical rate processes in industrial fermentation Part I. The interfacial area in gas-liquid contacting with mechanical agitation, *Trans. Inst. Chem. Eng.*, **1958**, *36*, 443.
  20. Wilke, C.R., Chang, P. Correlation of diffusion co-efficients in dilute solutions. *AIChE J.*, 1955, *1*, 26.
  21. (a) Paal, Z., Menon, P. G. Hydrogen effects in metal catalysts. *Catal. Rev. Sci. Eng.*, **1983**, *25*, 299. (b) Geus, J. Energetics of hydrogen adsorption on porous and supported metals. *Chem. Ind. (Dekker)*, **1988**, 85. (c) Christmann, K. R. Hydrogen sorption on pure metal surfaces. *Chem. Ind. (Dekker)*, **1988**, 3. (d) Engel, T., Kuipers, H. A molecular beam investigation of the scattering, adsorption and absorption of hydrogen and deuterium from/on/in palladium (111). *Surf. Sci.*, **1979**, *90 (1)*, 162.
  22. Benedetti, A., Fagherazzi, G., Pinna, F., Rampazzo, G., Selva, M., Strukul, G. The influence of a second metal component (Cu, Sn, Fe) on Pd/SiO<sub>2</sub> activity in hydrogenation of 2,4-Dinitrotoluene. *Catal. Lett.*, **1991**, *10*, 215.
  23. Vannice, M. A., Hyun, S. H., Kalpakci, B., Liauh, W. C. Entropies of adsorption in heterogeneous catalytic reactions. *J. Catal.*, **1979**, *56*, 358.
  24. Boudart, M. Two step catalytic reactions. *AIChE Journal*, **1972**, *18*, 465.
  25. Broderick, D. H., Gates B. C. Hydrogenolysis and hydrogenation of dibenzothiophene catalyzed by sulfided CoO-MoO<sub>3</sub>/γ-Al<sub>2</sub>O<sub>3</sub>: The reaction kinetics, *AIChE J.*, **1981**, *27*, 663.
  26. Chaudhari, R. V., Parande, M. G., Ramachandran, P. A., Brahme, P. H., Vadgaonkar, H. G., Jaganathan, R. Hydrogenation of butynediol to cis-butenediol catalyzed by Pd-Zn-CaCO<sub>3</sub>: Reaction kinetics and modeling of a batch slurry reactor, *AIChE J.*, **1985**, *31(11)*, 1891.
  27. Rajashekharam, M. V.; Jaganathan, R.; Chaudhari, R. V. A trickle-bed reactor model for hydrogenation of 2,4-dinitrotoluene: Experimental verification. *Chem. Eng. Sci.*, **1998**, *53 (4)*, 787.
  28. Bischoff, K.B. Effectiveness factors for general reaction rate forms. *AIChE J.*, **1965**, *11*, 351.
  29. Hochman, J. M.; Effron, E. Two phase cocurrent downflow in packed beds. *Ind. Eng. Chem. Fundam.*, **1969**, *8*, 63.
  30. Fukushima, S.; Kusaka, K. Liquid Phase volumetric and mass transfer coefficient, and boundary of hydrodynamic flow region in packed column with cocurrent downward flow. *J. Chem. Eng. Japan*, **1977**, *10 (6)*, 468.
  31. Satterfield, C. N.; Vab Eek, M. W.; Bliss, G. S. Liquid-solid mass transfer in packed beds with down flow cocurrent gas-liquid flow. *AIChE. J.*, **1978**, *24*, 709.
  32. Larachi, F.; Laurent, A.; Midoux, N.; Wild, G. Experimental Study of a Trickle-Bed Reactor Operating at High Pressure: Two-phase Pressure Drop and Liquid Saturation. *Chem. Eng. Sci.*, **1991**, *46 (5/6)*, 1233.
  33. Specchia, V.; Baldi, G. Heat transfer in trickle bed reactors. *Chem. Eng. Commun.*, **1979**, *3*, 483.
  34. Al-Dahhan, M. H.; Dudukovic, M. P. Catalyst wetting Efficiency In trickle-bed Reactors at high pressure. *Chem. Eng. Sci.*, **1995**, *50 (15)*, 2377.



## **Chapter 3**

# **Analysis of a Gas-Liquid-Liquid-Solid Catalytic Reaction: Kinetics and Modeling of a Semi Batch Slurry Reactor**

### 3.1. INTRODUCTION

Multiphase catalytic reactions have numerous applications in chemical industries including the emerging applications in fine chemicals and pharmaceuticals. The analysis of three phase catalytic reactions has been very well developed including both theoretical and experimental studies, in which detailed studies on understanding of rate behavior, kinetic modeling, role of mass transfer and performance characteristics of different types of reactors have been reported.<sup>1,2</sup> To achieve some specific advantages with respect to the overall rate and selectivity, more complex multiphase systems involving gas-liquid-liquid-solid reactions have also been proposed in recent years. Some important examples include selective hydrogenation of (i) benzene to cyclohexene using supported ruthenium catalysts,<sup>3,4,5</sup> (ii) unsaturated alcohols from unsaturated aldehydes using palladium based catalyst<sup>6</sup> and (iii) nitrobenzene to *p*-amino phenol in a four phase system.<sup>7</sup> While, these four phase reactions have already shown promising results from catalysis and process improvement point of view, a detailed analysis of the complex interface mass transfer effects, combined with reaction kinetics has not been addressed in the previous reports.

Dearomatization of aniline using supported metal catalysts is an industrially important reaction since the product cyclohexylamine has wide ranging applications such as devulcanizing agent, fuel additives, as a corrosion inhibitor in plastic films, in foam modeling, in removal of elemental sulfur etc.<sup>8</sup> Although there are many reports in the literature on hydrogenation of aniline in three phase slurry reactors,<sup>9,10,11,12</sup> and a few examples where water is used<sup>13,14,15</sup> as a solvent, there is no detailed study on the kinetics of this important reaction system using water as a separate phase. In this chapter a detailed study on hydrogenation of aniline in a gas-liquid-liquid-solid (four phase) system using ruthenium on alumina (Ru/Al<sub>2</sub>O<sub>3</sub>) as a catalyst is presented, in which the two immiscible liquids used were cyclohexane and water. Generally, four phase systems are not preferred due to a possibility of lower reaction rates resulting from inefficient contact of the liquid phases and hence, increased mass transfer resistances.<sup>16</sup> However, in several cases, use of four phase catalyst system has been found to be advantageous to achieve higher rate, selectivity and catalyst-product separation. As an illustration, the experimental results on hydrogenation of different substrates in four phase catalytic systems are also reported.

Further, a detailed rate analysis incorporating the interphase (gas-liquid and liquid-liquid) mass transfer effects has been presented.

## **3.2. EXPERIMENTAL SECTION**

### **3.2.1. Materials**

Ruthenium trichloride ( $\text{RuCl}_3 \cdot 3\text{H}_2\text{O}$ ) was purchased from S. D. Fine Chemical Limited, India. Aniline, cyclohexylamine, cyclohexane and other chemicals were purchased from E-Merck, India. Hydrogen gas with >99% purity was supplied by Inox Air Products Ltd., India and was used as received.

### **3.2.2. Analysis**

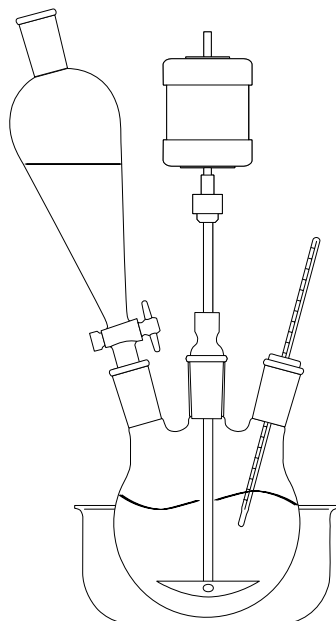
Liquid samples were analyzed by gas chromatography (series: HP 6890 chromatograph) using a HP-5 capillary column ( $30\text{m} \times 0.32\text{ mm} \times 0.25\text{ }\mu\text{m}$  film thickness with 5% phenyl methoxy siloxane as stationary phase). The GC conditions for organic phase analysis were as follows: oven: 323K (2 min)-40 K/min-373K (2 min)- 30 K/min-453K (1 min)- 40 K/min- 523K (1 min); pressure: 8.50 psi; inlet temperature: 523K; FID temperature: 523K; carrier gas: helium. A few samples were characterized using GC-MS (Shimadzu QP 2000A) for identification of the products.

The metal content of the catalyst was determined using a Perkin Elmer Plasma 1000 **ICP-OES** spectrometer. The X-ray diffraction (**XRD**) of the support ( $\gamma\text{-Al}_2\text{O}_3$ ) and the catalyst (2%  $\text{Ru}/\text{Al}_2\text{O}_3$ ) samples were recorded on Philips 1730 using Ni filtered  $\text{Cu K}\alpha$  radiation ( $\text{Cu K}\alpha$  radiation,  $\lambda=1.5418\text{ \AA}$ ) and a proportional counter detector at a scan rate of  $2^\circ/\text{min}$ . Metal particle size was obtained by Transmission Electron Microscopy (**TEM**) measurements on a JEOL 1200EX instrument operated at an accelerating voltage of 120 kV. Surface area of the powdered catalyst was measured using a Chembet-3000, Quantachrome instrument at 30% nitrogen.

### **3.2.3. Catalyst preparation and Characterization**

The catalyst 2%  $\text{Ru}/\text{Al}_2\text{O}_3$ , was prepared in our laboratory by precipitation technique. A schematic of the catalyst preparation set-up is shown in Figure 3.1. Required

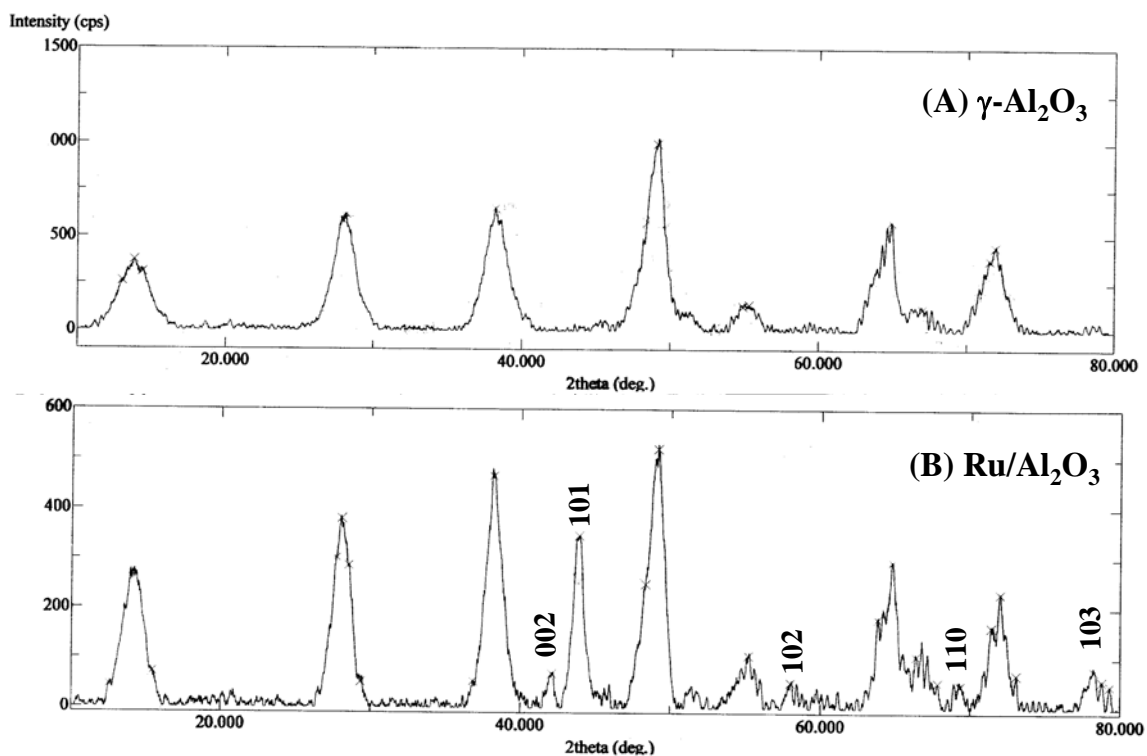
amount of support ( $\gamma\text{-Al}_2\text{O}_3$ ) was dispersed in distilled water, in a round bottom flask equipped with a half moon stirrer, condenser and an addition funnel, and the slurry was stirred for 2 hrs at 368-373K. Required amount of ruthenium trichloride dissolved in distilled water was added drop wise. After stirring for three hours, aqueous ammonia solution was added (pH:  $\sim 10$ ) to precipitate ruthenium hydroxide. The content was allowed to stir for 4 hrs, filtered, washed with hot distilled water to remove chloride ions and dried at 393 K for 8 hrs. The gray colored cake was powdered and activated under hydrogen flow for 7 hrs at 573 K. After activation, the catalyst was brought to room temperature, flushed with nitrogen and used for hydrogenation reactions.



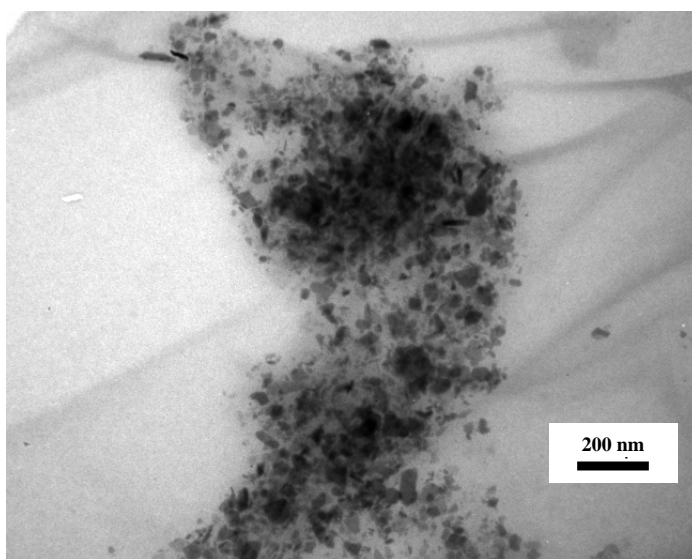
**Figure 3.1.** Set-up for Ru/Al<sub>2</sub>O<sub>3</sub> catalyst preparation

The powder XRD patterns of  $\gamma$ -alumina, and 2% Ru/Al<sub>2</sub>O<sub>3</sub> are shown in Figure 3.2. The characteristic Ru peaks were observed at  $2\theta$  values of  $42.19^\circ$  (32% intensity) and  $43.89^\circ$  (100% Intensity) corresponding to Ru 002 and 101 planes. Alumina peaks overlapped the peak at a  $2\theta$  value of  $38.38^\circ$  corresponding to Ru 100 plane. The Bragg reflections indicated in Figure 3.2 (B) are in good agreement with the hexagonal close

packed (*hcp*) Ru as reported in the literature.<sup>17</sup> The absence of peaks corresponding to RuO<sub>2</sub> species confirmed that most of the Ru species existed in Ru (0) state.



**Figure 3.2.** XRD patterns of (A)  $\gamma$ -alumina, and (B) 2% Ru/Al<sub>2</sub>O<sub>3</sub> recorded in the  $2\theta$  range  $10^\circ$ - $80^\circ$ . The Bragg reflections for Ru/Al<sub>2</sub>O<sub>3</sub> sample are indexed.



**Figure 3.3.** TEM image of 2%Ru/Al<sub>2</sub>O<sub>3</sub> Catalyst

The TEM micrograph for the 2% Ru/Al<sub>2</sub>O<sub>3</sub> catalyst prepared by precipitation technique is shown in Figure 3.3. Metal clusters on the support were not in uniform size and some of the agglomerates were of bigger size in the range of ~30 nm, where as smaller metal clusters of ~10-12 nm were also present. Specifications of the Ru/Al<sub>2</sub>O<sub>3</sub> catalyst are: ruthenium content: 2% (w/w); catalyst particle size:  $2 \times 10^{-5}$  m; metal particle size: 9 -30 nm; particle density:  $2 \times 10^3$  kg/m<sup>3</sup>; porosity: 0.5; tortuosity: 4; BET surface area:  $1.60 \times 10^5$  m<sup>2</sup>/kg.

### 3.2.4. Reactor Set-up

The hydrogenation reactions were carried out in a  $3 \times 10^{-4}$  m<sup>3</sup> high pressure stirred autoclave supplied by Parr Instrument Company, Moline, IL, as described in the previous chapter (Chapter 2, Figure 2.2). The reactor had a provision for operating up to 523 K and 10 MPa pressure. It was equipped with automatic temperature control, gas inlet, outlet, sampling of liquid, transducer for pressure, safety rupture disc and variable agitation speed controller. An intermediate reservoir was used for hydrogen storage from which gas was introduced into the reactor through a constant pressure regulator. In a typical hydrogenation reaction, required amount of aniline, cyclohexane and water were charged along with the catalyst into the autoclave. The total volume of the liquid phase was always kept constant ( $1 \times 10^{-4}$  m<sup>3</sup>) in all the experiments. It is important to mention here that aniline is immiscible with cyclohexane and water at room temperature, but completely soluble in cyclohexane above 45.6 °C.<sup>18</sup> Thus, beyond 45.6 °C the system involves two immiscible liquids with organic phase containing aniline and aqueous phase containing the catalyst. The catalyst was found to be predominantly in the aqueous phase below an aqueous phase hold up of 0.4. Interestingly, on increasing the aqueous phase hold up (>0.4), organic phase becomes a dispersed phase and the catalyst was generally observed to be present in the dispersed phase. This has been observed visually as shown in Figure 3.15. The reactor was flushed twice with nitrogen and twice with hydrogen at room temperature. The contents were then heated to the desired temperature, autoclave was pressurized with hydrogen and the reaction started by switching on the stirrer. Pressure drop in the reservoir as a function of time was recorded for all the experiments. Organic phase samples were analyzed at regular

time intervals. At the end of each experiment, aqueous phase was also analyzed for reactants and products.

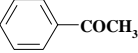
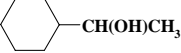
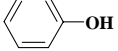
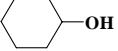
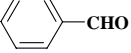
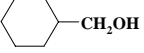
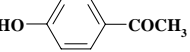
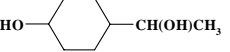
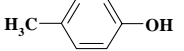

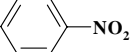
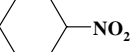
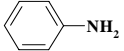
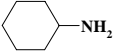
### 3.3. RESULTS AND DISCUSSIONS

#### 3.3.1. Preliminary Experiments

Several initial experiments on hydrogenation of various organic substrates using the 2% Ru/Al<sub>2</sub>O<sub>3</sub> catalyst were carried out in four phase as well as three phase systems and the results are summarized in Table 3.1. In the four phase (gas-liquid-liquid-solid) catalytic system, substrates and products were predominantly present in the organic phase, while the catalyst (2% Ru/Al<sub>2</sub>O<sub>3</sub>) was present only in the aqueous phase (at  $\epsilon_w < 0.4$ ) at the experimental conditions. The results presented in Table 3.1, clearly indicate that except for hydrogenation of phenol to cyclohexanol, the rates of reactions are higher for the four phase system compared to the three phase system. In hydrogenation of aromatic substrates, the promoting effect of water in ruthenium catalyzed hydrogenations<sup>19</sup> is known, which partly explains the rate enhancement in a four phase system. Another possibility is due to the presence of Ru/Al<sub>2</sub>O<sub>3</sub> catalyst in the aqueous phase wherein the reaction occurs by diffusion of reactants from organic phase to aqueous droplets followed by adsorption on catalyst surface and reaction. The liquid reactants and products, being sparingly soluble in water, are expected to remain in the organic phase in higher concentrations eliminating the possible effects of substrate and product inhibition.

In order to understand the rate behavior in such four phase (gas-liquid-liquid-solid) catalytic systems, a detailed study was undertaken using hydrogenation of aniline to cyclohexylamine as a model reaction. A few initial hydrogenation experiments were carried out with the aim of (i) identifying the products and defining the reaction scheme, (ii) study the intrinsic kinetics for hydrogenation of aniline in a slurry reactor with 2% Ru/Al<sub>2</sub>O<sub>3</sub> and (iii) understanding the performance of a semi-batch slurry reactor under isothermal conditions.

**Table 3.1.** Comparison of catalytic performance for three-phase and four-phase catalytic systems for different aromatic functionalities

No.	Substrate	Product	Time, min	Three phase			Four phase		
				Con., %	Sel., %	TOF, h <sup>-1</sup>	Con., %	Sel., %	TOF, h <sup>-1</sup>
1			60	70.6	15.2	1407	100	98.8	3994
2			30	100	98.7	6034	100	99.3	6021
3			120	23.4	98.5	473	100	100	2021
4			90	63.6	32.3	1729	97.5	94.8	2514
5			40	10.3	99.1	473	100	99.3	4540
6			90	100	35.2	2612	100	89.9	3926
7			90	31.5	88.7	584	100	90.5	1475

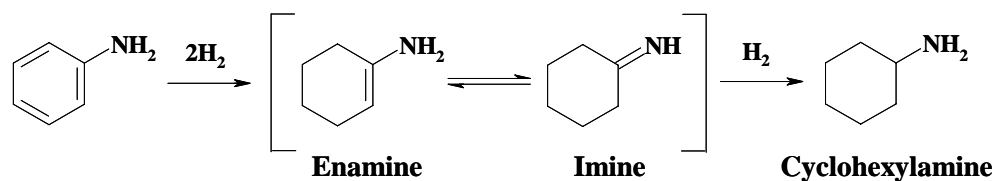
Reaction conditions: substrate:  $0.1 \times 10^{-3}$  kmol, catalyst: (2% Ru/Al<sub>2</sub>O<sub>3</sub>)  $0.5 \times 10^{-3}$  kg, temp.: 398K, P<sub>H<sub>2</sub></sub>: 4.8 MPa, agitation: 16.6 Hz, total liquid phase volume:  $100 \times 10^{-6}$  m<sup>3</sup>. TOF: in terms of total hydrogen consumed.

**Entry 1-5:** For three-phase: Methanol is the solvent; for four-phase: no organic solvent is used; aqueous phase:  $90 \times 10^{-6}$  m<sup>3</sup>

**Entry 6-7:** For three-phase: cyclohexane is the solvent; for four-phase: cyclohexane is the solvent; aqueous phase:  $30 \times 10^{-6}$  m<sup>3</sup>

### 3.3.1.1. Reaction Mechanism and Product Distribution

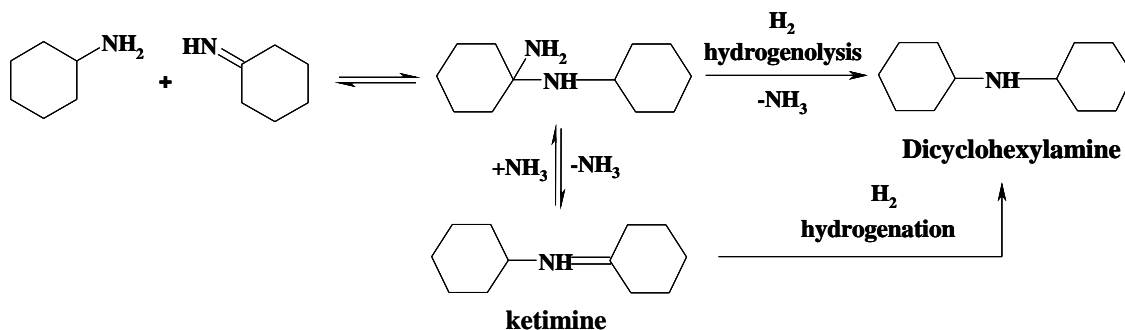
According to the literature, in hydrogenation of aniline, cyclohexylamine formed as the major product.<sup>20</sup> The mechanism of the formation of cyclohexylamine and other major byproduct, dicyclohexylamine, was discussed by Greenfield.<sup>21</sup> Catalytic hydrogenation of aniline proceeds with stepwise formation of enamine and imine intermediates, which further undergo hydrogenation to cyclohexylamine as shown in Scheme 3.1.



**Scheme 3.1.** Stepwise hydrogenation of aniline to cyclohexylamine



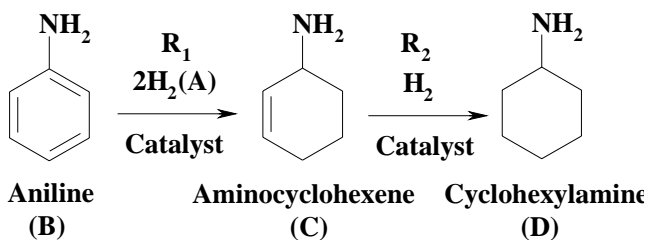
Dicyclohexylamine may also form by addition of cyclohexylamine with imine compound followed by hydrogenolysis or hydrogenation reactions as shown in Scheme 3.2.<sup>22</sup>



**Scheme 3.2.** Mechanism of formation of dicyclohexylamine during hydrogenation of aniline

Other side products such as cyclohexane ( $C_6H_{12}$ ) and cyclohexanol are also reported in the literature where ruthenium was used as a catalyst.<sup>23</sup> Cyclohexane is noticeable only at very high temperature hydrogenation (vapour phase) of aniline over transition metal catalysts.<sup>24</sup>

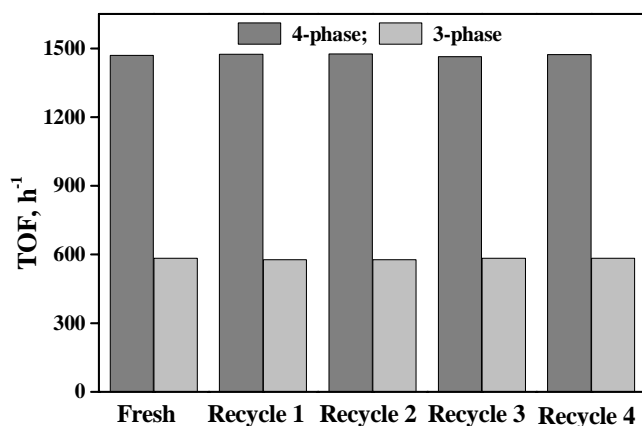
Our preliminary results revealed that cyclohexylamine was the major product in hydrogenation of aniline with 2% Ru/Al<sub>2</sub>O<sub>3</sub> catalyst formed by consecutive hydrogenation of aromatic double bonds. Small traces of dicyclohexylamine (< 0.5%) were detected in a few cases and hence not considered in kinetic analysis. The reaction scheme considered for the kinetic study is shown in Scheme 3.3.



**Scheme 3.3.** Reaction scheme for hydrogenation of aniline in a gas-liquid-liquid-solid system using 2% Ru/Al<sub>2</sub>O<sub>3</sub> catalyst

A few reactions were carried out without the catalyst and the results ensured the absence of any non-catalytic reactions. The constancy of the catalytic activity during the runs was confirmed by recycling the catalyst (Figure 3.4). After a reaction with fresh

catalyst, the organic and aqueous phases were separated by simple phase separation and the aqueous phase containing the catalyst was charged along with fresh organic phase for the recycle studies. The catalytic activity, presented in terms of turn over frequency (TOF,  $\text{h}^{-1}$  defined as number of moles of hydrogen consumed per mole of ruthenium per hour), remained almost constant even after four recycles. For the purpose of kinetic study, several experiments were carried out over a range of conditions given in Table 3.2, in which concentration-time profiles as well as hydrogen consumption vs time data were obtained.



**Figure 3.4.** Recycle experiments for hydrogenation of aniline using 2% Ru/Al<sub>2</sub>O<sub>3</sub> catalyst: a comparison between four-phase and three-phase systems  
Reaction conditions are as given in Table 3.1

**Table 3.2.** Range of operating conditions for kinetic study

Aniline concentration (w.r.t. organic phase), kmol/m <sup>3</sup>	0.75-3.0
Hydrogen partial pressure, MPa	2.1-6.3
Catalyst loading (w.r.t. aqueous phase), kg/m <sup>3</sup>	5-40
Temperature, K	378-418
Agitation speed, Hz	6.6-16.6
Volume of organic phase, m <sup>3</sup>	70×10 <sup>-6</sup>
Volume of aqueous phase, m <sup>3</sup>	30×10 <sup>-6</sup>
Total volume of liquid, m <sup>3</sup>	100×10 <sup>-6</sup>
Reaction time, hr.	1.5

### 3.3.2. Solubility Data

The saturation solubility of hydrogen ( $A^*$ , kmol/m<sup>3</sup>) at a particular temperature and composition was correlated with partial pressure of hydrogen ( $P_{H_2}$ , atm.) by Henry's Law as given below:

$$H_e = A^* / P_{H_2} \quad (3.1)$$

where,  $H_e$  is the Henry's constant, kmol/m<sup>3</sup>/atm.

#### 3.3.2.1. Solubility data for hydrogen in water

Solubility of hydrogen in water at different temperatures was calculated from the data reported by Pray et al.<sup>25</sup> The Henry's constant values at different temperatures are given in Table 3.3.

**Table 3.3.** Solubility data (Henry's constant) for H<sub>2</sub> in water at different temperatures

Temperature, K	$H_e \times 10^4$ , kmol/m <sup>3</sup> /atm.
378	6.58
398	6.97
418	7.8

#### 3.3.2.2. Solubility data for hydrogen in cyclohexane

The solubility of hydrogen in cyclohexane at various compositions of aniline in cyclohexane was measured by the procedure described in Chapter 2. The values of Henry's constant at different temperatures and compositions are presented in Table 3.4.

**Table 3.4.** Solubility data (Henry's constant) for H<sub>2</sub> in various compositions of aniline in cyclohexane at different temperatures

Temperature, K	$H_e \times 10^3$ , kmol/m <sup>3</sup> /atm.		
	5% aniline in cyclohexane	10% aniline in cyclohexane	20% aniline in cyclohexane
378	5.81	5.68	5.51
398	6.03	5.97	5.89
418	6.39	6.29	6.11

### 3.3.2.3. Partition coefficient of hydrogen and aniline in cyclohexane – water binary system

For hydrogenation of aniline to cyclohexylamine, at low aqueous phase hold up ( $\epsilon_w < 0.4$ ) the catalyst remained in the dispersed aqueous phase. Then for the hydrogenation reaction, hydrogen and aniline has to be transported from the organic phase to the aqueous phase. Therefore, the concentration of hydrogen and aniline in cyclohexane-water binary mixture is very important.

For hydrogen, the partition coefficient ( $\alpha_A$ ) value at the operating range of conditions was determined from the following equation:

$$(H_e)_{aq.} = \alpha_A (H_e)_{org.} \quad (3.2)$$

where,  $(H_e)_{aq}$  and  $(H_e)_{org}$  are the Henry's constants for aqueous and organic phases respectively at a particular temperature and composition, and  $\alpha_A$  is the partition coefficient of hydrogen in cyclohexane and water binary system. The average value of  $\alpha_A$  was obtained to be 0.116.

For aniline, the distribution of aniline in cyclohexane and water system was determined experimentally at various temperatures (378 – 418 K) and different initial concentration of aniline in cyclohexane (0.75-3.0 kmol/m<sup>3</sup>). It was observed that the aniline concentration in aqueous phase increased linearly with the organic phase aniline concentration. The obtained data was plotted and fitted by a linear equation (passing through zero)

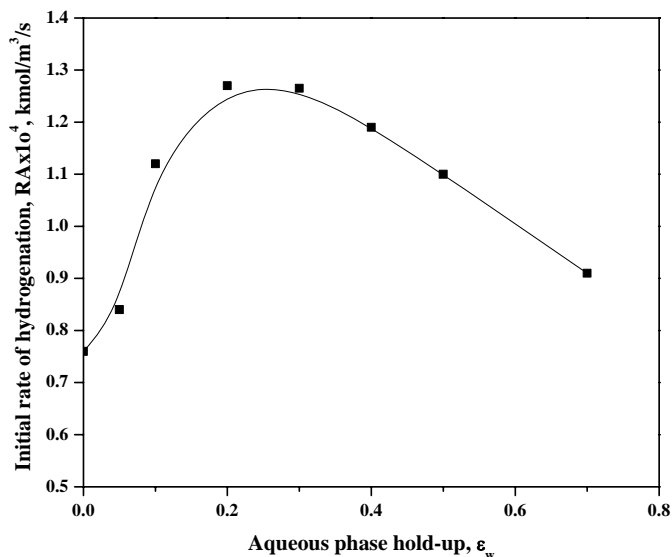
$$B_{l,w} = \alpha_B \cdot B_{l,o} \quad (3.3)$$

where,  $B_{l,w}$  and  $B_{l,o}$  are the aniline concentrations in aqueous and organic phases (kmol/m<sup>3</sup>) respectively,  $\alpha_B$  is the partition coefficient of aniline between cyclohexane and water. The average partition coefficient value was 0.260.

### 3.3.3. Analysis of Initial Rate Data

The initial rates of hydrogenation per unit volume of the total liquid phase were calculated from hydrogen consumption-time data for the following parameters: (a) aqueous phase hold-up, (b) agitation, (c) catalyst loading, (d) aniline concentration and (e) partial pressure of hydrogen. The initial rates of reaction vs aqueous phase hold up (hold up of a

particular phase was defined as the volume of that particular phase / volume of the total liquid phase) plot passed through a maxima as shown in Figure 3.5. This observation was typical of a four phase catalytic reaction and discussed in a later part of this chapter.



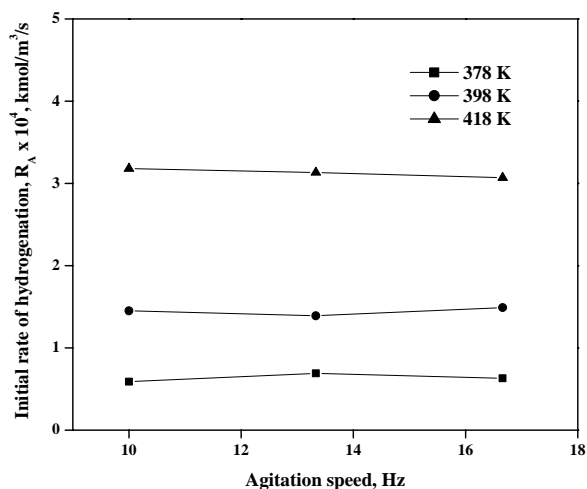
**Figure 3.5.** Effect of aqueous phase hold-up on initial rate of hydrogenation for hydrogenation of aniline in a four phase system using 2% Ru/Al<sub>2</sub>O<sub>3</sub>

Reaction conditions: aniline, 0.1 kmol; catalyst (2% Ru/Al<sub>2</sub>O<sub>3</sub>),  $0.6 \times 10^{-3}$  kg; P<sub>H<sub>2</sub></sub>, 4.8 MPa; temperature, 398K; total liquid volume,  $100 \times 10^{-6}$ m<sup>3</sup>.

The effect of agitation speed on initial rate of hydrogenation is shown in Figure 3.6. With an increase in agitation speed, the interfacial area between gas-liquid and liquid-liquid increases. Therefore, the gas-liquid as well as the liquid-liquid mass transfer rate would increase with agitation speed. From Figure 3.6, the initial rate of reaction was found to be independent of agitation speed beyond 10 Hz, which indicates the absence of gas-liquid and liquid-liquid mass transfer.

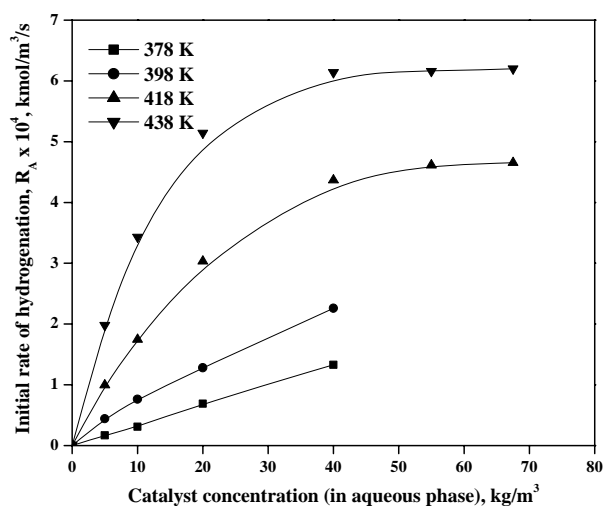
The effect of catalyst loading on initial rate of hydrogenation of aniline is shown in Figure 3.7. The initial rate increased linearly with catalyst loading at 378 and 398 K over the entire range indicating that the reactions occur in the kinetically controlled regime, where as at 418 K the reactions shifted towards the mass transfer regime with catalyst

loading above  $20 \text{ kg/m}^3$  (Figure 3.7). Therefore, the experiments for the kinetic study were carried out in the temperature range of 378-418K with catalyst loading of 5-20  $\text{kg/m}^3$  with respect to the aqueous phase holdup ( $\epsilon_w$ : 0.3) as shown in Table 3.2.



**Figure 3.6.** Effect of agitation speed on initial rate of hydrogenation for hydrogenation of aniline in a four phase system using 2% Ru/Al<sub>2</sub>O<sub>3</sub>

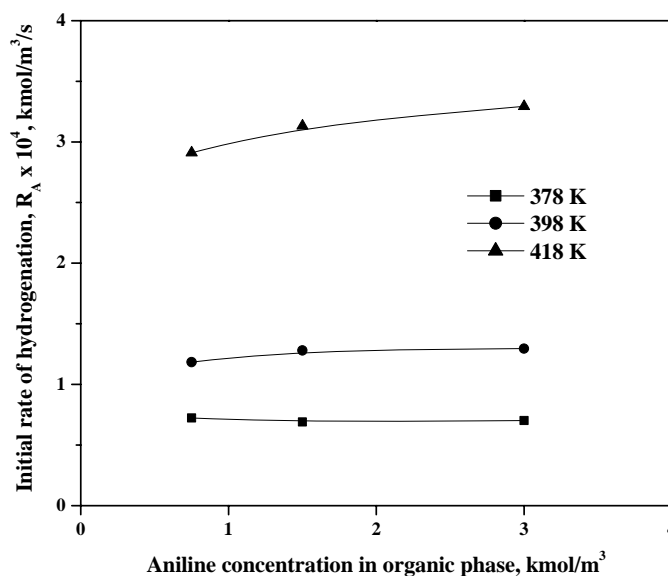
Reaction conditions: aniline,  $1.53 \text{ kmol/m}^3$ , catalyst (2% Ru/Al<sub>2</sub>O<sub>3</sub>),  $20 \text{ kg/m}^3$ ;  $P_{\text{H}_2}$ , 4.8 MPa; water,  $30 \times 10^{-6} \text{ m}^3$ ; aniline dissolved in cyclohexane, total liquid volume,  $100 \times 10^{-6} \text{ m}^3$ .



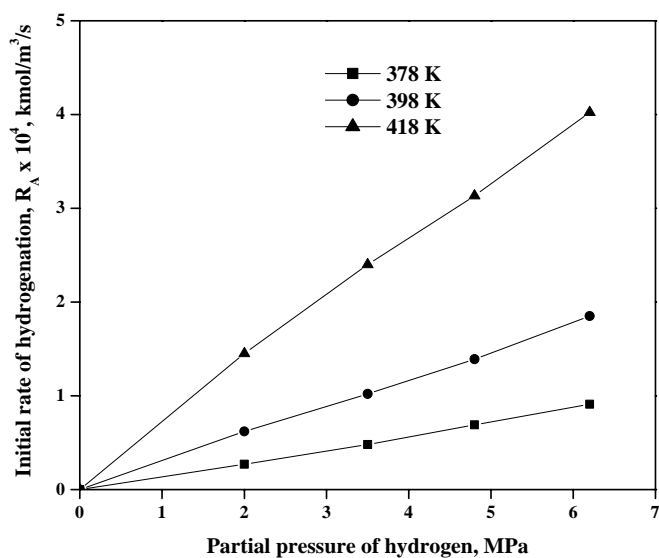
**Figure 3.7.** Effect of catalyst loading on initial rate of hydrogenation for hydrogenation of aniline in a four phase system using 2% Ru/Al<sub>2</sub>O<sub>3</sub>

Reaction conditions: aniline,  $1.53 \text{ kmol/m}^3$ ;  $P_{\text{H}_2}$ , 4.8 MPa; agitation, 16.66 Hz; water,  $30 \times 10^{-6} \text{ m}^3$ ; aniline dissolved in cyclohexane, total liquid volume,  $100 \times 10^{-6} \text{ m}^3$ .

The general trends of initial rates observed for other parameters were as follows: (i) the effect of aniline concentration on the initial rate of hydrogenation indicated zero order dependence over the entire range of aniline concentration studied (Figure 3.8) and (ii) initial rate of reaction was linearly dependent on hydrogen partial pressure as shown in Figure 3.9.



**Figure 3.8.** Effect of aniline concentration on initial rate of hydrogenation for hydrogenation of aniline in a four phase system using 2% Ru/Al<sub>2</sub>O<sub>3</sub>. Reaction conditions: catalyst (2% Ru/Al<sub>2</sub>O<sub>3</sub>), 20 kg/m<sup>3</sup>; P<sub>H<sub>2</sub></sub>, 4.8 MPa; Agitation, 16.66 Hz; water, 30 × 10<sup>-6</sup> m<sup>3</sup>; aniline dissolved in cyclohexane, total liquid volume, 100 × 10<sup>-6</sup> m<sup>3</sup>.



**Figure 3.9.** Effect of hydrogen partial pressure on initial rate of hydrogenation for hydrogenation of aniline in a four phase system using 2% Ru/Al<sub>2</sub>O<sub>3</sub>  
 Reaction conditions: aniline, 1.53 kmol/m<sup>3</sup>, catalyst (2% Ru/Al<sub>2</sub>O<sub>3</sub>), 20 kg/m<sup>3</sup>; agitation, 16.66 Hz; water, 30 × 10<sup>-6</sup> m<sup>3</sup>; aniline dissolved in cyclohexane, total liquid volume, 100 × 10<sup>-6</sup> m<sup>3</sup>.

### 3.3.4. Analysis of Mass Transfer Effects

Before going to develop an intrinsic kinetic model for hydrogenation of aniline in a gas-liquid-liquid-solid system, it was important to further check if the mass transfer limitations were significant using quantitative criteria. In a gas-liquid-liquid-solid catalytic reaction, following mass transfer steps must be considered: (a) gas-organic liquid phase mass transfer for hydrogen; (b) organic-aqueous phase mass transfer for hydrogen and aniline; and (c) aqueous phase to solid catalyst particles mass transfer for hydrogen and aniline and (d) intraparticle diffusion with surface reaction. Quantitative criteria to assess the significance of these steps, based on the approach described by Ramachandran and Chaudhari (1983) were used.

1. Gas-liquid mass transfer resistance can be negligible if,



$$\alpha_{gl} = \frac{R_A}{k_l a_b C_{A^*}} < 0.1 \quad (3.4)$$

where,  $k_l a_b$  is the gas-liquid mass transfer coefficient and calculated according to the correlation given below:<sup>26</sup>

$$k_l a_b = 1.48 \times 10^{-3} \times N^{2.18} \times \left( \frac{V_g}{V_l} \right)^{1.88} \times \left( \frac{d_i}{d_t} \right)^{2.16} \times \left( \frac{h_1}{h_2} \right)^{1.16} \quad (3.5)$$

2. Liquid-liquid mass transfer for hydrogen (X=A) or aniline (X=B) can be negligible if

$$\alpha_{ll,X} = \frac{R_A}{k_{lX} a_{ll} C_{X,Oi}} < 0.1 \quad (3.6)$$

where,  $k_{lX}$  is the liquid-liquid mass transfer coefficient and  $C_{X,Oi}$  is the concentration of hydrogen or aniline at the organic-aqueous interface. If it is considered that the dispersed aqueous phase is in the form of spherical droplets with a negligible slip velocity with respect to the continuous organic phase, liquid-liquid mass transfer coefficient can be calculated using  $Sh = 2$  by the following equation:<sup>27</sup>

$$k_{ll} = \frac{2 D_M}{d_d} \quad (3.7)$$

$$\text{and } a_{ll} = \frac{6 \varepsilon}{d_d} \quad (3.8)$$

where,  $D_M$  is the molecular diffusivity calculated from the correlation proposed by Wilke and Chang<sup>28</sup>

$$D_M = \frac{7.4 \times 10^{-8} T (\chi M_w)^{1/2}}{\mu_l \nu_M^{0.6}} \quad (3.9)$$

and  $d_d$  is the droplet diameter of the dispersed phase which can be obtained using the following equation given by Lagisetty et al.<sup>29</sup> for stirred liquid-liquid systems.

$$\left( \frac{d_d}{D} \right) = 0.125 \left( N^2 D^3 \rho_o / \sigma \right)^{-0.6} \quad (3.10)$$

3. Liquid-solid mass transfer resistance for hydrogen (X=A) or aniline (X=B) can be negligible if,

$$\alpha_{ls,X} = \frac{R_A}{k_{sX} a_p C_{X,W}} < 0.1 \quad (3.11)$$

where,  $a_p$  is the external surface area of the catalyst per unit volume

$$a_p = \frac{6w}{\rho_p d_p} \quad (3.12)$$

and  $k_s$  is the liquid-solid mass transfer coefficient and calculated by the correlation proposed by Sano et al.<sup>30</sup>

$$\frac{k_{s,X} d_p}{D_M F_c} = 2 + 0.4 \left[ \frac{e(d_p)^4 \rho_l^3}{\mu_l^3} \right]^{0.25} \left[ \frac{\mu_l}{\rho_l D_M} \right]^{0.333} \quad (3.13)$$

where,  $e$ , is the energy supplied to the liquid, was calculated according to Calderbank<sup>31</sup> and  $F_c$  is the shape factor assumed to be unity for spherical particles.

4. Pore diffusion resistance for hydrogen (X=A) or aniline (X=B) can be considered as negligible if,

$$\phi_{\text{exp},X} = \frac{d_p}{6} \left[ \frac{1}{2D_e} \frac{\rho_p R_A}{w C_{X,W}} \right]^{1/2} < 0.2 \quad (3.14)$$

where,  $D_e$  is the effective diffusivity, represented by

$$D_e = D_M \frac{\varepsilon}{\tau} \quad (3.15)$$

The values of different parameters required to calculate  $\alpha_1$ ,  $\alpha_2$  and  $\phi_{\text{exp}}$  are given in Table 3.5. For most cases, except catalyst loading  $>20 \text{ kg/m}^3$  (with respect to aqueous phase) and agitation speed below 16.66 Hz above 418 K, these criteria indicated absence of mass transport limitations as the values of  $\alpha_{gl}$ ,  $\alpha_{ll,A}$ ,  $\alpha_{ll,B}$ ,  $\alpha_{ls,A}$ ,  $\alpha_{ls,B}$ ,  $\phi_{\text{exp},A}$  and  $\phi_{\text{exp},B}$  were below  $3 \times 10^{-3}$ ,  $1.7 \times 10^{-2}$ ,  $3.6 \times 10^{-2}$ ,  $3.4 \times 10^{-2}$ ,  $4.6 \times 10^{-2}$ ,  $8 \times 10^{-3}$  and  $1.1 \times 10^{-2}$  respectively.

**Table 3.5.** Values of different parameters used in mass transfer analysis for hydrogen

Temperature, K	$k_l a_b$ , s <sup>-1</sup>	$d_p \times 10^4$ , m	$k_{ll} a_{ll}$ , s <sup>-1</sup>	$D_M \times 10^9$ , m <sup>2</sup> /s	$D_e \times 10^9$ , m <sup>2</sup> /s	$k_s a_p \times 10^1$ , s <sup>-1</sup>
378	0.268		1.448	4.8	0.60	4.25
398	0.268	1.49	1.758	5.7	0.71	5.97
418	0.268		2.012	6.1	0.76	8.07

However, the initial rate data in Figure 3.8-3.9 represent only the initial stage of the reaction and not applicable when the consecutive reactions were involved as shown in Scheme 3.3. Therefore, integral concentration-time data at different initial sets of conditions were used for evaluation of kinetic parameters.

### 3.3.5. Intrinsic Kinetics

The experimental concentration-time data in the kinetic regime were used to evaluate the rate equations. It was assumed that the solid catalyst particles are essentially present in the aqueous phase as also observed experimentally (for  $\varepsilon_w < 0.4$ ) and the product cyclohexylamine is quantitatively transferred from the aqueous phase to the organic phase with no changes in the volume of aqueous or organic phases and hence the liquid hold ups due to conversion. This is justified due to the low solubility of aniline and cyclohexylamine in water compared to that in cyclohexane. The following reaction mechanisms were considered to derive the rate equations (see Table 3.6):

- (1) Competitive adsorption of the reactants followed by reaction as the rate-limiting step,
- (2) Adsorption of molecular hydrogen on the catalyst surface (to form the active species) followed by reaction with the substrate as the rate-limiting step,
- (3) Hydrogen and aniline adsorbed competitively on the vacant catalyst sites and then hydrogen added to the aromatic moiety in sequential surface reaction steps,<sup>32</sup>
- (4) Dissociative adsorption of hydrogen and substrates on adjacent sites followed by surface reaction.

Along with the rate expressions based on mechanistic approach, three empirical models were also considered and the rate equations corresponding to all these models are shown in Table 3.6.

At isobaric and isothermal conditions a semi batch slurry reactor model was used to check the applicability of the equations. The material balance equations for different species in the organic phase on the basis of model 2 are given below as an example:

$$\frac{dC_{B,O}}{dt} = -\frac{\varepsilon}{(1-\varepsilon)} R_1 = -\frac{\varepsilon}{(1-\varepsilon)} \frac{k_1 w C_{A,W} C_{B,W}}{(1 + K_A C_{A,W} + K_B C_{B,W} + K_C C_{C,W})} \quad (3.16)$$

$$\frac{dC_{C,O}}{dt} = \frac{\varepsilon}{(1-\varepsilon)}(R_1 - R_2) = \frac{\varepsilon}{(1-\varepsilon)} \frac{wC_{A,W} (k_1 C_{B,W} - k_2 C_{C,W})}{(1 + K_A C_{A,W} + K_B C_{B,W} + K_C C_{C,W})} \quad (3.17)$$

$$\frac{dC_{D,O}}{dt} = \frac{\varepsilon}{(1-\varepsilon)} R_2 = \frac{\varepsilon}{(1-\varepsilon)} \frac{k_1 wC_{A,W} C_{C,W}}{(1 + K_A C_{A,W} + K_B C_{B,W} + K_C C_{C,W})} \quad (3.18)$$

and the initial conditions are:

$$\text{at } t = 0, C_{B,O} = (C_{B,O})_0 \text{ and } C_{C,O} = C_{D,O} = 0. \quad (3.19)$$

Here,  $k_1, k_2$  are the rate constants  $[(\text{kmol}/\text{m}^3)^{-1} (\text{kg}/\text{m}^3 (\text{aq. phase}))^{-1} \text{s}^{-1}]$  for step  $R_1$  and  $R_2$  respectively as shown in Scheme 3.3.  $R_1$  and  $R_2$  are the rates of reactions per unit volume of the dispersed phase with respect to B and C respectively as shown in Scheme 3.3.  $K_A, K_B$  and  $K_C$  are the adsorption constants for hydrogen (A), aniline (B) and aminocyclohexene (C) respectively. The concentrations in aqueous phase,  $C_{A,W}, C_{B,W}, C_{C,W}, C_{D,W}$  were in equilibrium with their respective concentrations in the organic phase ( $C_{A,O}, C_{B,O}, C_{C,O}, C_{D,O}$ ). For kinetic regime,  $C_{A,O}$  for hydrogen will be equal to saturation solubility  $C_{A^*,O} (=H_e \cdot P_{H_2})$ . Similarly,

$$C_{i,W} = C_{i,O} \alpha_i \quad (3.20)$$

where,  $i$  represents species A, B, C or D as mentioned in Scheme 3.3 and  $\alpha_i$  is the respective distribution coefficient. The partition coefficient value for A ( $\alpha_A$ ) and B ( $\alpha_B$ ) were 0.116 and 0.260 respectively (see Section 3.3.2.3). As the chemical nature of aniline (B) and aminocyclohexene (C) are quite similar, the distribution coefficients for B ( $\alpha_B$ ) and C ( $\alpha_C$ ) were assumed to be the same.

The overall rate of hydrogenation per unit volume of the total liquid dispersion can be written as:

$$R_{H_2} = \varepsilon_w (2R_1 + 3R_2) \quad (3.21)$$

To select the most suitable rate equation and to evaluate the suitability of the rate models, the above equations were solved using a fourth order Runge-Kutta method coupled with an optimization method based on Marquart's algorithm. The method also includes the following objective functions as optimization criterion:

$$\phi_{\min} = \sum_{i=1}^3 \sum_{i=1}^n (Yi_{\text{exp}} - Yi_{\text{mod}})^2 \quad (3.22)$$

and the mean average of relative residuals as:

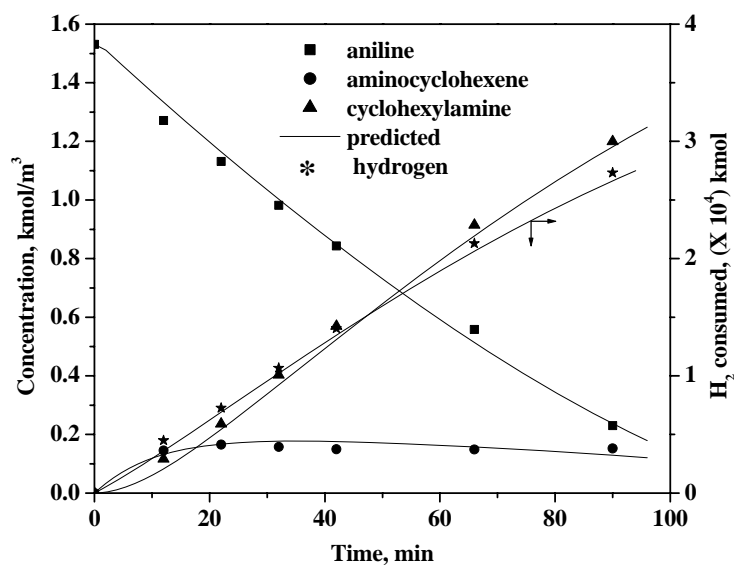
$$\%RR = \sum_{i=1}^4 \sum_{i=1}^n \frac{(Yi_{\text{exp}} - Yi_{\text{mod}})}{Yi_{\text{exp}}} \times 100 \quad (3.23)$$

The values of the optimized rate parameters and the objective functions for each rate model are given in Table 3.6. Minimum values of these objective functions were used as a criterion for model discrimination, but thermodynamic constraints such as positive values of rate parameters and activation energies were also considered as the most important criterion for the applicability of a model.<sup>33,34</sup> Based on these criteria, model 1 and 4 were discarded as one or two rate parameters were negative in those models. Model 2 had lower  $\phi_{\min}$  and % RR values compared to model 3, and hence was considered as the best model. We checked the applicability of these models by fitting the predicted and experimentally observed concentrations as functions of time. It was observed that only model 2 represented the experimental concentration-time profiles in very good agreement for all the initial sets of operating conditions at different temperatures. For example, Figures 3.10-3.12 represent the validity of the model 2 at three different temperatures.

**Table 3.6.** Rate equations and kinetic parameters

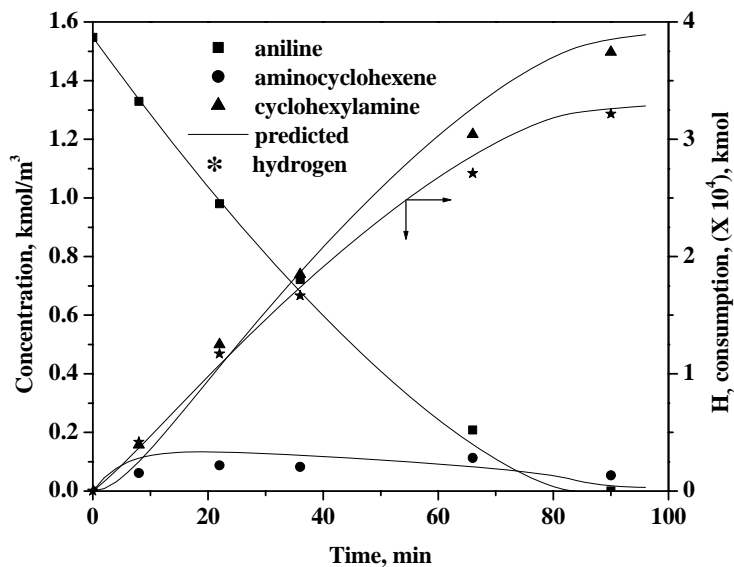
Model No.	Model	Temp., K	$k_1$	$k_2$	$K_A$	$K_B$	$K_C$	% RR	$\phi_{min}$
1	$R_i = \frac{k_i w C_{A,W} C_{i,W}}{(1 + K_A C_{A,W} + K_B C_{B,W} + K_C C_{C,W})^2}$	378	8.18	25.60	191.13	109.58	46.21	± 16	$8.7 \times 10^{-3}$
		398	24.79	38.81	165.61	76.62	-24.67	± 10	$6.2 \times 10^{-3}$
		418	44.72	75.33	103.24	24.25	24.17	± 13	$4.7 \times 10^{-3}$
2	$R_i = \frac{k_i w C_{A,W} C_{i,W}}{(1 + K_A C_{A,W} + K_B C_{B,W} + K_C C_{C,W})}$	378	$0.83 \times 10^{-2}$	$0.97 \times 10^{-2}$	38.19	34.82	61.41	± 8	$5.6 \times 10^{-4}$
		398	$1.51 \times 10^{-2}$	$2.20 \times 10^{-2}$	62.34	26.15	45.74	± 5	$5.6 \times 10^{-4}$
		418	$2.98 \times 10^{-2}$	$4.50 \times 10^{-2}$	81.99	9.7	33.7	± 7	$7.4 \times 10^{-4}$
3	$R_i = \frac{k_i w C_{A,W} C_{i,W}}{(1 + K_A C_{A,W} + (K_B C_{B,W})^{1/2} + K_C C_{C,W})^2}$	378	2.36	4.89	81.72	8.62	401.8	± 16	$4.7 \times 10^{-2}$
		398	4.43	10.58	186.4	3.53	367.3	± 11	$7.1 \times 10^{-2}$
		418	18.2	22.02	51.99	19.7	337.4	± 9	$1.2 \times 10^{-2}$
4	$R_i = \frac{k_i w C_{A,W}^{1/2} C_{i,W}}{(1 + K_A C_{A,W}^{1/2})(1 + K_B C_{B,W} + K_C C_{C,W})}$	378	$2.08 \times 10^{-3}$	$3.19 \times 10^{-3}$	-48.36	41.80	29.86	± 12	$5.1 \times 10^{-3}$
		398	$2.81 \times 10^{-3}$	$-1.5 \times 10^{-3}$	45.79	26.16	33.93	± 17	$5.5 \times 10^{-3}$
		418	$6.18 \times 10^{-3}$	$9.02 \times 10^{-3}$	57.81	23.11	21.88	± 14	$4.3 \times 10^{-1}$
5	$R_1 = \frac{k_1 w C_{A,W}}{(1 + K_A C_{A,W} + K_C C_{C,W})}$ $R_2 = \frac{k_2 w C_{A,W} C_{C,W}}{(1 + K_A C_{A,W} + K_C C_{C,W})}$	378	$1.41 \times 10^{-2}$	$2.17 \times 10^{-1}$	384.62	--	3.38	± 13	$5.1 \times 10^{-1}$
		398	$2.29 \times 10^{-2}$	$3.31 \times 10^{-1}$	599.11	--	4.57	± 11	$5.6 \times 10^{-1}$
		418	$5.53 \times 10^{-2}$	$5.91 \times 10^{-1}$	827.63	--	4.95	± 14	$6.9 \times 10^{-1}$

Model No.	Model	Temp., K	$k_1$	$k_2$	$K_A$	$K_B$	$K_C$	% RR	$\phi_{min}$
6	$R_1 = \frac{k_1 w C_{A,W}}{(1 + K_A C_{A,W} + K_C C_{C,W})^{1/2}}$ $R_2 = \frac{k_2 w C_{A,W} C_{C,W}}{(1 + K_A C_{A,W} + K_C C_{C,W})^{1/2}}$	378	$1.86 \times 10^{-4}$	$2.26 \times 10^{-3}$	81.92	--	69.54	$\pm 18$	$3.1 \times 10^2$
		398	$2.32 \times 10^{-4}$	$3.2 \times 10^{-3}$	$5.73 \times 10^5$	--	457.11	$\pm 21$	$2.6 \times 10^2$
		418	$3.72 \times 10^{-4}$	$5.21 \times 10^{-3}$	66.73	--	45.77	$\pm 16$	$2.9 \times 10^2$
7	$R_1 = \frac{k_1 w C_{A,W}}{(1 + K_A C_{A,W} + K_C C_{C,W})^2}$ $R_2 = \frac{k_2 w C_{A,W} C_{C,W}}{(1 + K_A C_{A,W} + K_C C_{C,W})^2}$	378	$3.14 \times 10^1$	$8.9 \times 10^2$	$6.84 \times 10^5$	--	326.8	$\pm 14$	$4.8 \times 10^1$
		398	$5.79 \times 10^1$	$1.94 \times 10^3$	$1.51 \times 10^6$	--	457.4	$\pm 13$	$5.6 \times 10^1$
		418	$4.96 \times 10^2$	$5.23 \times 10^3$	$7.50 \times 10^6$	--	957.7	$\pm 17$	$6.9 \times 10^1$



**Figure 3.10.** Concentration-time profile at 378 K

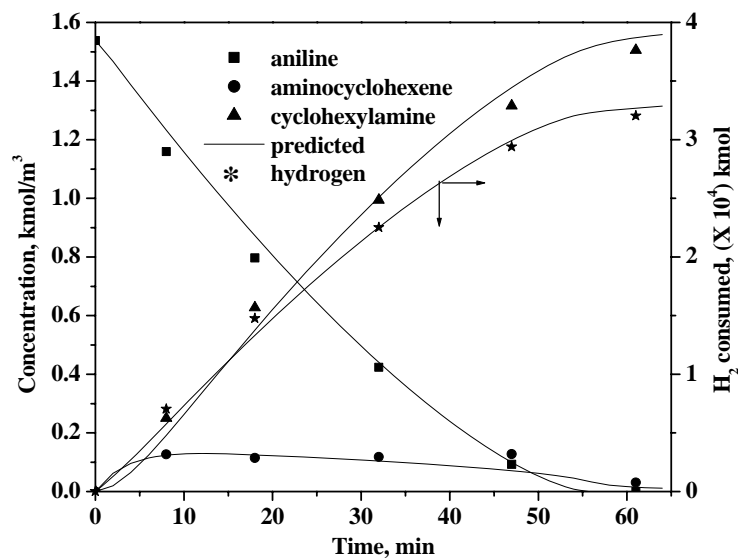
Reaction conditions: aniline,  $1.53 \text{ kmol/m}^3$ ; catalyst ( $2\% \text{ Ru/Al}_2\text{O}_3$ ),  $20 \text{ kg/m}^3$ ;  $P_{\text{H}_2}$ , 4.8 MPa; temperature, 378K; water,  $30 \times 10^{-6} \text{ m}^3$ ; aniline dissolved in cyclohexane, total liquid volume,  $100 \times 10^{-6} \text{ m}^3$ .



**Figure 3.11.** Concentration-time profile at 398 K

Reaction conditions: aniline,  $1.53 \text{ kmol/m}^3$ ; catalyst ( $2\% \text{ Ru/Al}_2\text{O}_3$ ),  $20 \text{ kg/m}^3$ ;  $P_{\text{H}_2}$ , 4.8 MPa; temperature, 398K; water,  $30 \times 10^{-6} \text{ m}^3$ ; aniline dissolved in cyclohexane, total liquid volume,  $100 \times 10^{-6} \text{ m}^3$ .

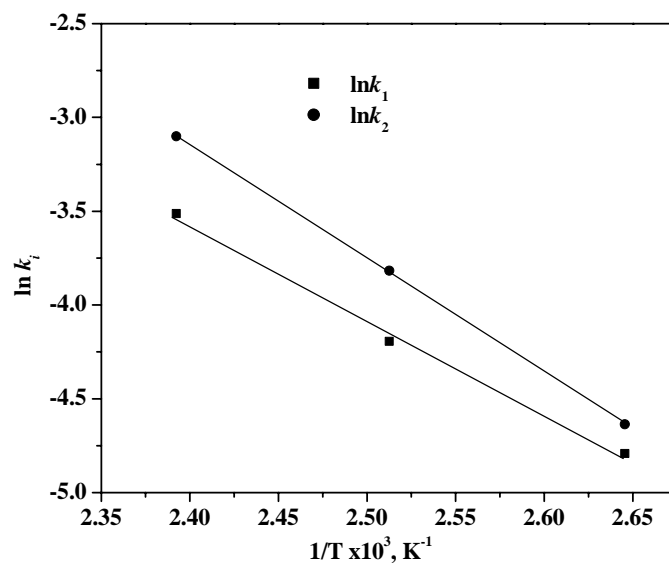




**Figure 3.12.** Concentration-time profile at 418 K

Reaction conditions: aniline,  $1.53 \text{ kmol/m}^3$ ; catalyst (2% Ru/Al<sub>2</sub>O<sub>3</sub>),  $20 \text{ kg/m}^3$ ; P<sub>H<sub>2</sub></sub>, 4.8 MPa; temperature, 418K; water,  $30 \times 10^{-6} \text{ m}^3$ ; aniline dissolved in cyclohexane, total liquid volume,  $100 \times 10^{-6} \text{ m}^3$ .

Activation energies of the reaction steps were calculated from the Arrhenius plots shown in Figure 3.13 as 41.97 and 50.386 kJ/mol for  $R_1$  and  $R_2$  respectively.



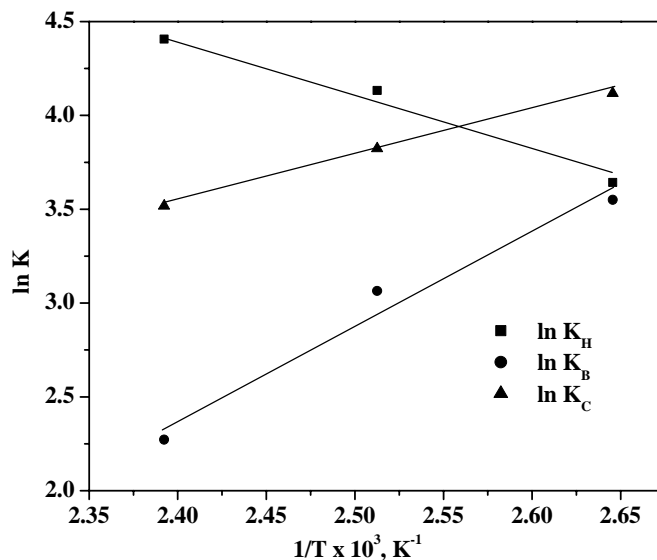
**Figure 3.13.** Temperature dependence of rate constants

The enthalpy ( $-\Delta H_i$ ) and entropy ( $\Delta S_i$ ) of adsorption for all the adsorbed species were calculated using the following equations<sup>35</sup>:

$$K_i = K_{i0} \exp\left(-\frac{\Delta H_i}{RT}\right) \quad (3.24)$$

$$K_{i0} = \exp\left(\frac{\Delta S_i}{R}\right) \quad (3.25)$$

where,  $K_{i0}$  was the pre-exponential factor and R is the universal gas constant. The  $\ln K_i$  vs.  $1/T$  plots for hydrogen (H), aniline (B) and amino cyclohexene (C) are shown in Figure 3.14. The slopes of these plots correspond to  $(-\Delta H_i/R)$  from which  $-\Delta H_i$  can be calculated. On the other hand, the intercept of the plots in Figures 3.14 to the Y-axis at  $1/T = 0$  represents the pre-exponential factor,  $K_{i0}$  from which  $\Delta S_i$  can be calculated according to Equation 3.25.



**Figure 3.14.** Temperature dependence of adsorption constants

The enthalpy of adsorption and entropy of adsorption for all the adsorbing species are given in Table 3.7. The negative value of enthalpy of adsorption for hydrogen ( $K_H$ ) was obtained which, though not so common, has also been previously reported for liquid phase

hydrogenation reactions by Broderick and Gates<sup>36</sup> and Chaudhari et al.<sup>37</sup> A plausible explanation for such unusual observation may be the endothermic chemisorption of hydrogen on the ruthenium metal surface.

**Table 3.7.** Values of enthalpy and entropy of adsorption

Adsorbate	$-\Delta H_i$ (kJ/mol)	$\Delta S$ (J/mol k)
Hydrogen	-25.09	38.57
Aniline	41.96	28.49
Aminocyclohexene	19.71	17.63

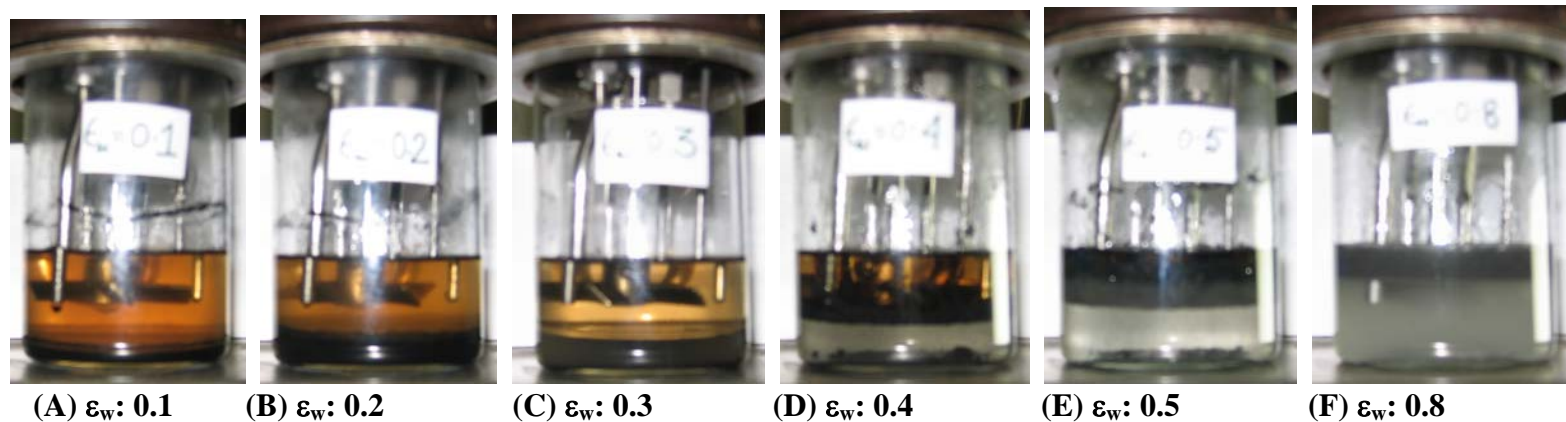
### 3.4. ANALYSIS OF A GAS-LIQUID-LIQUID-SOLID SYSTEM

The initial work on evaluation of catalysts clearly showed the advantages of using a four phase catalytic system involving two immiscible liquid phases for some hydrogenation reactions. In such reaction systems, the overall rate of reaction is dependent on interphase mass transfer, hydrodynamics of the complex multiphase system and reaction kinetics. In the previous section detailed kinetic modeling for hydrogenation of aniline to cyclohexylamine in a gas-liquid-liquid-solid system is presented. In this part, a theoretical analysis of the rate processes as a function of hold up of a particular phase involved in such gas-liquid-liquid-solid catalytic reaction systems has been described. For this purpose, hydrogenation of aniline in the cyclohexane–water in the presence of Ru/Al<sub>2</sub>O<sub>3</sub> catalyst was considered.

In hydrogenation of aniline to cyclohexylamine in a gas-liquid-liquid-solid system, the organic substrate produced equivalent moles of products, which due to its very low solubilities in aqueous medium, stayed in the organic phase only. Therefore, swelling or shrinkage of any phase didn't occur for this case. Hence, it is assumed that the volumes of organic and aqueous phases remain unchanged during the course of a reaction.

The important characteristic of the present four phase system was that at low aqueous phase hold up ( $\epsilon_w = 0.1 - 0.3$ ) the catalyst (2% Ru/Al<sub>2</sub>O<sub>3</sub>) remained in the aqueous phase and above which ( $\epsilon_w = 0.4 - 0.8$ ) the catalyst moved to the organic phase. These unusual observations are shown in Figure 3.15. Therefore, two different cases were considered to model the variation of initial rate of hydrogenation over the entire range of

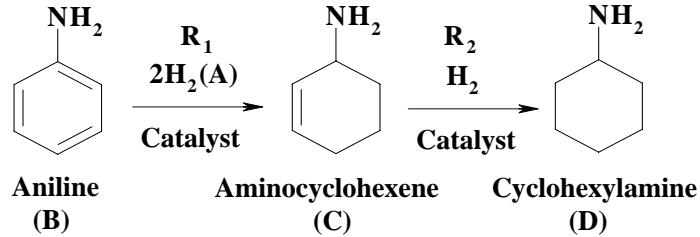
aqueous phase hold up: **(CASE-I)** At lower aqueous phase hold up, the catalyst was considered to be in the aqueous phase; and **(CASE-II)** At higher aqueous phase hold up, the equations were derived considering the catalyst in the organic phase.



**Figure 3.15.** Photographs of the glass reactor containing aniline in cyclohexane (organic phase; top yellow layer), water (aqueous phase; colorless bottom layer) and catalyst (black colored) at different hold ups of aqueous and organic phases. The total volume of the liquid phase was kept constant. A glass jar was fitted physically below the reactor head, which was used for the slurry reactions. A hot plate was used to heat the contents of the glass jar and temperature was controlled by the thermocouple fitted to the reactor.

### 3.4.1. Mathematical Model

The stepwise hydrogenation of aniline in gas-liquid-liquid-solid system using Ru/Al<sub>2</sub>O<sub>3</sub> catalyst is shown below.



The reaction scheme can be written as:



Kinetic studies showed that a rate equation of the following type is appropriate to represent the above reactions:

$$R_i = \frac{k_i w C_{A,W} C_{i,W}}{(1 + K_A C_{A,W} + K_B C_{B,W} + K_C C_{C,W})} \quad (3.28)$$

where,  $C_{i,w}$  represents the concentration of the  $i$ -th liquid phase component in the aqueous phase.  $C_{A,w}$  is the concentration of hydrogen in aqueous phase. Here it is important to note that  $R_i$  and  $k_i$  represent the rate of reaction and rate constants defined based on the volume of the dispersed phase. For the analysis of the rate process for such a gas-liquid-liquid-solid system, two different cases were considered.

**CASE-I:** When organic phase is continuous and aqueous phase is dispersed with catalyst in the dispersed aqueous phase

**CASE-II:** When aqueous phase is continuous and organic phase is dispersed with catalyst in the dispersed organic phase

#### **CASE-I: When organic phase is continuous and aqueous phase is dispersed**

This situation occurs when aqueous phase hold up,  $\varepsilon_w$  (the ratio of aqueous phase volume to total liquid volume) is  $\leq 0.3$ . Water droplets containing the catalyst particles remain in a pool of organic phase. In such a case, a number of steps have to occur before

aniline converts to the product over the active catalyst surface in a slurry reactor. The steps for gaseous reactant hydrogen (A) are as follows:

- (a) Transport of A from the bulk gas phase to the gas-liquid (organic) interface.
- (b) Transport of A from gas-liquid (organic) interface to the bulk liquid (organic) phase.
- (c) Transport of A from bulk liquid (organic) to liquid (organic)-liquid (water) interface.
- (d) Transport of A from liquid (organic)-liquid (water) interface to the bulk aqueous phase.
- (e) Transport of A from bulk aqueous phase to the solid catalyst surface.
- (f) Adsorption of A on the active catalyst surface.
- (g) Surface reaction to yield product.

To derive the mass balance equations the following assumptions were made:

**Assumptions:**

1. For gas-liquid mass transfer of hydrogen (A), the resistance from the gas side of gas-liquid film was considered to be negligible as pure hydrogen gas was used.
2. For liquid (organic)-liquid (aqueous) mass transfer for A, the resistance from the organic side liquid film was considered. For liquid-liquid mass transfer, the resistance from the aqueous liquid side of liquid-liquid film was considered to be negligible as it was assumed that the aqueous liquid film thickness was very small due to very small droplet size ( $< 1.5 \times 10^{-4}$  m).
3. As the concentrations of B and C were very high with respect to A, liquid-liquid mass transfer limitations for B and C were considered to be negligible. Concentrations of B and C in the aqueous phase will be related to the organic phase concentrations and the partition coefficient of the respective components in the cyclohexane-water system at the experimental condition as written in Equation 3.20.

4. Catalyst particles were surrounded by a thin film of water. Therefore, liquid-solid mass transfer resistances were considered to be negligible for all the components (A, B, C and D).
5. As the catalyst particles are very fine, intraparticle mass transfer resistance was considered to be negligible.
6. Steady state condition was assumed.

The concentration profile for A and B as it moved to the catalyst surface is shown in Figure 3.16.

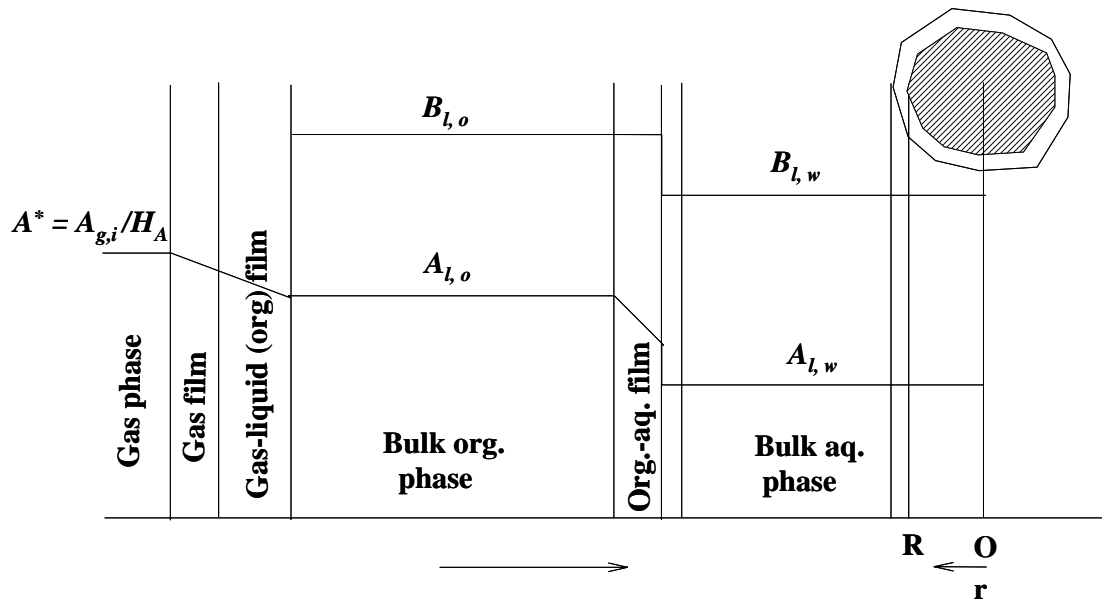


Figure 3.16. Concentration profile of species A and B in a gas-liquid-liquid-solid catalytic system

#### Mass balance for hydrogen (A)

The rate of mass transfer of hydrogen (A) from the bulk gas phase to the reaction at the catalyst surface can be derived according to the steps (a) to (g). The rate of gas-liquid (organic) mass transfer can be written as:

$$R_A = (K_{l,A}a_b)(A^* - A_{l,o}) \quad (3.29)$$

where,  $A^*$  and  $A_{l,o}$  are the saturation solubility and actual concentration of hydrogen in organic phase at that particular reaction condition.  $(K_{l,A}a_b)$  was the gas to liquid (organic) mass transfer coefficient. The details of the correlations used for the calculations were described in Section 3.3.4.



The rate of liquid (organic)-liquid (aqueous) mass transfer can be written as:

$$R_A = (K_{llA} a_{ll}) (A_{l,o} - A_{l,w} / \alpha_A) \quad (3.30)$$

where,  $A_{l,w}$  is the concentration of hydrogen in aqueous phase.  $\alpha_A$  is the partition coefficient of hydrogen in organic-water binary system.

The overall rate of hydrogenation per unit volume of total dispersion,  $R_A$  can be written as:

$$R_A = \varepsilon_w \left[ \frac{w A_{l,w} (2k_1 B_{l,w} + 3k_2 C_{l,w})}{(1 + K_A A_{l,w} + K_B B_{l,w} + K_C C_{l,w})} \right] \quad (3.31A)$$

$$= \varepsilon_w (2R_1 + 3R_2) \quad (3.31B)$$

As the liquid (aqueous) film surrounding the catalyst is very fine, we can assume that the liquid-solid mass transfer resistances are negligible.

At the steady state, the rate of gas-liquid, liquid-liquid mass transfers and the rate of chemical reaction per unit volume of the total dispersion are same. Therefore, combining Equations 3.29, 3.30 and 3.31 we can write:

$$R_A = (K_{l,A} a_b) (A^* - A_{l,o}) \quad (3.32A)$$

$$= K_{llA} a_{ll} (A_{l,o} - A_{l,w} / \alpha_A) \quad (3.32B)$$

$$= \varepsilon_w \left[ \frac{w A_{l,w} (2k_1 B_{l,w} + 3k_2 C_{l,w})}{(1 + K_A A_{l,w} + K_B B_{l,w} + K_C C_{l,w})} \right] \quad (3.32C)$$

From Equation 3.32B we have,

$$R_A = k_{ll,A} a_{ll} (A_{l,o} - A_{l,w} / \alpha_A)$$

which can be rearranged to,

$$\begin{aligned} \frac{R_A}{k_{ll,A} a_{ll}} &= (A_{l,o} - A_{l,w} / \alpha_A) \\ \Rightarrow A_{l,o} &= \frac{R_A}{k_{ll,A} a_{ll}} + A_{l,w} / \alpha_A \end{aligned} \quad (3.33)$$

From Equation 3.32A we have,

$$R_A = (K_{l,A} a_b) (A^* - A_{l,o})$$

Substituting  $A_{l,o}$  from Equation 3.33, we get

$$\begin{aligned} \frac{R_A}{K_{l,A} a_b} &= \left( A^* - \frac{R_A}{k_{l,A} a_{ll}} - A_{l,w} / \alpha_A \right) \\ \Rightarrow A_{l,w} / \alpha_A &= A^* - \frac{R_A}{k_{l,A} a_{ll}} - \frac{R_A}{K_{l,A} a_b} \\ \Rightarrow A_{l,w} &= \alpha_A A^* - \alpha_A R_A \left( \frac{1}{k_{l,A} a_{ll}} + \frac{1}{K_{l,A} a_b} \right) \end{aligned} \quad (3.34)$$

In Equation 3.34, the unknown surface concentration of hydrogen ( $A_{l,w}$ ) is represented in terms of known parameters.

Concentrations of B and C in the aqueous phase can be correlated to their corresponding organic phase concentrations by the following correlations:

$$B_{l,w} = \alpha_B B_{l,o} \quad (3.35)$$

$$C_{l,w} = \alpha_C C_{l,o} \quad (3.36)$$

The mass balance equations for B and C can be represented as:

$$-\frac{dB_{l,o}}{dt} = \frac{\varepsilon_w}{(1-\varepsilon_w)} R_1 = \frac{\varepsilon_w}{(1-\varepsilon_w)} \frac{k_1 w A_{l,w} B_{l,w}}{(1 + K_A A_{l,w} + K_B B_{l,w} + K_C C_{l,w})} \quad (3.37)$$

$$-\frac{dC_{l,o}}{dt} = \frac{\varepsilon_w}{(1-\varepsilon_w)} R_2 = \frac{\varepsilon_w}{(1-\varepsilon_w)} \frac{k_1 w A_{l,w} (k_2 C_{l,w} - k_1 B_{l,w})}{(1 + K_A A_{l,w} + K_B B_{l,w} + K_C C_{l,w})} \quad (3.38)$$

Now  $A_{l,w}$ ,  $B_{l,w}$  and  $C_{l,w}$  in 3.32C, 3.37 and 3.38 can be replaced in terms of known concentration terms by Equations 3.34 to 3.36 and can be solved. The rate of hydrogenation per unit volume of the total liquid dispersion was then calculated from Equation 3.32C.

### CASE II: When aqueous phase is continuous and organic phase is dispersed

This situation occurred when aqueous phase hold up,  $\varepsilon_w$  (the ratio of aqueous phase volume to total liquid volume) was  $\geq 0.4$ . Organic phase containing the liquid phase reactants (B and C) remained in a pool of aqueous phase. Catalyst particles were suspended in the organic phase. Therefore, reaction was occurring in the organic phase. In such a case,

number of steps has to occur before B and C converts to the product over the active catalyst surface in a slurry reactor. The steps for gaseous reactant hydrogen (A) are as follows:

- (a) Transport of A from the bulk gas phase to the gas-liquid (aqueous) interface.
- (b) Transport of A from gas-liquid (aqueous) interface to the bulk liquid (aqueous) phase.
- (c) Transport of A from bulk aqueous phase to liquid (aqueous)-liquid (organic) interface.
- (d) Transport of A from liquid (aqueous)-liquid (organic) interface to bulk organic phase.
- (e) Transport of A from bulk organic phase to the solid catalyst surface.
- (f) Adsorption of A on the active catalyst surface.
- (g) Surface reaction to yield product.

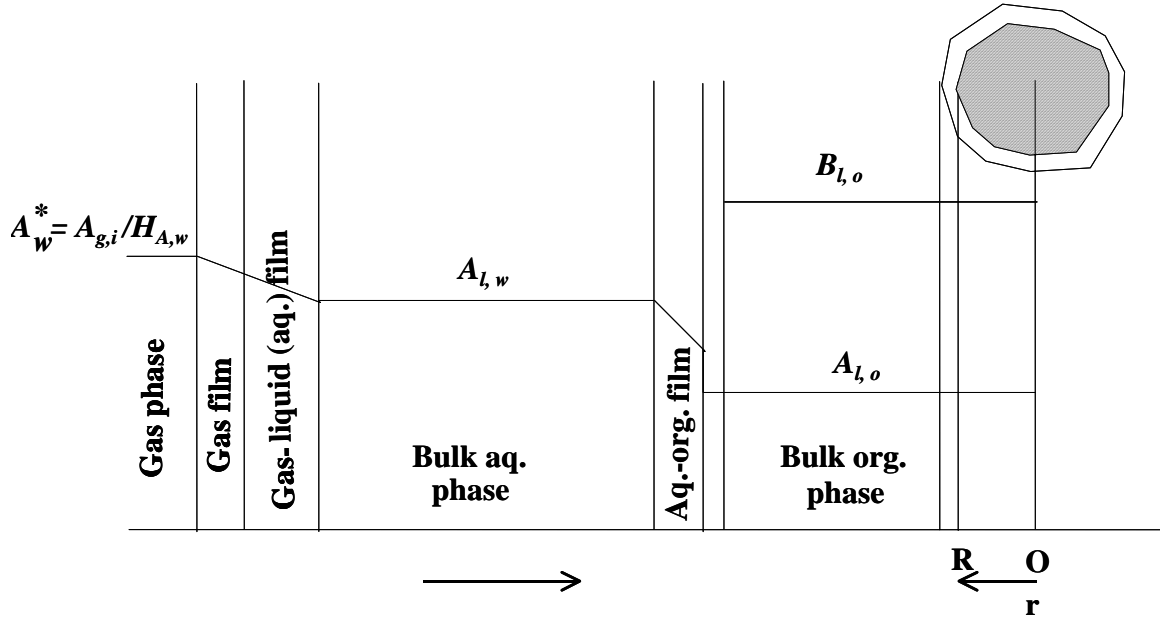
To derive the mass balance equations the following assumptions were considered:

**Assumptions:**

1. For gas-liquid mass transfer of hydrogen (A), the resistance from the gas side of gas-liquid (aqueous) film was considered to be negligible as pure hydrogen gas was used.
2. For liquid (aqueous)-liquid (organic) mass transfer for A, the resistance from the aqueous side liquid film was considered. For liquid-liquid mass transfer, the resistance from the organic liquid side of liquid-liquid film was considered to be negligible as it is assumed that the organic liquid film thickness was very small.
3. A (hydrogen) transferred only through gas-liquid (aqueous) film and then transferred to the organic phase. A (hydrogen) dissolve in organic phase and its mass transfer to the aqueous phase through liquid (organic)-liquid (aqueous) interface was assumed to be negligible.
4. Intraparticle mass transfer resistance was considered to be negligible.
5. Solvent effect on reaction kinetics was assumed to be negligible to use the same kinetic parameters.
6. Steady state condition was assumed.

The concentration profile for A and B as it moved to the catalyst surface is shown in Figure 3.17.

At steady state condition, the rate of hydrogenation per unit volume of the total liquid phase could be correlated to the gas-liquid (aqueous) mass transfer, liquid-liquid mass transfer and rate of surface reaction for hydrogen as:



**Figure 3.17.** Concentration profile of species A and B in a gas-liquid-liquid-solid catalytic system

$$R_A = (K_{l,A} a_b)_w (A_w^* - A_{l,w}) \quad (3.39A)$$

$$= (k_{ll,A} a_{ll}) (\alpha_A A_{l,w} - A_{l,o}) \quad (3.39B)$$

$$= (1 - \varepsilon_w) \frac{w A_{l,o} (2k_1 B_{l,o} + 3k_2 C_{l,o})}{(1 + K_A A_{l,o} + K_B B_{l,o} + K_C C_{l,o})} \quad (3.39C)$$

where,  $(K_{l,A} a_b)_w$  represented the gas-liquid mass transfer coefficient of A from the gas phase to the aqueous phase.  $A_w^*$  was the saturation solubility of A in aqueous phase.  $(k_{ll,A} a_{ll})$  was the liquid (aqueous)-liquid (organic) mass transfer coefficient for hydrogen.  $w$  was the catalyst loading per unit volume of the organic phase,  $\text{kg/m}^3(\text{org})$ .

From Equation 3.39B, we can get,

$$\begin{aligned}
R_A &= (k_{ll,A} a_{ll}) (\alpha_A A_{l,w} - A_{l,o}) \\
\Rightarrow \frac{R_A}{(k_{ll,A} a_{ll})} &= \alpha_A A_{l,w} - A_{l,o} \\
\Rightarrow A_{l,o} &= \alpha_A A_{l,w} - \frac{R_A}{(k_{ll,A} a_{ll})} \quad (3.40)
\end{aligned}$$

From Equation 3.39A, we can get,

$$\begin{aligned}
R_A &= (K_{l,A} a_b)_w (A_w^* - A_{l,w}) \\
\Rightarrow \frac{R_A}{(K_{l,A} a_b)_w} &= A_w^* - A_{l,w} \\
\Rightarrow A_{l,w} &= A_w^* - \frac{R_A}{(K_{l,A} a_b)_w} \quad (3.41)
\end{aligned}$$

Replacing  $A_{l,w}$  in Equation 3.40 by the expression in Equation 3.41, we get,

$$\begin{aligned}
A_{l,o} &= \alpha_A A_{l,w} - \frac{R_A}{(k_{ll,A} a_{ll})} \\
\Rightarrow A_{l,o} &= \alpha_A \left( A_w^* - \frac{R_A}{(K_{l,A} a_b)_w} \right) - \frac{R_A}{(k_{ll,A} a_{ll})} \\
\Rightarrow A_{l,o} &= \alpha_A A_w^* - \frac{\alpha_A R_A}{(K_{l,A} a_b)_w} - \frac{R_A}{(k_{ll,A} a_{ll})} \\
\Rightarrow A_{l,o} &= \alpha_A A_w^* - R_A \left( \frac{\alpha_A}{(K_{l,A} a_b)_w} + \frac{1}{(k_{ll,A} a_{ll})} \right) \quad (3.42)
\end{aligned}$$

The mass balance equations for B and C could be written as,

$$-\frac{dB_{l,o}}{dt} = R_1 = \frac{wk_1 A_{l,o} B_{l,o}}{(1 + K_A A_{l,o} + K_B B_{l,o} + K_C C_{l,o})} \quad (3.43)$$

$$-\frac{dC_{l,o}}{dt} = R_2 = \frac{wk_2 A_{l,o} C_{l,o}}{(1 + K_A A_{l,o} + K_B B_{l,o} + K_C C_{l,o})} \quad (3.44)$$

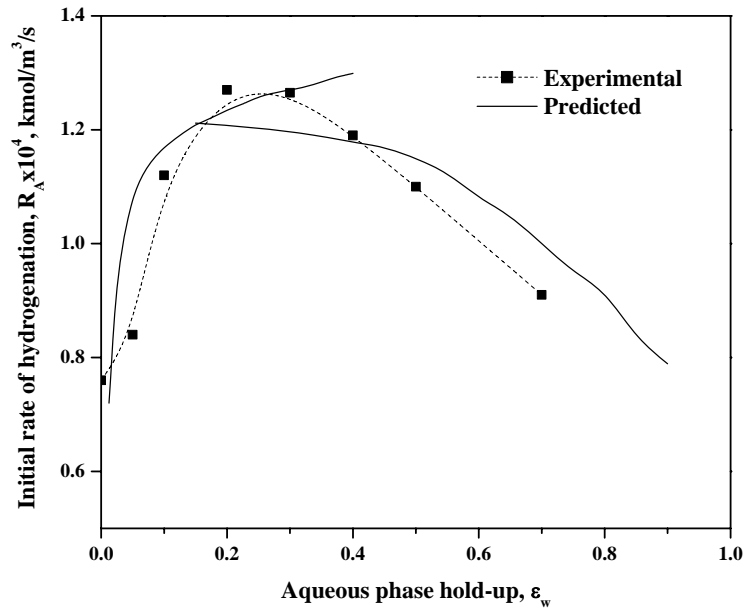
Now,  $A_{l,o}$  in Equation 3.43 and 3.44 could be replaced by the expression derived in Equation 3.42 and could be solved. Here,  $R_1$  and  $R_2$  were the rates of reaction per unit volume of organic phase hold up. Therefore, the rate of hydrogenation per unit volume of total liquid phase ( $R_A$ ) could be written as,

$$\begin{aligned}
R_A &= (1 - \varepsilon_w) \frac{wA_{l,o} (2k_1B_{l,o} + 3k_2C_{l,o})}{(1 + K_A A_{l,o} + K_B B_{l,o} + K_C C_{l,o})} \\
&= (1 - \varepsilon_w) (2R_1 + 3R_2)
\end{aligned} \tag{3.45}$$

### 3.4.1.1. Comparison of the model predictions with experimental results

In order to understand the effect of dispersed phase hold up on rate of hydrogenation, it is important to know the dispersion characteristics of the solid catalyst particles within the two liquid phases. As discussed earlier (Section 3.4, Figure 3.15), we observed that the solid catalyst particles are present primarily in dispersed phase. While at aqueous phase hold up of 0.1 to 0.3 catalyst particles are essentially present in the aqueous phase with a clear organic phase, at higher aqueous phase hold up ( $\varepsilon_w > 0.4$ ) wherein the organic phase is the dispersed phase the catalyst particles are predominantly present in the organic phase. Though this behavior may be different for different systems, in each case a quantitative account of rate of hydrogenation as a function of aqueous phase hold up can be made using the theoretical models discussed above for these two cases (CASE-I and II). The objective here was to examine whether the observed trend of initial rate of hydrogenation ( $R_A$ ) vs aqueous phase hold up ( $\varepsilon_w$ ) (at constant amount of catalyst and substrate aniline in the liquid-liquid dispersion) passing through a maxima can be achieved by the models. The model Equations 3.32C, 3.34-3.38 (for CASE-I) and 3.39C, 3.42-3.44 (for CASE-II) were used to calculate the initial rate of hydrogenation ( $R_A$ ) at different aqueous phase hold up ( $\varepsilon_w$ ) using the kinetic parameters ( $k_1, k_2$  and  $K_A, K_B, K_C$ ) for Model 2 presented in Table 3.6. The other model parameters required ( $K_{l,A}a_b, K_{l,A}, a_{ll}$ ) were all calculated by the correlations described in Section 3.3.4 (Equation 3.5, 3.7, 3.8). At this stage, very precise values of these parameters of gas-liquid-liquid-solid systems were not available and the predictions from these correlations may have some errors with respect to the true values. However, it was thought important to examine if the trend of maxima with respect to initial rate of hydrogenation ( $R_A$ ) vs aqueous phase hold up ( $\varepsilon_w$ ) is at least predictable. The predicted results along with experimental data for a specific set of reaction

conditions are shown in Figure 3.18, which indicates that the model equations proposed here predict the trend reasonably well.



**Figure 3.18.** Comparison of experimental and predicted results for initial rate of hydrogenation as a function of aqueous phase hold up at constant amount of aniline and catalyst

Reaction conditions: aniline,  $0.1 \times 10^{-3}$  kmol, catalyst (2% Ru/Al<sub>2</sub>O<sub>3</sub>),  $0.6 \times 10^{-3}$  kg; P<sub>H<sub>2</sub></sub>, 4.8 MPa; aniline dissolved in cyclohexane, total liquid volume,  $100 \times 10^{-6}$  m<sup>3</sup>.

The errors in the specific values in the initial rate predicted are obvious considering the uncertainty of some of the mass transfer and hydrodynamic parameters predicted by the correlations reported in the literature. From the study it is quite clear that the understanding of the overall rate of reactions in such multiphase catalytic reaction systems is rather complex due to coupled effect of interfacial mass transfer, hydrodynamics and kinetics of the reaction involved. Particularly, the influence of the liquid hold ups and catalyst particle distribution is important from the design and scale up point of view. More detailed investigation for such systems is necessary to arrive at generalized conclusions.

### 3.5. CONCLUSION

Gas-liquid-liquid-solid system showed better catalytic performance than the corresponding conventional gas-liquid-solid catalytic system with Ru/Al<sub>2</sub>O<sub>3</sub> catalyst for dearomatization of aromatic compounds by hydrogenation. Kinetics of aniline hydrogenation to cyclohexylamine was studied in a tetra phase system over a temperature range of 378-418K. It was found that the experimental data were in the kinetic regime in most cases except higher catalyst loading and agitation speed below 16 Hz. Different rate models were developed and based on the observed concentration-time data intrinsic kinetic parameters estimated. A rate model considering adsorption of hydrogen on the catalyst surface followed by reaction with the liquid phase components as the rate-limiting step was found to give the best fitting of the experimental concentration-time as well as the hydrogen consumption-time data at different initial sets of reaction conditions. Activation energy, heat of adsorption and entropy of adsorption were evaluated. Theoretical model was developed to predict the initial rate data as a function of aqueous phase hold up. An unusual property of catalyst phase inversion with increase in aqueous phase hold up was observed and hence two separate models based on availability of the catalyst in a particular phase were derived. Predictions of the two models were in good agreement with experimental results.

#### Nomenclature

$a_p$  = external surface area of the catalyst per unit volume, m<sup>2</sup>/m<sup>3</sup>

$C_{A^*,O}$  = saturation solubility of hydrogen in the organic phase, kmol/m<sup>3</sup>

$(C_{B,0})_0$  = initial concentration of aniline in organic phase, kmol/m<sup>3</sup>

$C_{i,O}$  = concentration of *i*-th species in organic phase, kmol/m<sup>3</sup>

$C_{i,W}$  = concentration of *i*-th species in aqueous phase, kmol/m<sup>3</sup>

$D$  = reactor diameter, m

$d_p$  = particle diameter, m

$D_M$  = molecular diffusivity, m<sup>2</sup>/s

$D_e$  = effective diffusivity, m<sup>2</sup>/s

$E_i$  = activation energy of *i*-th species, kJ/mol



$\Delta H$  = enthalpy of adsorption, kJ/mol

$k_1$ - $k_2$  = rate constants for the hydrogenation steps,  $(\text{kg/m}^3)^{-1} (\text{kmol/m}^3)^{-1} \text{s}^{-1}$

$K_H$  = adsorption equilibrium constant for hydrogen,  $(\text{kmol/m}^3)^{-1}$

$K_B$  &  $K_C$  = adsorption equilibrium constants for aniline and aminocyclohexene respectively,  $(\text{kmol/m}^3)^{-1}$

$k_{la}$  = gas-liquid mass-transfer coefficient,  $\text{s}^{-1}$

$k_s$  = liquid-solid mass-transfer coefficient,  $\text{m s}^{-1}$

$N$  = speed of agitation, Hz

$R_A$  = initial rate of hydrogenation,  $(\text{kmol/m}^3) \text{s}^{-1}$

$R_1$ - $R_2$  = individual rates of reaction for the four steps,  $(\text{kmol/m}^3) \text{s}^{-1}$

$R_{H_2}$  = overall rate of hydrogenation,  $(\text{kmol/m}^3) \text{s}^{-1}$

$R$  = universal gas constant, kJ/kmol/K

$\Delta S$  = entropy of adsorption, J/(mol K)

$u_g$  = gas velocity, m/s

$V_L$  = liquid volume,  $\text{m}^3$

$w$  = catalyst weight with respect to aqueous phase hold up,  $\text{kg/m}^3$

$Y_{i,exp}$  = experimental concentration of i-th species

$Y_{i,mod}$  = predicted concentration of i-th species

#### *Greek Letters*

$\alpha_i$  = distribution coefficient of i-th species

$\alpha_{gl}$  = parameter defined by eq 1-1

$\alpha_{ll,x}$  = parameter defined by eq 1-2

$\phi_{exp}$  = parameter defined by eq. 1-11

$\phi_{min}$  = parameter defined by eq. 7

$\mu_l$  = viscosity of the liquid, P

$\rho_l$  = density of liquid,  $\text{kg/m}^3$

$\varepsilon$  = aqueous phase hold up

$(1-\varepsilon)$  = organic phase hold up

$\tau$  = tortuosity

$\rho_p$  = particle density,  $\text{kg/m}^3$

$\sigma$  = interfacial tension, dynes/cm

$\rho_o$  = density of the continuous phase,  $\text{g/cm}^3$

## Literature Cited:

1. Ramachandran, P. A.; Chaudhari, R. V. *Three Phase Catalytic Reactors*. Gordon and Breach, New York, USA, **1983**.
2. Mills, P. L.; Chaudhari, R. V. Multiphase catalytic reactor engineering and design for pharmaceuticals and fine chemicals. *Catalysis Today*, **1997**, *37*, 367.
3. Drinkard W. C. Selective hydrogenation of aromatic compounds to cycloolefinic compounds, *GB patent 1381048 A* to Dupont de Nemours, **1972**.
4. Doebert, F.; Gaube, J. Partial hydrogenation of benzene to cyclohexene in a continuously operated slurry reactor. *Catalysis Letters*, **1995**, *31*(4), 431.
5. (a) Mitsui, O.; Fukuoka, Y. Process for producing a cycloolefin. *US Patent 4678861* to Asahi Chemical Ind., **1987**. (b) Nagahara, H.; Konishi, M. Process for producing cycloolefins. *US Patent 4734536* to Asahi Chemical Ind., **1988**.
6. Yamada, H., Urano, H.; Goto, S. Selective hydrogenation of unsaturated aldehydes in gas-liquid-liquid-solid four phases. *Chem. Eng. Sci.*, **1999**, *54*, 5231.
7. Rode, C. V.; Vaidya, M. J.; Jaganathan, R.; Chaudhari, R. V. Hydrogenation of nitrobenzene to *p*-aminophenol in a four-phase reactor: reaction kinetics and mass transfer effects. *Chem. Eng. Sci.*, **2001**, *56*, 1299.
8. (a) Tindal, B. J. R. Fuel additive. *GB patent 2156848 A1*, 1985. (b) Martin, V. T. H.; Schenz, L. F.; Ledwig, D. Anti-corrosive plastic film and process and anti-corrosive agent for the production thereof. *DE patent 3417149*, **1985**. (c) Fakhriev, A. M.; Mazgarov, A. M.; Vil'danov, A. F.; Kashevarov, L. A. Method for removing elemental sulfur. *SU patent 948876 A1*, **1982**.
9. Hayes, K. S. Industrial processes for manufacturing amines. *Applied Catalysis A: General*, **2001**, *221*, 187.
10. Darsow, G.; Niemeier, W.; Petruck, G. Process for the preparation of a mixture of cyclohexyl amine and dicyclohexyl amine. *US Patent 5728883 A1*, **1997**.
11. Mink, G.; Horvath, L. Hydrogenation of aniline to cyclohexylamine on NaOH-promoted or lanthana supported nickel., *React. Kinet. Catal. Lett.*, **1998**, *65*(1), 59.
12. Langer, R.; Petruck, G. Hydrogenation of aromatic amines to cycloaliphatic amines and catalyst therefor. *EP patent 965579 A2*, 1999.
13. Pitara, E. L.; N'Zemba, B.; Barbier, J.; Barbot, F.; Miginiac. Catalytic hydrogenation of aniline in aqueous media. *J. Mol. Catal. A: Chemical*, **1996**, *106*, 235.
14. Ualikhanova, A.; Mailyubaev, B. T.; Temirbulatova, A. E.; Sokol'skii, D. V. Reaction of aniline in the presence of hydrogen on transition metals. *Izv. Akad. Nauk Kaz. SSR, Ser. Khim.*, **1989**, *4*, 24.
15. Sokol'skii, D. V.; Ualikhanova, A.; Temirbulatova, A. E. Hydrogenation of aniline under pressure on some Group VIII metals. *Zh. Org. Khim.*, **1986**, *18*(10), 2078.
16. Struijk, J.; d'Agremont, M.; Lucas-de Regt, W. J. M.; Scholten, J. J. F. Partial liquid phase hydrogenation of benzene to cyclohexene over ruthenium catalysts in the presence of an aqueous salt solution: I. Preparation, characterization of the catalyst and study of a number of process variables. *Appl. Catal. A*, **1992**, *86*, 263.
17. Gao, S.; Zhang, J.; Zhu, Y-F; Che, C.-M. A convenient solvothermal route to ruthenium nanoparticles. *New Journal of Chemistry*, **2000**, *24*(10), 739.
18. Sazonov, V. P.; Filippov, V. V.; Sazonov, N. V. Liquid-liquid equilibria for aniline + cyclohexane + water. *J. Chem. Eng. Data*. **2001**, *46*, 959.
19. Mathew, S. P. Catalytic hydrogenation of aromatic ketones in multiphase reactors: catalysis and reaction engineering studies. *Thesis submitted to The University of Pune, India*.
20. (a) Isao, N.; Tatsuo, K. Continuous manufacture of cyclohexylamine compounds via hydrogenation of aniline compounds. *JP 01070446*, **1989**. (b) Das, J. K.; Hanamshet, P. M.; Mhalas, J. G.; Sahasrabudhe, V. D.; Sriram, M. An improved process for the conversion of aniline to cyclohexylamine. IN 172839, 1993.
21. Greenfield H. Hydrogenation of aniline to cyclohexylamine with platinum metal catalysts. *J. Org. Chem.*, **1964**, *29*, 3082.
22. (a) Immel, O.; Darsow, G.; Waldmann, H.; Petruck, G. M. Supported noble metal catalysts and their preparation and use in manufacture of mixture of mono- and dicyclohexylamines. EP 501265, **1992**. (b) Immel, O.; Schwarz, H. H. Process and catalysts for the manufacture of cyclohexylamines and dicyclohexylamines from anilines. *EP patent 324984 A1*, **1989**.

23. (a) Sokol'skii, D. V.; Temirbulatova, A. E.; Ualikhanova, A. Hydrogenation of aniline using a ruthenium/alumina catalyst in a hydrogen atmosphere under pressure. *Izv. Akad. Nauk Kaz. SSR, Ser. Khim.*, **1982**, 2, 34. (b) Sokol'skii, D. V.; Ualikhanova, A.; Temirbulatova, A. E.; Mailyubaev, B. T. Liquid-phase hydrogenation of aniline, along with its conversion products, in the presence of ruthenium on magnesium oxide. *Zh. Org. Khim.*, **1986**, 22(8), 1693. (c) Sokol'skii, D. V.; Ualikhanova, A.; Temirbulatova, A. E. Hydrogenation of aniline in the presence of ruthenium (IV) hydroxide trichloride. *Zh. Prikl. Khim.*, **1986**, 59(7), 1643.
24. (a) Vishwanathan, V.; Narayanan, S. A direct correlation between dispersion, metal area, and vapor phase hydrogenation of aniline; a first report. *J. Chem. Soc., Chem. Commun.*, **1990**, 1, 78.
25. Pray, H. A.; Schweickert, C. E.; Minnich, B. H. Solubility of hydrogen, oxygen, nitrogen and helium in water at elevated temperatures. *Ind. Eng. Chem.*, **1952**, 44, 1146.
26. Chaudhari, R. V.; Gholap, R. V.; Emig, G.; Hofmann, H. Gas-liquid mass transfer in dead end reactors. *Can. J. Chem. Eng.*, **1987**, 65, 744.
27. Lekhal, A.; Chaudhari, R.V.; Wilhelm, A.M.; Delmas, H. Mass transfer effects on hydroformylation catalyzed by a water soluble complex. *Catalysis Today*, **1999**, 48, 265.
28. Wilke, C.R., Chang, P. Correlation of diffusion co-efficients in dilute solutions. *AIChE J.*, **1955**, 1, 264.
29. Lagisetty, J. S.; Das, P. K.; Kumar, R.; Ghandhi, K. S. Breakage of viscous and non-Newtonian drops in stirred dispersions. *Chem. Eng. Sci.*, **1986**, 41(1), 65.
30. Sano, Y., Yamaguchi, N., Adachi, T. Mass transfer coefficients for suspended particles in agitated vessels and bubble columns. *J. Chem. Eng. Jpn.*, **1974**, 1, 255.
31. Calderbank, P. H. Physical rate processes in industrial fermentation Part I. The interfacial area in gas-liquid contacting with mechanical agitation, *Trans. Inst. Chem. Eng.*, **1958**, 36, 443.
32. (a) Smeds, S.; Murzin, D.; Salmi, T. Kinetics of ethyl benzene hydrogenation on Ni/Al<sub>2</sub>O<sub>3</sub>. *Appl. Catal. A*, **1995**, 125, 271. (b) Toppinen, S.; Rantakylae, T. K.; Salmi, T.; Aittamaa, J. Kinetics of the liquid phase hydrogenation of di- and trisubstituted alkyl benzenes over a nickel catalyst. *Ind. Eng. Chem. Res.*, **1996**, 35(12), 4424.
33. Vannice, M. A.; Hyun, S. H.; Kalpakci, B.; Liauh, W. C. Entropies of adsorption in heterogeneous catalytic reactions. *J. Catal.*, **1979**, 56, 358.
34. Boudart, M. Two step catalytic reactions. *AIChE Journal*, **1972**, 18, 465.
35. Zhu, X. D.; Valerius, G.; Hofmann, H.; Haas, T.; Arntz, D. Intrinsic kinetics of 3-hydroxypropanal hydrogenation over Ni/SiO<sub>2</sub>/Al<sub>2</sub>O<sub>3</sub> catalyst. *Ind. Eng. Chem. Res.*, **1997**, 36, 2897.
36. Broderick, D. H., Gates B. C. Hydrogenolysis and hydrogenation of dibenzothiophene catalyzed by sulfided CoO-MoO<sub>3</sub>/γ-Al<sub>2</sub>O<sub>3</sub>: The reaction kinetics, *AIChE J.*, **1981**, 27, 663.
37. Chaudhari, R. V., Parande, M. G., Ramachandran, P. A., Brahme, P. H., Vadgaonkar, H. G., Jaganathan, R. Hydrogenation of butynediol to *cis*-butenediol catalyzed by Pd-Zn-CaCO<sub>3</sub>: Reaction kinetics and modeling of a batch slurry reactor, *AIChE J.*, **1985**, 31(11), 1891.

## **Chapter 4**

# **Pt and Pd Nanoparticles Immobilized on Amine-functionalized Zeolite: Catalytic Applications for Hydrogenation and Heck Reactions**

## 4.1. INTRODUCTION

Metal nanoparticles are of considerable interest to the scientific community as they exhibit unique electronic, optical, and catalytic properties, due to their quantum size effects.<sup>1</sup> These nanoparticles are presently under intensive study for applications in optoelectronic devices,<sup>2</sup> ultra sensitive chemical and biological sensors,<sup>3</sup> and as catalysts in chemical and photochemical reactions.<sup>4</sup> In particular, the high surface area-to-volume ratio of the metal nanoparticles makes them highly attractive tools for catalysis. A key challenge in the application of these materials in catalysis is the agglomeration of the nanoparticles, which can be overcome through surface functionalization/stabilization.<sup>5</sup> Application of metal nanoparticles in catalysis has predictably centered on Pt and Pd nanoparticles.<sup>6,7</sup> As far as Pt nanoparticles are concerned, a number of processes have been developed for their synthesis in an aqueous environment,<sup>6,7,8</sup> in non-polar organic solutions<sup>9</sup> and by phase transfer of aqueous nanoparticles into organic solutions.<sup>10</sup> Though, Pt/Pd nanoparticles in aqueous and organic<sup>9c</sup> media as well as soluble platinum, palladium complexes exhibit high reactivity and high selectivity<sup>11</sup> in hydrogenation and Heck reactions, they have some drawbacks, similar to that of homogeneous catalysis such as difficulties in quantitative separation (purity of the product), recovery and regeneration of the catalyst. In addition to separation problems, deactivation of the homogeneous catalysts by formation of inactive colloidal species is encountered at comparatively higher reaction temperatures.<sup>12</sup> Therefore, efficient catalyst-product separation and hence product purity, regeneration of the catalysts are the challenging issues.

Attempts have been made to overcome problems concerning thermal stability (high reaction temperature), separation and recovery of the catalyst by the use of heterogeneous catalyst systems. Heterogeneous noble metal catalysts are generally prepared by deposition of metals onto preformed supports,<sup>13</sup> resulting in limited control over the metal particle size and dispersion. Heterogeneous catalysts and in particular porous materials such as alumina, silica, and zeolites have many advantages as supports because of their high surface areas, shape/size selectivity, and easy separation from reaction mixtures. Mesoporous structures would seem to be ideal for forming a scaffold in which three-dimensional dispersions of metal nanoparticles could be supported. For these reasons, the use of metal nanoparticles deposited on such porous materials has increased recently.<sup>14</sup> Generally, these catalysts have

been prepared either by chemical vapor deposition of volatile metal compounds and their subsequent decomposition in the porous structure,<sup>15</sup> or by impregnation<sup>16</sup> and ion-exchange<sup>17</sup> methods by immersing the calcined porous materials in an aqueous solution of metal precursors<sup>14</sup> followed by reduction with hydrogen at high temperature (>573K). Although, these methods have been successfully used to introduce a higher metal content into the pores, these methods are very complex, take a long time, and particle size and shape control is poor. Furthermore, these metal particles are usually formed both inside and outside the channels of the porous support. The catalyst particles inside the pores suffer from molecular accessibility limitations for the reactants and consequently, poor activity. The use of directed self-assembly to construct heterogeneous catalysts in a ‘bottom-up’ fashion presents a promising alternative, preventing agglomeration while providing the inherent advantages of heterogeneous catalysts, such as ease of product separation and catalyst recycling.

A possible strategy to overcome these drawbacks could be based on the immobilization of the metal nanoparticles on the surface of zeolites where active sites of the nanoparticles can be easily accessible to reactants. Since, the size of the nanoparticles is extremely important for retention of high catalytic activity,<sup>18</sup> it is necessary to stabilize the nanoparticles on the surface of the zeolite during the reactions. It is fairly well accepted that amine groups bind strongly to platinum and palladium nanoparticles,<sup>9c,19</sup> and therefore, attempts have been made here to immobilize aqueous platinum and palladium nanoparticles on the surface of micron-sized NaY zeolite particles functionalized with amine groups and thereafter use the platinum/palladium-nano-decorated zeolite particles in different important reactions. In this context, easily available silica gel can also be an alternative support to zeolites for immobilization of metal nanoparticles. However, in a recent work Mukhopadhyay et al.<sup>20</sup> have shown that anchored Pd complex on APTS modified silica gave considerable amount of Pd metal leaching (~ 15%) during hydrocarboxylation of aryl olefins and alcohols. This is the reason why silica is not considered as a support in the present study.

Catalyst-mediated hydrogenation reactions represent a high percentage of industrially important processes. In such hydrogenation reactions, supported platinum and palladium metals are the most commonly used catalysts. The Heck reaction (Pd-catalyzed

carbon-carbon bond formation between aryl halides and olefins) is one of the most versatile tools in modern synthetic chemistry and has great potential for future industrial applications.<sup>21</sup> Although, recent advances in homogeneous and heterogeneous Heck catalysis have attracted considerable attention, homogeneous catalysts suffer from the above mentioned problems while heterogeneous systems suffer from a lower turnover numbers (TON) and limited lifetime of the catalysts.<sup>22</sup> Hitherto used metallic palladium catalysts such as Pd/SiO<sub>2</sub>,<sup>23</sup> Pd/C,<sup>24</sup> Pd/Al<sub>2</sub>O<sub>3</sub>,<sup>25</sup> Pd/resin,<sup>25</sup> Pd(0) modified zeolites,<sup>26</sup> have yielded poor to moderate conversion and selectivity in the Heck olefination of haloarenes.

In this chapter, a simple but generic synthesis procedure for the immobilization of platinum and palladium nanoparticles on the surface of amine-functionalized zeolite and their evaluation as heterogeneous catalysts for hydrogenation and Heck reactions are reported. These new catalysts exhibit excellent turnover frequencies, selectivity and reusability for both hydrogenation and Heck reactions. The nanomaterials are characterized in details using spectroscopic techniques such as UV, FTIR, powder XRD, TGA, TEM, XPS etc.

## **4.2. EXPERIMENTAL SECTION**

### **4.2.1. Chemicals**

3-aminopropyltrimethoxysilane (APTS), chloroplatinic acid (H<sub>2</sub>PtCl<sub>6</sub>), palladium nitrate di-hydrate [Pd(NO<sub>3</sub>)<sub>2</sub>]. 2H<sub>2</sub>O, sodium borohydride (NaBH<sub>4</sub>), styrene and iodobenzene were obtained from Aldrich Chemicals and used as received. Nitrobenzene, triethylamine, cyclohexane, N, N-dimethyl acetamide (DMAC) were obtained from Merck and used without any further purification. 5% Pd/C and 5% Pt/C were purchased from Arrora Mathey, India.

### **4.2.2. Synthesis**

In the procedure for synthesis of catalysts, there are two steps:

- (i) Synthesis of Na-Y zeolite and functionalization of the zeolite surface by amine groups and,

(ii) Synthesis of platinum and palladium nanoparticles in aqueous medium and immobilization of those metal nanoparticles on the surface of the amine-functionalized Na-Y zeolite.

**(i) Synthesis and functionalization of Na-Y zeolite by APTS grafting (APTS-Y):**

The zeolite Na-Y has been synthesized according to the procedure described by Mukhopadhyay et. al.<sup>27</sup> In a typical synthesis, seed crystals were made separately by stirring the aqueous solution containing Na<sub>2</sub>SiO<sub>3</sub> (95 mmol, 28% SiO<sub>2</sub> and 8.4% Na<sub>2</sub>O), NaAlO<sub>2</sub> (9.76 mmol, 43% Al<sub>2</sub>O<sub>3</sub> and 39% Na<sub>2</sub>O) and NaOH (70 mmol) for 1 h and keeping in rest for 18 h. The seed solution followed by NaAlO<sub>2</sub> (34.2 mmol), NaOH (92.5 mmol), Al<sub>2</sub>(SO<sub>4</sub>)<sub>3</sub>.16H<sub>2</sub>O (6.02 mmol) and 35 ml of water were added into an aqueous solution of Na<sub>2</sub>SiO<sub>3</sub> (355 mmol) under constant stirring conditions for 2 h. The final molar gel composition of the zeolite Na-Y was 25.0 SiO<sub>2</sub>/4.9 Al<sub>2</sub>O<sub>3</sub>/27.0 Na<sub>2</sub>O/552 H<sub>2</sub>O. The gel was aged for 12 h at 373 K, cooled to ambient temperature, filtered and washed several times with distilled water.

For amine functionalization of Na-Y zeolite, 5.73 mmol APTS was added slowly into a slurry containing 1 g calcined Na-Y in anhydrous dichloromethane at room temperature and atmospheric pressure. The slurry was allowed to stir for 16 h. The white solid was filtered and washed repeatedly with dichloromethane. The white amine functionalized cake (APTS-Y) was dried in vacuum and used for further application.

**(ii) Synthesis of platinum and palladium nanoparticle solutions and immobilization on the surface of the amine-functionalized Na-Y zeolite:**

In a typical experiment, 100 mL of a 10<sup>-4</sup> M concentrated aqueous solution of chloroplatinic acid (H<sub>2</sub>PtCl<sub>6</sub>) was reduced by 0.01 g of sodium borohydride (NaBH<sub>4</sub>) at room temperature to yield a blackish-brown colored solution, which indicates the formation of Pt nanoparticles. Similarly, Pd nanoparticles were prepared from the aqueous solution of palladium nitrate (Pd(NO<sub>3</sub>)<sub>2</sub>, 2H<sub>2</sub>O). These colloidal platinum and palladium solutions were used for immobilization on amine-functionalized Na-Y zeolite. 0.02 g of APTS-Y was added into the Pt or Pd colloidal solutions and stirred for 12 h at room temperature. The solid was allowed to settle, filtered and washed several times with hot water to remove chloride ions. The mass loading of the zeolite particles by platinum and palladium



nanoparticles was estimated by inductively coupled plasma (ICP) measurements to be 4.5 and 3.6 wt % for platinum and palladium respectively. Nomenclature used in the text for the samples of platinum and palladium nanoparticles immobilized on amine-functionalized Na-Y zeolite are **[Pt]-APTS-Y** and **[Pd]-APTS-Y** respectively.

### 4.2.3. Instrumentation

UV-visible (UV-vis) spectroscopic studies were performed on a Shimadzu dual beam spectrometer (model UV- 1601 PC) operated at a resolution of 1 nm. UV-vis spectra of the platinum and palladium nanoparticles immobilized on APTS modified Na-Y zeolite (**[Pt]-APTS-Y** and **[Pd]-APTS-Y** respectively) was measured after sonication of the samples in water. Fourier transform infrared (FTIR) spectra of the amine functionalized zeolite (APTS-Y) and immobilized Pt metal nanoparticle (**[Pt]-APTS-Y**) were recorded in the diffuse reflectance mode on a Perkin-Elmer Spectrum One FTIR spectrometer in the range of 450-4000  $\text{cm}^{-1}$  and at a resolution of 4  $\text{cm}^{-1}$ . The APTS-grafted and the metal nanoparticle -immobilized zeolite samples were prepared for FTIR measurement on a Si (111) wafer by drop-casting from solution. TGA profiles of carefully weighed quantities of powders of APTS modified Na-Y zeolite, **[Pt]-APTS-Y** and **[Pd]-APTS-Y** were recorded on a Seiko Instruments model TG/DTA 32 instrument at a heating rate of 10°C/min. Transmission electron microscopy (TEM) measurements were performed on a JEOL model 1200EX instrument operated at an accelerating voltage of 120 kV. Samples of **APTS-Y**, **[Pt]/[Pd]-APTS-Y** before and after different reactions were made on carbon-coated grids after dispersing the powders in isopropanol for transmission electron microscopy (TEM) measurements. These films were allowed to dry for 1 min following which the extra solution was removed using a blotting paper. Powder X-ray diffraction (XRD) measurements were performed on a Philips PW 1830 instrument consisting of a rotating anode generator with a copper target (Cu  $K_{\alpha}$  radiation,  $\lambda=1.5418\text{\AA}$ ) operating at 40 kV and a current of 30 mA. The XRD patterns of the parent Na-Y zeolite, **APTS-Y** and **[Pt]/[Pd]-APTS-Y** samples were recorded in the range 5° - 85° at a scan rate of 1° per minute. X-ray Photoemission Spectroscopy (XPS) measurements of the **[Pt]-APTS-Y** and **[Pd]-APTS-Y** samples were carried out on a VG MicroTech ESCA 3000 instrument at a pressure  $<1 \times 10^{-9}$  Torr. The general scan and the C1s, Pt 4f and Pd 3d core level spectra were recorded with

un-monochromatized Mg K $\alpha$  radiation (photon energy,  $h\nu = 1253.6$  eV) at pass energy of 50 eV and electron takes off angle (angle between electron emission direction and surface plane) of 60°. The overall resolution was 1 eV for the XPS measurements. The core level spectra were background corrected using the Shirley algorithm<sup>28</sup> and the chemically distinct species were resolved using a non-linear least squares fitting procedure. The core level binding energies (BE) were aligned with the adventitious carbon binding energy of 285 eV. The metal content of the catalysts was determined using a Perkin Elmer Plasma 1000 ICP-OES spectrometer. The liquid and catalyst samples after the hydrogenation and Heck reactions were also analyzed for metal content to examine the extent of leaching of the metals during reactions.

The hydrogenation and Heck reactions were carried out in a 50 ml stirred pressure reactor supplied by Parr Instrument Company, Moline, USA. The reactor was equipped with a heating arrangement, overhead stirrer, thermo well, pressure gauge as well as a pressure transducer, gas inlet, gas outlet and sampling valve. The temperature inside the reactor could be controlled to an accuracy of  $\pm 1^\circ\text{C}$  and agitation speed could be varied between 0-2000 rpm. In a typical hydrogenation reaction, a known amount of substrate in cyclohexane and the catalyst were charged into the reactor. The reactor was flushed thrice with nitrogen and then with hydrogen. After setting the reaction temperature, the heater was put-on under slow stirring rate for uniform heat distribution. After attaining the temperature, hydrogen gas was introduced into the reactor to the desired pressure level from a hydrogen reservoir. Liquid sample was withdrawn as an initial sample and the reaction started by putting the stirrer on to a higher agitation speed (1200 rpm). The reactor was maintained at a constant pressure during reactions by supplying hydrogen from a reservoir vessel using a constant pressure regulator between the reactor and the reservoir. The reaction was stopped when the gas absorption ceased. The reactor contents were cooled and the liquid sample was taken for analysis. In recycle studies, the supernatant liquid was pipetted out and fresh reactant and solvent were added. For hydrogenation of nitrobenzene, initial and final samples were analyzed by gas chromatography (GC) technique (model number HP 6890) using a HP-5 capillary column (5% phenyl methyl siloxane). For other hydrogenation reactions HP-FFAP capillary column consisting of (poly(ethylene glycol)-TPA was used as the stationary phase. Activity of the catalysts was

represented in terms of turnover frequency (TOF) calculated from the hydrogen consumption per g-atom of the metal per hour. For the reactions studied here, it was observed that the hydrogen and substrate consumed were stoichiometrically consistent with the products formed.

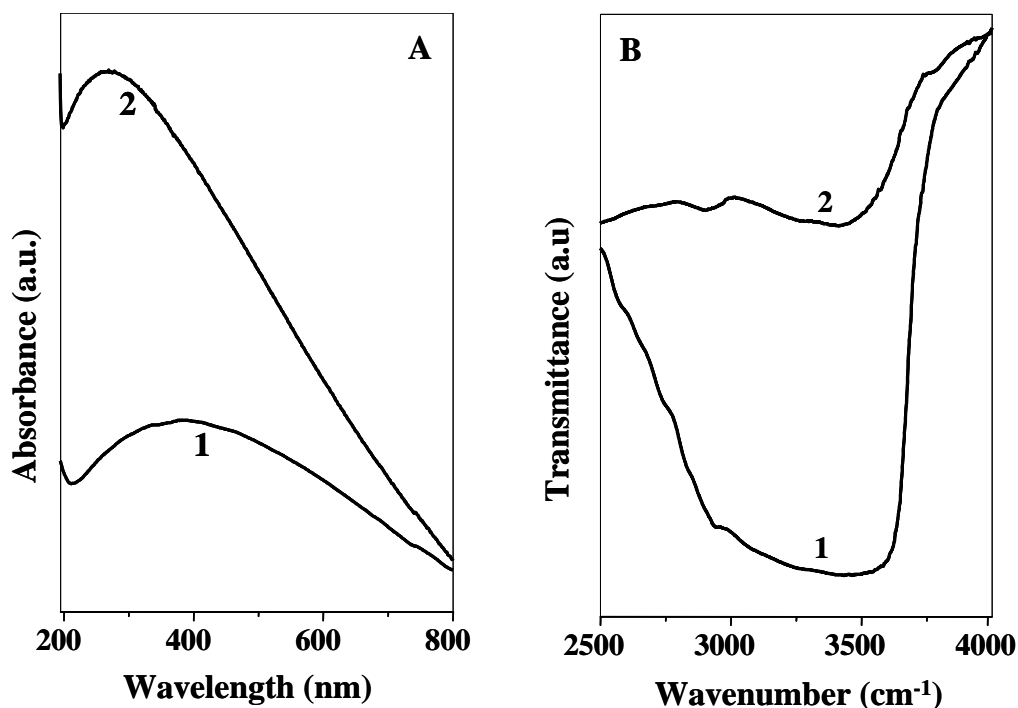
In a typical Heck arylation reaction, a known amount of arylhalide, olefin and base were dissolved in DMAC (N, N-dimethyl acetamide) and charged along with a known amount of **[Pd]-APTS-Y** catalyst to the reactor. The reactor was flushed with nitrogen for three times and the heating started under slow stirring rate. When the temperature was attained, agitation speed was increased to 1200 rpm to start the reaction. Intermediate samples were taken at different time intervals. For recycle studies, the liquid was withdrawn from the reactor bomb and a fresh charge of reactants was added. The reactions were carried out for two hrs. The catalyst was allowed to settle and then the clear liquid was withdrawn for analysis of reactants and products. A HP 6890 GC with HP-5 capillary column (5% phenyl methyl siloxane) was used to analyze the samples. Activity of the catalysts was represented in terms of turnover frequency (TOF) calculated as moles of arylhalide (limiting reactant) consumed per g-atom of palladium per hour.

## **4.3. RESULTS AND DISCUSSION**

### **4.3.1. Characterization**

With a goal to examine the catalytic performance of Pt and Pd nanocatalysts for hydrogenation and Heck reactions (well-known catalysts for hydrogenation and Heck reactions), and to demonstrate their advantages over supported metal catalysts with respect to activity and reusability, the synthesis, characterization and performance of Pt and Pd nanocatalysts (**[Pt]-APTS-Y** and **[Pd]-APTS-Y**) are presented in this part. Amine groups bind very strongly to platinum and palladium nanoparticles and consequently, we have attempted to entrap aqueous platinum and palladium nanoparticles on the surface of micron-sized Na-Y zeolite particles functionalized with amine groups to prepare **[Pt]-APTS-Y** and **[Pd]-APTS-Y** catalysts.

Figure 4.1A shows UV-vis spectra recorded for the samples [Pt]-APTS-Y (curve 1) and [Pd]-APTS-Y (curve 2), respectively after dispersion in water. The broad absorption bands from the samples [Pt]-APTS-Y and [Pd]-APTS-Y can be clearly seen at ca. 400 nm (curve 1) and 258 nm (curve 2) respectively, which arise due to excitation of surface plasmon vibrations in platinum<sup>29</sup> and palladium<sup>30</sup> nanoparticles respectively. This clearly indicates the formation of nanosized platinum and palladium particles on the amine-functionalized zeolite.

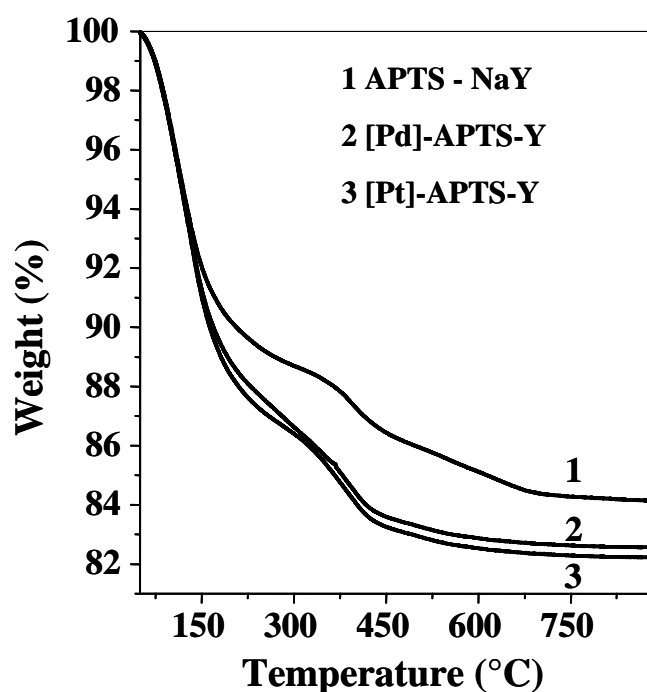


**Figure 4.1.** (A) UV-vis spectra recorded for the samples [Pt]-APTS-Y (curve 1) and [Pd]-APTS-Y (curve 2) after dispersion in water; (B) FTIR spectra recorded from drop-coated films of amine-functionalized zeolite (curve 1) and platinum-nanoparticle-bound zeolite (sample [Pt]-APTS-Y) material (curve 2) on Si(111) substrates.

Figure 4.1B shows the FTIR spectra recorded from the drop-coated films of the amine-functionalized zeolite (curve 1) and the platinum nano-zeolite composite (sample [Pt]-APTS-Y) (curve 2) on Si(111) substrates in the range of 2500-4000  $\text{cm}^{-1}$ . The FTIR spectrum of the amine-functionalized zeolite film (curve 1) shows an asymmetric, broad band centered at around 3484  $\text{cm}^{-1}$ . This broad resonance arises from excitation of N-H

stretch vibrations of the amine groups (usually centered at ca.  $3350\text{ cm}^{-1}$ ) and O-H stretch vibrations from silanol groups in the zeolite material ( $3400\text{-}3600\text{ cm}^{-1}$  region). In the film of [Pt]-APTS-Y sample (curve 2), this band becomes narrower with an apparent loss in intensity of the  $3350\text{ cm}^{-1}$  N-H stretch component. This result indicates binding of the platinum nanoparticles to the zeolite particles through the amine groups.

There have been very few reports in the literature on capping palladium and platinum nanoparticles with amine functionalized molecules and therefore, it is important to study the strength and nature of the interaction between the amine and the palladium/platinum nanoparticle surface. Figure 4.2 shows a plot of the TGA data recorded from a carefully weighed quantity of the amine-functionalized Na-Y zeolite powder (curve 1), after immobilization of palladium and platinum nanoparticles on the amine-functionalized zeolite (curves 2 and 3 for [Pd]-APTS-Y and [Pt]-APTS-Y samples respectively).

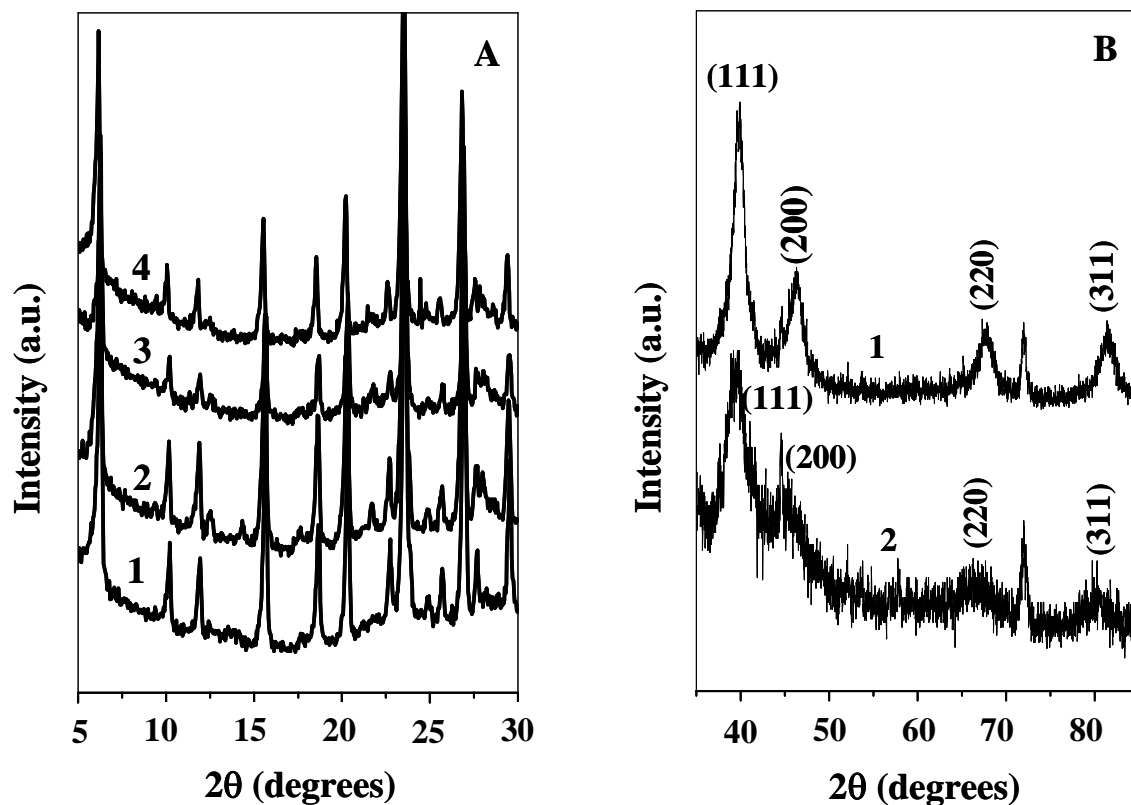


**Figure 4.2.** TGA data recorded from a carefully weighed quantity of the APTS functionalized Na-Y zeolite powder (curve 1), after immobilization of palladium and platinum nanoparticles on the amine-functionalized zeolite (curves 2 and 3 for [Pd]-APTS-Y and [Pt]-APTS-Y samples respectively).

Two monotonic weight losses of 7% and 8% are observed in the temperature interval of 50-142°C and 145-725°C respectively for APTS modified zeolite. The weight loss in the temperature interval of 50-142°C is attributed to desorption of water molecules present in the amine functionalized Na-Y zeolite powder, while the weight loss in the temperature interval 145-725°C is due to desorption of surface-bound APTS molecules from the surface of the Na-Y zeolite (curve 1). Comparing the curves 2 and 3 with the curve 1 it is observed that the nature of the curves 2 and 3 are similar with the curve 1, however the percentage (%) of weight losses are more in case of **[Pd]-APTS-Y** and **[Pt]-APTS-Y** samples (curves 2 and 3 respectively) compared to amine functionalized zeolite (curve 1). In curves 2 and 3, the weight losses are 7% upto 142°C due to desorption of water molecules present in the zeolites whereas in the temperature interval of 145-725°C the weight losses are ca. 10% and 10.5% for **[Pd]-APTS-Y** and **[Pt]-APTS-Y** respectively. In the temperature interval of 145-725°C the 2% and 2.5% higher weight losses for **[Pd]-APTS-Y** and **[Pt]-APTS-Y** samples respectively were observed compared to only APTS modified zeolite. When desorption of surface bound APTS molecules occurs from the surface of Na-Y zeolites, the palladium and platinum molecules are also desorbed with the APTS molecules and a higher percentage of weight loss is attributed to desorption of palladium and platinum nanoparticles bound on the Na-Y zeolite surface through binding with the amine group of the APTS molecules. From the TGA data, it is clearly seen that strength of the interaction between amine group of the APTS molecule and palladium and platinum molecules are strong enough, at least up to 145°C (desorption of surface bound APTS molecules starts at ca. 145°C). Therefore **[Pd]-APTS-Y** and **[Pt]-APTS-Y** catalysts are stable in our experimental conditions (maximum 120°C). From the above discussion it can be concluded the platinum and palladium nanoparticles are bound on the zeolite through binding with the amine group of the APTS molecules only.

Figure 4.3A shows the XRD patterns recorded in the  $2\theta$  range 5°-30° from the Na-Y zeolite before amine functionalization (curve 1), after amine-functionalization of the Na-Y zeolite powder (curve 2), after immobilization of platinum and palladium nanoparticles on the amine-functionalized zeolite (curves 3 and 4 for **[Pt]-APTS-Y** and **[Pd]-APTS-Y** samples respectively). After amine functionalization and binding of platinum and

palladium nanoparticles to the underlying zeolite template, there are no significant changes in the peak positions and peak width of the Bragg reflections arising from the zeolite. This indicates that if amorphisation occurs during the modification of the surface of Na-Y zeolite with APTS molecules and immobilization of Pt and Pd nanoparticles, the percentage of amorphisation is extremely small. Kelate et al.<sup>31</sup> have reported that encapsulation of hetero polyanions in channels of Si-MCM41 lead to a loss in crystallinity of the mesoporous template. The XRD results in Figure 4.3A thus show that the platinum and palladium nanoparticles are bound to the surface of the zeolite particles and are not trapped within the pores of the zeolite.

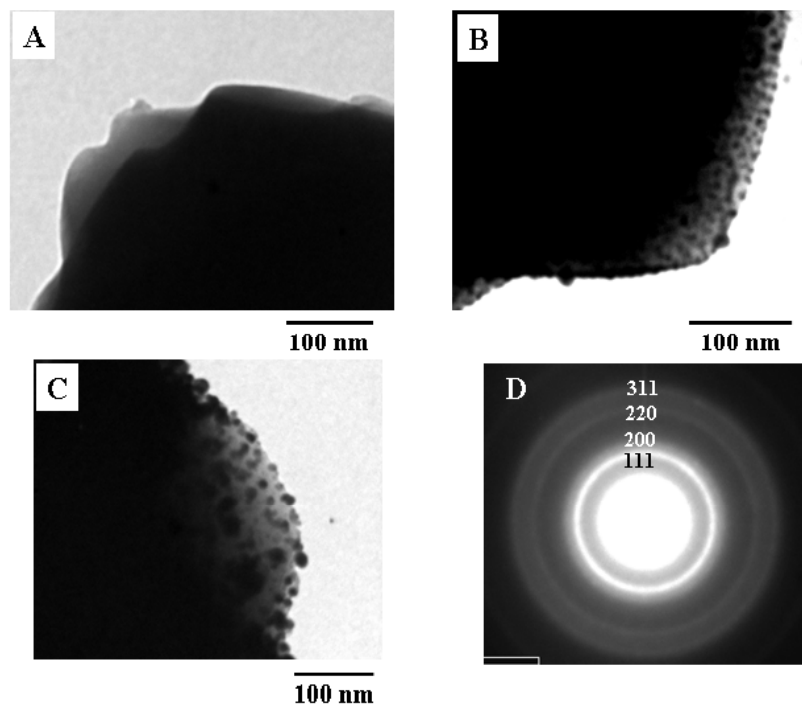


**Figure 4.3.** (A) XRD patterns recorded from the samples of Na-Y zeolite (curve 1), amine-functionalized Na-Y zeolite (curve 2), [Pt]-APTS-Y (curve 3) and [Pd]-APTS-Y (curve 4) in the  $2\theta$  range  $5^\circ$ - $30^\circ$ ; (B) XRD patterns recorded from the samples [Pd]-APTS-Y (curve 1) and [Pt]-APTS-Y (curve 2) in the  $2\theta$  range  $35^\circ$ - $85^\circ$ . The Bragg reflections for both samples are indexed.

Figure 4.3B shows the XRD patterns recorded in the  $2\theta$  range  $35^\circ$ - $85^\circ$  from the samples **[Pd]-APTS-Y** (curve 1) and **[Pt]-APTS-Y** (curve 2). The positions of the Bragg reflections (indexed in the curves 1 and 2 Figure 4.3B) correspond very well with those reported in the literature for face centered cubic (fcc) Pt<sup>32</sup> and Pd.<sup>33</sup> The broadening of the Bragg reflections from platinum and palladium bound to the amine-functionalized Na-Y zeolite template (curves 1 and 2) clearly indicates that the particles are nanocrystalline. The nano-size of the immobilized Pt and Pd is corroborated by TEM measurements presented below.

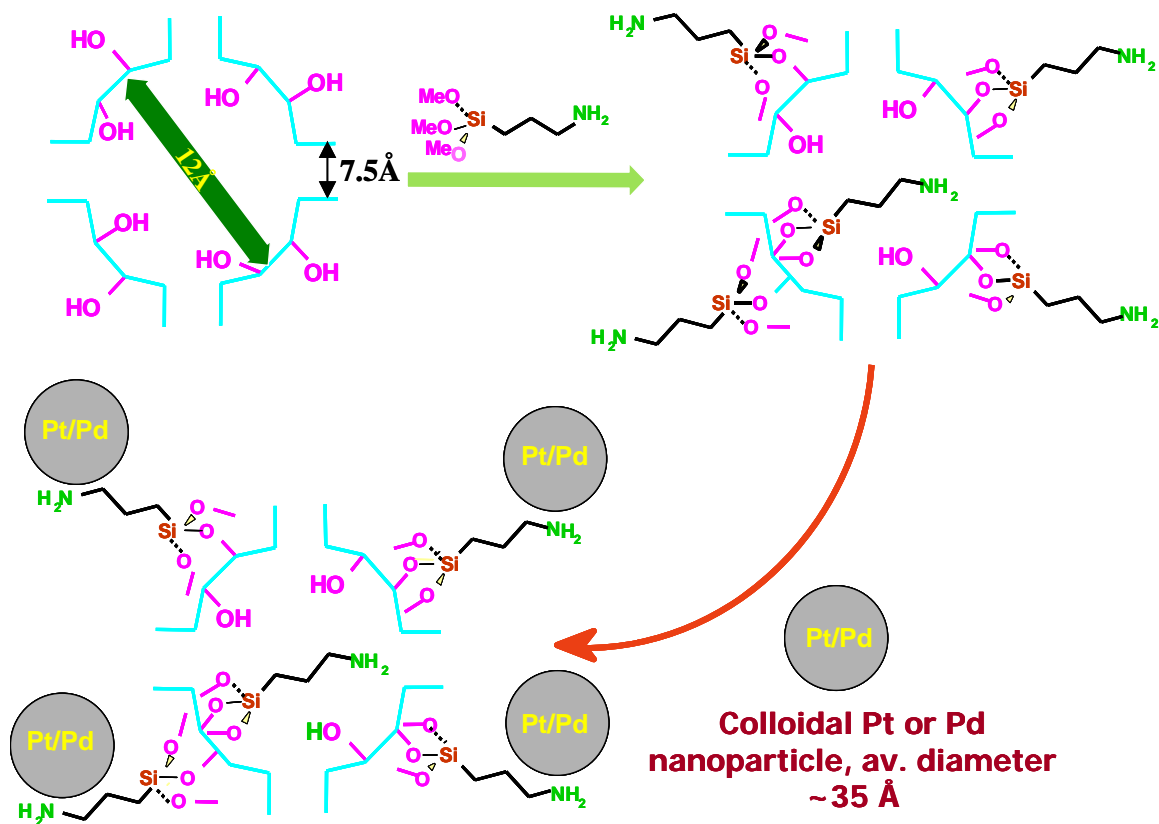
To examine the immobilization of platinum and palladium nanoparticles on the amine-functionalized Na-Y zeolite, TEM measurements of the samples were carried out at different stages. Figure 4.4A and B show representative TEM micrographs of the as-prepared amine-functionalized zeolite particles (A), after immobilization of platinum nanoparticles on the amine-functionalized Na-Y zeolite (sample **[Pt]-APTS-Y**) (B). In Figure 4.4A, it is clearly seen that the surface of the amine-functionalized Na-Y zeolite is clean and smooth, whereas after immobilization of platinum nanoparticles on the zeolite the surface is covered by the platinum nanoparticles (4.4B). In the Figure 4.4B, platinum nanoparticles (dark spots) decorating the surface of the zeolite particles and a dense population of platinum nanoparticles on the surface can be clearly seen which indicates that the platinum nanoparticles are bound to the zeolites at fairly high concentration. Figure 4.4D shows the selected area electron diffraction (SAED) pattern recorded from the platinum nanoparticles shown in Figure 4.4B. The diffraction rings have been indexed in the figure and are clearly due to a face centered cubic (fcc) platinum unit cell structure.





**Figure 4.4.** (A) - (C) Representative TEM images of amine-functionalized zeolite, [Pt]-APTS-Y before reaction and [Pt]-APTS-Y after reaction respectively on a carbon-coated TEM grid (see text for details). (D) Selected area electron diffraction (SAED) pattern recorded from the platinum nanoparticles shown in B.

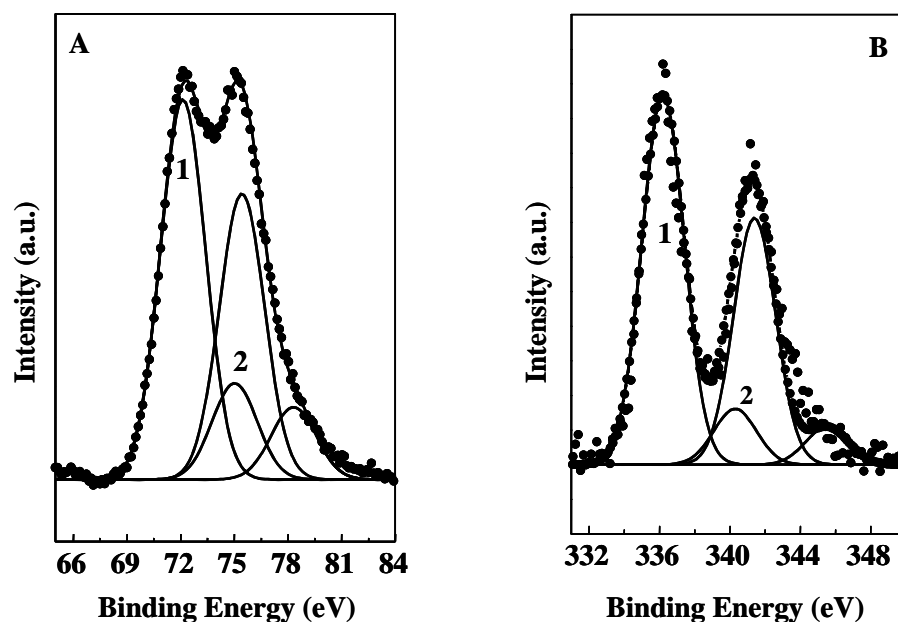
Though FTIR, XRD, TGA and TEM measurements proved that the metal nanoparticles are selectively on the outer surface of the zeolite, a semi-theoretical explanation can also be given to prove that the metal nanoparticles are immobilized only on the outer surface of the zeolite Y. Zeolite Y has a large supercage of 12 Å connected to four channels of 7.4 Å each. If we assume that APTS molecule can bind to the silanol groups inside the channels, the tethered moiety ((-O)<sub>3</sub>SiCH<sub>2</sub>CH<sub>2</sub>CH<sub>2</sub>NH<sub>2</sub>) will have a length of 6.065 Å (using Mercury 1.1.2 software, Cambridge Crystallographic Data Center). But the bare platinum and palladium nanoparticles possess an average particle size in the range of 4-5 nm, which are far bigger than the channels of the zeolite Y. Therefore, though the amine functionalities of APTS molecules are present inside the supercages, those are not accessible to the bare Pt and Pd nanoparticles. From this discussion, it is understood that the Pt and Pd nanoparticles are bound to the surface of the zeolite and not inside the cages.



**Scheme 4.1.** Schematic representation of selective outer-cage synthesis of [Pt]/[Pd]-APTS-Y nanocomposites

A chemical analysis of the [Pt]-APTS-Y and [Pd]-APTS-Y samples were also performed using XPS and the metal core level spectra obtained for these samples (Pt 4f and Pd 3d) are shown in Figures 4.5A and B respectively. The general scan spectra of the above samples showed the presence of C 1s, N 1s, Cl 2p, Pt 4f and Pd 3d core levels with no evidence of impurities. In Figure 4.5A, the Pt 4f spectrum could be resolved into two spin-orbit pairs (spin-orbit splitting  $\sim 3.36$  eV) with a  $4f_{7/2}$  binding energies (BEs) of 72 eV (curve 1 in Figure 4.5A) and 75.3 eV (curve 2 in Figure 4.5A) respectively.<sup>34</sup> The low BE component at 72 eV (curve 1) corresponds to metallic Pt while the high BE component at 75.3 eV (curve 2) is assigned to unreduced  $\text{PtCl}_6^{2-}$  ions, possibly bound to the surface of the Pt metal core. In addition to the additional components of Pt 4f spectrum, a strong Cl 2p signal was also observed in the samples supporting the contention that unreduced  $\text{PtCl}_6^{2-}$  ions are present on the surface of the platinum nanoparticles (data not shown). In a similar

study, capping of gold nanoparticles by unreduced  $\text{AuCl}_4^-$  ions has also been observed previously.<sup>35</sup> In Figure 4.5B, the Pd 3d level shows the presence of two chemically distinct spin-orbit pairs centered at 336.1 (curve 1) and 340.3 eV (curve 2) BE. As in the case of Pd nanoparticles, the low BE component corresponds to fully reduced Pd nanoparticles while the high BE peak is due to unreduced  $\text{Pd}^{2+}$  ions on the surface of the metal core.<sup>36</sup> Therefore, Pt(IV) and Pd(II) species are present in minor quantities along with the Pt(0) and Pd(0) species in [Pt]-APTS-Y and [Pd]-APTS-Y nanocomposites respectively.



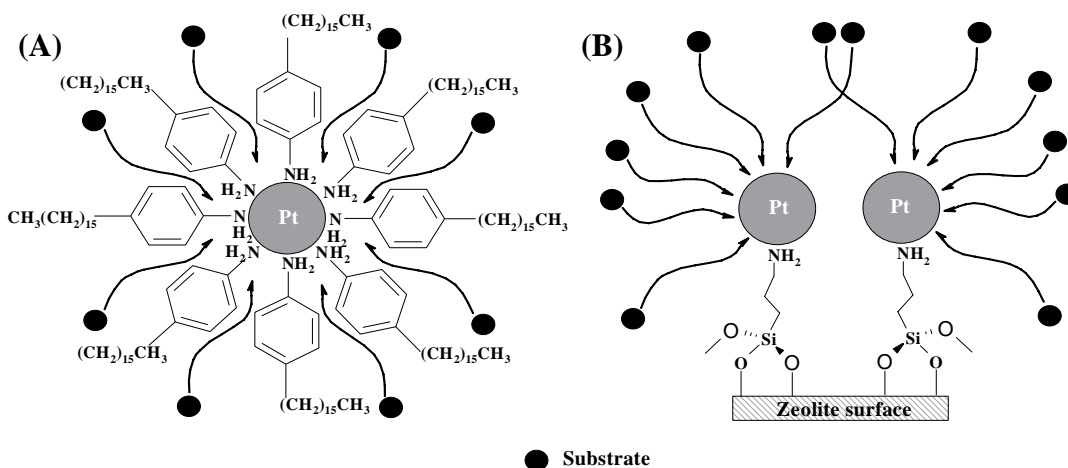
**Figure 4.5.** (A) and (B) - Pt 4f and Pd 3d core level spectra recorded for [Pt]-APTS-Y and [Pd]-APTS-Y samples respectively.

### 4.3.2. Catalysis

One important direction of heterogeneous catalysis research is to develop catalyst systems with high activity, selectivity and stability. To accomplish this, it is necessary to design and identify the atomic level catalyst ingredients that control the performance. The hydrogenation of various hydrocarbon compounds has been employed from time to time as a convenient test reaction for evaluating the catalytic properties of supported Pt or Pd metals. Platinum and palladium are superior catalysts for a variety of hydrogenation reactions under suitable reaction conditions (reactants composition, pressure, and

temperature). Therefore, catalytic activity of the [Pt]-APTS-Y and [Pd]-APTS-Y nanocomposites was tested for hydrogenation reactions. Catalytic activity of the platinum and palladium nanoparticles after immobilization on the surface of amine-functionalized zeolite for a hydrogenation reaction involving the conversion of styrene to ethylbenzene, phenylacetylene to ethylbenzene and nitrobenzene to aniline was studied in a 50 ml reactor (Hastelloy-C, supplied by Parr Instrument Company, USA).

Table 4.1 shows the activity of the catalyst [Pt]-APTS-Y for hydrogenation of different substrates. The hydrogenation of styrene to ethylbenzene showed a remarkable jump in activity expressed as TOF (mol/g-atom/hr) in comparison to our previous results obtained under the same reaction conditions with 4-hexadecylaniline (HDA) stabilized platinum nanoparticles (TOF: 655 h<sup>-1</sup>).<sup>9c</sup> In HDA capped platinum nanoparticle synthesis, free movement of HDA molecules allowed the HDA molecules to bind with the platinum nanoparticles from all the sites and hence suffered from less accessibility for the reactant molecules (Scheme 4.2A). However, in the present synthesis procedure, in the first step the stabilizer APTS molecules are bound with the solid zeolite surface, which restricts their free movements. In the second step of synthesis, when platinum nanoparticles are immobilized on the surface of the zeolite, the Pt nanoparticles are stabilized by APTS molecules binding with the amine group through one site only and therefore other sites will be accessible for reactant molecules (Scheme 4.2B).



**Scheme 4.2.** Schematic diagram of (A) HDA capped colloidal Pt nanoparticle and (B) [Pt]-APTS-Y nanocomposite catalysts. Active catalyst surface is more accessible with [Pt]-APTS-Y for the substrate molecules for catalytic hydrogenation reactions.

**Table 4.1.** Hydrogenation reactions using immobilized Pt nanoparticles on APTS modified NaY zeolite

Substrate	Conditions	Time	Conv., %		Sel., %		TOF, h <sup>-1</sup>	
			[Pt]- APTS- Y	5% Pt/C	[Pt]- APTS- Y	5% Pt/C	[Pt]- APTS- Y	5% Pt/C
Styrene (1.7525 g)	353K, 200 psig	30 min	100	95	ETB: 99.2	ETB: 99.5	19480	17141
Phenylacetylene (2.36 g)	353K, 200 psig	90 min	100	100	ETB: 66.3 Styrene: 32.9	ETB: 57.89 Styrene: 41.88	14394	12710
Nitrobenzene (2.37 g)	383K, 500 psig	40 min	100	94	Aniline: 100	Aniline: 100	52613	44510

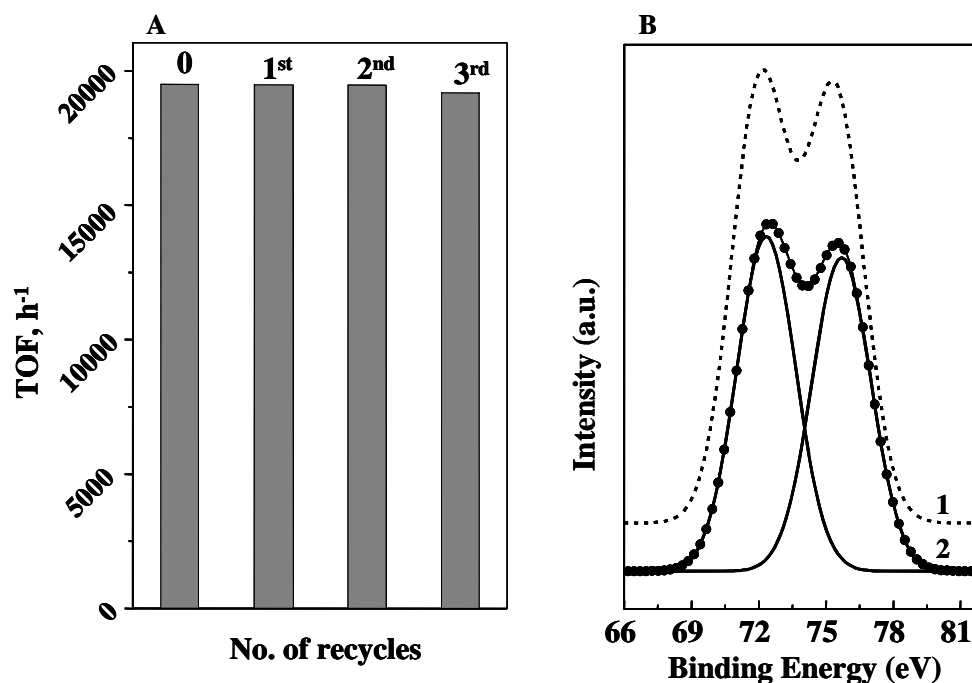
Catalyst taken: 0.0075 g, metal loading for [Pt]-APTS-Y: 4.5%

From Table 4.1, it is seen that the [Pt]-APTS-Y catalyst is very active for hydrogenation reactions. An important point concerning the use of heterogeneous catalysts is their lifetime/reusability and therefore we checked the recyclability of the [Pt]-APTS-Y catalyst in hydrogenation reactions. The catalyst [Pt]-APTS-Y was efficiently recycled 3 times for the hydrogenation of styrene to ethylbenzene, which has been shown by the bar, diagram in Figure 4.6 A, which showed that there is no change in the activity even after three recycles. This indicates that the nano structure and dispersivity of the platinum nanoparticles has not changed after the recycle reactions. This is supported by the TEM image of the catalyst after recovering from the reaction mixture of the third recycle (Figure 4.4C). Hardly any differences were recognized in the size of the platinum nanoparticles on the surface of the zeolite for the samples before and after the reaction (Figure 4.4B and C respectively). This indicates that no significant aggregation or sintering of platinum nanoparticles on zeolite occurred during the hydrogenation reactions. The catalytic activity depends on the size of the nanoparticles and in our study the size of the platinum nanoparticles on the zeolite surface did not change as also the activity of the catalyst for

hydrogenation reactions. Generally during recycle of the hydrogenation catalysts consisting of supported metal nanoparticles, increase in size of the nanoparticles due to agglomeration leads to deactivation of the catalyst. However, in this study, due to strong binding of the platinum nanoparticles with the amine groups on the surface of the zeolite, there is no aggregation of the platinum nanoparticles on the zeolite surface observed during the reaction, which is consistent with the efficient reusability of the catalyst and the TEM picture after the reaction.

From the XPS data in the Figure 4.5A it was clearly seen that before the reaction, unreduced Pt (IV) ions were present in the **[Pt]-APTS-Y** sample. Therefore, a question arises as to which oxidation state of the platinum nanoparticles in **[Pt]-APTS-Y** is responsible for the hydrogenation reactions. Therefore, a chemical analysis of the **[Pt]-APTS-Y** sample after hydrogenation reactions was also performed using XPS and the metal core level spectra obtained for this sample (Pt 4f) are shown in Figure 4.6B. The general scan spectra of the above samples showed the presence of C 1s, N 1s and Pt 4f core levels with no evidence of impurities. Figure 4.6B shows the Pt 4f spectra recorded for **[Pt]-APTS-Y** sample after 1<sup>st</sup> recycle (curve 1) and after 3<sup>rd</sup> recycle (curve 2) of the hydrogenation reaction respectively (these spectra have been shifted vertically for clarity). The Pt 4f spectrum in all cases could be resolved into a single spin-orbit pair (spin-orbit splitting  $\sim 3.35$  eV) with a 4f<sub>7/2</sub> binding energy (BE) of 72.07 eV (Figure 4.6, curve 2), which corresponds to Pt (0).

There was no evidence for the presence of Pt (IV) oxidation state in the Pt 4f spectra after the 1<sup>st</sup> and 3<sup>rd</sup> recycles (curves 1 and 2 respectively) of the hydrogenation reactions. During the 1<sup>st</sup> recycle of the hydrogenation reaction a small amount of unreduced Pt(IV) ions, (present before the reaction) are completely converted to Pt (0) and the same catalyst was used for other cycles of the hydrogenation reaction. If Pt (IV) oxidation state (present in the **[Pt]-APTS-Y** sample before the reaction) is responsible for the hydrogenation reaction, then after the 1<sup>st</sup> recycle the activity should go down, but it did not happen (from Figure 4.6A). From these results, it may be concluded that Pt (0) state is only responsible for hydrogenation reaction and the small amount of unreduced Pt (IV) ions present in **[Pt]-APTS-Y** converts to Pt (0) during a hydrogenation reaction.



**Figure 4.6.** (A) Recycle experiments for hydrogenation of styrene to ethylbenzene using [Pt]-APTS-Y; and (B) Pt 4f core level spectra from [Pt]-APTS-Y after 1<sup>st</sup> (curve 1) and 3<sup>rd</sup> (curve 2) cycle of the hydrogenation reaction.

In Table 4.2, the results on the activity of the [Pd]-APTS-Y catalyst for hydrogenation reactions for different substrates are presented. Though the hydrogenation results are comparable for [Pt]-APTS-Y and [Pd]-APTS-Y catalysts for styrene and phenyl acetylene, the former showed higher activity (~ double) for nitrobenzene hydrogenation. In order to compare these results with commercial supported platinum and palladium catalysts, we conducted the hydrogenation reactions with commercial 5% Pt/C and 5%Pd/C catalysts (Arora Matthey) and the results were compared in terms of conversion, product distribution and TOF with [Pt]-APTS-Y (in Table 4.1) and [Pd]-APTS-Y (in Table 4.2) catalysts.

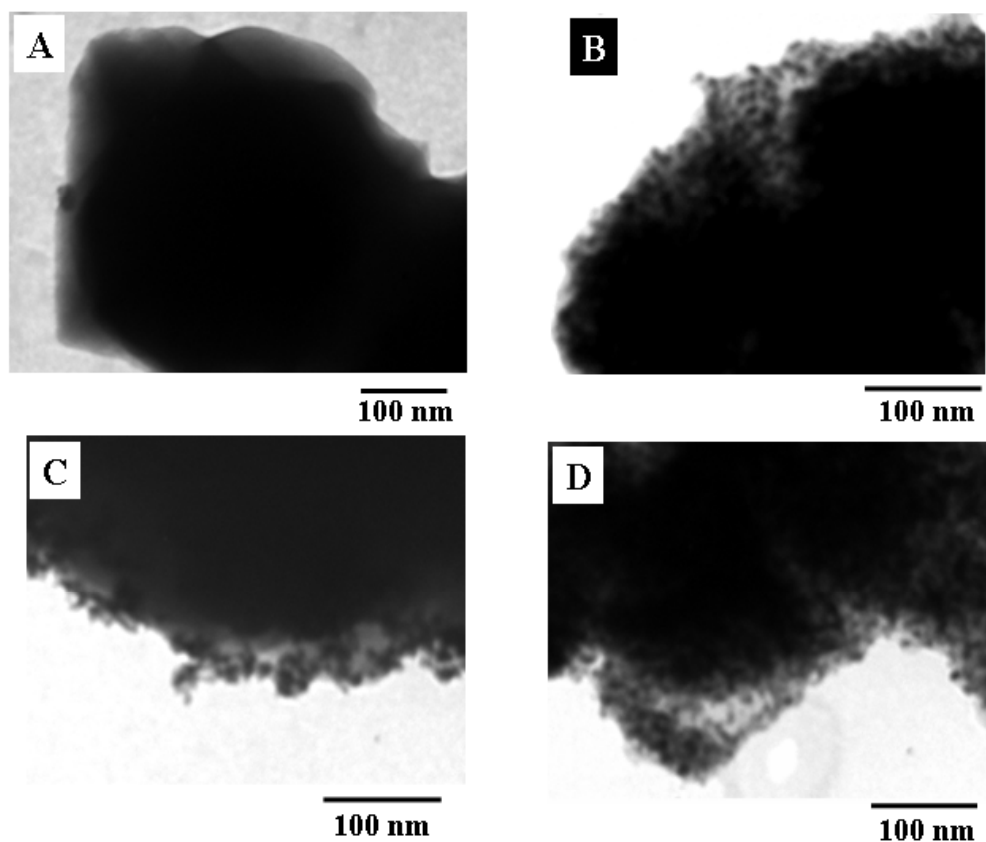
**Table 4.2.** Performance of **[Pd]-APTS-Y** catalyst for hydrogenation reactions

Substrate	Cond <sup>n</sup> .	Time	Conversion, %		Selectivity, %		TOF, h <sup>-1</sup>	
			[Pd]- APTS- Y	5% Pd/C	[Pd]- APTS-Y	5% Pd/C	[Pd]- APTS- Y	5% Pd/C
Styrene (2.087 g)	353K, 200 psig	30 min	100	100	ETB: 99.2	ETB: 99.2	15815	11386
Phenyl- acetylene (2.0440 g)	353K, 200 psig	80 min	100	100	ETB: 85.9 Styrene: 14.0	ETB: 81.2 Styrene: 18.8	10993	7728
Nitro- benzene (2.35 g)	383K, 500 psig	50 min	100	58.95	Aniline: 100	Aniline: 100	26431	11604

Catalyst: 0.0075 g, metal loading for [Pd]-APTS-Y: 3.6%(w/w)

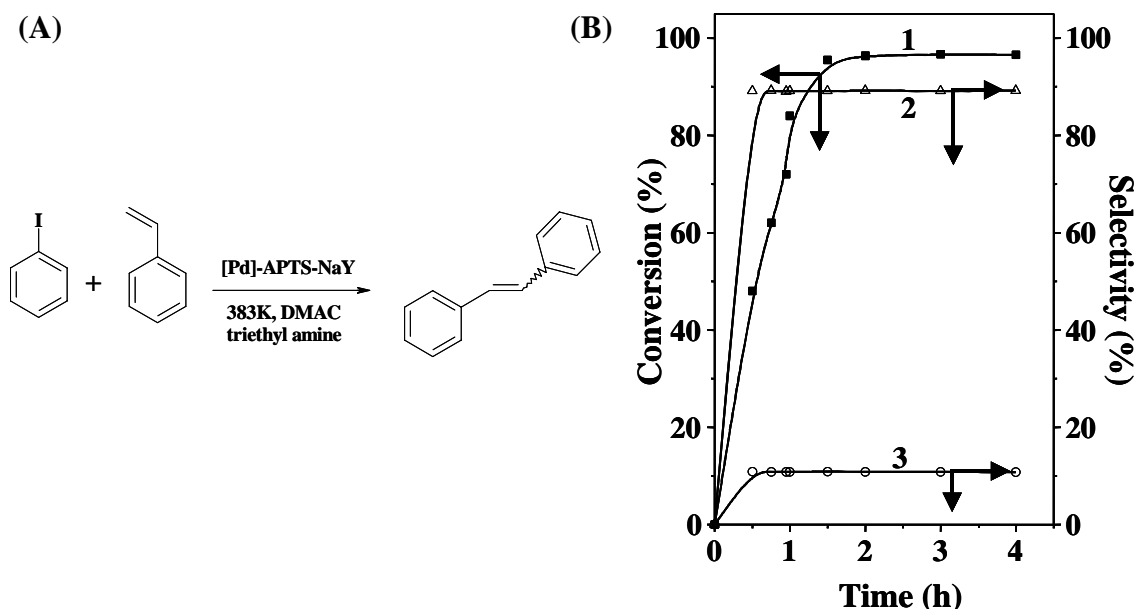
There is a remarkable difference in activity between **[Pd]-APTS-Y** and Pd/C. From Table 4.2 it is clearly seen that the **[Pd]-APTS-Y** catalyst is more active for the hydrogenation of nitrobenzene (26431 h<sup>-1</sup> and 11604 h<sup>-1</sup> respectively, Table 4.2). After the reaction, we also made TEM analysis of **[Pd]-APTS-Y** catalyst sample for examining if a change in particle size occurred during the hydrogenation reaction. Figure 4.7C shows the TEM image of **[Pd]-APTS-Y** catalyst after hydrogenation reaction of styrene to ethyl benzene. Comparing the TEM images of the sample **[Pd]-APTS-Y** before and after hydrogenation reaction (Figure 4.7 B & C respectively) it is clearly seen that there is no change in the population and the size of the palladium nanoparticles during the reaction. Furthermore, observations of TEM indicated that no substantial aggregation of palladium nanoparticles on the zeolite surface occurred during hydrogenation reactions and suggested that no appreciable sintering of the palladium nanoparticles occurs during the reaction.





**Figure 4.7.** (A) - (D) Representative TEM images of the samples of amine-functionalized zeolite, **[Pd]-APTS-Y** before reaction, **[Pd]-APTS-Y** after hydrogenation reaction and after 2<sup>nd</sup> cycle of Heck reaction respectively on a carbon-coated TEM grid.

The Heck reaction is one of the most versatile tools in modern synthetic chemistry for C-C bond formation and has great potential for future industrial applications. However, the heterogeneous palladium catalysts suffer from lower turnover numbers (TON/TOF) and reusability<sup>21</sup> due to either aggregation of the particles or leaching from the support materials<sup>37,38</sup> during the reactions. Therefore, performance of the **[Pd]-APTS-Y** nanocomposite catalyst was evaluated for the arylation of styrene with iodobenzene (Figure 4.8A). Triethylamine was used as a base to remove the hydriodic acid formed during the reaction. The products obtained were only *cis*-stilbene and *trans*-stilbene in all the cases. Figure 4.8B shows a typical conversion-selectivity profile of the reaction with time where curves 2 and 3 represent the selectivity patterns of *trans*- and *cis*-stilbene respectively.



**Figure 4.8.** (A) Reaction scheme for Heck arylation of styrene: an application of [Pd]-APTS-Y catalyst; (B) A typical conversion-time profile (1: iodobenzene; 2: *trans*-stilbene; 3: *cis*-stilbene)

The catalyst [Pd]-APTS-Y was recycled thrice in the Heck olefination of iodobenzene with styrene and after the completion of the reaction the catalyst was recovered by filtration and washed thoroughly with isopropanol and sample was made for TEM measurement. The fresh reaction showed 95.4% conversion of iodobenzene after 2 h with a TOF of 1881 h<sup>-1</sup>. After 1<sup>st</sup> and 2<sup>nd</sup> cycles of the Heck reaction, the conversion of iodobenzene obtained was 95.52% and 94.41% with TOF 1882 h<sup>-1</sup> and 1860 h<sup>-1</sup> respectively (Table 4.3).

Thus, recycled catalyst showed activities comparable to the fresh catalyst. The recycle results show that the catalyst is still active for Heck arylation of styrene even after two cycles, which indicates neither agglomeration nor leaching of the palladium nanoparticles from the supports during the reaction. ICP-OES analysis of the supernatant liquids withdrawn after each recycle reactions showed almost no metal leaching (1, 0.7 and 0.3 ppm respectively with respect to total metal loading) from the catalyst.

**Table 4.3.** Heck arylation of iodobenzene with styrene using [Pd]-APTS-Y

Catalyst	Entry	Conversion, %	Stilbene Selectivity, %		TOF, h <sup>-1</sup>
			<i>cis</i> -	<i>trans</i> -	
[Pd]-APTS-Y	Recycle-0	95.4	10.8	89.15	1881
	Recycle-1	95.52	10.8	89.1	1882
	Recycle-2	94.41	10.7	89.3	1860
[Pd]-APTS-Y	Recycle-0	96.1	10.6	89.35	1893
after keeping in	Recycle-1	94.3	11.2	88.8	1858
H <sub>2</sub> atmosphere	Recycle-2	95.1	10.8	89.2	1874
<b>[Pd]-NaY</b>					
Without APTS modification		18.1	10.7	89.2	4256

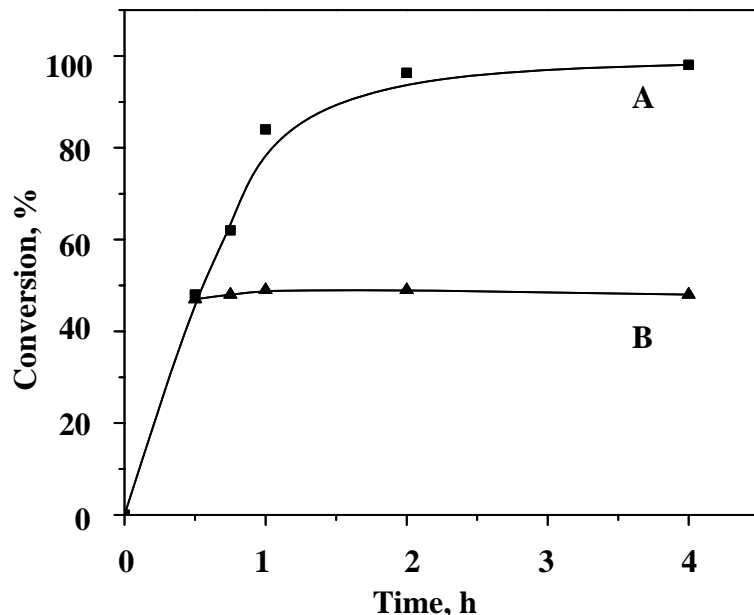
**Reaction conditions:** Iodobenzene: 10 mmol, Styrene: 15 mmol, triethylamine: 15 mmol, Solvent: DMAC, Temperature: 393 K, Catalyst: 0.0075 g (in all cases), reactions carried out under nitrogen atmosphere, Reaction time: 2 h.

Figure 4.7D shows the TEM image of [Pd]-APTS-Y sample after 2<sup>nd</sup> recycle of Heck reaction. Comparing the TEM images of the sample [Pd]-APTS-Y before and after Heck reaction (Figure 4.7 B & D respectively), it is clearly seen that there is a no change in the density and size of the palladium nanoparticles on the surface of the zeolite during the reaction. As the population of the palladium nanoparticles on the zeolite surface is not decreased after the reaction, this also indicates that there is no leaching of the palladium nanoparticles during the Heck reaction. It is known that in the Heck reaction, palladium particles get leached out from the support<sup>37</sup> and the metal leaching is a common phenomenon in heterogeneous Heck coupling reactions<sup>38</sup> leading to loss in catalyst activity. In some cases up to 79% Pd metal leaching was observed using commercial 1% Pd/Al<sub>2</sub>O<sub>3</sub> catalyst.<sup>39</sup> Several authors reported loss in activity of palladium nanoparticle catalysts for these reactions.<sup>40</sup> Zhuangyu et. al. reported Heck coupling between styrene and iodobenzene using p-C<sub>6</sub>H<sub>4</sub> phen/Pd catalyst and showed remarkable decrease in activity from 70.3 h<sup>-1</sup> to 41.4 h<sup>-1</sup> in the first recycle.<sup>41</sup> The same group reported a slight improvement in recycle efficiency from 70.3 h<sup>-1</sup> to 57.7h<sup>-1</sup> after 5<sup>th</sup> recycle.<sup>42</sup> Therefore, in

Heck reaction the reusability of the catalyst without loss in activity has been a major challenge. A recent report on Heck coupling of iodobenzene and styrene using organically modified Pd-silica catalysts has good recycleability, but the catalyst system has poor activity (highest  $129\text{h}^{-1}$ ).<sup>43</sup> However, in the present study, the synthesized catalyst **[Pd]-APTS-Y** showed excellent performance without loss in activity even after 2<sup>nd</sup> recycles of the Heck reaction with iodobenzene and styrene. The palladium nanoparticles on the surface of the zeolite are neither aggregated nor leached out from the surface of the zeolite due to strong binding with the amine group on the surface of the zeolite and for these reasons there is no loss in activity of the catalyst. From the above results it is clearly seen that our synthesized catalyst is also a good candidate for Heck reaction showing significant improvement over the previously known catalysts.

#### **4.3.2.1. Trojan Horses or Truly Heterogeneous?**

Though the **[Pd]-APTS-Y** catalyst showed very good activity as well as selectivity, stability is also a *sine qua non* for its practical utility. According to Sheldon et al.,<sup>44</sup> a heterogeneous catalyst, which simply releases its active species into solution - like Greek warriors from the Trojan horse - is likely to have limited practical utility. The authors had also mentioned that conventional recycling of a catalyst for several times without significant loss of activity is also not an adequate proof for heterogeneity, because in many heterogeneous catalyzed reactions, the supported catalyst comes out to the liquid phase during the reaction and sits back on the support surface after cooling or completion of the reaction.<sup>45</sup> As suggested in the literature, hot filtration experiment was carried out to confirm if there is Pd metal leaching or not during the reaction. The **[Pd]-APTS-Y** catalyzed Heck reaction between iodobenzene and styrene was allowed to continue till 20-50% conversion of iodobenzene and filtered in the hot condition. The liquid without the solid material was used to continue the reaction. The results are shown in Figure 4.9, which confirms that there was no leaching of the palladium nanoparticles from the supports during the reaction. This is also indirectly supported by the TEM image of the **[Pd]-APTS-Y** catalyst taken after the heck reaction as discussed in the previous paragraph (see Figure 4.7 D). If the Pd metal leaches out during the reaction, then its deposition may not be too similar to the TEM image taken before the reaction.



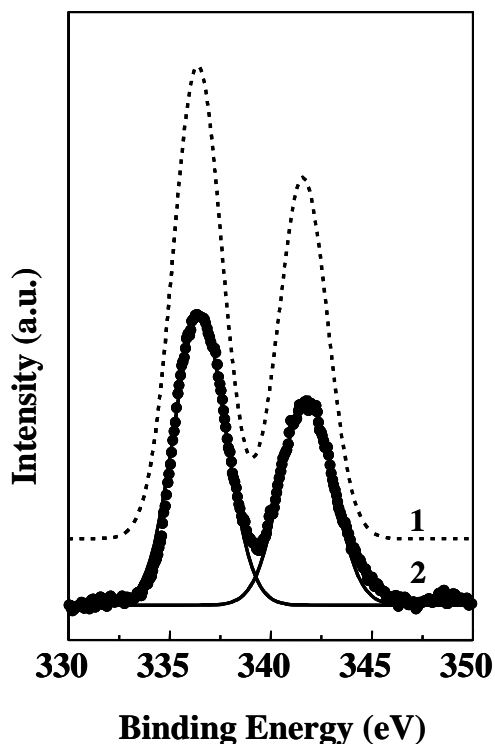
**Figure 4.9.** Hot filtration experiment to check the heterogeneity of [Pd]-APTS-Y catalyst for Heck arylation of styrene with iodobenzene. (A) [Pd]-APTS-Y catalyzed reaction; (B) reaction continued with liquid separated out from [Pd]-APTS-Y by filtration after ~50% conversion. Conditions are as given in Table 4.3.

#### 4.3.2.2. Active Pd species for Heck Reaction

A similar strategy to [Pt]-APTS-Y was used to check the active species in [Pd]-APTS-Y catalyst responsible for Heck reaction. In the XPS data shown in Figure 4.5 B, it was clearly seen that before reaction there were unreduced palladium ions ( $\text{Pd}^{2+}$ ) present in the [Pd]-APTS-Y sample. Therefore, it was doubtful that which oxidation state of the palladium nanoparticles present in [Pd]-APTS-Y sample is responsible for the Heck reaction. For this reason we kept the catalyst [Pd]-APTS-Y in presence of hydrogen atmosphere for the complete reduction of even small amount of  $\text{Pd}^{2+}$  ions to Pd (0) state. The hydrogen-pretreated catalyst was used for Heck coupling reaction. A chemical analysis of the [Pd]-APTS-Y samples after the reactions were also performed using XPS and the metal core level spectra obtained for these samples (Pd 3d) are shown in Figure 4.10, in which the spectra have been shifted vertically for clarity. Curve 1 in Figure 4.10 shows the Pd 3d core level spectrum recorded from the [Pd]-APTS-Y sample after keeping in

hydrogen atmosphere and the Pd 3d spectrum could be resolved into a single spin-orbit pair (spin-orbit splitting  $\sim 5.2$  eV) with a  $3d_{5/2}$  binding energy (BE) of 336.4 eV (Figure 8, curve 1). There was no evidence for additional components for Pd (II) oxidation state in the Pd 3d spectrum after reduction by hydrogen (curves 1) which indicates the presence of Pd (0) state only and complete reduction of  $Pd^{2+}$  ions to Pd (0). This catalyst (after complete reduction of  $Pd^{2+}$  ions to Pd (0), containing only Pd (0) state) was used for further Heck reactions.

Curve 2 in Figure 4.10 shows the Pd 3d core level spectrum recorded from the **[Pd]-APTS-Y** sample after 2<sup>nd</sup> recycle of the Heck reaction and the Pd 3d spectrum has been resolved into a single spin-orbit pair (spin-orbit splitting  $\sim 5.2$  eV) with a  $3d_{5/2}$  binding energy (BE) of 336.5 eV (Figure 4.10, curve 2). There was no evidence for additional components of Pd (II) oxidation state in the Pd 3d spectrum after reaction (curve 2), which indicates the absence of  $Pd^{2+}$  ions in the sample. If  $Pd^{2+}$  ions present in the **[Pd]-APTS-Y** catalyst were responsible for Heck reaction, after complete reduction of  $Pd^{2+}$  to Pd (0) species it should not show any catalytic activity. The conversions after 0 (fresh reaction), 1<sup>st</sup> and 2<sup>nd</sup> recycles in the Heck olefination of iodobenzene with styrene were 96.1%, 94.3% and 95.1% with TOF 1893 h<sup>-1</sup>, 1858 h<sup>-1</sup> and 1874 h<sup>-1</sup> respectively (Table 4.3). The recycle results show that the catalyst is still active and there is neither agglomeration nor leaching of the palladium nanoparticles from the catalyst during the reaction. Therefore it can be concluded that Pd (0) oxidation state in the **[Pd]-APTS-Y** sample is responsible for Heck reaction.

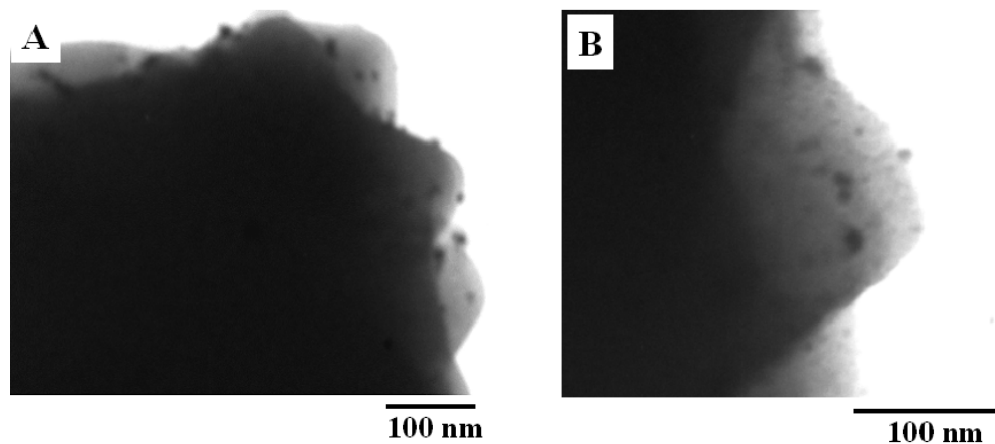


**Figure 4.10.** Pd 3d core level spectra recorded from [Pd]-APTS-Y sample after keeping in hydrogen atmosphere (curve 1) and after 2<sup>nd</sup> recycle (curve 2) of the Heck reaction. The spectrum in curve 2 has been decomposed into two components by a nonlinear least-squares procedure and the spin-orbit components are shown.

#### 4.3.2.3. Role of Surface Modification by APTS

APTS modified Na-Y zeolite was used to immobilize the palladium nanoparticles on the surface of the zeolite binding through the amine group of the APTS molecules. Are the APTS molecules really required to immobilize the Pd nanoparticles on the surface of the Na-Y zeolite? To check the role of APTS molecule, a control experiment was performed wherein Pd nanoparticles were tried to immobilize on the surface of the Na-Y zeolite without modifying the surface with APTS molecules ([Pd]-NaY). The loading of metal nanoparticles (Pd) on the surface of unmodified Na-Y zeolite is very low (0.3 %), which was measured by ICP. From the TEM images as shown in Figure 4.11, it is also visible that on the surface of the zeolite, numbers of metal nanoparticles (dark spots) are very few compared to the TEM images shown in Figure 4.7B where the Pd nanoparticles were immobilized on the APTS modified zeolite. We carried out the Heck arylation

reaction between styrene and iodobenzene with **[Pd]-NaY** (without APTS) in identical reaction conditions to compare its activity with **[Pd]-APTS-Y** catalyst and the results are shown in Table 4.3. With the **[Pd]-NaY** catalyst, conversion in the Heck reaction is very poor (18.1%) (Table 4.3). This is due to the poor loading of the metal nanoparticles on the surface of the zeolite without modifying the surface of zeolite with APTS molecules.



**Figure 4.11.** Representative TEM images of Pd nanoparticles immobilized on the surface of Na-Y zeolite without APTS modification

Thus, modification of the surface of Na-Y zeolite with APTS molecules is an important step to immobilize the Pd nanoparticles on the surface of the zeolite. Pd nanoparticles were immobilized on the surface of the zeolite through binding with the amine group of APTS molecules present on the surface of the zeolite and strong interaction of Pd nanoparticles with the amine group of the APTS molecule stabilized the metal nanoparticles and increased the loading of the metal nanoparticles on the surface of the zeolite, which is responsible for good catalytic activity in the Heck reactions.

#### **4.4. CONCLUSION**

In this chapter it is demonstrated that platinum and palladium nanoparticles immobilized on the surface of amine-functionalized zeolite provides highly active, recyclable heterogeneous catalysts for hydrogenation and carbon-carbon bond formation



reactions. Detailed characterizations have been done to understand the exact nature of the nanocomposites and are summarized below.

- ❖ UV-visible spectra confirm the formation of Pt and Pd metal nanoparticles
- ❖ FTIR spectra and TGA data confirm that the Pt and Pd nanoparticles are bound to the zeolite surface through the amine functionality of APTS molecule
- ❖ TGA data also indicates that the **[Pt]-APTS-Y** and **[Pd]-APTS-Y** nanocomposites are stable till 145°C
- ❖ Powder XRD data indicates that the zeolite structure remains unchanged during the surface grafting by APTS molecules and metal immobilization. The formation of face centered cubic Pt and Pd nanoparticles on the outer surface of Na-Y zeolite is also interpreted by the XRD data. These observations are supported by TEM measurements
- ❖ Different oxidation states of Pt and Pd present in the **[Pt]-APTS-Y** and **[Pd]-APTS-Y** nanocomposites are confirmed by XPS studies.

The synthesized platinum and palladium nanoparticles show very good catalytic activity for hydrogenation and Heck coupling reactions and more importantly, the stability of these catalysts was found to be good. The high activity of the catalysts can be attributed to the nano size of the metal nanoparticles where as the large grain size of the zeolite take care of easy separation of the catalyst from the liquid phase after reaction. The methodology reported here for the synthesis of supported nano catalysts has great potential for synthesis of heterogeneous catalysts useful for practical applications.

## Reference:

1. (a) Schmid, G. In *Clusters and Colloids*; VCH: Weinheim, **1994**. (b) Lewis, L. N. Chemical catalysis by colloids and clusters. *Chem. Rev.* **1993**, *93*(8), 2693. (c) Alivisatos, A. P. Semiconductor clusters, nanocrystals, and quantum dots. *Science*, **1996**, *271*(5251), 933. (d) Henglein, A. Small-particle research: physicochemical properties of extremely small colloidal metal and semiconductor particles. *Chem. Rev.*, **1989**, *89*(8), 1861.
2. Colvin, V. L.; Schlamp, M. C.; Alivisatos, A. P. Light-emitting diodes made from cadmium selenide nanocrystals and a semiconducting polymer. *Nature*, **1994**, *370*(6488), 354.
3. (a) Emory, S. R.; Nie, S. Screening and Enrichment of Metal Nanoparticles with Novel Optical Properties. *J. Phys. Chem. B*, **1998**, *102*(3), 493. (b) Bruchez, M., Jr.; Moronne, M.; Gin, P.; Weiss, S.; Alivisatos, A. P. Semiconductor nanocrystals as fluorescent biological labels. *Science*, **1998**, *281*(5385), 2013. (c) Chan, W. C. W.; Nile, S. Quantum dot bioconjugates for ultrasensitive nonisotopic detection. *Science*, **1998**, *281*(5385), 2016.
4. (a) Toshima, N.; Nakata, K.; Kitoh, H. Giant platinum clusters with organic ligands: preparation and catalysis. *Inorg. Chim. Acta*, **1997**, *265*(1-2), 149. (b) Schmidt, T. J.; Noeske, M.; Gasteiger, H. A.; Behm, R. J.; Britz, P.; Bonnemann, H. PtRu alloy colloids as precursors for fuel cell catalysts. A combined XPS, AFM, HRTEM, and RDE study. *J. Electrochem. Soc.*, **1998**, *145*(3), 925.
5. (a) Lewis, L. N. Chemical catalysis by colloids and clusters. *Chem. Rev.*, **1993**, *93*(8), 2693. (b) Underhill, R. S.; Liu, G. Preparation and Performance of Pd Particles Encapsulated in Block Copolymer Nanospheres as a Hydrogenation Catalyst. *Chemistry of Materials*, **2000**, *12*(12), 3633.
6. Alvarez, J.; Liu, J.; Roman, E.; Kaifer, A. E. Water-soluble platinum and palladium nanoparticles modified with thiolated  $\beta$ -cyclodextrin. *Chem. Commun.*, **2000**, *13*, 1151.
7. Crooks, R. M.; Zhao, M.; Sun, L.; Chechik, V.; Yeung, L. K. Dendrimer-encapsulated metal nanoparticles: synthesis, characterization, and applications to catalysis. *Acc. Chem. Res.*, **2001**, *34*(3), 181.
8. Mizukoshi, Y.; Oshima, R.; Maeda, Y.; Nagata, Y. Preparation of platinum nanoparticles by sonochemical reduction of the Pt(II) ion. *Langmuir*, **1999**, *15*(8), 2733.
9. (a) Horswell, S. L.; Kiely, C. J.; O'Neil, I. A.; Schiffrin, D. J. Alkyl Isocyanide-derivatized platinum nanoparticles. *J. Am. Chem. Soc.*, **1999**, *121*(23), 5573. (b) Yee, C.I.; Scotti, M.; Ulman, A.; White, H.; Rafailovich, M.; Sokolov, J. One-phase synthesis of thiol-functionalized platinum nanoparticles. *Langmuir*, **1999**, *15*(13), 4314. (c) Mandal, S.; Selvakannan, P. R.; Roy, D.; Chaudhari, R. V.; Sastry, M. A new method for the synthesis of hydrophobized, catalytically active Pt nanoparticles. *Chem. Comm.* **2002**, *24*, 3002
10. (a) Zhao, S.-Y.; Chen, S.-H.; Wang, S.-Y.; Li, D.-G.; Ma, H.-Y. Preparation, phase transfer, and self-assembled monolayers of cubic Pt nanoparticles. *Langmuir*, **2002**, *18*(8), 3315. (b) Sarathy, K. V.; Raina, G.; Yadav, R. T.; Kulkarni, G. U.; Rao, C. N. R. Thiol-Derivatized Nanocrystalline Arrays of Gold, Silver, and Platinum. *J. Phys. Chem. B*, **1997**, *101*(48), 9876.
11. Meijiere, A.; Meyer, F. E. Clothes make the people: the Heck reaction in new clothing. *Angew. Chem.* **1994**, *106*, 2473. (See also *Angew. Chem., Int. Ed. Engl.*, 1994, *33*(23/24), 2379-411. (b) Jeffery, T. On the efficiency of tetraalkylammonium salts in Heck type reactions. *Tetrahedron*, **1996**, *32*, 10113. (c) Herrmann, W. A.; Brommer, C.; Reisinger, C. -P.; Riermeier, T. H.; Ofele, K.; Beller, M. *Chem. Eur. J.* **1997**, *1357*.
12. Beller, M.; Fisher, H.; Kuhlein, K.; Reisinger, C.-P.; Herrmann, W.A. First palladium-catalyzed Heck reactions with efficient colloidal catalyst systems. *J. Organomet. Chem.*, **1996**, *520*, 257.
13. (a) Blaser, H. -U.; Indolese, A.; Schnyder, A.; Steiner, H.; Studer, M. Supported palladium catalysts for fine chemicals synthesis. *J. Mol. Catal. A: Chem.* **2001**, *173*, 3. (b) Toebes, M. L.; van Dillen J. A.; de Jong, Y. P. Synthesis of supported palladium catalysts. *J. Mol. Catal. A: Chem.*, **2001**, *173*, 75. (c) Anastas, P. T.; Bartlett, L. B.; Kirchhoff, M. M.; Williamson, T. C. The role of catalysis in the design, development, and implementation of green chemistry. *Catal. Today*, **2000**, *55*, 11.
14. (a) Jackson, S. D.; McLellan, G. D.; Webb, G.; Conyers, L.; Keegan, M. B. T.; Mather, S.; Simpson, S.; Wells, P. B.; Whan, D. A.; Whyman, R. Supported metal catalysts: preparation, characterization, and function. V. Activities and selectivities of platinum catalysts in the reactions of cyclopropane, ethene, 1,3-butadiene, and 2-butyne with dihydrogen. *Catal.* **1996**, *162*, 10. (b) Jacobs, G.; Ghadiali, F.; Pisanu, A.; Borgna, A.; Alvarez, W. E.; Resasco, D. E. Characterization of the morphology of Pt clusters incorporated

- in a KL zeolite by vapor phase and incipient wetness impregnation. Influence of Pt particle morphology on aromatization activity and deactivation. *Appl. Catal. A* **1999**, *188*, 79. (c) Englisch, M.; Jentys, A.; Lercher, J. A. Structure sensitivity of the hydrogenation of crotonaldehyde over Pt/SiO<sub>2</sub> and Pt/TiO<sub>2</sub>. *J. Catal.*, **1997**, *166*(1), 25. (d) Cocco, G.; Campostrini, R.; Cabras, M. A.; Carturan, G. Propene hydrogenation on low-temperature reduced Pt/TiO<sub>2</sub>. Effects of TiO<sub>2</sub> phases and H<sub>2</sub> treatment on specific catalytic activity. *J. Mol. Catal.* **1994**, *94*, 299.
15. Raja, R.; Sankar, G.; Hermann, S.; Shephard, D.S.; Bromley, S.; Thomas, J.M.; Johnson, B.F.G. Preparation and characterization of a highly active bimetallic (Pd-Ru) nanoparticle heterogeneous catalyst. *Chem. Commun.*, **1999**, *16*, 1571.
  16. Han, Y. J.; Kim, J. M.; Stucky, G. D. Preparation of Noble Metal Nanowires Using Hexagonal Mesoporous Silica SBA-15. *Chem. Mater.* **2000**, *12*, 2068
  17. Yang, C. M.; Sheu, H. S.; Chao, K. J. Templated synthesis and structural study of densely packed metal nanostructures in MCM-41 and MCM-48. *Adv. Funct. Mater.* **2002**, *12*, 143.
  18. El-Sayed, M. A. Some interesting properties of metals confined in time and nanometer space of different shapes. *Acc. Chem. Res.* **2001**, *34*, 257
  19. Crooks, R.M.; Zhao, M.; Sun, L.; Chechnik, V.; Yeung, L.K. Dendrimer-encapsulated metal nanoparticles: synthesis, characterization, and applications to Catalysis. *Acc. Chem. Res.* **2001**, *34*, 181.
  20. Mukhopadhyay, K.; Sarkar, B. R.; Chaudhari, R. V. Anchored Pd Complex in MCM-41 and MCM-48: Novel Heterogeneous Catalysts for Hydrocarboxylation of Aryl Olefins and Alcohols. *J. Am. Chem. Soc.* **2002**, *124*, 9692.
  21. (a) Heck, R. F. Arylation, methylation, and carboxylation of olefins by group VIII metal derivatives. *J. Am. Chem. Soc.* **1968**, *90*, 5518. (b) Tsuji, J. *Palladium Reagents and Catalysts*; Wiley: New York, 1995 (c) Choudary, B. M.; Madhi, S.; Chowdari, N. S.; Kantam, M. L.; Sreedhar, B. Layered double hydroxide supported nanopalladium catalyst for heck-, suzuki-, sonogashira-, and stille-type coupling reactions of chloroarenes. *J. Am. Chem. Soc.*, **2002**, *124*(47), 14127. (d) Reetz, M. T.; Lohmer, G. Propylene carbonate stabilized nanostructured palladium clusters as catalysts in Heck reactions. *Chem. Comm.* **1996**, 1921. (e) Crisp, G. T. Variations on a theme: recent developments on the mechanism of the Heck reaction and their implications for synthesis. *Chem. Soc. Rev.* **1998**, *27*, 427. (f) Genet, J. P.; Savignac, M. J. Recent developments of palladium(0) catalyzed reactions in aqueous medium. *J. Organomet. Chem.* **1999**, *576*, 305. (g) Beletskaya, I. P.; Cheprakov, A. V. The Heck Reaction as a Sharpening Stone of Palladium Catalysis. *Chem. Rev.* **2000**, *100*(8), 3009. (h) Albrecht, M.; van Koten, G. Platinum group organometallics based on "pincer" complexes: sensors, switches, and catalysts. *Angew. Chem., Int. Ed.* **2001**, *40*, 3750. (i) Biffis, A.; Zecca, M.; Basato, M. Palladium metal catalysts in Heck C-C coupling reactions. *J. Mol. Catal. A: Chem.* **2001**, *173*(1-2), 249.
  22. DeVries, R. A.; Mendoza, A. Synthesis of high-purity o- and p-vinyltoluenes by the heck palladium-catalyzed arylation reaction. *Organometallics*, **1994**, *13*, 2405.
  23. Zhao, F.; Bhanage, B. M.; Shirai, M.; Arai, M. Heck reactions of iodobenzene and methyl acrylate with conventional supported palladium catalysts in the presence of organic and/or inorganic bases without ligands. *Chem. Eur. J.*, **2000**, *6*, 843.
  24. Julia, M.; Duteil, M.; Gard, C.; Kuntz, E. *Bull. Soc. Chim. Fr.* **1973**, 2791.
  25. Biffis, A.; Zecca, M.; Basato, M. Metallic palladium in the Heck reaction: active catalyst or convenient precursor? *Eur. J. Inorg. Chem.* **2001**, *5*, 1131.
  26. (a) Djakovitch, L.; Koehler, K. Heck Reaction Catalyzed by Pd-Modified Zeolites. *J. Am. Chem. Soc.* **2001**, *123*(25), 5990. (b) Djakovitch, L.; Koehler, K. Heterogeneously catalyzed Heck reaction using palladium modified zeolites. *J. Mol. Catal. A: Chem.* **1999**, *142*(2), 275.
  27. Mukhopadhyay, K.; Mandale, A. B.; Chaudhari, R. V. Encapsulated HRh(CO)(PPh<sub>3</sub>)<sub>3</sub> in microporous and mesoporous supports: Novel heterogeneous catalysts for hydroformylation. *Chem. Mater.*, **2003**, *15*(9), 1766.
  28. Shirley, D. A. High-Resolution X-Ray Photoemission Spectrum of the Valence Bands of Gold. *Phys. Rev. B.* **1972**, *5*, 4709.
  29. Zhao, M.; Crooks, R. M. Intradendrimer Exchange of Metal Nanoparticles. *Chem. Mater.*, **1999**, *11*(11), 3379.
  30. Henglein, A. Colloidal palladium nanoparticles. Reduction of Pd(II) by H<sub>2</sub>; Pd<sub>Core</sub> Au<sub>Shell</sub> Ag<sub>Shell</sub> particles. *J. Phys. Chem. B.*, **2000**, *104*(29), 6683.

- 
31. Kaleta, W.; Nowinska, K. Immobilization of heteropoly anions in Si-MCM-41 channels by means of chemical bonding to aminosilane groups. *Chem. Commun.* **2001**, 6, 535.
  32. Scheeren, C. W.; Machado, G.; Dupont, J.; Fichtner, P. F. P. Teixeira, S. R. Nanoscale Pt(0) particles prepared in imidazolium room temperature ionic liquids: synthesis from an organometallic precursor, characterization, and catalytic properties in hydrogenation reactions. *Inorg. Chem.*, **2003**, 42(15), 4738.
  33. Kim, S-W.; Park, J.; Jang, Y.; Chung, Y.; Hwang, S.; and Hyeon, T. Synthesis of monodisperse palladium nanoparticles. *Nano Letters*, **2003**, 3(9), 1289.
  34. Fachini, E. R.; Cabrera, C. R. Adsorption and decomposition of Ru<sub>3</sub>(CO)<sub>9</sub>(CH<sub>3</sub>CN)<sub>3</sub> at platinum surfaces: An X-ray photoelectron spectroscopy and Fourier transform-infrared spectroscopy study. *Langmuir*, **1999**, 15(3), 717.
  35. Kumar, A.; Mandal, S.; Selvakannan, P. R.; Pasricha, R.; Mandale, A. B. Sastry, M. Investigation into the interaction between surface-bound alkylamines and gold nanoparticles. *Langmuir*, **2003**, 19(15), 6277.
  36. Venezia, A. M.; Liotta, L. F.; Deganello, G. IR and XPS study of NO and CO interaction with palladium catalysts supported on aluminosilicates. *Langmuir*, **1999**, 15(4), 1176.
  37. Mehnert, P.; Weaver, D. W.; Ying, J. Y.; Heterogeneous Heck catalysis with palladium-grafted molecular sieves. *J. Am. Chem. Soc.*, **1998**, 120(47), 12289.
  38. (a) Schmidt, A. F.; Mametova, L. V. Main features of catalysis in the styrene phenylation reaction. *Kinet. Catal.* **1996**, 37, 406. (b) Wagner, M.; Köhler, K.; Djakovitch, L.; Weinkauf, S.; Hagen, V.; Muhler, M. Heck reactions catalyzed by oxide-supported palladium - structure-activity relationships. *Topics in Catal.* **2000**, 13(3), 319. (c) Zhao, F.; Bhanage, B. M.; Shirai, M.; Arai, M. Heck reactions of iodobenzene and methyl acrylate with conventional supported palladium catalysts in the presence of organic and/or inorganic bases without ligands. *Chem. Eur. J.* **2000**, 6(5), 843.
  39. Biffis, A.; Zecca, M.; Basato, M. *Eur. Metallic palladium in the Heck reaction: active catalyst or convenient precursor? J. Inorg. Chem.* **2001**, 5, 1131.
  40. a) Rahim, E. H.; Kamounah, F. S.; Frederiksen, J.; Christensen, J. B. Heck reactions catalyzed by PAMAM-dendrimer encapsulated Pd(0) nanoparticles. *Nano Letters*, **2001**, 1(9), 499. (b) Mehnert, C. P.; Ying, J. Y. Palladium-grafted mesoporous MCM-41 material as heterogeneous catalyst for Heck reactions. *Chem. Comm.*, **1997**, 22, 2215.
  41. Zhuangyu, Z.; Hongwen, H.; Tsi-Yu, K. *React. Polym.*, **1988**, 9, 249.
  42. Zhuangyu, Z.; Hongwen, H.; Tsi-Yu, K. *React. Polym.*, **1990**, 12, 229.
  43. Molnár, Á.; Papp, A.; Miklós, K.; Forgo, P. Organically modified Pd-silica catalysts applied in Heck coupling. *Chem. Commun.*, **2003**, 20, 2626.
  44. Sheldon, R. A.; Wallau, M.; Arends, I. W. C. E.; Schuchardt, U. Heterogeneous Catalysts for Liquid-Phase Oxidations: Philosophers' Stones or Trojan Horses? *Acc. Chem. Res.*, **1998**, 31(8), 485.
  45. (a) Lempers, H. E. B.; Sheldon, R. A. Allylic oxidation of olefins to the corresponding  $\alpha,\beta$ -unsaturated ketones catalyzed by chromium aluminophosphate-5. *Appl. Catal., A*, **1996**, 143(1), 137. (b) Lempers, H. E. B.; Sheldon, R. A. The stability of chromium in chromium molecular sieves under the conditions of liquid phase oxidations with tert-butyl hydroperoxide. *Stud. Surf. Sci. Catal.*, **1997**, 105B (Progress in Zeolite and Microporous Materials, Pt. B), 1061.

## **Publications & Symposia**

### **Published Papers**

1. *A new method for the synthesis of hydrophobized, catalytically active Pt nanoparticles*  
Saikat Mandal, P. R. Selvakannan, **Debdut Roy**, Raghunath V. Chaudhari and Murali Sastry  
*Chemical Communications*, **2002**, 3002-3003
2. *Pt and Pd Nanoparticles Immobilized on Amine-Functionalized Zeolite: Excellent Catalysts for Hydrogenation and Heck Reactions*  
Saikat Mandal, **Debdut Roy**, Raghunath V. Chaudhari and Murali Sastry  
*Chemistry of Materials*, **2004**, 16, 3714-3724
3. *Kinetic Modeling of Reductive Alkylation of Aniline with Acetone Using Pd/Al<sub>2</sub>O<sub>3</sub> Catalyst in a Batch Slurry Reactor*  
**Debdut Roy**, Rengaswamy Jaganathan and Raghunath V. Chaudhari  
*Ind. Eng. Chem. Res.*, **2005**, 44, 5388-5396
4. *Analysis of a Gas-Liquid-Liquid-Solid Catalytic Reaction: Kinetics and Modeling of a Semi Batch Slurry Reactor*  
**Debdut Roy** and Raghunath V. Chaudhari  
*Ind. Eng. Chem. Res.*, **2005**, 44, 9586-9593
5. *Kinetics of Reductive Alkylation of p-Phenylenediamine with Methyl Ethyl Ketone Using 3% Pt/Al<sub>2</sub>O<sub>3</sub> Catalyst in a Slurry Reactor*  
Narendra G. Patil, **Debdut Roy**, Amit S. Chaudhari and Raghunath V. Chaudhari  
*Ind. Eng. Chem. Res.*, **2006**. Accepted for publication.

## **Presentations in National & International Symposiums**

1. Synthesis of catalytically active platinum nanoparticles immobilized on surface modified Na-Y zeolite.

International Conference on Nanoscience and Technology (**ICONSAT 2003**), 17-20 December 2003, at Kolkata, India

### **Poster Presentation**

2. Kinetic modeling of reductive alkylation of aniline with acetone using Pd/Al<sub>2</sub>O<sub>3</sub> catalyst in a batch slurry reactor.

**Recent Trends in Catalysis Research**, 28<sup>th</sup> October 2004, at National Chemical Laboratory, Pune, India: *A symposium in honour of Dr. S. Sivasankar on his 60<sup>th</sup> Birth Anniversary.*

### **Oral Presentation**

3. Analysis of a gas-liquid-liquid-solid reaction: kinetics and modeling of a semi batch slurry reactor.

5<sup>th</sup> International Symposium on Catalysis in Multiphase Reactors & 4<sup>th</sup> International Symposium on Multifunctional Reactors (**CAMURE-5 & ISMR-4**), 15-18 June, 2005 at Portoroz-Portorose, Slovenia

### **Oral Presentation**

4. Synthesis of Catalytically Active Platinum and Palladium Nanoparticles Grafted on Surface Modified Na-Y Zeolite.

2<sup>nd</sup> Catalysis Research Scholars Meet, a student symposium organized by Catalysis Society of India, Mumbai Chapter (**Catschol-2005**), 19<sup>th</sup> November, 2005 at University Institute of Chemical Technology (UICT), Mumbai, India

### **Oral Presentation**